

Theoretical Studies of Oxidative Addition and Reductive Elimination

Thesis by

John James Low

**In Partial Fulfillment of the Requirements
For the Degree of Doctor of Philosophy**

**California Institute of Technology
Pasadena, California**

1985

(Submitted May 27, 1985)

© 1985

John James Low

ALL RIGHTS RESERVED

Acknowledgment

First of all I would like thank Bill Goddard for providing me the opportunity to do research in Quantum Chemistry. We did not always agree but he allowed me to make many of my own decisions and mistakes. I do appreciate the faith he showed in me and that he trusted me enough to give me important tasks and responsibilities. I hope that I did not and will not disappoint him too often. I would also like to acknowledge my high school instructor in chemistry, Mr. Gerad A. Kass. He first kindled my interest in understanding chemistry at a fundamental level.

I would to thank my parents for providing me with the talents and for raising me the way they did. I am sure that I would not have persevered for as long as I have, if it was not for the good start they gave me.

I have appreciated the help that various Goddard group members have given me. Most of all, I would like to thank Tony Rappé, Ray Bair and Tom Upton for helping me get started in research and Mike Stiegerwald for many helpful discussions. A special thanks goes to Adria McMillan not only for her secretarial skills, but for her encouragement and for reminding me that there is life after Cal. Tech.

I would like thank Horia Metiu and Dick Messmer for their encouragement, advice and helpful discussions. They showed me that one could be a good scientist and a good person as well.

I have made a few good friends here (Steve Witt, Greg Voth, Dan Zirin Mark Brusich, Tom Gibson, Bill Finch, The Lynches, Walther Ellis, Eric Hood, Mike Weimer, and Heidi Tanicar). They have gotten drunk with me (except Eric) and made me laugh on many occasions. I thank the Weenies for competitive softball and the Sierra Club for many relaxing excursions.

A special thanks goes to the Blankenburgs for always being supportive and providing a retreat for me to regain equilibrium. I acknowledge Tikoos for his many loans and for being a good friend, Aunt Eleanor for good food and lots of beer, and Annette and Debbie (a future Blankenburg) for proofreading assistance.

I would like to acknowledge One West and Chippendales for many exciting friday nights.

I finally would like thank Claudia Troesch. She was a good companion at a time when I needed a lot of support.

ABSTRACT

Chapter 1: *Ab initio* calculations (Hartree-Fock, generalized valence bond, and configuration interaction), utilizing relativistic core potentials, have been used to follow the oxidative addition of H_2 to $Pt(PH_3)_2$. We find an activation barrier of 2.3 kcal/mol and an exothermicity of 15.9 kcal/mol. From examination of the geometries and wavefunctions, we find that up to the transition state the H-H bond is still intact. The role of the Pt s^1d^9 and d^{10} states in oxidative addition is described, and the effects of including electronic correlation are discussed. The implications for reductive elimination of the dimethyl and hydridomethyl complexes are also discussed.

Chapter 2: *Ab initio* calculations have been carried out on MR_2 complexes (where $M = Pd$ or Pt and $R = H$ or CH_3) to model concerted reductive coupling from MR_2L_2 complexes (where L is a substituted phosphine). The results of these calculations support the following two conclusions. (1) The differences in the driving force for reductive elimination from $Pd(II)$ and $Pt(II)$ complexes with the same R groups is very close (0-4 kcal/mol) to the difference in the s^1d^9 - d^{10} state splittings of these elements (32 kcal/mol). Thus reductive elimination is exothermic from Pd complexes (since Pd prefers d^{10}) and endothermic from Pt complexes (since Pt prefers s^1d^9), where the metal product is in its d^{10} state. This supports the conclusion, derived from qualitative considerations of generalized valence bond wavefunctions, that $Pt(II)$ and $Pd(II)$ complexes have their metal atoms in a s^1d^9 configuration and the metal atoms in $Pt(0)$ and $Pd(0)$ complexes are in a d^{10} configuration. (2) The activation barriers for

C-C coupling are approximately twice that for C-H coupling. There are essentially no barriers for processes involving H-H bonds. The origin of this trend is the directionality of the methyl sp^3 orbital, which destabilizes the transition state for the case where an M-C bond is being converted to a C-C or C-H bond. Conversely, the spherical H 1s orbital can form multicenter bonds easily, allowing it to break M-H bonds while forming an H-H bond and leading to low intrinsic barriers. These results are consistent with the experimentally observed trends.

Chapter 3: *Ab initio* calculations were carried out on $Pt(CH_3)_2(Cl)_2(PH_3)_2$ and on various $Mt(R_1)(R_2)(PH_3)_2$ complexes (where $Mt = Pd$ or Pt ; $R_1, R_2 = H$ or CH_3) in order to elucidate the differences in reductive H-C and C-C coupling from $Pd(II)$, $Pt(II)$, and $Pt(IV)$ complexes. These studies explain why (1) reductive C-C coupling is facile for $Pd(II)$, favorable for $Pt(IV)$, and unobserved for $Pt(II)$ systems, while (2) reductive H-C coupling is facile for $Pt(II)$ and $Pd(II)$ systems, and (3) oxidative addition is favorable only for addition of H_2 to $Pt(0)$ systems.

Chapter 4: *Ab initio* calculations were carried out on CH_x and NH_x molecular fragments on small clusters of Ni atoms (Ni_{13} and Ni_{14}), as a model for chemisorption on the Ni(100) surface. The results presented here show that these species make strong π bonds to the surface which cause methylidyne and imidogen to be the most stable CH_x and NH_x species on this surface. The results have also been used to estimate ΔH_f^0 for various intermediates important for methanation and ammonia decomposition on Ni surfaces.

Table of Contents

Chapter 1:

Theoretical Studies of Oxidative Addition and Reductive Elimination: $\text{H}_2 + \text{Pt}(\text{PH}_3)_2 \rightarrow \text{Pt}(\text{H})_2(\text{PH}_3)_2$	1
I. Introduction	2
II. Summary of Results	3
III. Results	4
IV. Computational Details	10

Chapter 2:

Theoretical Studies of Oxidative Addition and Reductive Elimination: II. Reductive Coupling of H-H, H-C, and C-H Bonds from Pd and Pt Complexes	12
I. Introduction	13
II. Summary of Results	18
III. Comparison With Experiment	32
IV. Comparison With Other Theoretical Work	36
V. Computational Details	40
Appendix A	46
Appendix B	49
References and Notes	50
Tables	59
Figures	75

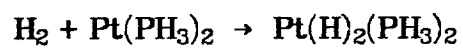
Chapter 3:

Theoretical Studies of Oxidative Addition and Reductive Elimination: III. C-H and C-C Reductive Coupling from Pd and Pt Bisphosphine Complexes	86
I. Introduction	87
II. Summary of Results	90
III. Discussion	113

IV. Computational Details.....	121
References and Notes.....	126
Tables	134
Figures.....	149
Chapter 4:	
Theoretical Studies of CH _x and NH _x Species Chemisorbed on Ni Clusters	160
I. Introduction	161
II. Results.....	163
III. Computational Details.....	174
IV. Conclusions.....	178
Appendix A.....	179
References.....	186
Tables	191
Figures.....	204

CHAPTER 1

Theoretical Studies of Oxidative Addition and Reductive Elimination:



The following chapter has appeared in the *Journal of the American Chemical Society*, **1984**, *106*, 6928-6937.

Reprinted from the Journal of the American Chemical Society, 1984, 106, 6928.
Copyright © 1984 by the American Chemical Society and reprinted by permission of the copyright owner.

Theoretical Studies of Oxidative Addition and Reductive Elimination: $H_2 + Pt(PH_3)_2 \rightarrow Pt(H)_2(PH_3)_2$

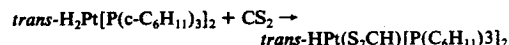
John J. Low and William A. Goddard III*

Contribution No. 6995 from the Arthur Amos Noyes Laboratory of Chemical Physics, California Institute of Technology, Pasadena, California 91125. Received March 5, 1984

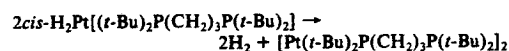
Abstract: Ab initio calculations (Hartree-Fock, generalized valence bond, and configuration interaction), utilizing relativistic core potentials, have been used to follow the oxidative addition of H_2 to $Pt(PH_3)_2$. We find an activation barrier of 2.3 kcal/mol and an exothermicity of 15.9 kcal/mol. From examination of the geometries and wave functions, we find that up to the transition state the H-H bond is still intact. The role of the Pt s^1d^9 and d^{10} states in oxidative addition is described, and the effects of including electronic correlation are discussed. The implications for reductive elimination of the dimethyl and hydridomethyl complexes are also discussed.

I. Introduction

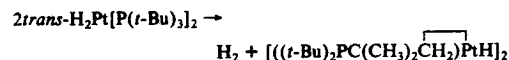
Oxidative addition and reductive elimination are important steps in many organometallic reactions.¹ In particular, the oxidative addition of a hydrogen molecule to a PtL_2 complex (where L is a substituted phosphine) has been observed for a number of different ligands, L [e.g., $P(c-C_6H_{11})_3$, $P(i-Pr)_3$].^{2,3} H_2PtL_2 complexes have been observed to undergo many types of reactions, including insertion,⁴⁻⁶ e.g.,



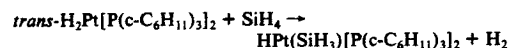
dimer formation,^{7,8} e.g.,



metallation,⁹ e.g.,

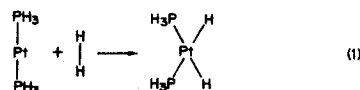


and oxidative addition followed by reductive elimination of H_2 ,^{2,3,10-12} e.g.,

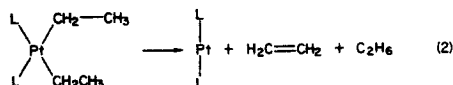


Such species have also been proposed as intermediates in the catalysis of the water-gas shift reaction¹³ and of alkene hydrogenation.⁷

As a first step in gaining a better understanding of the formation of covalent bonds through reductive elimination and the scission of bonds via oxidative addition, we have examined the process



Of particular interest in analyzing these results will be to explain why (i) the addition of hydrogen to PtL_2 occurs at room temperature, but reductive elimination is quite slow;^{2,3,14} (ii) the reductive elimination of methane from $(H)(CH_3)Pt(L)_2$ proceeds at room temperature;¹⁵ but (iii) $Pt(II)$ diacyl complexes tend to be stable with respect to forming carbon-carbon bonds through reductive elimination. Thus, diacyl complexes will disproportionate through β -hydride elimination



rather than reductively eliminate when they thermally decompose.¹⁶⁻²⁰ Only for $Pt(II)$ diacyl complexes, where β -elimination is impossible, have carbon-carbon bonds been formed through reductive elimination at high temperatures.²¹ On the other hand, (iv) $Pd(II)$ dimethyl complexes are quite unstable with respect to reductive elimination to yield C-C coupling.²²

In this paper we develop a relatively simple model of reaction 1 by examining the energetics, geometries, and wave functions along the reaction coordinate. These results indicate that oxidative addition of H_2 to PtL_2 depends crucially on the relative positions of the $5d^{10}$ and $6s^15d^9$ states of the platinum atom. The resulting energetics explain the observed differences regarding oxidative

- (1) Collman, J. P.; Hegedus, L. S. "Principles and Applications of Organotransition Metal Chemistry"; University Science Books: Mill Valley, CA, 1980; Chapter 4.
- (2) Yoshida, T.; Otsuka, S. *J. Am. Chem. Soc.* **1977**, *99*, 2134-2140.
- (3) Fornies, J.; Green, M.; Spencer, J. L.; Stone, F. G. A. *J. Chem. Soc., Dalton Trans.* **1977**, 1006-1009.
- (4) Albinati, A.; Musco, A.; Carturan, G.; Strukul, G. *Inorg. Chim. Acta* **1976**, *18*, 219-223.
- (5) Immirzi, A.; Musco, A. *Inorg. Chim. Acta* **1977**, *22*, L35-L36.
- (6) Clark, H. C.; Goel, A. B.; Wong, C. S. *J. Organomet. Chem.* **1978**, *152*, C45-C47.
- (7) Yoshida, T.; Yamagata, T.; Tulip, T. H.; Ibers, J. A.; Otsuka, S. *J. Am. Chem. Soc.* **1978**, *100*, 2063-2073.
- (8) Tulip, T. H.; Yamagata, T.; Yoshida, T.; Wilson, R. D.; Ibers, J. A.; Otsuka, S. *Inorg. Chem.* **1979**, *18*, 2239-2250.
- (9) Clark, H. C.; Goel, A. B.; Ogini, W. O. *J. Organomet. Chem.* **1978**, *157*, C16-C18.
- (10) Ebsworth, E. A. V.; Maranian, V. M.; Reed, F. J. S.; Gould, R. O. *J. Chem. Soc., Dalton Trans.* **1978**, 1167-1170.
- (11) Clark, H. C.; Goel, A. B.; Billard, C. *J. Organomet. Chem.* **1979**, *182*, 431-440.
- (12) Paonessa, R. S.; Troglor, W. C. *Organometallics* **1982**, *1*, 768-770.
- (13) Yoshida, T.; Ueda, Y.; Otsuka, S. *J. Am. Chem. Soc.* **1978**, *100*, 3941-3942.
- (14) Paonessa, R. S.; Troglor, W. C. *J. Am. Chem. Soc.* **1982**, *104*, 1138-1140.
- (15) Abis, L.; Ayusman, S.; Halpern, J. *J. Am. Chem. Soc.* **1978**, *100*, 2915-2916.
- (16) Whitesides, G. M.; Gaasch, J. F.; Stedronsky, E. R. *J. Am. Chem. Soc.* **1972**, *94*, 5258-5270.
- (17) Nuzzo, R. G.; McCarthy, T. J.; Whitesides, G. M. *J. Am. Chem. Soc.* **1981**, *103*, 3404-3410.
- (18) McCarthy, T. J.; Nuzzo, R. G.; Whitesides, G. M. *J. Am. Chem. Soc.* **1981**, *103*, 1676-1678.
- (19) McCarthy, T. J.; Nuzzo, R. G.; Whitesides, G. M.; *J. Am. Chem. Soc.* **1981**, *103*, 3396-3403.
- (20) Komiya, S.; Yoshiyuki, M.; Yamamoto, A.; Yamamoto, T. *Organometallics* **1982**, *1*, 1528-1536.
- (21) Braterman, P. S.; Cross, R. J.; Young, G. B. *J. Chem. Soc., Dalton Trans.* **1976**, 1310.
- (22) Gillie, A.; Stille, J. K. *J. Am. Chem. Soc.* **1980**, *102*, 4933-4941.

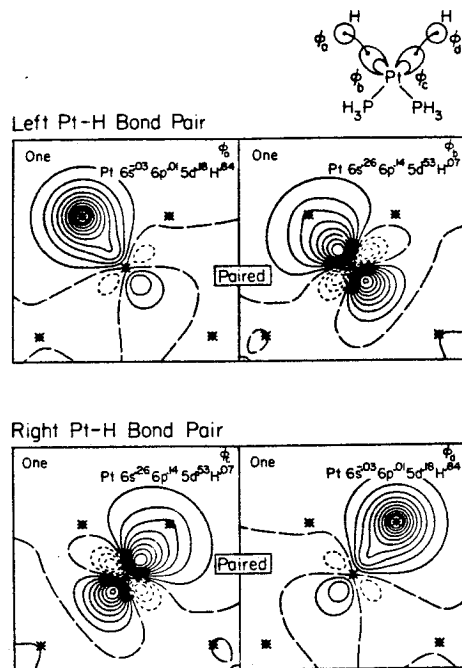
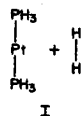


Figure 1. GVB orbitals for the Pt-H bonds of $\text{H}_2\text{Pt}(\text{PH}_3)_2$ at equilibrium. Hybridization for each singly occupied GVB orbital is shown on each plot. Each contour represents a change of 0.05 in amplitude. Solid lines represent positive amplitude. Dashed lines represent nodes. Dotted lines represent negative amplitude. Asterisks represent the position of atoms.

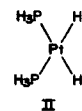
addition/reductive elimination in Pt and Pd complexes.

II. Summary of Results

The details of the calculations are described in section IV. Here we will emphasize the main lessons from the theoretical studies. In the ground state of the reactants,



the lone pairs of the phosphines make strong Lewis base bonds to the Pt atom, stabilizing the (d^{10}) configuration and leading to a linear complex. The oxidative addition product is square-planar,



with an HPtH angle of 79.4° and a PPtP angle of 99.9° . Despite the terminology "oxidative addition", we find that there is essentially no charge transfer from the Pt to the H's. Instead, we find that the Pt in II corresponds to a $(6s)^1(5d)^9$ configuration of Pt, allowing the formation of two covalent bonds to the H atoms. The generalized valence bond (GVB) orbitals for these bond pairs are shown in Figure 1 where each bond involves one electron in an $\text{H}1s$ -like orbital and one electron in a $6s$ - $5d$ hybrid (60% d) pointing at the H.

The net exothermicity of reaction 1 is calculated to be 16 kcal/mol, so that one can consider the two Pt-H bonds of II to

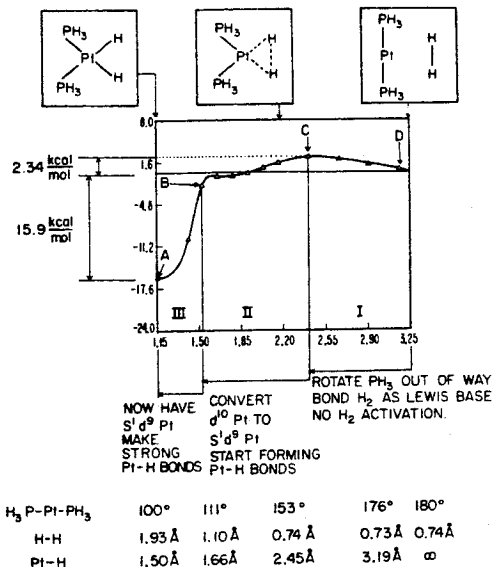


Figure 2. Potential energy curve along the reaction coordinate.

be worth 60 kcal/mol each. [If the geometry of the $\text{Pt}(\text{PH}_3)_2$ fragment were kept fixed, then the average Pt-H bond energy would be 72 kcal/mol.] The next question is how do the orbitals change as the system goes from I to II? This process is orbital symmetry allowed²³ and indeed we find in Figure 2 that the reaction has only a 2.3-kcal/mol barrier. In examining the potential curve in Figure 2, three distinct phases in the process of oxidative addition are discerned.

(i) **Lewis Base/Lewis Acid Bonding of H_2 to $\text{Pt}(\text{PH}_3)_2$ (D → C in Figure 2).** Since the platinum atom is in a d^{10} state, the Pt 6s orbital is empty and can serve as an electron acceptor. As the hydrogen molecule approaches the diphosphine complex, the H_2 electrons utilize the Pt 6s orbital, making a Lewis acid/Lewis base bond. As this occurs, the phosphine ligands bend back (a) to lower steric interactions between the hydrogen molecule and the phosphine ligands and (b) to increase the overlap between the Pt 6s orbital and the H-H bonding orbital. The overlap between the Pt 6s and H-H bonding orbitals increases because the Pt 6s orbital polarizes away from the phosphines (hybridizes with the 6p orbital) to get orthogonal to the phosphine lone-pair orbitals. By the transition state, the P-Pt-P bond angle has decreased from 180° to 153° , but the H-H bond length remains essentially constant (changing by only 0.003 Å). The overall energy increase is 2.3 kcal/mol, whereas to bend the P-Pt-P angle the same amount in the diphosphine complex would cost 9 kcal/mol. Therefore we can consider the H_2 -Pt Lewis base/Lewis acid interaction to be worth 7 kcal/mol at the transition state.

(ii) **Electronic Promotion of the Platinum Atom (C → B in Figure 2).** Once the H_2 molecule has passed the transition state (point B in Figure 2), the platinum atom begins to build in some d^9s^1 character. As the phosphines bend back from 153° to 113° , this becomes more favorable because the splitting between the d^{10} (1A_1) ground state and the lowest s^1d^9 state (3B_1) decreases as the P-Pt-P angle decreases. Thus, as the P-Pt-P angle decreases from 180° to 140° and then to 90° , this splitting decreases from 107 kcal/mol, to 63 kcal/mol, and then to 20 kcal/mol. The mixing of the d^9s^1 and the d^{10} states occurs mainly through the delocalization of the H_2 electrons into the Pt 6s orbital and the back-donation of the Pt $6d_{yz}$ electrons into the H-H antibonding

(23) Tatsumi, K.; Hoffmann, R.; Yamamoto, A.; Stille, J. K. *Bull. Chem. Soc. Jpn.* 1981, 54, 1857.

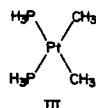
orbital. As these electronic changes occur, the H-H bond lengthens from 0.74 to 0.87 Å.

(iii) Covalent Bonding (B → A in Figure 2). By point B in Figure 2, the platinum atom is in the d^9s^1 state, allowing it to form two covalent Pt-H bonds. As the Pt-H bonds decrease from 1.72 Å to their equilibrium bond lengths (1.50 Å), the energy decreases rapidly. In this region the P-Pt-P bond angle changes from 113° to 100° and the H-H distance increases from 0.87 to 1.93 Å.

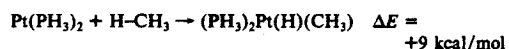
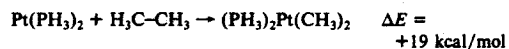
An important point from the calculations is that the final bonds are covalent; thus the oxidative addition of H_2 to Pt is not oxidative. Rather, the electronic state of the Pt is promoted from d^{10} to s^1d^9 because the d^{10} state cannot make covalent bonds, while the s^1d^9 state can make two covalent bonds. Therefore one might denote these states as Pt^0 and Pt^{II} , respectively, where the superscript indicates not oxidation state but rather maximum covalency (maximum number of covalent bonds). Substantiation of this idea that H_2 addition is not oxidative is given by the observed promotion of H_2 addition to Ir(I) complexes by electron-withdrawing substituents (opposite of the expected trend if one has assumed significant charge transfer to the hydrogens).²⁴

A second point of the calculations is that a low barrier for the H_2 oxidation requires that the adduct (H_2) must be a sufficiently good Lewis base that it can activate the Pt by pushing back the phosphine ligands while forming a Lewis acid-base bond. The activation of the Pt corresponds to the stabilization of the s^1d^9 (Pt^{II}) state that can form the covalent bonds.

Implications for other systems are as follows. Preliminary calculations for



indicate an average Pt-C bond energy of $D_{PtC} = 36$ kcal/mol, whereas the work presented here leads to $D_{PtH} = 60$ kcal/mol. Extrapolating the same bond energies to $H(CH_3)Pt(PH_3)_2$ gives the following energetics:



The above energetics can be used to explain the relative energetics of hydridomethylplatinum(II) and dihydride complexes. The platinum dihydrides are stable under 0.5 atm of hydrogen at room temperature and decompose slowly under vacuum.¹⁴ The only known *cis*-hydridomethylplatinum(II) complex decomposes quickly at room temperature.¹⁵ Since the Pt(II) dimethyl complex has been calculated to have a larger driving force for reductive elimination, and it is known experimentally that these complexes are more stable than the hydridomethylplatinum(II) complex, there must be a larger barrier to reductively eliminate ethane than to reductively eliminate methane. This is plausible since the directional character of the Pt-C bond requires that the methyl groups must rotate away from the Pt in order to overlap each other in forming the C-C bond. In contrast, for H_2 the s orbital used in the Pt-H bond can also be used in the H-H bond. Thus, for reductive elimination of ethane directly from $L_2Pt(CH_3)_2$, it is plausible that a barrier exists even if the process is exothermic. (Preliminary calculations on this process for a Pd complex confirm these expectations.²⁵)

On the other hand, in the hydridomethyl complex, the hydrogen orbital can overlap both the carbon sp^3 orbital and a Pt sd hybrid

Table I. Pt Atom State Splittings (in kcal/mol)

state	expt ^c	HF	GVB- (5/10) ^a	RCI- (5/10) ^a	GVBCI- (5/10) ^a
$^3D(s^1d^9)^b$	0.0	0.0	0.0	0.0	0.0
$^1S(d^{10})$	11.0	31.4	27.0	12.3	12.2
$^3F(s^2d^8)$	14.7	8.4	11.2	18.5	14.2

^a See Computational Details section. ^b The total energies of the 3D state are -27.50619 hartrees at the HF level, -27.51933 hartrees at the GVB-PP level, and -27.55129 hartrees at the RCI(5/10) level (using the relativistic effective core potential of ref 37). ^c The energies in this column are actually the average of experimentally observed j states derived from each Russell-Sanders term.

orbital as methane reductively eliminates. This should lead to an activation barrier for reductive elimination of methane from hydridomethylplatinum(II) complexes that is intermediate between those for breaking H-H and forming C-C bonds, in agreement with the observed reactivities of hydridomethyl complexes.¹⁵

We find that oxidative addition of H_2 to $Pt(PH_3)_2$ proceeds with a small activation barrier (2.3 kcal/mol) and the overall reaction is sufficiently exothermic that the products should be stable with respect to reductive elimination. This is in agreement with the results of Paonessa and Trogler.¹⁴ They have prepared the dihydrides of the sterically unhindered $Pt(PMe_3)_2$ and $Pt(PEt_3)_2$ and found these complexes to be stable under 0.5 atm of H_2 and to decompose slowly under vacuum. The singular difference between Pd and Pt is that the Pd atom prefers the d^{10} configuration by 22 kcal/mol,²⁶ while Pt prefers the d^9s^1 configuration by 11.0 kcal/mol.²⁶ Thus Pd has a total bias of about 33 kcal/mol in favor of the d^{10} configuration. Since the reductive eliminations considered here involve mostly changing from s^1d^9 to d^{10} , this means that the increased splitting should make the Pd(II) complexes considerably (about 34 kcal/mol) less stable than their Pt counterparts. This is in agreement with observed reductive elimination of ethane from $Pd(CH_3)_2L_2$ complexes²² (where $L = PPh_3, PPh_2CH_3$; $L_2 = PPh_2PCH_2CH_2PPh_2$) and the fact that hydrogen will not oxidatively add to a Pd diphosphine complex but does add for the corresponding platinum complex.²

III. Results

A. Platinum Atom. The changes occurring during oxidative addition are partly determined by the electronic structure of the Pt atom. As with Ni and Pd, the platinum atom has three low-lying states, $^3D(s^1d^9)$, $^1S(d^{10})$, and $^3F(s^2d^8)$. We find that the Pt complexes tend to have the character of one or another of these atomic states and that the chemistry is dominated by this atomic character. In Table I, we summarize the relative energies of these states for various levels of calculations and experimental results.²⁷

Clearly, Hartree-Fock (HF) calculations are strongly biased against the d^{10} state. In the jargon of theorists, electron correlation is far more important if the two electrons are in a $5d$ orbital than if the electrons are in different orbitals ($5d$ or $6s$). A simple way to account for the major electron correlation errors implicit in the HF or molecular orbital (MO) description is the use of the GVB wave function, which allows each electron to have a differently shaped orbital and allows the orbitals for singlet-coupled electrons to overlap. Thus, in GVB each doubly occupied valence orbital of the HF wave function is described by a pair of overlapping GVB orbitals. For an atom with a doubly occupied d orbital in the HF wave function, the GVB wave function converges to one tight d orbital (near the nucleus) and one diffuse d orbital (farther from the nucleus). We have chosen to describe the doubly occupied s orbital of the 3F state by tight and diffuse s orbitals in order to be consistent with the correlation included in the GVB pairs describing d electrons.²⁸

(26) Moore, C. E. "Atomic Energy Levels"; National Bureau of Standards: Washington, DC, 1971; Vol. III (averaged over j states to cancel out spin-orbit coupling).

(27) Herzberg, G. "Molecular Spectra and Molecular Structure, Part III. Electronic Spectra and Electronic Structure of Polyatomic Molecules"; D. Van Nostrand Co., Inc.: Princeton, NJ, 1966.

(24) Crabtree, R. *Acc. Chem. Res.* 1979, 12, 331-388.

(25) Low, J. J.; Goddard, W. A., III *J. Am. Chem. Soc.*, submitted for publication.

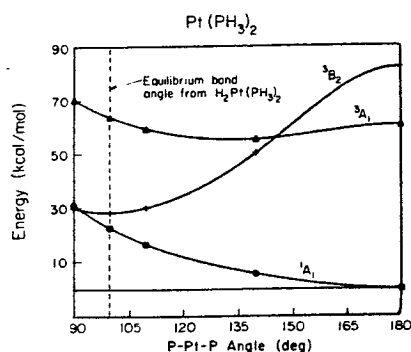


Figure 3. Potential energy curves for the low-lying states of $\text{Pt}(\text{PH}_3)_2$ as a function of P-Pt-P angle.

In many systems, electron correlation plays an important chemical role only for certain orbitals. In the platinum atom most of the electronic correlation important for state splittings occurs in the Pt 5d and 6s orbitals. Thus, if all ten d electrons in the Pt $^1\text{S}(d^{10})$ state are correlated in the GVB wave function, we denote this wave function as GVB(5/10) [here the 5 is the number of singlet-coupled electron pairs, while the 10 is the number of orbitals used to describe the five pairs]. If only one pair of electrons were to be correlated (i.e., for the bonding pair of electrons in Pt-H), we would use a GVB(1/2) wave function.

When there is more than one pair to correlate, there are additional options in describing the wave function. The simplest description is for each pair to have singlet spin coupling as a simple valence bond (VB) wave function. This is denoted as GVB-PP and is the usual form in which the orbitals are calculated. However, for a system with five pairs of electrons (ten VB orbitals), there are 42 VB structures or spin couplings that should all be included in calculating the final wave function. In addition, there are interpair correlation effects, wherein if the two electrons in the d_{xy} orbitals are at some instant closer to the nucleus, the two electrons in the d_{yz} orbital will at that instant tend to be farther from the nucleus. These spin coupling and interpair correlation effects are included by carrying out a configuration interaction (CI) calculation in which the two electrons in each pair of orbitals are simultaneously allowed all possible occupations of those two orbitals, leading to what is termed a GVB-RCI wave function. Thus, for a GVB-PP(5/10) wave function, there are $3^5 = 243$ configurations in the GVB-RCI wave function.

The most complete wave function that can be described with just the GVB orbitals is to carry out a full CI with use of all possible occupations of these orbitals. This is termed GVB-CI, and for a GVB-PP(5/10) wave function, this leads to 8953 configurations. Since the GVB-RCI and GVB-CI are based on GVB orbitals, we can interpret these CI wave functions in terms of simple VB concepts. As is evident from the results in Table I, the GVB-RCI wave function gives results that are as consistent as the GVB-CI results but with significantly fewer configurations. For the purposes of this paper, the GVB-RCI provides the best combination of accuracy and simplicity.

B. $\text{Pt}(\text{PH}_3)_2$. When two phosphines are added to a platinum atom, the major effect is to raise the energy of the platinum 6s orbital relative to the Pt 5d orbitals. This occurs because the phosphine lone pair makes a Lewis acid-base bond by overlapping with (donating into) the Pt 6s orbital. The net result is that the ground state of $\text{Pt}(\text{PH}_3)_2$ is a singlet ($^1\text{A}_1$) state derived from the $^1\text{S}(d^{10})$ state of the platinum atom. In this state, the phosphines minimize their steric repulsions by increasing the P-Pt-P bond angle to 180° . The low-lying triplet states of $\text{Pt}(\text{PH}_3)_2$ are both

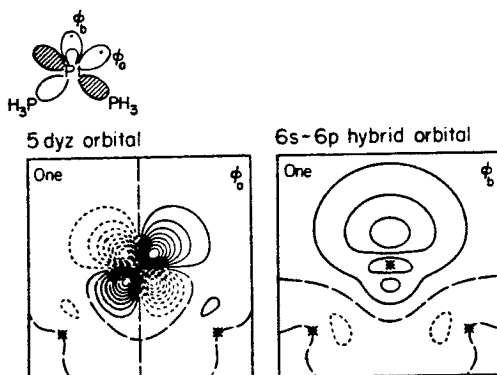


Figure 4. Open-shell orbitals for the $^3\text{B}_2$ state for bent (100°) $\text{Pt}(\text{PH}_3)_2$.

Table II. State Splittings for the d^{10} and d^9s^1 States of $\text{Pt}(\text{PH}_3)_2$

state	$\text{PH}_3\text{-Pt-PH}_3$ angle, deg	state splittings (kcal/mol)		
		HF	GVB(5/10)	RCI(5/10)
$^1\text{A}_1$ ^a	180.0	0.0	0.0	0.0
$^3\text{B}_2$	180.0	81.9	89.2	106.5
$^3\text{A}_1$	180.0	65.7	53.3	69.6
$^3\text{B}_2$	99.0 ^b	28.5	35.2	51.5
$^1\text{A}_1$	99.0 ^b	22.8	22.1	24.6
$^3\text{A}_1$	99.0 ^b	72.9	58.0	75.3

^a The total energies for the $^1\text{A}_1$ are -712.170 592 hartrees at the HF level, -712.199 127 hartrees at the GVB-PP(5/10) level, and -712.260 738 hartrees at the RCI(5/10) level. ^b 99.0° is the optimum bond angle for the $^3\text{B}_2$ state.

derived from the $^3\text{D}(s^1d^9)$ state of the platinum atom. When two hydrogen atoms make bonds to $\text{Pt}(\text{PH}_3)_2$, we find that the Pt atom changes from d^{10} to s^1d^9 character in order to make covalent Pt-H bonds. In making these bonds, there is a major change in the P-Pt-P angle of PtL_2 . In order to assess the role of this geometric change upon the energetics of the Pt d^{10} and s^1d^9 states, we show in Figure 3 the energies of the $\text{Pt}(\text{PH}_3)_2$ complex as a function of P-Pt-P bond angle. [The internal coordinates of the phosphine were frozen at the internal coordinates of free phosphine²⁹ (H-P-H angle = 93.3° , P-H bond distance = 1.420 Å). The Pt-P distance was chosen to be 2.268 Å.³⁰ The H-P-Pt angles were fixed (at 122.9°) so that the C_3 axis of the phosphine groups would pass through the platinum atom.]

The lowest excited state of $\text{Pt}(\text{PH}_3)_2$ is the $^3\text{B}_2$ state with an s^1d^9 configuration. This state has a singly occupied $5d_{yz}$ orbital and a singly occupied 6s orbital. The phosphines would prefer to have their lone pairs overlap the singly occupied d_{yz} orbital as much as possible, which would imply a bond angle of 90° or 180° ; however, the 90° geometry allows the 6s pair to hybridize away from the phosphines, stabilizing this geometry. Steric interactions of the phosphines cause the bond angle to open up slightly, leading to an optimum bond angle of 99.0° (HF). A plot of the singly occupied orbitals for the $^3\text{B}_2$ state is shown in Figure 4, where we note that the singly occupied 6s orbital has been polarized away from the phosphines. This occurs because the 6s orbital must be orthogonal to the phosphine lone pairs.

In Table II, we show the state splittings at various levels of calculation for several states.

The $^3\text{A}_1$ state has a singly occupied Pt d_{xz} orbital and a singly occupied Pt p orbital (see Figure 5). In this case a bond angle of 180° is favored since the phosphines can both overlap the singly occupied d_{xz} orbital while simultaneously minimizing their steric

(28) The best (lowest energy) two-orbital description of the 6s pair of electrons would be in terms of two sp hybrid orbitals, $\psi_a = c_1\psi_s + c_2\psi_p$ and $\psi_b = c_1'\psi_s - c_2'\psi_p$, as for Be, Mg, Zn, etc.²⁹

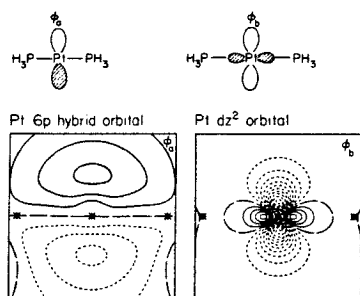
(29) Goddard, W. A., III; Harding, L. B. *Annu. Rev. Phys. Chem.* 1978, 29, 363-396.

(30) Noell, J. O.; Hay, P. J. *J. Am. Chem. Soc.* 1982, 104, 4578-4584.

Table III. Summary of Results for Pt-H

	R , Å	D_e , kcal/mol	total energy, ^c hartrees	ω_e , ^b cm ⁻¹	dipole moment, ^c Debye	Mulliken pop. on Pt	Mulliken pop. on H
HF	1.516	37.3	-28.065 612	2027	2.52	10.07	0.93
GVB-PP(1/2)	1.526	51.6	-28.088 370	1948	1.89	10.10	0.90
GVB-PP(5/10)	1.530	58.1	-28.098 619	1930	1.88	10.10	0.90
RCI(5/10)	1.544	48.9	-28.128 813	1914	1.86	10.11	0.89
GVB-CI(5/10)	1.549	52.8	-28.136 407	1909	1.90	10.10	0.90
DC-CI	1.51 ^d	60.6					
experiment ^a	1.528	<79.3		2260			

^a Huber, K. P.; Herzberg, G. "Molecular Spectra and Molecular Structure. IV. Constants of Diatomic Molecules"; Van Nostrand-Reinhold Co.: New York, 1979. ^b Frequencies were obtained from the curvature at R_e which was obtained from a cubic spline fit. ^c The positive sign implies Pt⁺H⁻. ^d This calculation was only carried out at this bond distance. ^e All total energies are reported for $R = 1.51$ Å.

Figure 5. Open-shell orbitals for the 3A_1 state for linear Pt(PH₃).

interactions. However, in this geometry the s orbital cannot as easily polarize out of the way of the phosphine lone pairs, leading to a higher energy. In fact, for this state the Pt s electron has been promoted to the p orbital³¹ (see Figure 5). The 3B_2 state is the best triplet because it allows both phosphines to overlap the singly occupied d orbital, while allowing the platinum s orbital to polarize out of the way of the phosphine lone pairs.

Comparisons between Pd and Pt complexes are useful because both atoms have low-lying d^9s^1 and d^{10} atomic states but yield different ground states. In palladium the atom has a d^{10} ground state (22.9 kcal/mol below the d^9s^1 state), while in platinum the d^9s^1 state is the ground state (11.0 kcal/mol below the d^{10} state). This should lead to $d^{10}s^1d^9$ splittings for the Pd diphosphines that are 33.9 kcal/mol larger (disfavoring oxidative addition to Pd) and hence should result in much weaker Pd-H and Pd-C σ bonds for Pd diphosphine complexes than for the corresponding Pt complexes. Consistent with these expectations, hydrogen has not been observed to add to PdL₂ while it has for PtL₂ [e.g., L = P(c-C₆H₁₁)₃, P(*i*-Pr)₃].² In addition, Gillie and Stille²² have observed reductive elimination of ethane from Pd(II) dimethyl complexes, while Pt(II) dimethyl complexes are much more stable. These cases demonstrate how the $d^{10}s^1d^9$ splittings for these ML₂ complexes affect the driving forces for reductive elimination and oxidative addition.

C. Pt-H. Calculations were performed on the platinum hydride diatomic molecule to determine how the energetics of the Pt-H bond are affected by the level of the calculations. These studies also help demonstrate the nature of the Pt-H bond. Five levels of calculation have been performed: HF, GVB(1/2), GVB(5/10), RCI(5/10), and GVB-CI(5/10). The results of these calculations are shown in Table III where we see that bond distance (R_e), bond energy (D_e), and vibrational frequency (ω_e) are fairly insensitive to the level of calculation once the Pt-H bond pair was correlated. Thus, description of the Pt-H bond at the GVB(1/2) level provides a quite adequate description of the bond and should be a suitable level for use in the Pt-H bonds in H₂Pt(PH₃)₂ and in reductive elimination from this complex.

(31) We have used C_{2v} symmetry to classify the states in this discussion. At a P-Pt-P angle of 180° the Pt(PH₃)₂ complex would actually have D_{3h} symmetry. The 3A_1 state would be one component of the $^3E'$ state.

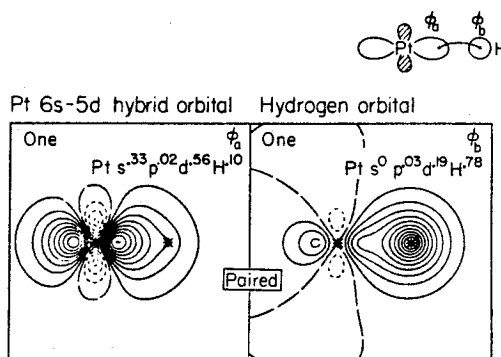


Figure 6. GVB orbitals for diatomic PtH.

Experimental characterization of PtH includes the bond length and vibrational frequency but only an upper bound for the bond energy. This compares well with the experimental geometry (1.5% long) but is 15% low for the vibrational frequencies. The best theoretical bond energy of 60.6 kcal/mol was obtained from a dissociation-consistent configuration interaction (DC-CI) calculation.³² This calculation involves all single and double excitations from the active space defined by the Pt-H bond pair from a GVB-PP(1/2) calculation times all single excitations from the semiactive space defined by the remaining platinum valence electrons. This calculation was carried out at only a single point (1.51 Å), so a vibrational frequency is not reported for this level of calculation. This calculated bond energy is 20 kcal/mol smaller than the experimental upper bound of 80 kcal/mol.

The calculated Mulliken populations and dipole moments show that the PtH bond is essentially covalent. This is consistent with the small difference in Pauling electronegativities of Pt (2.2) and H (2.1).³³ However, detailed comparison of the dipole moment and Mulliken populations appears to give conflicting results. The dipole moment indicates a transfer of 0.26 e^- to the hydrogen atom, while the Mulliken populations indicate a transfer of 0.10 e^- from the H. This apparent conflict is partly due to the Pt part of the bond orbital being a Pt sd hybrid with some Pt p character so that it is polarized toward the hydrogen. This polarization contributes to the dipole moment but not to the Mulliken charge transfer. To obtain a qualitative measure of the polarization taking place, we have calculated the dipole moment of the platinum orbitals from a GVB(1/2) calculation on PtH. This calculation included the localized Pt GVB orbital from the Pt-H GVB bond pair and the other five Pt-like nonbonding sd orbitals (four doubly occupied and the singly occupied d_{z^2} orbital), where in each case any hydrogen character was deleted (and the orbitals were renormalized). This calculation on the Pt atom yields a dipole moment of 1.08 D, over half the total dipole moment of Pt-H. Subtracting

(32) Bair, R. A.; Goddard, W. A., III *J. Chem. Phys.*, submitted for publication. Bair, R. A. Ph.D. Thesis, California Institute of Technology, 1981.

Table IV. Geometries along the Reaction Coordinates 1-13

	1	2	3	4	5	6	7	8	9	10	11	12	13
$R_{\text{Pt-H}_2}$ ^a	1.166	1.417	1.542	1.667	1.792	1.917	2.042	2.167	2.417	2.667	2.917	3.167	∞
$R_{\text{Pt-P}}$	2.447	2.417	2.387	2.372	2.356	2.335	2.336	2.348	2.351	2.330	2.334	2.325	2.318
$R_{\text{H-H}}$	1.926	1.570	1.104	0.865	0.812	0.780	0.762	0.750	0.740	0.733	0.728	0.732	0.743
$R_{\text{Pt-H}}$	1.504	1.620	1.628	1.723	1.838	1.957	2.077	2.199	2.445	2.692	2.940	3.188	
$R_{\text{Pt-H}_2}$	1.525	1.522	1.519	1.524	1.525	1.525	1.526	1.529	1.530	1.525	1.518	1.526	1.527
$R_{\text{Pt-H}_2}$	1.529	1.526	1.526	1.526	1.525	1.526	1.525	1.527	1.526	1.525	1.522	1.527	1.527
$\theta_{\text{H-Pt-H}}$	99.9	102.5	108.1	113.5	122.3	127.2	133.8	137.4	152.9	167.2	170.1	175.2	180.0
$\theta_{\text{H-Pt-H}}$	79.4	58.0	39.4	29.1	25.5	23.0	21.1	19.6	17.4	15.6	14.3	13.2	
$\theta_{\text{H-Pt-H}}$	96.6	96.8	95.9	95.3	95.0	95.2	94.9	94.8	95.1	95.6	94.3	95.7	96.2
$\theta_{\text{H-Pt-H}}$	95.5	95.5	95.5	94.9	94.7	94.8	95.2	95.0	95.5	95.7	95.8	95.8	96.2
$\theta_{\text{H-Pt-H}}$	119.3	120.2	121.2	123.8	123.1	124.4	124.8	124.8	124.9	120.7	122.9	121.1	120.7
$\theta_{\text{H-Pt-H}}$	121.4	120.9	121.0	120.4	121.1	120.2	120.0	120.2	119.7	121.4	121.3	121.1	120.7

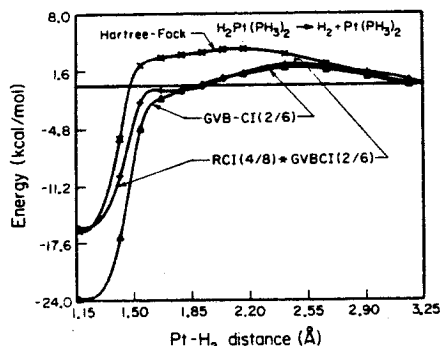
^a All R in Å. ^b All θ in deg.

Figure 7. Plot of energy along the reaction coordinate for HF, GVB-CI(2/6), and RCI(4/8)+GVB-CI(2/6) wave functions.

this dipole moment due to Pt atom polarization from the total dipole moment leads to a residual molecular moment of 0.81 D, corresponding to a transfer of only 0.11 e^- to the hydrogen atom. Therefore, a large fraction of the dipole moment is due to polarization of the Pt valence orbitals. The remaining discrepancy of $Q_{\text{H}} = 1.11 e^-$ from the dipole moment vs. $Q_{\text{H}} = 0.90 e^-$ from the Mulliken populations represents a deficiency in the Mulliken analysis, namely, the equal partitioning of overlap terms tends to underestimate the population on H. Summarizing, the charge transfer in the Pt-H bond is small so that the Pt-H bond should be described as covalent.

The Mulliken populations for the GVB orbitals (see Figure 6) of the Pt-H bond show that the GVB orbital localized on the Pt atom is about 60% Pt d character and 40% Pt sp character. This hybridization of the Pt d_{z^2} orbital makes the density along the z axis larger than it would be for either a pure Pt 6s orbital or a pure Pt d_{z^2} orbital. This increases the overlap (and contragradience) between the platinum orbital and the hydrogen orbital.³⁴

D. $\text{H}_2\text{Pt}(\text{PH}_3)_2$. The changes in the electronic structure that occur during oxidative addition can most easily be elucidated by following a reaction path from reactants to products. We used the distinguished coordinate method to find a good approximation to the reaction coordinate at various levels of calculation.³⁵ The distinguished coordinate method freezes one internal coordinate of the system to be studied while optimizing all the others for lowest energy. By repeating this procedure for a number of values for the frozen coordinate, one can generate a potential curve that is only a function of one variable and changes continuously from products to reactants. These optimizations were performed at the HF level with use of an analytic gradient technique.³⁶ HF

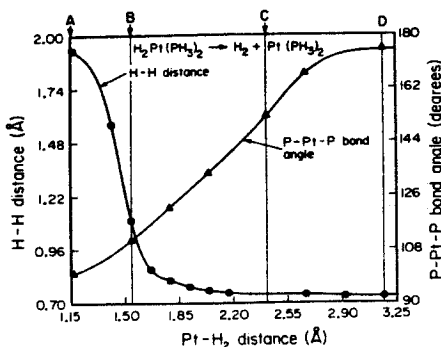


Figure 8. Changes in the P-Pt-P bond angle and H-H distance along the reaction coordinate.

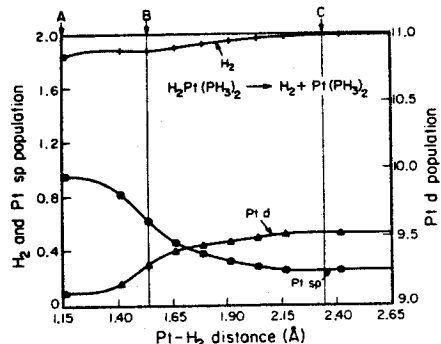


Figure 9. Mulliken population along the reaction coordinate.

provides accurate equilibrium geometries for various platinum complexes³⁷ and leads to exothermicities and barrier heights similar to correlated wave functions.

The geometries resulting from the distinguished coordinate method are listed in Table IV. For more details on how these calculations were carried out, see section IV. The distinguished coordinate used in these calculations was the Pt-H₂ distance. The HF potential as a function of Pt-H₂ distance is shown in Figure 7.

As the Pt-H₂ distance was varied, only two other internal coordinates changed significantly. The P-Pt-P angle changed from 180° to 100° through the reaction path. The H-H distance increased a small amount as the hydrogen molecule approached the Pt(PH₃)₂ complex up to a Pt-H₂ distance of 2.0 Å. For Pt-H₂

(33) Pauling, L. "The Nature of the Chemical Bond", 3rd ed.; Cornell University Press: Ithaca, New York, 1960; pp 88-98.

(34) Steigerwald, M. L. Ph.D. Thesis, California Institute of Technology, 1983.

(35) Rothman, M. J.; Lohr, L. L. *Chem. Phys. Lett.* **1980**, *70*, 405.

(36) Low, J. J.; Goddard, W. A., III, manuscript in preparation.

(37) Noell, J. O.; Hay, P. J. *Inorg. Chem.* **1982**, *21*, 14-20.

distances less than 2.0 Å, the H-H distance increased rapidly from 0.76 to 1.926 Å. These geometry changes as a function of Pt-H₂ distance are shown in Figure 8.

E. Charge Populations. The Mulliken populations of the Pt d, Pt s and H₂ orbitals are plotted as a function of Pt-H₂ distance in Figure 9. This plot shows that the amount of Pt 6s character increases and the amount of Pt 5d character decreases as H₂ approaches the Pt(PH₃)₂ complex. At the dissociated limit, the Pt population has 9.51 d electrons and 0.38 s electrons. At equilibrium, the population has 9.10 d electrons and 0.96 s electrons. Although Mulliken populations are not truly quantitative measures for the character and locations of the electrons, as shown above for Pt-H, they can be used to provide qualitative ideas of how charge is distributed. At equilibrium, the Mulliken populations show that the platinum atom is in a d⁹s¹ state. At the dissociated limit and at the transition state, the platinum atom is in a state that is mainly d¹⁰ and singlet.

In Noell's population analysis,³⁸ charges are assigned to atoms by partitioning space. All charge within the covalent radius of the Pt atom was assigned to this center. The space outside this sphere was partitioned into cones with 45° angles of rotation about each ligand. The charge in a particular cone was assigned to the ligand that was contained in the cone. The remaining charge outside the covalent radius of the platinum atom was assigned to the platinum atom. This partitioning resulted in a positively charged platinum atom (1.22 e⁻), negatively charged hydrogen atoms (-0.29 e⁻), and negatively charged PH₃ groups (-0.32 e⁻). Noell feels that this is a more reasonable assignment because it is closer to the formal oxidation states of the platinum and hydrogen atoms. One problem with Noell's analysis is that a relatively large fraction of the platinum atom d basis (11%) and sp basis (37%) is outside the covalent radius of the platinum atom. When the platinum atom is in a s¹d⁹ state, this would result in 1.36 e⁻ being assigned to the ligands! Clearly this is not a fair division of density.

Comparing the Pauling electronegativities³³ of platinum (2.2) and hydrogen (2.1), we see that the hydrogen atom should be slightly negatively charged. But such a small difference in the electronegativity should lead to a bond that is essentially covalent (less than 4% ionic by Pauling's formula).³³ The dipole moment of Pt-H indicates that the Pt-H bond is more polar than Pauling would predict, as discussed in section III. This is due largely to the polarization of the Pt valence electrons rather than to charge transfer. Although the Mulliken population leads to the wrong polarity (Pt⁺), it is particularly useful in determining the relative amounts of Pt s, p, and d character in a wave function. Qualitatively, the Mulliken populations indicate that there is not a large amount of charge transfer, and this is in agreement with the dipole moments.

F. Forms for the Wave Functions. In analyzing the character of bond orbitals, it is important to use wave functions that change smoothly as one goes from one extreme with a doubly occupied Pt d_{xy} orbital and H-H bond pair to the other extreme with Pt-H bonds. The simplest wave function providing a good description of the Pt-H bonds is the GVB(2/4) wave function. This wave function contains one GVB pair for each Pt-H bond, as shown in Figure 1. These orbitals involve combinations of the platinum 5d_{xy} and 6s orbitals and of the two hydrogen atomic orbitals. The best GVB orbitals at the dissociated limit are shown in Figure 10. These orbitals involve combinations of a tight Pt 5d_{xy} orbital, a diffuse 5d_{xy} orbital, and two hydrogen atomic orbitals. Thus the GVB(2/4) wave function is *not* consistent throughout the reaction path because different types of correlation are required to describe the electrons localized on the platinum atom at the different limits. At the dissociated limit, the pair of Pt electrons involved in the Pt-H bonds are both in d_{xy} orbitals and are correlated in-out. In other words, one electron is in close to the platinum atom while the other is farther away. After the two Pt-H bonds are formed, the bonding Pt electrons are both in sd hybrid orbitals.

A more consistent wave function for this reaction would be to allow the Pt pair of bonding electrons to use a tight d orbital, a

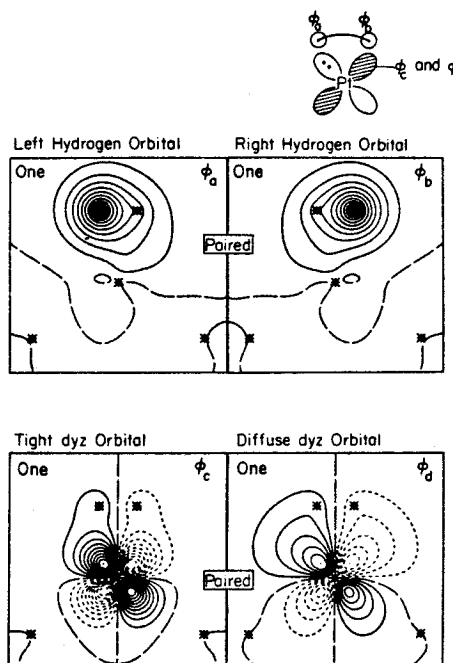


Figure 10. GVB orbitals for H₂ + Pt(PH₃)₂ near the transition state.

Table V. Energies along the Reaction Path

$R_{\text{Pt-H}_2}$ Å	HF, kcal/mol	GVB-CI(2/6), kcal/mol	GVB-CI(2/6)- *RCI(4/8), kcal/mol
1.166	-16.21	-23.79	-15.90
1.417	-5.92	-16.91	-10.09
1.542	2.26	-4.76	-1.86
1.667	3.12	-1.41	-0.56
1.792	3.42	-0.55	-0.51
1.917	3.69	0.13	-0.13
2.042	4.00	0.86	0.70
2.167	4.04	1.25	1.40
2.417	3.47	1.96	2.34
2.667	2.37	1.71	2.05
2.917	1.26	0.92	1.40
3.167	0.15	0.02	0.52
∞ ^a	0.0	0.0	0.0

^aThe total energies at the dissociated limit (∞) are -713.330 533 hartrees at the HF level, -713.363 061 hartrees at the GVB-CI(2/6) level, and -713.449 931 hartrees at the GVB-CI(2/6)*RCI(4/8) level.

diffuse d orbital, and a Pt s orbital. This would allow this pair of electrons to have both in-out correlation and the optimum d⁹s¹ mixture throughout the reaction. In order that the two GVB pairs involved in the bonding be treated equivalently, we have permitted each of them to have three natural orbitals (rather than two). At the dissociated limit, this corresponds to a Pt pair, as was described above, and to an H₂ molecule described at the GVB(1/3) level (in-out plus left-right correlation).

In considering the effects of electron correlation on this reaction, we examined the HF, GVB-CI(2/6), and GVB-CI(2/6)*RCI(4/8) wave functions. The GVB-CI(2/6) wave function includes electronic correlation terms differential in describing the Pt-H bonds. The GVB-CI(2/6)*RCI(4/8) wave function includes both the Pt-H bonding terms of the GVB-CI(2/6) level as well as the d-d correlations important in determining the d⁹s¹-d¹⁰ splitting on the platinum atom. For more calculational details, see section IV.

Table VI. Transition State as a Function of Electronic Correlation for $\text{Pt}(\text{PH}_3)_2 + \text{H}_2 \rightarrow \text{H}_2\text{Pt}(\text{PH}_3)_2$

level of electronic correlation	Pt-H ₂ distance, Å	activation energy, kcal/mol	exothermicity, kcal/mol
HF	2.199	4.04	-16.21
GVB-CI(2/6)	2.417	1.96	-23.79
RCI(4/8)*GVB-CI(2/6)	2.417	2.34	-15.90

Table VII. Comparison of the HF Activation Barrier for $\text{Pt}(\text{PH}_3)_2 + \text{H}_2 \rightarrow \text{Pt}(\text{PH}_3)_2(\text{H})_2$ and Important Geometric Parameters at the Transition State Obtained in Various ab Initio Studies

	ΔE_{act} , kcal/mol	$R_{\text{Pt-H}}$, Å	$R_{\text{H-H}}$, Å	$\theta_{\text{Pt-Pt-H}}$, deg
Noell and Hay ^a	17.4	1.81	0.90	120
Kitaura et al. ^b	5.2	2.066	0.766	147.7
this work	4.04	2.199	0.750	137.4

*Reference 30. ^aReference 39.

The potential curves are shown in Figure 7, and the calculated energies are tabulated in Table V. The main effect of correlating the Pt-H bonds at the GVB-CI(2/6) level is to increase the exothermicity of the reaction and to move the transition state to longer distances. Correlating the nonbonding d electrons at the GVB-CI(2/6)*RCI(4/8) level makes the exothermicity for the reaction smaller than for the GVB-CI(2/6) level wave function, but gets essentially the same transition-state geometry and barrier. Correlating the nonbonding d electrons does not affect the long-range behavior of the Pt-H bonds. The GVB-CI(2/6) wave function (in which the nonbonding d electrons are doubly occupied) does as well as the GVB-CI(2/6)*RCI(4/8) wave function (which has the nonbonding d electrons correlated) near the transition state. This implies that this transition-state geometry is less sensitive to the s^1d^9 - d^{10} splitting than is the exothermicity.

Qualitatively, these potential curves all have similar shapes. The potential curves for the correlated wave functions can be divided into three regions similar to those for the HF surface. This implies that the HF level wave function could have been used to elucidate the electronic structure of the mechanism. Unfortunately HF yields orbitals that are delocalized and difficult to interpret, whereas the GVB types of wave functions lead to orbitals that are localized and easier to interpret. Also, the GVB wave function allows one to interpret the various types of correlation and to see how each one affects the wave function. The GVB-CI(2/6) wave function leads to an improved description of the long-range attractive terms in the wave function, leading to a lower activation energy and a longer Pt-H bond distance at the transition state. At the GVB-CI(2/6)*RCI(4/8) level, we also include interpair correlations of the nonbonding d electrons on the platinum atom. These correlations were not important at the transition state because the Pt atom still has a d^{10} -like configuration. On the other hand, these d-d correlations have a big effect on the d^{10} - s^1d^9 separation, and hence they have a big effect on the reaction exothermicity. These correlation effects stabilize d^{10} relative to s^1d^9 and have led to a smaller exothermicity. In Table VI we present a summary of the energetics for oxidative addition at the different levels of calculation.

G. Comparison with Previous Results. The previous two ab initio studies of this system gave different results for activation barrier and transition state. A comparison of the results presented in this paper with the results from Noell and Hay and from Kitaura et al.³⁹ is shown in Table VII.

The transition-state geometry found in our studies and by Kitaura et al.³⁹ is much closer to products than Noell and Hay's³⁰ transition state. Also, our HF activation barrier (4.04 kcal) for oxidative addition is close to the value (5.2 kcal) found by Kitaura et al.³⁹ Noell and Hay,³⁰ on the other hand, found a significantly

larger activation barrier (17.4 kcal/mol). Since we have used the same effective potential as Noell and Hay³⁷ and completely optimized the geometry for every fixed value of Pt-H₂ distance, Noell and Hay's³⁰ high activation barrier must be due to their partial optimization, which apparently did not converge to the lowest energy point along the reaction coordinate.

The differences between our transition-state geometry and that of Kitaura et al.³⁹ must be due to the different effective potentials and basis sets used. Our results should be more reliable for the following reasons. (1) We have used Noell and Hay's³⁷ Pt potential, which includes the f-projected terms required when f electrons are included in the effective potential, whereas the Kitaura et al.³⁹ calculations used an effective potential with only s and p projections. (2) We have used a larger hydrogen basis than Kitaura et al.³⁹ This larger basis includes the more diffuse character needed to describe the long-range Pt-H₂ interactions at the transition state.

The energies of reaction found from HF calculations in these three studies were also very different. Our ΔE (-16.2 kcal/mol) is larger than that found by Noell and Hay³⁰ (-6.7 kcal/mol), but smaller than the ΔE (-36.9 kcal/mol) of Kitaura et al.³⁹ We obtain a larger ΔE than Noell and Hay for this reaction because we allowed the Pt-P bond lengths to change along the reaction path. Noell and Hay held this parameter fixed at a value closer to the optimum for $\text{Pt}(\text{PH}_3)_2$, which should favor the dissociated limit and give a smaller ΔE . The Pt potential used by Kitaura et al.³⁹ is known to give Pt-H bonds that are 11.6 kcal/mol too strong.³⁰ Applying this correction factor to Kitaura et al.'s³⁹ ΔE leads to a corrected ΔE of 13.7 kcal/mol, which is very close to our value.

Comparing geometries with the available X-ray structures, we see that our Pt-P bond distances are too long by 0.1 to 0.2 Å. For $\text{Pt}(\text{PCy}_3)_2$, the experimental distance was found to be 2.231 Å,⁵ while our calculated Pt-P bond distance for $\text{Pt}(\text{PH}_3)_2$ is 2.32 Å. Typical Pt-P bond distances for Pt(II) complexes are 2.25 Å for $t\text{-H}_2\text{Pt}(\text{PCy}_3)_2$,⁴⁰ 2.268 Å for $t\text{-PtHCl}[\text{P}(\text{C}_6\text{H}_5)_2\text{C}_2\text{H}_5]_2$,⁴¹ and 2.248 Å for $c\text{-PtCl}_2(\text{PMe}_3)_2$.⁴² Our calculated Pt-Pt bond distance for $c\text{-H}_2\text{Pt}(\text{PH}_3)_2$ is 2.45 Å, which is 0.2 Å too long. This elongation of the Pt-P bond length was also found by Noell and Hay³⁷ when they optimized the geometry of $\text{Pt}(\text{PH}_3)_2$ and found a Pt-P distance of 2.36 Å (using a different effective potential and basis set on the phosphorus). This effect appears to be systematic for phosphorus Lewis acid/Lewis base bonds treated at the HF level with a valence double- ζ basis.

In BH_3PH_3 , where phosphorus is making a similar Lewis acid/Lewis base bond, we find a B-P bond length of 2.180 Å at the HF level using a double- ζ basis.⁴³ When the geometry was optimized with polarization functions on both the phosphorus and boron,⁴³ the B-P distance was found to be 2.055 Å. The experimental⁴⁴ B-P distance in BH_3PH_3 is 1.937 Å. Therefore, approximately 0.1 Å of the error observed in P Lewis acid/Lewis base bonds is due to the use of an unpolarized basis. Ahlrichs and Koch⁴⁵ have carried out calculations on BH_3PH_3 using a smaller basis set with both HF and correlated wave functions (CEPA). The smaller basis set yields a shorter B-P bond distance of 1.99 Å at the HF level. For the correlated wave function, their B-P bond distance is 0.04 Å shorter than their HF results. This indicates a large part of the remaining discrepancy must be due to electronic correlation.

Kitaura et al.³⁹ found Pt-P bonds that were short by 0.1 Å, but this is most likely due to the small basis set (STO-2G) used to optimize their geometries, which would underestimate bond distances for Lewis acid-Lewis base bonds.

(40) Immirzi, A.; Musco, A.; Carturan, G.; Belluco, U. *Inorg. Chim. Acta* 1975, 12, L13.(41) Eisenberg, R.; Ibers, J. A. *Inorg. Chem.* 1965, 4, 473.(42) Meesmer, G. G.; Amma, E. L.; Ibers, J. A. *Inorg. Chem.* 1967, 6, 725.

(43) Dunning, T. H.; Hay, P. J. In "Modern Theoretical Chemistry: Methods of Electronic Structure Theory"; Schaefer, H. F., III, Ed.; Plenum Press: New York, 1977; Vol. 3, Chapter 1, pp 1-27.

(44) Durig, J. R.; Li, Y. S.; Carreira, L. A.; Odom, J. D. *J. Am. Chem. Soc.* 1973, 95, 2491-2496.(45) Ahlrichs, R.; Koch, W. *Chem. Phys. Lett.* 1978, 53, 341-344.(38) Noell, J. O. *Inorg. Chem.* 1982, 21, 11-14.(39) Kitaura, K.; Obara, S.; Morokuma, K. *J. Am. Chem. Soc.* 1981, 103, 2891-2892.

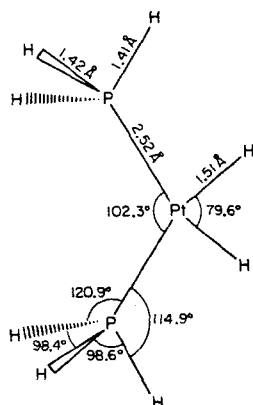


Figure 11. Geometry of $\text{H}_2\text{Pt}(\text{PH}_3)_2$ obtained by using a double- ζ basis on phosphines.

Hoffmann and co-workers²³ have performed an analysis of reductive elimination reactions using the extended Hückel method. Three major conclusions were presented in this work: (1) The better the σ -donating capability of the leaving group, the more readily the elimination proceeds. (2) Stronger donor ligands trans to the leaving groups give a higher barrier for the elimination reaction. (3) A lower positioning of the $\text{MA}_2 \text{b}_2$ orbital facilitates the reductive elimination of R_2 . A lower $\text{MA}_2 \text{b}_2$ energy will be given by a lower metal d orbital energy.

Our studies concur with the third conclusion of Hoffmann et al. A more stable d orbital implies a more stable d^{10} state of the metal relative to s^0d^9 that will in turn increase the driving force for reductive elimination. This should also decrease the barrier for reductive elimination. Our results do not bear on the first two points since we have studied only the one system.

Balazs et al.⁴⁶ have also studied (1) using the SCF-X α -SW approach. However, they do not report calculated geometries or transition states nor do they report calculated bond energies or activation energies; thus there is little with which to compare our work. The electronic densities from X α agree with our results, indicating neutral H atoms (charge of -0.04 e).

IV. Computational Details

A. Potentials and Basis Sets. On platinum atom we used the relativistic effective potential of Noell and Hay.³⁷ For the hydrogen atoms bonded directly to the Pt atom we used a triple- ζ contraction of Huzinaga's six-Gaussian basis.⁴⁷ For phosphorus we used the SHC effective potentials of Rappé et al.⁴⁸ with a minimum basis contraction based on the atomic orbitals. The hydrogen atoms bonded to P were described with a minimum basis set based on Huzinaga's four-Gaussian basis (unscaled). To determine whether the use of minimum basis phosphines affected the geometries or energetics for oxidative addition, we carried out geometry optimizations on $\text{H}_2\text{Pt}(\text{PH}_3)_2$ and $\text{Pt}(\text{PH}_3)_2$ using full double- ζ basis sets on the phosphine ligands. The results are shown in Figures 11 and 12. The exothermicity calculated for this reaction with double- ζ phosphines is 13.84 kcal/mol, only 2.47 kcal/mol smaller than the result with minimum basis set phosphines. This represents only a 1.25-kcal/mol error per Pt-H bond.

B. GVB-PP (Generalized Valence Bond with Perfect Pairing Restrictions).⁴⁹ In this wave function each correlated pair of

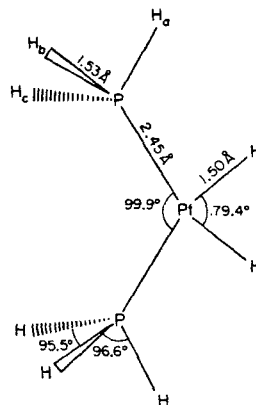


Figure 12. Geometry of $\text{H}_2\text{Pt}(\text{PH}_3)_2$ obtained by using a minimum basis on phosphines.

electrons is described as a spin singlet state $\varphi_a\varphi_b + \varphi_b\varphi_a$. This description can be transformed to a natural orbital description

$$c_1\varphi_1^2 - c_2\varphi_2^2$$

where

$$\varphi_1 = \frac{(\varphi_a + \varphi_b)}{(2(1 + S))^{1/2}} \quad \varphi_2 = \frac{(\varphi_a - \varphi_b)}{(2(1 - S))^{1/2}}$$

$c_2/c_1 = (1 - S)/(1 + S)$, $c_1^2 + c_2^2 = 1$, and $S = \langle \varphi_a | \varphi_b \rangle$. These natural orbitals are then used in higher level CI calculations.

C. GVB-RCI (Restricted Configuration Interaction). The GVB-RCI calculation includes the configurations φ_1^2 , φ_2^2 , and $\varphi_1\varphi_2$ for each GVB pair. When the configuration $\varphi_1\varphi_2$ is multiplied by similar configurations in the other GVB pairs, more general spin couplings are included that will optimize the total spin eigenfunction of the electronic wave function. This spin optimization can be important in describing the dissociation of multiple bonds and in describing the changes in the spin multiplicity in different atomic states. This wave function also includes interpair correlations important in the atomic $\text{d}^{10}\text{-s}^0\text{d}^9$ splittings. This type of wave function is useful because it still maintains orthogonal GVB pairs of electrons, facilitating the interpretation of the wave function.

When comparing singlet and triplet states of the platinum atom and of $\text{Pt}(\text{PH}_3)_2$, we counted the two open-shell orbitals as a GVB pair in the RCI(5/10) nomenclature. This is consistent since the triplet wave function contains all the configurations that the singlet contains except for those that have two electrons in one of the open-shell orbitals.

D. GVB-CI (Generalized Valence Bond Configuration Interaction). This type of CI is carried out by using all possible configurations that can be formed from the various occupations of the GVB orbitals from the GVB-PP calculation. This wave function includes all the terms of the RCI wave function plus terms that allow the GVB pairs to overlap and to change shape by allowing linear combinations between pairs. Such terms are particularly important near the region where the Pt-H bonds are just starting to form. Omission of such terms (as in a GVB-PP or RCI calculations) would lead to an artificial hump in the transition region.

Figure 13 demonstrates the importance of full correlation among the four electrons that are involved with the oxidation/reduction process. The GVB-PP wave function can describe the two Pt-H bonds at equilibrium or the doubly occupied d orbital and H-H bond at the dissociated limit. Near the region where both of the above VB descriptions are important, the energy of the GVB-PP wave function becomes artificially high. This gives a transition state near 1.55 Å for the GVB-PP wave function that disappears

(46) Balazs, A. C.; Johnson, K. H.; Whitesides, G. M. *Inorg. Chem.* **1982**, *21*, 2162-2174.

(47) Huzinaga, S. *J. Chem. Phys.* **1965**, *42*, 1293-1302.

(48) Rappé, A. K.; Smedley, T. A.; Goddard, W. A., III. *J. Phys. Chem.* **1981**, *85*, 1662-1666.

(49) Bobrowicz, F. W.; Goddard, W. A., III. In "Modern Theoretical Chemistry: Methods of Electronic Structure Theory"; Schaefer, H. F., III, Ed.; Plenum Press: New York, 1977; Vol. 3, Chapter 4, pp 79-127.

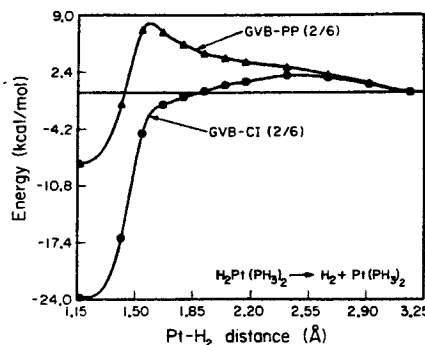


Figure 13. Comparison of energies along the reaction coordinate for GVB-PP(2/6) and GVB-CI(2/6) wave functions.

for the GVB-CI wave function (which can describe both VB wave functions).

E. Geometry Optimizations. All of the geometry optimizations were obtained by using an analytic gradient procedure (GVBGRAD). This program was based on (a) the GVB2P5⁴⁹ program to evaluate density matrices for restricted HF and GVB-PP wave functions, (b) the HONDO⁵⁰ program to calculate derivatives of the ab initio terms in the energy expression, and (c) routines from the GAUSS 80⁵¹ program and the Los Alamos effective potential program⁵² to calculate the effective potential terms of the derivative. For the optimization of the geometries we used a relatively simple Newton-Raphson technique³⁶ in which the second derivative matrix is updated after every gradient calculation (except for the starting geometry).

The end-on approach of H₂ to Pt(PH₃)₂ was not considered in this work since the side-on approach of H₂ to Pt(PH₃)₂ gave a low barrier. The end-on approach should give a higher barrier because it would require breaking an H-H bond (104 kcal/mol) and promoting PtL₂ to a triplet state (~50 kcal/mol) while only getting ~72 kcal/mol back in the Pt-H bond. [Kitauro et al.³⁹ found that the C_{2v} transition state is a true saddle point (i.e., there is only one negative root in the curvature matrix).]

F. Hybrid Wave Functions. In examining the effect of electronic correlation along the reaction path, we calculated a GVB-CI(2/6)*RCI(4/8) wave function where the orbitals were optimized for the full 3360 configuration (8568 spin eigenfunctions) wave function by using the GVB3⁵³ program. We used this wave function to examine the effects of correlating the nonbonding d electrons on the energetics along the reaction coordinate. The electrons in the Pt-H bonds were treated at the GVB-CI level for the reasons described above. The d nonbonding orbitals were treated at the RCI(4/8) level because this level was needed to get reasonable triplet-singlet splittings for the atom. The resulting wave function is therefore a product of the GVB(2/6) wave function for the Pt-H bonds and a RCI(4/8) for the nonbonding

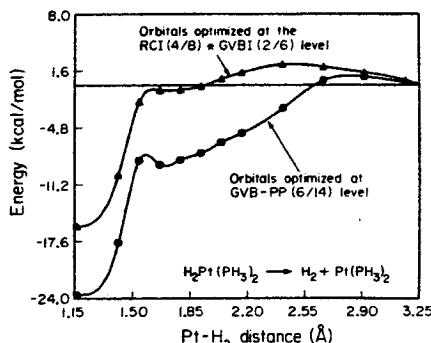


Figure 14. Comparison of energies along the reaction coordinate for RCI(4/8)*GVB-CI(2/6) and GVB-PP(6/14) wave functions.

d electrons. This wave function was optimized self-consistently by using the GVB3 multiconfigurational self-consistent-field program⁵³ because the nonbonding d natural orbitals did not change smoothly from equilibrium to the dissociated limit at the GVB-PP level unless they were optimized at the CI level.

Often it is sufficient to use the orbitals from the GVB-PP wave function for RCI or GVB-CI wave functions. For example, orbitals obtained at the GVB-PP level were adequate for the GVB-CI(2/6) wave function. Optimizing the orbitals at the GVB-CI level lowered the energy of the GVB-CI wave function by less than 0.002 hartree (1.255 kcal/mol) relative to the GVB-CI calculation by using orbitals obtained at the GVB-PP level. This energy lowering remained essentially constant along the reaction path. Thus, although the GVB-PP wave function yields an unreasonable potential curve in the transition region, it does provide orbitals yielding a proper description of Pt-H bonding formation. This occurs because the GVB-CI includes the recoupling of bonding electrons necessary in describing the reaction.

However, for the GVB-CI(2/6)*RCI(4/8) wave function it is essential to self-consistently reoptimize the orbitals for the full wave function, as illustrated in Figure 14. The upper potential curve was obtained from the fully self-consistent wave function, while the lower curve is for a wave function for which the orbitals were optimized at the GVB-PP level. Use of incompletely optimized orbitals (GVB-PP) is biased against the Pt d¹⁰ state (the dissociated limit) and leads to an irregularly stepped potential curve. The reason for this behavior is that for Pt(PH₃)₂ the RCI wave function includes terms differential in the d¹⁰-s¹d⁹ splitting. When the orbitals are optimized for a wave function including these terms, orbital shape changes occur that are differential for these state splittings. These differential terms affect the shape of the potential curve (and the transition state) because the platinum atom changes its electronic state during the reaction.

Acknowledgment. This work was supported in part by a grant from the National Science Foundation (No. CHE80-17774). One of the authors (J.J.L.) wishes to acknowledge financial support in the form of a fellowship from Exxon.

Registry No. Pt(H)₂(PH₃)₂, 76832-29-6; Pt(PH₃)₂, 76830-85-8; H₂, 1333-74-0.

(50) Dupuis, M.; King, H. F. *J. Chem. Phys.* **1978**, *68*, 3998-4004.
(51) Binkley, J. S.; Whiteside, R. A.; Krishnan, R.; Seeger, R.; DeFrees, D. J.; Schlegel, H. B.; Topiol, S. W.; Kahn, L. R.; Pople, J. A. "Gauss 80", unpublished.

(52) Hay, P. J.; Wadt, W. R.; Kahn, L. R., unpublished results.

(53) Yaffe, L. G.; Goddard, W. A., III *Phys. Rev. A* **1976**, *13*, 1682.

CHAPTER 2

Theoretical Studies of Oxidative Addition and Reductive Elimination:

II. Reductive Coupling of H-H, H-C, and C-C Bonds

from Pd and Pt Complexes

The following chapter has been submitted for publication to *Organometallics*

I. Introduction

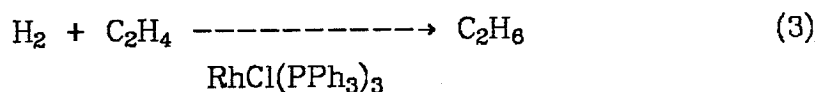
The concepts of oxidative addition



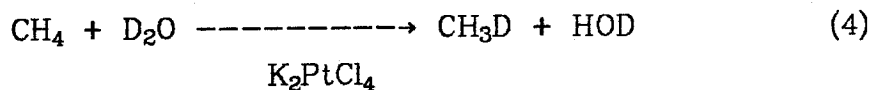
and reductive elimination



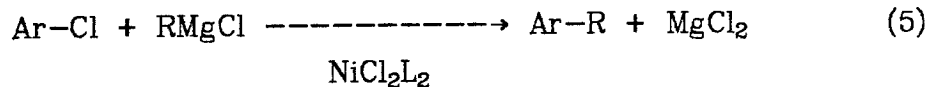
are prevalent in the literature on organometallic chemistry.¹ Thus, catalytic hydrogenation of alkenes often requires oxidative addition of H₂ to form the activated complex MH₂,² e.g.,



involves formation of Rh(H)₂(Cl)(PPh₃)₃. Similarly, an important step in the H-D exchange in alkanes³ is the oxidative addition of C-H bonds, e.g.,



may involve formation of Pt(H)(CH₃)(Cl)₄⁻. In addition, reductive coupling to form C-C bonds is an important step in the cross coupling reaction catalyzed by Ni(II) and Pd(II),⁴ e.g.,



involves Ni(Ar)(R)L₂ → NiL₂ + Ar-R.

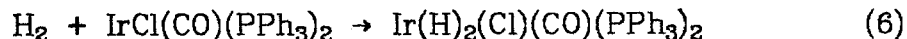
Because of the central role of oxidative addition/reductive elimination in organometallic chemistry, a number of recent experimental studies have been directed toward elucidating the details of such reactions.

However, a number of puzzles remain and there is yet no unified theoretical framework for understanding such processes for H-H, H-C, and C-C systems. The purpose of this paper is to add toward building this framework.

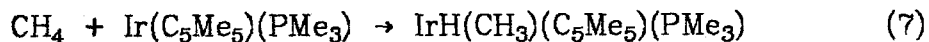
Current experimental evidence relating to these reactions is as follows.

A. *Experimental Evidence for Mechanism*

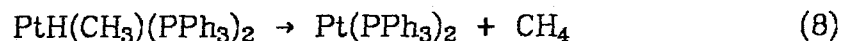
Mechanistic studies have been carried out on activation of H₂ by Ir(I) complexes,⁵



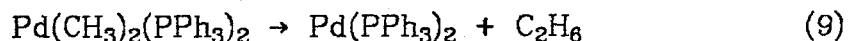
C-H activation by Ir(I)⁶ and Rh(I)⁷ complexes,



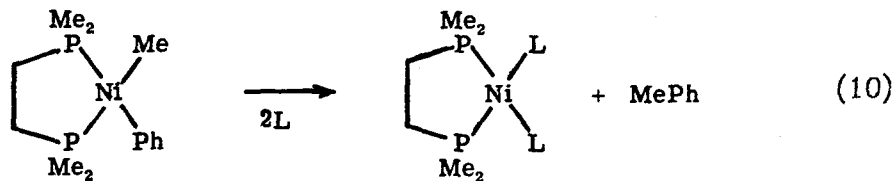
reductive coupling of C-H bonds from Pt(II)hydridomethyl complexes,⁸



and reductive coupling of C-C bonds from Pd(II)⁹



and Ni(II)¹⁰ complexes.



In all cases there is good evidence that these H-H, C-H, and C-C coupling or activation processes are concerted. Some of the evidence is as follows.

The activation of H₂ by Ir(I) complexes, (6), is believed to be concerted because (i) the oxidative addition of H₂ to Ir(I) complexes almost

always yields a *cis*-product,^{5,11} (ii) the kinetics of the addition reaction are first-order in both H₂ and the Ir(I) complex;^{5abd} and (iii) the entropy of activation $\Delta S^\ddagger \approx -23 \pm 3$ e.u. for oxidative addition of H₂ is very close to the entropy of reaction, $\Delta S \approx -28 \pm 3$ e.u. (which is dominated by the loss of the translational and rotational entropy of the H₂ molecule).^{5b}

Activation of C-H bonds by Ir(I) complexes, (7), has been observed by a number of different research groups.⁶ Janowics and Bergman^{6c} conducted crossover experiments and measured the relative rates of insertion in different types of C-H bonds. Their results appear to be most consistent with a concerted process.

The mechanism of reductive elimination from Pt(II) hydridoalkyls, (8), has been studied by two research groups.⁸ Abis, Sen, and Halpern^{8a} used isotope labeling experiments to follow the decomposition of various Pt(H)(Me)L₂ complexes and found that reductive elimination is intramolecular. Michelin *et al.*^{8b} studied the decomposition of *cis*-Pt(H)(CH₂CF₃)(PPh₃)₂ [which decomposes at a slower rate than the hydridomethyl Pt(II) complexes] and found that (i) the rate of decomposition is first-order in the reaction, and (ii) the reaction has low values for the entropy of activation ΔS^\ddagger (2-8 e.u.). These results are consistent with a concerted unimolecular reductive elimination.

The mechanism of reductive elimination from Pd(II) dimethyl complexes, (9), has been studied by Stille *et al.*^{9a-c} and by Ozawa *et al.*^{9d} The lack of crossover products in the decomposition of Pd(CH₃)₂L₂ and Pd(CD₃)₂L₂ and the unimolecular kinetics observed in these experiments are consistent with a concerted process. Note, however, that the corresponding Pt complex will *not* reductively eliminate ethane;



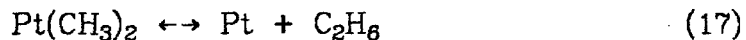
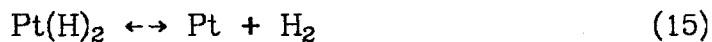
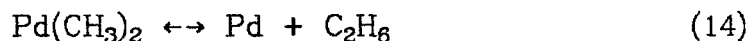
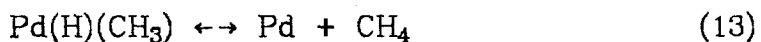
it can, in fact, be sublimed before it will decompose.¹²

B. Theoretical Strategy

Four issues we wish to address here are:

- (i) Are the processes concerted?
- (ii) What are the relative barriers for H-H, H-C, and C-C coupling (and activation)?
- (iii) How does the nature of the metal affect the reaction? [Why is Pt(II) so different from Pd(II)?]
- (iv) What relation should there be between the processes for metal complexes versus those for metal atoms?

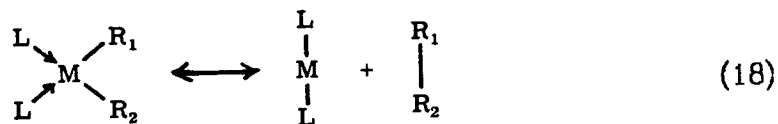
For reasons to be discussed below, we wanted to consider two related classes of systems where one class has exothermic reductive coupling for all three cases of $R_1, R_2 = H, CH_3$, and where the other class has exothermic oxidative addition for all three cases. Consequently, we examined the following reactions:



where the first three are exothermic (to the right) while the last three are endothermic. The Pd-H, Pd-CH₃, Pt-H, and Pt-CH₃ bonds in these sys-

terms should typify the M-H and M-C bonds of other organometallic complexes involving metals of comparable electronegativity and oxidation state.

From various previous studies,¹³ we concluded that the reactions



[where $\text{R}_1, \text{R}_2 = \text{H}, \text{CH}_3$ and $\text{M} = \text{Pt}(0), \text{Pd}(0)$] involve a change in the effective electronic configuration of M from an s^1d^9 configuration for $\text{M}(\text{R}_1)(\text{R}_2)\text{L}_2$ to a d^{10} configuration for ML_2 . Since the ground state of the Pd atom is d^{10} (with the lowest s^1d^9 state lying 22 kcal/mol higher),¹⁴ the Pd *atom* should be a fair model for facile reductive elimination from various low valent Group VIII transition metal complexes (18). On the other hand, the ground state of the Pt atom is s^1d^9 (with the d^{10} state lying 11 kcal/mol higher),¹⁴ favoring oxidative addition and making the Pt atom a good model for facile oxidative addition processes.

The theoretical results for reactions (12)-(17) are described in Section II, compared with experiment in Section III, and compared with other theoretical work in Section IV and Appendix A. Computational details are described in Section V.

II. Summary of Results

A. *Electronic Promotion Versus Charge Transfer*

A major conclusion from these studies is that *oxidative addition requires promotion of the metal from the d^{10} atomic configuration to the s^1d^9 configuration*. We find for $R = H, CH_3$, that the M-R bonds are covalent for both $M = Pd$ and Pt , with each bond involving one electron in an orbital on R and one electron in an sd hybrid orbital on the metal. The d^{10} configuration cannot make covalent bonds since all five d orbitals are doubly-occupied; however, the s^1d^9 configuration with two singly-occupied orbitals can mix these two orbitals to form two sd hybrids capable of forming covalent bonds to the two ligands. Thus *the metal atom is not oxidized* during the oxidative addition of H_2 , CH_4 , and C_2H_6 to Pd and Pt. Rather, the metal is promoted from the d^{10} state incapable of forming covalent bonds to the s^1d^9 state capable of forming two covalent bonds.

Generalized valence bond (GVB) orbitals for the complexes studied in this work are shown in Figures 1, 2, and 3, with the hybridization of each orbital indicated just above the lower boundary of each orbital plot (these populations of GVB orbitals are summarized in Table I). In each case the ligand GVB orbital has 0.80 ± 0.03 electrons on the ligand with 0.17 ± 0.02 electrons on the Pt atom. For the Pt complexes, the metal GVB orbital has 0.08 ± 0.01 electrons on the ligand, 0.62 ± 0.02 electrons in a Pt d orbital, and 0.30 ± 0.02 electrons in Pt 6s and 6p orbitals (94% s and 5% p). Thus the metal orbitals are sd^2 hybrids. In the Pd complexes there is more variety in the character of the GVB orbital describing the metal part of the metal-carbon bond pair, with 0.24 electrons on the CH_3 for $Pd(CH_3)_2$, but 0.12 for $Pd(H)(CH_3)$. In addition, the sd hybrid character varies [from $s^1d^{1.7}$ for PdH_2 to $s^1d^{1.3}$ for the Pd-H bond of $Pd(H)(CH_3)$ and

from $s^1d^{3.8}$ for the Pd-C bond of $PdH(CH_3)$ to $s^1d^{2.9}$ for $Pd(CH_3)_2$]. We do not believe that these variations are as significant as the general result that the GVB orbitals for both Pt and Pd use sd hybrid orbitals to form bonds to H and CH_3 groups. These sd hybrids are similar in all cases, with somewhat more d than s character. The carbon atoms in methyl groups bonded to the metal are tetrahedral (within 1°) and sp^3 hybridized (see Appendix B). From total Mulliken populations (see Table II), the Pt complexes on the average have 9.03 d electrons and 1.06 s electrons, while Pd complexes have 9.23 d electrons and 0.69 s electrons (a difference expected from the preference of Pd for d electrons).

The fact that Pd-H, Pd-C, Pt-H, and Pt-C bonds are covalent is consistent with the Pauling electronegativities: Pd(2.2) and Pt(2.2) versus H(2.1) and C(2.5).¹⁵ Crabtree *et al.*^{5f-i} have also suggested that the addition of H_2 to Ir(I) complexes is not oxidative based on observations that the oxidative addition of H_2 to cationic Ir(I) cyclooctadiene complexes is promoted by electron-withdrawing ligands and inhibited by electron donors^{5f} and that an upfield shift of the vinyl carbon resonance occurs in the ^{13}C NMR of $Ir(COD)_2^+$ (COD = 1,5-cyclooctadiene) on addition of H_2 .^{5g}

Summarizing, the oxidative addition of H_2 , CH_4 , and C_2H_6 to d^{10} metal centers should be thought of in terms of promoting an electron from a doubly-occupied d orbital to an unoccupied s orbital in order to accommodate the formation of two covalent bonds rather than the transfer of one electron to each ligand. For Pd and Pt this promotion corresponds to the electronic transition from d^{10} to s^1d^9 instead of ionizing two electrons from $d^{10} M(0)$ to form a $d^8 M(II)$.

B. Reaction Energetics and Bond Energies

1. Reaction Energetics

Before discussing the details of the reactions, we will examine the overall energetics (see Figures 4 and 5). For Pd, H-H, H-C, and C-C coupling is *exothermic* (with ΔH_{298}^{16} of -4.0, -17.2, -19.0 kcal/mol resulting from ΔE 's of -3.6, -20.1, and -16.0 kcal/mol, respectively), while for Pt these processes are *endothermic* (with ΔH_{298} of 33.2, 19.0, 15.5 kcal/mol resulting from ΔE 's of 33.6, 16.1, and 18.3 kcal/mol ΔE , respectively; see Table III). (For Pt these energies are for the lowest spin-allowed process, leading to d^{10} Pt atom.) These differences between Pd and Pt are easily understood on the basis of relative atomic excitation energies. Reductive coupling changes the metal from s^1d^9 to d^{10} , but for Pd the s^1d^9 state is 22 kcal/mol *higher* than d^{10} , while for Pt the s^1d^9 state is 11 kcal/mol *below* d^{10} . Thus, reductive coupling from Pd should be favored by 33 kcal/mol (theoretical value 32 kcal/mol) over comparable reductive coupling from Pt. Indeed, we find the differences [ΔH_{298} for (2)] to be 37.2 kcal/mol for the dihydrides, 36.2 kcal/mol for hydridomethyl complexes, and 34.3 kcal/mol for the dimethyl complexes. Thus the GVB model of bonding allows one to use atomic excitation energies and the relative energetics of reductive coupling for one metal complex to estimate the energetics for other metals.

2. Average Bond Energies

For semi-quantitative comparisons of various systems, it is often useful to have an idea of average bond energies for various types of bonds. There are two simple ways of doing this:

Method 1: Adiabatic Bond Energies

The adiabatic bond energy is defined as

$$\bar{D}_A(M-R) = \frac{1}{2} [\Delta H_{298}(MR_2 \rightarrow M + R_2) + \Delta H_{298}(R_2 \rightarrow 2R\cdot)].$$

The calculated reaction enthalpy for the reductive coupling is added to the R_2 bond energy¹⁷ for a free R_2 , and then the total is divided in half to give the adiabatic bond energy. This leads to $\bar{D}_A(Pt-H) = 69$ kcal/mol, $\bar{D}_A(Pt-C) = 53$ kcal/mol, $\bar{D}_A(Pd-H) = 50$ kcal/mol, and $\bar{D}_A(Pd-C) = 36$ kcal/mol. As a check on the consistency of average bond energies, we can use the bond energies calculated from the ΔH_{298} of reactions (12), (14), (15), and (17) to predict ΔH_{298} for reactions (13) and (16). This yields predicted values of ΔH_{298} of -19 kcal/mol for reaction (13) and 17 kcal/mol for reaction (16), which are both 2 kcal/mol lower than the calculated values of -17.2 and 19.0 kcal/mol. Overall, the Pd-R bonds are 19 and 17 kcal/mol weaker than the corresponding Pt-R bonds, which just represents the preference of Pd for d^{10} over s^1d^9 .

Method 2: Intrinsic Bond Energies

In order to eliminate the effect of s^1d^9 - d^{10} state splittings on the average bond energies, we define an intrinsic bond energy as

$$\bar{D}_I(M-R) = \frac{1}{2} [\Delta H_{298}(MR_2 \rightarrow M + R_2) + \Delta H_{298}(R_2 \rightarrow 2R\cdot) + \Delta E(d^{10} \rightarrow s^1d^9)].$$

where the final state of the metal atom is taken as the s^1d^9 state. This is the intrinsic bond strength where the electronic state of the atom is not allowed to relax to a d^{10} state. In this case, we obtain very similar bond energies for Pd and Pt, with $\bar{D}_I(Pd-H) = 60$ kcal/mol and $\bar{D}_I(Pt-H) = 62$ kcal/mol, while $\bar{D}_I(Pd-CH_3) = 45$ kcal/mol, and $\bar{D}_I(Pt-CH_3) = 47$ kcal/mol (see Table IV). Thus, these intrinsic energies plus atomic excitation energies should be most useful in using results for one metal to predict

results for another.

3. Energetics on Metal Surfaces

For metal surfaces, one might expect that metal-metal bonding would tend to keep the surface atoms for the Ni triad in s^1d^9 states. If so then the \bar{D}_1 should provide a reasonable estimate for the bond energy at metal surfaces.¹⁸ (Band calculations for Pd and Pt have been interpreted in terms of an average $s^{0.4}d^{9.6}$ configuration,¹⁹ somewhat more d occupation than in our complexes.) The predicted results for



are

$$\Delta H_{298} = -15 \text{ kcal/mol (Pd) and } -20 \text{ kcal/mol (Pt) for H}_2$$

$$\Delta H_{298} = -4 \text{ kcal/mol (Pd) and } -8 \text{ kcal/mol (Pt) for H-CH}_3$$

$$\Delta H_{298} = -10 \text{ kcal/mol (Pd) and } -14 \text{ kcal/mol (Pt) for H-C}_2\text{H}_5$$

and

$$\Delta H_{298} = 0 \text{ kcal/mol (Pd) and } -5 \text{ kcal/mol (Pt) for CH}_3\text{-CH}_3.$$

The experimental heats of adsorption for H_2 on Pt and Pd surfaces are 20.8 kcal/mol,²⁰ on Pd(111), 24.4 kcal/mol, on Pd(110),²⁰ 9.5 kcal/mol, on Pt(111),²¹ and 12 kcal/mol on Pt[9(111) \times (111)].²¹ Thus our one-center Pd numbers predict surface Pd-H bonds about 3 kcal/mol weaker than experiment, whereas our numbers for Pt indicate surface Pt-H bonds about 5 kcal/mol stronger than observed.

Using the experimental results on H_2 to calibrate the predictions for the other reactions leads to

$\Delta H = -10$ kcal/mol (Pd) and $+1$ kcal/mol (Pt) for $H-CH_3$

$\Delta H = -16$ kcal/mol (Pd) and -6 kcal/mol (Pt) for $H-C_2H_5$

$\Delta H = -6$ kcal/mol (Pd) and $+4$ kcal/mol (Pt) for CH_3-CH_3

As experimental data become available for such surface reactions, it will be interesting to see how energetics can be extrapolated between homogeneous and heterogeneous systems.

4. Barriers for Reductive Coupling

For the $Pd(R_1)(R_2)$ complexes, it is exothermic to reductively couple H-H, H-C, or C-C bonds; however, the barriers for these processes depend dramatically upon the nature of the ligands (see Figure 6):

$$\Delta E_{H-H}^\ddagger = 1.6 \text{ kcal/mol}, \quad \Delta H_{298}^\ddagger_{H-H} = 0.4 \text{ kcal/mol}$$

$$\Delta E_{H-C}^\ddagger = 10.4 \text{ kcal/mol}, \quad \Delta H_{298}^\ddagger_{H-C} = 9.5 \text{ kcal/mol}$$

$$\Delta E_{C-C}^\ddagger = 22.6 \text{ kcal/mol}, \quad \Delta H_{298}^\ddagger_{C-C} = 23.6 \text{ kcal/mol}.$$

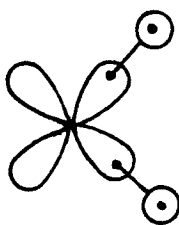
Similarly, for the corresponding Pt complexes (see Figure 7), the barriers for H-C and C-C coupling are far larger than the endothermicity

$$E_{H-C}^\ddagger = 29.0 \text{ kcal/mol}, \quad H_{298}^\ddagger_{H-C} = 28.1 \text{ kcal/mol}$$

$$E_{C-C}^\ddagger = 53.5 \text{ kcal/mol}, \quad H_{298}^\ddagger_{C-C} = 54.5 \text{ kcal/mol}.$$

Such dramatically different barriers would explain why $Pt(H)(CH_3)(PH_3)_2$ will reductively couple H-C bonds, whereas $Pt(CH_3)_2(PH_3)_2$ will *not* reductively couple C-C bonds. However, the question now is *why* the dramatic differences in barriers?

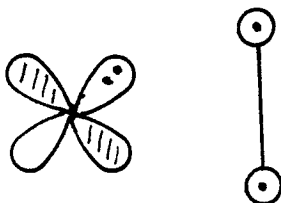
As discussed in more detail in Section II.6, the reductive coupling process starts with a configuration having two covalent bonds involving sd hybrids on the metal,



(19)

s^1d^9 Resonance Configuration

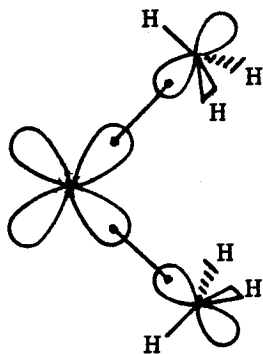
and converts this to a wavefunction with one covalent bond between the ligands and a doubly-occupied d orbital on the metal,



(20)

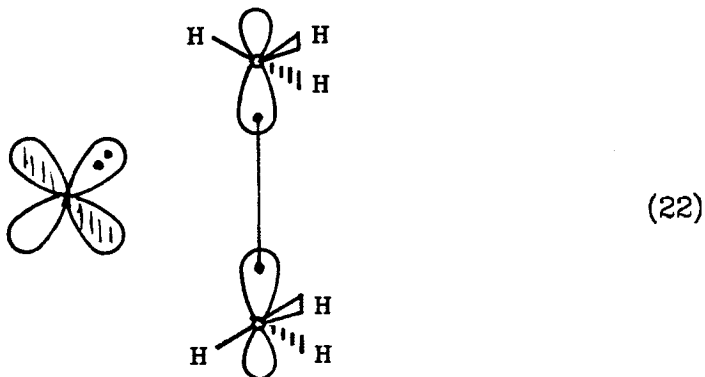
d^{10} Resonance Configuration

At the transition state geometry, both configurations must come into the wavefunction, wherein lies the difficulty. A hydrogen s orbital at the transition state is equally suited for either bonding configuration (19) or (20); however, for methyl the bonding orbital is an sp^3 hybrid that can be directed *either* for making an M-C bond,



(21)

or for making a C-C bond



but *not* both. This is illustrated in Figures 8 and 9, which show the various orbitals for (12), (13), and (14) at a geometry near the saddle point. The CH_3 radical orients itself to a position intermediate between the geometries appropriate for (21) and for (22), leading to too weak a bond for either. The consequence of these effects is that each methyl group leads to a doubling of the barrier.

Clearly this methyl orientation effect can account for the observed differences in the efficacy of H-C versus C-C coupling in Pt phosphine complexes. These results are consistent with the facile H-C coupling on Pt and C-C coupling on Pd, with the apparent lack of stability of the *cis*- $\text{Pd}(\text{H})(\text{CH}_3)(\text{PH}_3)_2$ complex, and with the difficulty of C-C coupling from Pt dimethyl complexes.

5. Geometries

The bond distances for Pd-CH_3 and Pt-CH_3 bonds are nearly identical [$1.96 \pm 0.01 \text{ \AA}$] for all complexes. For M-H bonds there is more variation with $\text{Pd-H} = 1.51 \pm 0.01 \text{ \AA}$ and $\text{Pt-H} = 1.48 \pm 0.01 \text{ \AA}$. On the other hand, the bond angles for the various $\text{M}(\text{H})_2$, $\text{M}(\text{H})(\text{CH}_3)$, and $\text{M}(\text{CH}_3)_2$ complexes vary considerably, being 73° , 80° , and 92° for Pd and 82° , 89° , and 98° for Pt.

The ideal bond angle between two bonds formed with symmetric linear combinations of a Pt s and a Pt d orbital is 90° . Thus, if the repulsive steric interactions were solely responsible for the trend of bond angle with methyl substitution, one would expect to find R-M-R angles greater than 90° , but most of the equilibrium geometries have R-M-R angles less than 90° . Of course the actual hybridization is not exactly sd, and the calculated angles between the lobes of the metal-like GVB orbitals vary between 86° and 100° [86° for PtH_2 , 91° for $\text{Pt(H)(CH}_3\text{)}$, and 100° for $\text{Pt(CH}_3\text{)}_2$, leading to the an average of 92°] for Pt complexes and the average for Pd complexes is $88^\circ \pm 1^\circ$. The observed angles between the metal-like GVB orbitals for Pt track closely with the actual bond angle (80, 91, and 100 versus 82, 89, and 98, respectively); however, this does not constitute an explanation since we have not provided an *a priori* criterion for predicting the hybridization leading to these angles (other than being $s^{1.0}d^{1.0}$ to correspond to the s^1d^9 state). Thus, compared with the 90° expected from the s^1d^9 configuration, there must be attractive interactions between the ligands bound to the metal atom. This attractive interaction can be explained by noting that the d^{10} resonance structure has an R-R bonding interaction. The more important the d^{10} resonance structure, the more attractive the interaction between ligands and the smaller the R-M-R angle. Since the d^{10} resonance structure is more important in PdR_2 than in PtR_2 , there will be greater bonding character between the R groups in PdR_2 , providing a rationalization for the R-Pd-R bond angles being 10° smaller than the corresponding bond angles in the PtR_2 complexes (see Figures 4 and 5).

6. Changes Along Reaction Path

As discussed above, there are two important resonance structures in the $M(R_1)(R_2)$ complexes responsible for determining the relative amounts of s and d character. The dominant resonance structure for PdR_2 and PtR_2 has the metal atom in an s^1d^9 configuration, shown schematically in (19) and denoted as the s^1d^9 resonance structure. Here the singly-occupied s and d orbitals rehybridize to form sd hybrid orbitals that spin-pair (or form bonds) to the singly-occupied orbitals of the R group. The second resonance structure, which dominates the wavefunction at the dissociated limit, has the metal atom in a d^{10} configuration and an R-R bond, as shown schematically in (20). This is referred to as the d^{10} resonance structure. As oxidative addition proceeds, the dominant resonance structure changes from the d^{10} structure to the s^1d^9 structure. Since Pd prefers d^{10} while Pt prefers s^1d^9 , PdR_2 should have more of the d^{10} resonance structure than PtR_2 . This is consistent with the observation that PdR_2 complexes have larger d populations than PtR_2 complexes.

The Mulliken populations as a function of reaction coordinate for reaction (12) (see Table V) show that at the dissociated limit the Pd atom is in a d^{10} state, and as the hydrogen molecule approaches, the Pd atom mixes in s^1d^9 character. Finally, when two Pd-H bonds have formed, the Pd atom has 75% s^1d^9 character (defined by the occupation of the Pd s orbital).

The spherically symmetric H_{1s} orbital allows it to form bonds in more than one direction at a time. This multi-centered bonding increases the H-H bonding character of the d^{10} resonance structure, causes the H atoms to have an attractive interaction in the dihydrides, and leads to

smaller H-M-H bond angles.

The sp^3 hybrid orbital of the CH_3 group is more directional than the H_{1s} orbital. The shape of this orbital makes it difficult for this orbital to bond in more than one direction at a time. Consequently, there will be less bonding character in the d^{10} resonance structure of the hydridomethyl complexes than in the dihydrides. This will cause the hydridomethyl complexes to have larger bond angles than the dihydrides.

Since the sp^3 orbitals of the methyl groups are directed at the metal, they have trouble forming the C-C bond in the d^{10} structure. Consequently, the dimethyl complexes have the least amount of bonding character in the d^{10} resonance structure. Therefore, the dimethyl complexes should have the largest bond angles.

The increased ligand-ligand bonding in the d^{10} resonance structure should stabilize it relative to the s^1d^9 resonance structure. This will cause metal d populations to be larger for dihydride complexes and smaller for the dimethyl complexes, which is consistent with the Mulliken populations in Table II.

The potential curves along the reaction paths are shown in Figures 6 and 7. In each of the potential curves the R_1-M-R_2 bond angle ($\theta_{R_1R_2}$) was fixed, and all other geometric parameters were fully optimized (see Section V). In this manner, we were able to obtain the energy as a function of $\theta_{R_1R_2}$ from the MR_2 complex to the dissociated limit ($\theta_{R_1R_2} = 0^\circ$).

The potential curves for reactions (12)-(14), (16), and (17) can be partitioned into three regions:

1. The MR_2 complex region, where the metal atom has s^1d^9 character and each R group forms a covalent bond to the metal.

2. The transition state region, where the M-R bonds are breaking and the R-R bond is forming (or vice versa), with a strong mixture of both the d^{10} and s^1d^9 resonance structures.
3. The dissociated limit, where the R-R bond is fully formed and the metal is in the d^{10} state.

In region 1 the M-R bond lengths change by less than 0.02 Å as the $\Theta_{R_1R_2}$ is varied, indicating that the M-R bond is still intact. As the complex enters region 2, the M-R bonds begin to stretch and the methyl groups in the hydridomethyl and dimethyl complexes rotate so that their sp^3 orbitals are directed more toward the other R group.

At the transition state, the ligand-ligand bond distances are generally closer to the bound complex geometry than to the dissociated limit. Pd complexes have smaller distortions (they are more reactant-like) than the corresponding Pt complexes (see Figures 4 and 5) at the transition state, as would be expected from the Hammond Postulate. The dimethyl complexes have the largest distortions. $Pt + H_2 \rightarrow PtH_2$ differs from the other reactions studied here in that there is no barrier to oxidative addition (it is quite exothermic, 33.6 kcal/mol).

Past the transition state there exists a second minimum for the Pd + H_2 , Pd + CH_4 , and Pt + CH_4 cases. In this bound complex, the H-H or C-H bonds are intact and behave as Lewis bases, while the d^{10} configuration of the transition metal serves as a Lewis acid (empty valence s orbital). The geometries for the Lewis acid/Lewis base complex are shown in Figure 10. These geometries were not separately optimized but were interpolated from the calculations along the reaction path. [Notice the lack of symmetry in the $M(CH_4)$ complexes.] As a result, the geometry obtained for each complex is not particularly accurate [the internal coordinates of H_2

and CH₄ in these complexes should be accurate, while the error in metal-ligand distance (± 0.2 Å) and in orientation ($\pm 10^\circ$) will be larger]. However, Lewis acid/Lewis base complexes in these systems are clearly stable with respect to the dissociated limit. There seems to be a small increase in the H-H bond length (0.07 Å) and very little distortion in the C-H bond lengths of methane (two CH bonds of methane interact with the metal atom in this region). Our reaction path restricted the orientation of the methyl group in such a way that at most two C-H bonds could complex to the metal atom. Therefore, the Lewis acid/Lewis base complexes, with three C-H bonds complexed to the metal atom (probably the most stable), were not examined.

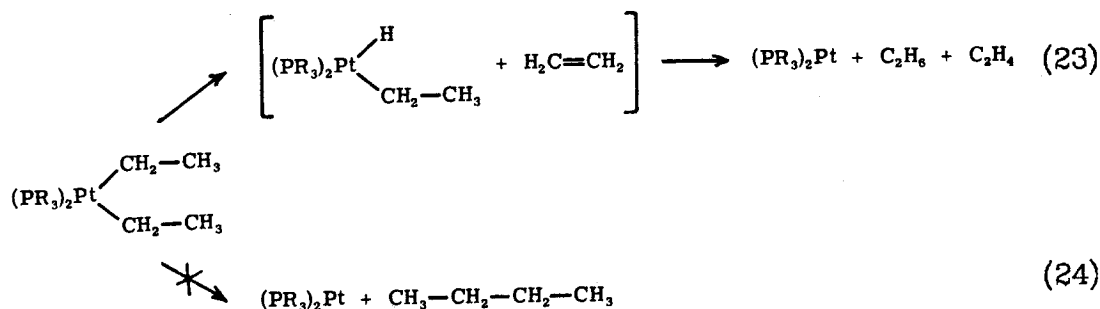
Previous calculations found a similar bound complex for PdH₂²² and described it as a van der Waals complex. Since our wavefunction does not include the electronic configurations involved in the dynamic polarizations responsible for van der Waals forces (nor the f functions needed on the Pt for a proper description of such effects), our results cannot be explained in terms of a van der Waals complex.²³ Rather, they should be thought of as weak Lewis acid/Lewis base complexes. Similar η^2 bonding of H₂ to a transition metal has been observed experimentally in M(CO)₃(PR₃)₂H₂ (M = Mo, W; R = Cy, i-Pr) complexes studied by Kubas *et al.*^{24a} and theoretically by Hay.^{24b}

The interactions responsible for these Lewis base/Lewis acid complexes of CH₄ to metal atoms are probably identical to those involved in "agostic"^{25a} interactions of C-H bonds and transition metals observed experimentally^{25a} and theoretically^{25b} in several complexes. This type of interaction has thus far only been observed for C-H bonds of ligands that are also covalently bound to the complex. The very small binding ener-

gies found in our calculations [5 kcal/mol for $\text{Pd}(\text{H}_2)$, 2 kcal/mol for $\text{Pd}(\text{CH}_4)$, and 4 kcal/mol for $\text{Pt}(\text{CH}_4)$] are insufficient to balance the entropic contribution to the free energy of binding at room temperature (~ 10 kcal/mol), indicating that such bonds to alkyl groups that are not already part of the complex will in gas phase only be observed at low temperatures.

III. Comparison With Experiment

The results presented in the previous section explain many of the experimentally observed trends. Halpern *et al.*^{8a} and Michelin *et al.*^{8b} observed intramolecular reductive coupling from various hydridoalkyl-bisphosphine Pt(II) complexes. However, reductive coupling from Pt(II) dialkyls to form C-C bonds has never been reported, even though this reaction is thought to be thermodynamically favored.²⁶ Rather, the Pt(II) dialkyls prefer β -hydride elimination,²⁷



despite the fact that (24) is favored thermodynamically (by $\Delta H_{300} = -22.5$ kcal/mol and $\Delta G_{300} = -11.0$ kcal/mol).²⁸ These observations are consistent with our findings that C-H reductive coupling leads to a barrier half that for CC reductive coupling. This trend should be applicable to concerted addition/elimination reactions for other Group VIII metals because it depends primarily on the relative shapes of H 1s and CH_3 sp^3 orbitals.

Unlike their Pt analogs, Pd(II) dimethyl complexes do reductively eliminate ethane, a result we attribute to the strong preference (by 34 kcal/mol relative to Pt) of Pd for the d^{10} configuration, which leads to a greatly reduced barrier [we estimate 10 kcal/mol for $\text{Pd}(\text{CH}_3)_2(\text{PH}_3)_2$ compared with 40 kcal/mol for $\text{Pt}(\text{CH}_3)_2(\text{PH}_3)_2$].²⁹ This is in agreement with observed reductive elimination of ethane from $\text{Pd}(\text{CH}_3)_2\text{L}_2$ complexes^{9a,d} (where $\text{L} = \text{PPh}_3$, PPh_2CH_3 ; $\text{L}_2 = \text{PPh}_2\text{PCH}_2\text{CH}_2\text{PPh}_2$) and the

fact that hydrogen will not oxidatively add to a Pd bisphosphine complex but does add to the corresponding Pt complex.³⁰

Oxidative addition of H₂ to square planar Ir(I) complexes is the most thoroughly studied system experimentally, and it is believed to involve a concerted mechanism.⁵ In contrast to the results presented here for the addition of H₂ to Pt and Pd and earlier work for H₂ addition to Pt(PH₃)₂, the Ir(I) complexes have a relatively high barrier to oxidative addition (10-12 kcal/mol for Vaska's complex^{5a,b,d}) and reductive elimination (25 kcal/mol). This difference probably arises from the difference in electronic configurations, with Pt and Pd having a spherically symmetric d¹⁰ shell of electrons on the metal atom, while Ir(I) leads to square planar four-coordinate complexes. Thus Pt(PH₃)₂,¹³ has a P-Pt-P angle of 180°, being determined by steric interactions between phosphines. Promoting the Pt(PH₃)₂ complex to a triplet state leads to a P-Pt-P bond angle of 100°, where the phosphine lone pairs maximize their overlap with the singly-occupied d_{yz} orbital of the triplet state.¹³ On the other hand, Ir(I) has a strong preference for square planar geometries. Addition of H₂ to such complexes should lead to a distortion of ligands toward the six-coordinate Ir(III) product.^{5b} Here a significant distortion away from square planar is required at the transition state in order to allow the d² → s¹d¹ excitation required for formation of the new Ir-ligand covalent bonds. Thus the higher barrier in Ir(I) is attributed to the lack of a symmetric d¹⁰ shell and the concomitant strong preference for square planar geometries. Indeed, Vaska and Werneke^{5b} proposed a similar effect, the "reorganization or rehybridization energy," whose magnitude was deduced from the trends observed in ΔH[‡] and ΔH for oxidative addition of H₂ to Ir(I) complexes. They equated this reorganization energy to the ΔH[‡]

for reductive elimination of H_2 . We find low barriers for concerted reactions of H_2 with Pd, Pt(1S), and Pt(PH_3) $_2$; therefore, the reorganization energy must be very small (~ 2 kcal/mol) for these d^{10} systems.

It has generally been believed that oxidative addition (being oxidative) should be promoted by electron-rich metals.^{6c} However, C-H activation of C-H bonds has been observed to occur for both electron-rich^{6a-d} and electrophilic Ir systems.^{6e} Since the electronegativity¹⁴ of Ir(2.2) is the same as for Pt(2.2) and Pd(2.2), we expect it to form covalent bonds to H and CH_3 so that the electron density on the metal should have little effect on the energetics for oxidative addition (as observed).

In every case where stable hydridoalkyl complexes have been formed by oxidative addition of M to sp^3 C-H bonds, a photochemically generated Cp^*ML ($L = CO$ or PMe_3) ($M = Ir^{6a-d}$ or Rh^7) ($Cp^* = \eta^5-C_5Me_5$) complex has been involved. The Cp^* ligand can easily occupy three coordination sites of the octahedral complex for Ir(III) or Rh(III). However, Cp^{*-} cannot occupy three coordination sites of a square planar complex. Thus, the Cp^*ML complexes are distorted significantly away from the square planar preferred by Ir(I) and Rh(I), and hence have smaller reorganization energy for oxidative addition than does Vaska's complex [they are much closer to the octahedral geometry favored by Ir(III) and Rh(III) complexes].³¹⁻³³ Therefore, these complexes will have lower activation barriers and greater driving forces favorable for oxidative addition. Constraining the geometry of the ligands appears to be a more important effect than the electron richness of the metal center. Similar analyses have also been given by Saillard and Hoffmann,³¹ Sevin,³² and Dedieu and Strich.³³

We find that oxidative addition of H_2 , CH_4 , and C_2H_6 to the Pd atom is

uphill energetically. These results suggest that the Pd atom is unreactive with respect to H_2 , CH_4 , and C_2H_6 . This is consistent with the results of Klabunde and Tanaka^{34c} who found no reaction of Pd codeposited with CH_4 at 10°K. This lack of reactivity of Pd at low temperatures is due to the unreactive nature of the d^{10} state of Pd and the large excitation energy (21.9 kcal/mol) needed to promote the Pd atom to the s^1d^9 configuration that can make two covalent bonds.

In fact, no transition metal in its ground state has been found to be reactive with CH_4 at low temperatures.³⁴ This can be easily explained despite the diverse nature of transition metal atoms. Every transition metal except Pd has either a singly- or doubly-occupied valence s orbital in its ground state. In reactions (12), (13), and (16), the empty s orbital gave rise to attractive Lewis acid/Lewis base interactions at long M-R distances, resulting in an decreased barrier for oxidative addition. For a metal where the s orbital is occupied, this orbital must become orthogonal to the incoming R-R bond, leading to a repulsive interaction at long M-R₂ distances. Thus, one would expect every transition metal in its ground state to have an activation barrier to oxidative addition.

For excited states of transition metal atoms, one can have states in which the s orbital is unoccupied and for which oxidative addition is exothermic. For example, we find that $\text{Pt}(^1\text{S}) + \text{H}_2 \rightarrow \text{PtH}_2(^1\text{A}_1)$ leads to no barrier. These predictions are consistent with experiments³⁴ that find photoexcited metal atoms reactive with methane at low temperatures. [Extended Hückel calculations of Sevin and Chaquin³⁵ lead to similar results.]

IV. Comparison With Other Theoretical Work

Several previous theoretical studies^{22b,23,36,37} have addressed various issues relevant to the oxidative addition/reductive elimination of H₂, CH₄, and C₂H₆ to transition metal complexes, although most have not examined the full reaction surfaces. Using fixed bond distances, Tatsumi *et al.*^{36a} calculated activation energies at the extended Hückel level for reductive elimination of C₂H₆ from Pd(CH₃)₂(PH₃)₂ and H₂ from (PdH₄)⁻⁴ models. They found higher barriers for reductive couplings for C-C bonds (39.1 kcal/mol) than for H-H bonds (4.6 kcal/mol) because of the "weakening necessitated by the rocking motion"^{36a} of the methyl group.

Balacz *et al.*^{36b} carried out muffin-tin X α calculations at assumed geometries for various complexes and suggested, on the basis of the shapes of the molecular orbitals, that three-center bonding might be more important in the reductive elimination of H₂ from H₂PtL₂ than for CH₄ from H(CH₃)PtL₂ or for C₂H₆ from (CH₃)₂PtL₂. (They did not calculate barriers or geometries.)

Previous theoretical studies^{22,23} of Pd(H)₂ did not find the local minimum corresponding to the Pd-H bonded complex. However, these calculations did *not* include relativistic effects and consequently the s¹d⁹ (³D) state [important in the Pd(H)₂ complex] is 15 kcal/mol too high³⁸ relative to the d¹⁰ state. Since our calculated barrier for reductive coupling is only 1.5 kcal/mol, it is not surprising that nonrelativistic calculations of this minimum do not find a Pd-H bonded complex.

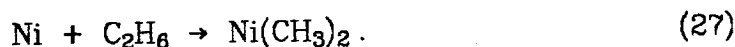
Obara *et al.*^{16a} have recently reported *ab initio* calculations on oxidative addition of H₂ and CH₄ to Pt(PH₃)₂. Their transition state geometry for H₂ addition is in reasonable agreement with our previously published results on the same system.¹³ The transition state geometry for CH₄

addition calculated by Obara *et al.*^{16a} (C-Pt-H angle = 36°, Pt-CH₃ distance = 2.27 Å, and Pt-H distance = 1.59 Å) is remarkably close to ours (C-Pt-H angle = 42°, Pt-CH₃ distance = 2.12 Å, and Pt-H distance = 1.57 Å), considering the lack of phosphines in our model. Their energetics, however, are difficult to compare with ours since the Pt effective core potential used by Obara *et al.*³⁹ is known to give stronger Pt-H bonds that are far too strong.⁴⁰ [We used the Hay⁴¹ effective core potential which gives excellent bond energies and excitation energies.] The similarity of the transition states indicates that the PH₃ ligands do not significantly affect the reaction path for reductive coupling of C-H bonds. We would expect PH₃ ligands to lower the barrier for reductive elimination, since phosphines stabilize the d¹⁰ configuration relative to s¹d⁹ and increase the driving force for reductive elimination from Pt(H)₂(PH₃)₂,¹³ Pt(H)(CH₃)(PH₃)₂,²⁹ Pt(CH₃)₂(PH₃)₂,²⁹ and Pd(CH₃)₂(PH₃)₂.²⁹

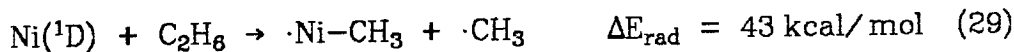
No other *ab initio* theoretical studies on oxidative addition/reductive elimination to Pd and Pt atoms have been reported; however, similar studies have been reported for oxidative addition of H₂, CH₄, and C₂H₆ to the lowest singlet state of the Ni atom.^{22b,37a,b} These results on Ni differ considerably from ours on Pd and Pt. For example, Siegbahn *et al.*^{22b,37a,b} find oxidative addition barriers of 4.2 kcal/mol for H₂, 54.1 kcal/mol for CH₄, and 42.3 kcal/mol for addition to the CC bond of C₂H₆. In addition, they report an unusually small equilibrium bond angle of 57° for NiH₂. There are significant differences in the properties of Ni versus Pd and Pt, even though they are in the same column. For example, Ni is much more electropositive than Pd or Pt (Pauling electronegativities¹⁵ of 1.8 versus 2.2 and 2.2). In addition, the ground state of Ni has nearly degenerate s²d⁸ (³F) and s¹d⁹ (³D) triplet states, with the d¹⁰ (¹S) state 40 kcal/mol

higher.¹⁴ For Ni the lowest singlet state is s^1d^9 (1D) at 7.7 kcal/mol.¹⁴ On the other hand, Pd has a d^{10} (1S) ground state with the s^1d^9 (3D) triplet at 22 kcal/mol, while the lowest singlet for Pt is also d^{10} (1S) with s^1d^9 (3D) 11 kcal/mol lower.¹⁴ Consequently, we include in Appendix A some calculations performed on the Ni + H₂ system for comparison purposes.

Siegbahn and co-workers^{22b,37b} calculated potential surfaces at the contracted CI level for the reactions



They find, in contrast to our results, higher barriers for C-H activation than for C-C activation. Since this trend parallels the trend in C-H versus C-C bond energies, it is possible that Siegbahn's calculations are modelling *nonconcerted* additions of Ni to CH₄ and C₂H₆.^{37b} To estimate the ΔE 's for the formation of the radical intermediates (ΔE_{rad}), we used Siegbahn's ΔE for Ni + H₂ → NiH₂^{37a} (-9.6 kcal/mol) and Ni + C₂H₆ → Ni(CH₃)₂^{37b} (5.3 kcal/mol) to estimate average Ni-H ($\bar{D}_1 = 56$ kcal/mol) and Ni-CH₃ bond energies ($\bar{D}_1 = 45$ kcal/mol).⁴²



These ΔE_{rad} 's are very close to the ΔE^\ddagger 's for C-H activation (54 kcal/mol) and C-C activation (42 kcal/mol), as calculated by Siegbahn *et al.*,^{37b} suggesting that their calculations are not modelling the concerted processes. On the other hand, for our studies on Pd and Pt, a similar analysis leads to energies of formation for radical intermediates far higher than our calculated barriers for the concerted processes. The sole

exception is for C-C activation of Pt where the ΔH_{rad} is 43 kcal/mol, which is close to the ΔH^\ddagger for oxidative addition of 39 kcal/mol. This suggests that radical processes are competitive with concerted processes for reactions (17), (26), and (27).

For the organometallic systems being modeled in this paper, the metal atoms will generally have other ligands (e.g., phosphines) on them. We have shown¹³ that the effect of phosphines is to stabilize the d^{10} versus s^1d^9 states in $\text{Pt}(\text{PH}_3)_2$ and expect the same effect for $\text{Pd}(\text{PH}_3)_2$ and $\text{Ni}(\text{PH}_3)_2$. The lowest *singlet* states of Pd and Pt are d^{10} , like the $\text{M}(\text{PR}_3)_2$ complexes that we are modelling, whereas the lowest singlet state of Ni is s^1d^9 . Thus, the calculations for oxidative coupling of Pd and Pt atoms are more relevant for organometallic chemistry than similar calculations^{37a,b} on Ni. Since the lowest singlet state of Ni differs so much from the lowest singlet state of Pd, Pt, and $\text{M}(\text{PR}_3)_2$ ($\text{M} = \text{Ni}, \text{Pd}, \text{Pt}$), it is not surprising that Siegbahn's results are different from ours and run counter to the observed experimental trends.

V. Computational Details

A. Potentials and Basis Sets

We used *ab initio* effective core potentials (ECP) to represent the core electrons of Ni, Pd, and Pt. For Ni we used the ECP of Melius *et al.*,⁴³ with the five-gaussian d basis of Rappé *et al.*,⁴⁴ and the sp basis associated with the SHC potential of Rappé.⁴⁵ The relativistic effective core potentials (RECP) and basis of Hay⁴¹ were used on Pd and Pt with a valence double zeta basis. The Dunning⁴⁶ double zeta contraction of the Huzinaga (9s5p) gaussian basis was used on carbon. The active hydrogens bound directly to metal atoms were described by a triple zeta contraction of the Huzinaga six-gaussian basis.⁴⁷ The nonactive methyl hydrogen atoms were described by a double zeta contraction of the Huzinaga four-gaussian hydrogen basis scaled by a factor of 1.2.^{46,47} For highly accurate bond energies and geometries, f functions should be included on the metal center, d functions on the C atoms, and p functions on the H atoms. However, the present basis is expected to be adequate for extracting the important issues about these various reactions.

B. Configuration Interaction Calculations

For PdH₂ and PtH₂ there are 12 valence electrons with four electrons involved in M-H bonds and eight involved in four pairs of metal d orbitals. As the H₂ molecule is eliminated, the four bonding electrons change dramatically, leading to two electrons describing H-H bonding and two describing a doubly-occupied d orbital on the metal, while the other eight electrons change little. [Note that the spin-allowed product M(H)₂ → M + H₂ involves a d¹⁰ singlet state for both Pd and Pt.] Thus, to provide a balanced description of this system, we described each of the four fairly constant pairs of electrons in terms of a standard (one orbital

per electron) GVB description. This is denoted as GVB(1/2) for each pair and GVB-PP(4/8) to indicate four pairs of electrons, each with two GVB orbitals for a total of eight. The PP (for perfect-pairing) indicates that the spin coupling is that of a simple valence bond wavefunction with each of these four pairs singlet-spin paired. Expanded as a configuration interaction (CI) wavefunction in terms of natural orbitals, the GVB-PP(4/8) wavefunction leads to $2^4 = 16$ configurations. Instead, we allowed the two electrons of each pair to recouple in all three possible ways using two orbitals, leading to a total of $3^4 = 81$ configurations, a calculation referred to as GVB-RCI(4/8). This GVB-RCI level of wavefunction allows the spin-coupling terms often important in transition metal systems and allows the interpair correlation so important for doubly-occupied d orbitals.

The other four electrons have very different requirements for $\text{Pd}(\text{H}_2)$ versus $\text{Pd} + \text{H}_2$. Thus, for $\text{Pd}(\text{H})_2$, a standard GVB wavefunction leads to two localized orbitals for describing each Pd-H bond pair (as shown in Figure 1). In terms of symmetry orbitals, this would lead to two a_1 and two b_2 orbitals. On the other hand, for separated H_2 and Pd, the standard GVB(2/4) description has two localized orbitals on the H_2 (leading to one a_1 and one b_2) and a correlated d_{yz} orbital (leading to *two* b_2 orbitals). In order to provide an unbiased description of these reactions all along the reaction path, we used a wavefunction with three a_1 and three b_2 orbitals for the four bonding electrons. Allowing all possible occupations of the four electrons among these six orbitals leads to a wavefunction with 48 configurations and is referred to as GVB-CI(2/6). For all points along the reaction path we combined the GVB-RCI(4/8) and GVB-CI(2/6) wavefunctions to obtain a composite containing 8568 configurations⁴⁸ and denoted

as GVB-RCI(4/8)×GVB-CI(2/6). The orbitals for this wavefunction were optimized for this 8568 configuration wavefunction using the GVB3 program.⁴⁹

For calculations involving methyl groups, the inactive C-H bonds were uncorrelated [as in Hartree-Fock (HF)], and the M-C, active C-H and C-C bonds were included in the GVB-CI space. All the other metal electrons were described in the same manner as MH_2 .

A special virtue of this GVB approach to wavefunctions is that since the orbitals are divided into active (GVB-CI), semi-active (GVB-RCI), and inactive (HF) orbitals, the number of configurations does not increase when ligands are added, so large systems [e.g., $\text{Pt}(\text{CH}_3)_2(\text{PH}_2)_2$]²⁹ can be treated nearly as easily as small ones.

Often it has been convenient to calculate the GVB-RCI wavefunction using orbitals from corresponding GVB-PP calculations. This saves considerable time because the GVB-PP calculation does not require transformation of electron repulsion integrals to the molecular orbital basis. Indeed, such GVB-RCI calculations, using orbitals from GVB wavefunctions, yield atomic state splittings that are in good agreement with state splittings calculated self-consistently at the GVB-RCI level (see Table VI). However, it is necessary to optimize orbitals at the full GVB-RCI(4/8)×GVB-CI(2/6) level of wavefunction in order to self-consistently include the resonance between the d^{10} and s^1d^9 configurations near the transition states for reactions (12)-(17).

To indicate how well this type of wavefunction does for atomic state splittings, we show in Table VII comparisons with experiment for HF and GVB-RCI(5/10)^{13,50} state splittings. Here the GVB-RCI involves a total of ten optimized GVB orbitals for each state (d^{10} , s^1d^9 , or s^2d^8), and we see

that GVB-RCI does quite well, with errors of 1 to 3 kcal/mol in the $^1S(d^{10})$ to $^3D(s^1d^9)$ excitation, and 0 to 6 kcal/mol in the energy of $^1D(s^1d^9)$ relative to $^1D(s^1d^9)$. These three states describe the dominant character of the wavefunction for the reactions studied in this paper. [Larger errors occur for the s^2d^8 state because angular correlation of the s pair of electrons, which is important for this state, was not included in this wavefunction. However, the s^2d^8 state is destabilized by addition of phosphine ligands, and it will not play a significant role³⁰ in the chemistry of such complexes.] In contrast, HF wavefunctions lead to errors of 20 to 60 kcal/mol in the $^1S(d^{10})$ to $^3D(s^1d^9)$ excitation and 2 to 11 kcal/mol in the position of $^1D(s^1d^9)$ relative to $^3D(s^1d^9)$.

Configurations with more than six singly-occupied orbitals in the GVB-RCI wavefunction lead to numerous spin eigenfunctions (SEF) (e.g., a triplet with ten open shells has 90 SEF's). In order to save computer time, it is convenient to restrict the wavefunction so that there is a maximum of six open shells in any configuration. Thus the GVB-RCI for the 1S state of Pt restricted to six open shells contains 72 configurations and 328 SEF's, whereas the full GVB-RCI contains 81 configurations with 642 SEF's. Table VI shows the differences in state splittings of Pt atom for calculations in which the number of open shells was restricted to a minimum of six compared with the case where no restrictions were made (up to ten open shells). The restriction of a maximum of six open shells leads to errors of only ~ 0.2 kcal/mol in the atomic state splitting relevant for this work, an error quite tolerable for our studies. We should emphasize that inclusion of at least six open shells is required in order to describe inter-pair correlations (a single excitation within one GVB pair times a single excitation within another GVB pair) for both the triplet and open-shell

singlet states of the atom. In conclusion, the use of the six-open-shell restriction is justified for these studies, and all wavefunctions reported here are restricted to a maximum of six open shells unless otherwise noted.

C. Geometry Optimization

We used a distinguished coordinate method⁵¹ to follow the potential curve from reactants to products. Each geometry was calculated by holding the R-M-R angle fixed and optimizing all other geometric parameters for the HF wavefunction. Using this sequence of geometries, we then carried out the self-consistent GVB-RCI(4/8)×GVB-CI(2/6) calculations. This allowed us to follow a continuous path from reactant to products for each system studied and to extract the concepts permitting us to explain the various features and to interpret the experiments. To obtain various critical points (minima and saddle points), we fitted the variations in energy and all other geometric parameters along the reaction path to cubic splines and interpolated the geometric parameters for the optimum energy. Thus, the geometries are not as accurate as they would be if separate energy optimizations had been carried out.

To determine the effect of electronic correlation on geometry, we calculated (see Table VIII) the equilibrium bond angles for PdH₂, PtH₂, PdH(CH₃), and NiH₂ at the HF, GVB-CI(2/6) and GVB-RCI(4/8)×GVB-CI(2/6) levels. For Pd and Pt complexes, the bond angle determined at the HF level is within 5° of the GVB-RCI(4/8)×GVB-CI(2/6) level. On the other hand, the equilibrium geometry of NiH₂ is strongly affected by electronic correlation, as discussed in Appendix A.

In order to test the effects of correlation on the transition state geometries, we reoptimized the geometry of PdH₂ at the GVB-RCI(4/8)×GVB-CI(2/6) level. This optimized transition state has a Pd-H

distance of 1.595 Å and an H-Pd-H bond angle of 50.6°, with an activation energy of 0.74 kcal/mol (versus 1.547 Å, 50.8°, and 1.551 kcal/mol for interpolated value based on the HF distinguished coordinate studies followed by GVB-RCI). These changes of 0.048 Å in Pd-H distance, 0.2° in bond angle, and 0.81 kcal/mol in activation barrier⁵² indicate that use of the GVB calculations along the HF reaction path provides a reasonable description for these reactions.

Our calculations for reductive elimination of dimethyl and dihydride complexes assume a transition state with C_{2v} symmetry. It is possible that the transition state for these reactions has lower symmetry.⁵³ However, it has been shown that the C_{2v} transition state is a true saddle point in recent *ab initio* calculations on a similar system, oxidative addition of H_2 to $Pt(PH_3)_2$.^{16a,54} Therefore it is plausible that the C_{2v} transition state for H-H coupling from PdH_2 and C-C coupling from $Pd(CH_3)_2$ is also a true saddlepoint; however, we did not demonstrate this (by solving for the eigenvectors of the Hessian and showing there to be one negative eigenvalue).

Acknowledgments: This work was supported by a grant from the National Science Foundation (No. CHE83-18041). One of the authors (J. J. L.) was an Exxon Education Foundation Fellow (1983) and then an Atlantic Richfield Foundation Summer Fellow (1984) during part of the time the project was in process.

Appendix A.

Although not strictly required for the studies of this paper, we carried out some limited calculations on NiH_2 in order to compare with a series of studies carried out by Siegbahn and co-workers^{22b,37a,b} on $\text{Ni}(\text{R}_1)(\text{R}_2) \rightarrow \text{Ni} + \text{R}_1-\text{R}_2$ processes.

The calculations by Siegbahn and co-workers^{37a} on NiH_2 started with a CASSCF in which three pairs of electrons are correlated. Thus, of the 12 valence electrons, six are in doubly-occupied orbitals, while the other six are described by a full CI in which six electrons are distributed among five orbitals. All orbitals are solved for self-consistently in this wavefunction [denoted as CASSCF (3/5)], which corresponds closely to our GVB-CI(2/6) wavefunction, except that we have four doubly-occupied orbitals (rather than three) and four electrons distributed among six orbitals (rather than six electrons distributed among four orbitals), all of which are optimized self-consistently [thus our wavefunction could be denoted CASSCF(2/6)]. In addition, we also calculated the wavefunction in which all four doubly-occupied orbitals were correlated simultaneously at the GVB-RCI(4/8) level. This calculation is denoted GVB-RCI(4/8)×GVB-CI(2/6) (see Section V), where all orbitals are solved for self-consistently for the full wavefunction. We find that the GVB-RCI wavefunction gives a balanced description of the s^2d^8 , s^1d^9 , and d^{10} atomic states (see Section V), and this is the level used in the various calculations on Pd and Pt systems.

However, Siegbahn and co-workers³⁷ considered an alternative wavefunction in which several dominant configurations from the CASSCF were selected (all configurations with coefficients larger than 0.05),^{37a} and all single and double excitations from the dominant configurations to

all virtuals were allowed. Siegbahn's contracted CI method⁵⁵ was used to solve for this CI wavefunction. On top of this, the multi-reference analog of Davidson's correction⁵⁶ was used to estimate the effect of quadruple excitations.

To mimic Siegbahn's CI calculation, we carried out a CI calculation (denoted CISD) that involved all single and double excitations from the three dominant spatial configurations of the CASSCF wavefunction, accounting for about $99.0 \pm 0.1\%$ of the CASSCF wavefunction for the geometries considered. This size-consistent CI involved 6324 spatial configurations and 19,740 spin eigenfunctions.⁵⁷ We also added the multi-reference analog of Davidson's correction⁵⁶ for quadruple excitations (denoted CISD+Q). We also carried out HF, GVB-CI(2/6), GVB-RCI(4/8) \times GVB-CI(2/6), and CASSCF calculations (without p functions on the hydrogens to be consistent with how PdH₂ and PtH₂ were calculated). CASSCF, CISD, and CISD+Q levels were also calculated with polarization functions on each hydrogen to be consistent with the basis set used by Blomberg and Siegbahn.^{37a} The effect of hydrogen p functions is to make the H-Ni-H angle larger by 2° at the CASSCF level. (All calculations with p functions of hydrogens will henceforth have an apostrophe after their names, e.g., CASSCF'.) These results are presented in Figure 11, where we see that the equilibrium H-Ni-H bond angle decreases as the level of correlation increases. Since the H-Ni-H angle is the same at the CISD' and CISD+Q' levels, this angle has probably converged to 69° with respect to electronic correlation. This bond angle is significantly different from the 57° bond angle found by Blomberg and Siegbahn^{37a} and is closer to the GVB-RCI(4/8) \times GVB-CI(2/6) result of 76°.

We believe that the smaller bond angle found by Blomberg and

Siegbahn^{37a} is due to the fact that their CI calculation was not a "fully variational CI calculation".^{37c} Siegbahn's contracted CI method has been shown to give errors of 2% of the total correlation energy in simple systems such as CH₂, CH₃, and CH₅.⁵⁵ In NiH₂, the total correlation energy is on the order of 0.30 hartrees (HF energy minus CISD+Q energy). Thus, 2% errors in the contracted CI would lead to changes of about 6 millihartrees = 3.8 kcal/mol. Since the difference in energy between the 57° geometry and the 69° geometry (from CISD+Q) is only 0.5 millihartrees, we conclude that the contracted CI should not be reliable for such geometric quantities.

It is appropriate to examine why electron correlation has such a large effect on the bond angle in NiH₂ (99° at HF, 76° at GVB-RCI, and 69° at the best CI; see Table A-I). For all three systems, NiH₂, PdH₂, and PtH₂, the dominant resonance structure is the same, s¹d⁹. However, the second resonance structure for NiH₂ is different from PdH₂ and PtH₂ [see (19) and (20)], as should be expected since the lowest singlet state for Pd and Pt is d¹⁰, whereas it is s¹d⁹ (¹D) for Ni. Thus, while the second resonance structure of PdH₂ and PtH₂ is d¹⁰, it is expected to be s¹d⁹ for the Ni atom. But the s¹d⁹ open-shell singlet cannot be described by the closed-shell HF wavefunction. This bias against the s¹d⁹ singlet state of the Ni atom leads to repulsive interactions between hydrogen atoms and a large H-Ni-H bond angle at the HF level. The CI wavefunction includes a good description of s¹d⁹ singlet and hence leads to significantly smaller bond angles. Therefore, HF bond angles should be accurate for the Pd and Pt complexes but not for NiH₂.

Appendix B.

We report here (in Tables B.I-VI) the optimized geometries along the reaction path for the various reactions studied in this paper. All of the geometries were optimized at the HF level (described in Section V). We also report energies for HF, GVB-CI(2/6), and GVB-RCI(4/8)×GVB-CI(2/6) wavefunctions, all of which were found¹³ to be consistent levels of calculation for the reaction $\text{H}_2 + \text{Pt}(\text{PH}_3)_2 \rightarrow \text{H}_2\text{Pt}(\text{PH}_3)_2$.

The following trends can be observed from these results. In going from HF to GVB-CI(2/6), oxidative addition always becomes *more* favorable (or reductive elimination is made less favorable). This occurs because the GVB-CI(2/6) wavefunction includes terms that provide a better description of the two M-R bonds, which have larger correlation errors than the corresponding pairs for the dissociated limit (involving a metal d pair and an H-H bond pair). In going from the GVB-CI(2/6) level to the GVB-RCI(4/8)×GVB-CI(2/6) level, we have added terms to describe the correlation effects between d electrons. These terms are needed to get accurate d^{10} - s^1d^9 splittings. These correlation terms always stabilize the d^{10} (^1S) state relative to the s^1d^9 (^3D) state and make oxidative addition *less* favorable (and reductive elimination more favorable). Thus there is some degree of cancellation in the correlation errors for HF.

Table B.VII shows the effect of electron correlation on ΔE^\ddagger , R-M-R angle at the transition state, and ΔE . The trends in ΔE^\ddagger follow the same general trend as the ΔE for these reactions except with smaller magnitudes.

References and Notes

- (1) Collman, J. P.; Hegedus, L. S. "Principles and Applications of Organotransition Metal Chemistry," University Science Books: Mill Valley, California, 1980.
- (2) (a) James, B. R. "Homogeneous Hydrogenation," Wiley: New York, 1973;
(b) James, B. R. *Adv. Organometal. Chem.* **1979**, *17*, 319-405;
(c) Brothers, P. J. *Prog. Inorg. Chem.* **1981**, *28*, 1-61.
- (3) (a) Parshall, G. W. *Catalysis (London)* **1977**, *1*, 335-368;
(b) Shilov, A. E.; Shteinman, A. A. *Coord. Chem. Rev.* **1977**, *24*, 97-143;
(c) Webster, D. E. *Adv. Organomet. Chem.* **1977**, *15*, 147-188.
- (4) (a) Tamao, K.; Sumitani, K.; Kiso, Y.; Zembayashi, M.; Fujioka, A.; Kodama, S.; Nakajima, I.; Minato, A.; Kumada, M. *Bull. Chem. Soc. Jpn.* **1976**, *49*, 1958;
(b) Negishi, E. "Aspects of Mechanism and Organometallic Chemistry," Brewster, J.H., Ed.; Plenum Press: New York 1978;
(c) Kumado, M. *Pure Appl. Chem.* **1980**, *52*, 669-679;
(d) Negishi, E. *Acc. Chem. Res.* **1982**, *15*, 340-348.
- (5) (a) Chock, P. B.; Halpern, J. *J. Am. Chem. Soc.* **1966**, *88*, 3511-3514;
(b) Vaska, L.; Werneke, M. F. *Trans. N.Y. Acad. Sci.* **1971**, *33*, 70-86;
(c) Mays, M. J.; Simpson, R. N. F.; Stefanini, F. P. *J. Chem. Soc. (A)* **1970**, 3000-3002;
(d) Hyde, E. M.; Shaw, B. L. *J. Chem. Soc. Dalton Trans.* **1975**, 765-767;
(e) Longato, B.; Morandini, F.; Bresadola, S. *Inorg. Chem.* **1976**, *15*,

- 650-655;
- (f) Crabtree, R. H. *Acc. Chem. Res.* **1979**, *12*, 331-338;
- (g) Crabtree, R. H.; Quirk, J. M. *J. Organomet. Chem.* **1980**, *199*, 99-106;
- (h) Crabtree, R. H.; Hlatky, G. G. *Inorg. Chem.* **1980**, *19*, 571-572;
- (i) Crabtree, R. H.; Morehouse, S. M. *ibid.* **1982**, *21*, 4210-4213;
- (j) Harrod, J. F.; Hamer, G.; Yorke, W. J. *J. Am. Chem. Soc.* **1979**, *101*, 3987-3989;
- (k) Harrod, J. F.; Yorke, W. J. *Inorg. Chem.* **1981**, *20*, 1156-1159;
- (l) Drouin, M.; Harrod, J. F. *ibid.* **1983**, *22*, 999-1001.
- (6) (a) Janowicz, A. H.; Bergman, R. G. *J. Am. Chem. Soc.* **1982**, *104*, 352-354;
- (b) Hoyano, J. K.; Graham, W. A. G. *ibid.* **1982**, *104*, 3723-3725;
- (c) Janowicz, A. H.; Bergman, R. G. *ibid.* **1983**, *105*, 3929-3939;
- (d) Wax, M. J.; Stryker, J. M.; Buchananan, J. M.; Kovac, C. A.; Bergman, R. G. *ibid.* **1984**, *106*, 1121-1122;
- (e) Burk, M. J.; Crabtree, R. H.; Parnell, C. P.; Uriarte, R. J. *Organometallics* **1984**, *3*, 816-817.
- (7) (a) Jones, W. D.; Feher, F. J. *J. Am. Chem. Soc.* **1984**, *106*, 1650-1663;
- (b) Periana, R. A.; Bergman, R. G. *Organometallics* **1984**, *3*, 508-510.
- (8) (a) Abis, L.; Sen, A.; Halpern, J. *J. Am. Chem. Soc.* **1978**, *100*, 2915-2916; Halpern, J. *Acc. Chem. Res.* **1982**, *15*, 332-338;
- (b) Michelin, R. A.; Faglitz, S.; Uguagliati, P. *Inorg. Chem.* **1983**, *22*, 1831-1834.

- (9) (a) Gillie, A.; Stille, J. K. *J. Am. Chem. Soc.* **1980**, *102*, 4933-4941;
(b) Loar, M. K.; Stille, J. K. *ibid.* **1981**, *103*, 4174-4181;
(c) Moravskiy, A.; Stille, J. K. *ibid.* **1981**, *103*, 4182-4186;
(d) Ozawa, F.; Ito, T.; Nakamura, Y.; Yamamoto, A. *Bull. Chem. Soc. Jpn.* **1981**, *54*, 1868-1880.
- (10) Kohara, T.; Yamamoto, T.; Yamamoto, A. *J. Organomet. Chem.* **1980**, *192*, 265-274.
- (11) Harrod *et al.* have observed a trans product from H₂ addition to Ir(I);^{5j} however, this is believed not to be an initial product of the oxidative addition but rather the result of a rearrangement of one of the initial cis-products.^{5l}
- (12) (a) Chatt, J.; Shaw, B. L. *J. Chem. Soc.* **1959**, 705-716;
(b) Ruddick, J. D.; Shaw, B. L. *J. Chem. Soc.* **1969**, 2801-2808.
- (13) Low, J. J.; Goddard III, W. A. *J. Am. Chem. Soc.* **1984**, *106*, 6928-6937.
- (14) Moore, C. E. "Atomic Energy Levels," NBS: Washington, D.C., 1971; Vol. III. (These state splittings were averaged over j states to cancel out spin-orbit coupling.)
- (15) Pauling, L. "The Nature of the Chemical Bond," 3rd ed.; Cornell University Press: Ithaca, 1960; pp 88-98.
- (16) The vibrational frequencies used to estimate the zero point energies were taken from those calculated for Pt(H)₂(PH₃)₂ and PtH(CH₃)(PH₃)₂.^{16a}
(a) Obara, S.; Kitaura, K.; Morokuma, K. *J. Am. Chem. Soc.* **1984**, *106*, 7482-7492;
(b) The C-Pt-C bend was calculated using the angle bending force

constant derived from the potential of reaction (14). This gave a frequency for the $\text{H}_3\text{C}-\text{Pt}-\text{CH}_3$ bend of 190 cm^{-1} .

- (17) The D_{298} used in these calculations are $D_{298}(\text{H}-\text{H}) = 104.2\text{ kcal/mol}$, $D_{298}(\text{H}-\text{CH}_3) = 105.1\text{ kcal/mol}$ and $D_{298}(\text{H}_3\text{C}-\text{CH}_3) = 90.4\text{ kcal/mol}$. These bond energies were derived from spectroscopic measurements of H_2 ^{17a} and the reported D_{298} ^{17b} for $\text{H}_3\text{C}-\text{CH}_3$ and $\text{H}-\text{CH}_3$.

(a) Huber, K.P.; Herzberg, G. "Constants of Diatomic Molecules," Van Nostrand: New York, 1979;

(b) McMillen, D. F.; Golden, D. M. *Ann. Rev. Phys. Chem.* **1982**, *33*, 493-352.

- (18) The vibrational frequencies (550 , 1230 , and 1230 cm^{-1}) used to calculate the zero point energy correction of chemisorbed H are those from the EELS spectra of H on Pt(111).^{18a} The zero point energy correction for chemisorbed CH_3 is that calculated and estimated for CH_3 chemisorbed on Ni(001).^{18b}

(a) Baro, A. M.; Ibach, H.; Bruchmann, H. D. *Surf. Sci.* **1979**, *88*, 384-398.

(b) Low, J. J. Ph.D. Thesis, California Institute of Technology, Pasadena, California, 1985, Chapter 4.

- (19) MacDonald, A. H.; Daams, J. M.; Vosko, S. H.; Koelling, D. D. *Phys. Rev. B* **1981**, *23*, 6377-6398.

- (20) Conrad, H.; Ertl, G.; Latta, E. E. *Surf. Sci.* **1974**, *41*, 435-446.

- (21) Weinberg, W. H. *Survey of Progress in Chemistry* **1983**, *10*, 1-59.

- (22) (a) Bagatur'yants, A.; Anikin, N.; Zhidomirov, G.; Kazanskii, V. *Zh. Fiz. Khim.* **1981**, *55*, 2035-2039;

(b) Blomberg, M.; Brandemark, U.; Pettersson, L.; Siegbahn, P. *Int.*

- J. Quant. Chem.* **1983**, *23*, 855-863.
- (23) Brandemark, U. B.; Blomberg, M. R. A.; Pettersson, L. G. M.; Siegbahn, P. E. M. *J. Phys. Chem.* **1984**, *88*, 4617-4621. In this paper, convincing proof is provided that the Pd(H₂) complex is not a van der Waals complex.
- (24) (a) Kubas, R.; Ryan, R.; Swanson, B.; Vergamini, P.; Wasserman, H. *J. Am. Chem. Soc.* **1984**, *106*, 451-452;
(b) Hay, P. J. *Chem. Phys. Lett.* **1984**, *103*, 466-469.
- (25) (a) Brookhart, M.; Green, M. L. H. *J. Organomet. Chem.* **1983**, *250*, 395-408, and references therein;
(b) Koga, N.; Obara, S.; Morokuma, K. *J. Am. Chem. Soc.* **1984**, *106*, 4625-4626.
- (26) Halpern, J. *Acc. Chem. Res.* **1982** *15*, 238-244.
- (27) (a) Whitesides, G. M.; Gaasch, J. F.; Stedronsky, E. R. *J. Am. Chem. Soc.* **1972**, *94*, 5258-5270;
(b) McDermott, J. X.; White, J. F.; Whitesides, G. M. *ibid.* **1976**, *98*, 6521-6528;
(c) Young, G. B.; Whitesides, G. M. *ibid.* **1978**, *100*, 5808-5815;
(d) McCarthy, T. J.; Nuzzo, R. G.; Whitesides, G. M. *ibid.* **1981**, *103*, 1676-1678;
(e) McCarthy, T. J.; Nuzzo, R. G.; Whitesides, G. M. *ibid.* **1981**, *103*, 3396-3403;
(f) Nuzzo, R. G.; McCarthy, T. J.; Whitesides, G. M. *ibid.* **1981**, *103*, 3404-3410;
(g) Komiya, S.; Morimoto, Y.; Yamamoto, A.; Yamamoto, T. *Organometallics* **1982**, *1*, 1528-1536.

- (28) $\text{Pt}(\text{Et})_2(\text{PEt}_3)_2$ is known to decompose via β -hydride elimination to yield ethylene ($\Delta H_{f300}^0 = 12.5 \text{ kcal/mol}$, $S_{300} = 52.4 \text{ e.u.}$) and ethane ($\Delta H_{f300}^0 = -20.2 \text{ kcal/mol}$, $S_{300} = 54.9 \text{ e.u.}$) rather than by reductive elimination to give n-butane ($\Delta H_{f300}^0 = -30.2 \text{ kcal/mol}$, $S_{300} = 74.1 \text{ e.u.}$) even though n-propane is the thermodynamically favored product ($\Delta H_{300} = -22.5 \text{ kcal/mol}$, $\Delta S_{300} = -34.2 \text{ e.u.}$, $\Delta G_{300} = -11.0 \text{ kcal/mol}$ for $\text{C}_2\text{H}_4 + \text{C}_2\text{H}_6 \rightarrow \text{n-C}_4\text{H}_{10}$). The ΔH_{f300}^0 and S_{300}^0 were taken from Benson, S. W. "Thermochemical Kinetics," 2nd ed.; J. Wiley and Sons: New York, 1976.
- (29) Low, J.J. Ph.D. Thesis, California Institute of Technology, Pasadena, CA, 1985; Chapter 3.
- (30) Yoshida, T.; Otsuka, S. *J. Am. Chem. Soc.* **1977**, *99*, 2134-2140.
- (31) Saillard, J.; Hoffmann, R. *J. Am. Chem. Soc.* **1984**, *106*, 2006-2028.
- (32) Sevin, A. *Nouv. J. Chim.* **1981**, *5*, 233-241.
- (33) Dedieu, A; Strich, A. *Inorg. Chem.* **1979**, *10*, 2940-2943.
- (34) (a) Billups, W. E.; Kararski, M. M.; Hauge, R. H.; Margrave, J. L. *J. Am. Chem. Soc.* **1982**, *102*, 7394-7396;
(b) Ozin, G. A.; McCaffrey, J. G. *ibid.* **1982**, *104*, 7351-7352;
(c) Klabunde, K.J.; Tanaka, Y. *ibid.* **1983**, *105*, 3544-3546.
- (35) Sevin, A.; Chaquin, P. *Nouv. J. Chim.* **1983**, *7*, 353-360.
- (36) (a) Tatsumi, K.; Hoffmann, R.; Yamamoto, A.; Stille, J. K. *Bull. Chem. Soc. Jpn.* **1981**, *54*, 1857-1867;
(b) Balazs, A. C.; Johnson, K. H.; Whitesides, G. M. *Inorg. Chem.* **1982**, *21*, 2162-2174.
- (37) (a) Blomberg, M. R. A; Siegbahn, P. E. M. *J. Chem. Phys.* **1983**, *78*, 986-987;

- (b) Blomberg, M. R. A; Brandemark, U.; Siegbahn, P. E. M. *J. Am. Chem. Soc.* **1983**, *104*, 5557-5563;
- (c) Siegbahn, P. E. M.; Blomberg, M. R. A; Bauschlicher, C. W. *J. Chem. Phys.* **1984**, *81*, 1373-1382.
- (38) Martin, R. L.; Hay, P. J. *J. Chem. Phys.* **1981**, *75*, 4539-4545.
- (39) Basch, H.; Topiol, S. *J. Chem. Phys.* **1979**, *71*, 802-814.
- (40) Noell, J. O.; Hay, P. J. *J. Am. Chem. Soc.* **1982**, *104*, 4578-4584.
- (41) Hay, P. J. *J. Am. Chem. Soc.* **1981**, *103*, 1390-1393.
- (42) It is important to point out here that the multi-reference singles and doubles CI method is not size-consistent at every section of the potential surface.^{37c} The number of configurations reported in ref. 37a "varied between 30,000 and 130,000 for Ni(CH₃)₂ depending on the part of the potential surface." Small inconsistencies at different geometries can generate large errors in the optimum geometries if the potential surface has small curvatures. It appears that the energetics derived from these calculations are reasonable and useful in discussing the properties of Ni atom vs Pd and Pt. We have used the following D_e and state splitting to calculate average bond energies and energetics; D_e(H-H) = 109.6, D_e(H₃C-H) = 112.6, D_e(H₃C-CH₃) = 95.0, and ³D-¹D splitting of 7.1 kcal/mol.^{42a}
- (a) Blomberg, M. R. A.; Siegbahn, P. E. M.; Roos, B. O. *Mol. Phys.* **1982**, *47*, 127-143.
- (43) Melius, C. F.; Olafson, B. D.; Goddard III, W. A. *Chem. Phys. Lett.* **1974**, *28*, 457-462.

- (44) Rappé, A. K.; Smedley, T. A.; Goddard III, W. A. *J. Phys. Chem.* **1981**, *85*, 2607-2611.

- (45) Rappé, A. K., unpublished results.

We have tested the SHC basis sp basis by reoptimizing the H-Ni-H angle with the 5p basis associated with the one-electron MEP of Upton and Goddard [Upton, T. H.; Goddard III, W. A. "Chemistry and Physics of Solid Surfaces," Vanselow, R; England, W.; Eds.; CRC Press: Boca Raton, 1982; Vol. 3, pp 127-162]. The MEP basis yielded an H-Ni-H angle of 83.2° at the GVB-CI(2/6) level, while the SHC gave 81.0° at the same level of calculation.

- (46) Dunning, Jr.; T. H.; Hay, P. J. In "Modern Theoretical Chemistry: Methods of Electronic Structure Theory," Schaefer III, H.F., Ed.; Plenum Press: New York, 1977; Vol. 3, Chapter 1, pp 1-27.

- (47) Huzinaga, S. *J. Chem. Phys.* **1965**, *42*, 1293-1302.

- (48) This CI level was restricted to allow only six open shells. This was found to be an adequate level for the state splittings of Ni, Pd, and Pt atoms.

- (49) Yaffe, L. G.; Goddard III, W. A. *Phys. Rev. A* **1976**, *13*, 1682-1691.

- (50) This level is very close to atomic wavefunctions at the dissociated limit of reactions (1)-(6).

- (51) (a) Rothman, M. J.; Lohr, L. L. *Chem. Phys. Lett.* **1980**, *70*, 405;
(b) Williams, I. H.; Maggiora, G. M. *J. Mol. Structure, THEOCHEM*, **1982**, *89*, 365-378. Williams and Maggiora have shown that the distinguished coordinate method can yield a discontinuous reaction path if multiple local minima exist for the same value of distinguished coordinate. Since the M-H and M-CH₃ equilibrium bond

lengths are much longer than the corresponding R-H and R-CH₃ bond lengths, it is not likely that more than one local minimum can exist for any value of R₁-M-R₂ bond angle in the bound complex to transition state region. The M-R bond lengths in this region are close to those of the bound complex. If another minimum existed, it would have an R₁-R₂ distance closer to those of the products, which would force unphysically short M-R bond lengths. The typical symptom of a discontinuous reaction path would be a discontinuous change in geometric parameters, which is not evident in our results (see Appendix B).

- (52) A similar energy lowering would be expected for the PdH₂ complex if the geometry was reoptimized at the RCI(4/8)×GVB-CI(2/6) level.
- (53) (a) Metiu, H.; Ross, J.; Silbey, R.; George, T. F. *J. Chem. Phys.* **1974**, *8*, 3200-3209;
(b) Stanton, R. E.; McIver, J. W. *J. Am. Chem. Soc.* **1975**, *97*, 3632-3646;
(c) Pechukas, P. *J. Chem. Phys.* **1976**, *64*, 1516-1521.
- (54) Kitaura, K.; Obara, S.; Morokuma, K. *J. Am. Chem. Soc.* **1981**, *103*, 2891-2892.
- (55) Siegbahn, P. E. M. *Chem. Phys.* **1977**, *25*, 197-205.
- (56) Davidson, E. R. In "The World of Quantum Chemistry," Daudel, R.; Pullman, B., Eds.; Reidel: Dordrecht, 1974.
- (57) Unfortunately no total energies or number of configurations were reported for Siegbahn's calculations^{37a} on NiH₂, so a comparison of how closely our calculations mimic his results is not possible.

Table I. Mulliken Populations for the GVB Bond Pairs of $M(R_1)(R_2)$. For each bond there are two listings, the top one is the metal-like GVB orbital and the bottom one is the ligand-like orbital.

System			Populations of GVB Orbitals	
M	R ₁	R ₂	M - H	M - CH ₃
Pd	H	H	$s^{0.28} p^{0.02} d^{0.57} H^{0.12}$	-
			$(sp)^{0.02} d^{0.18} H^{0.80}$	-
Pd	H	CH ₃	$s^{0.3} p^{0.02} d^{0.43} C^{0.04} H^{0.19}$	$s^{0.17} p^{0.01} d^{0.68} C^{0.12}$
			$(sp)^{0.02} d^{0.15} C^{0.02} H^{0.81}$	$(sp)^{0.02} d^{0.17} C s^{0.10} p^{0.67}$
Pd	CH ₃	CH ₃	-	$s^{0.16} p^{0.03} d^{0.55} C^{0.24}$
			-	$(sp)^{0.01} d^{0.20} C s^{0.28} p^{0.52}$
Pt	H	H	$s^{0.29} p^{0.02} d^{0.63} H^{0.07}$	-
			$(sp)^{0.02} d^{0.19} H^{0.80}$	-
Pt	H	CH ₃	$s^{0.30} p^{0.02} d^{0.60} H^{0.08}$	$s^{0.28} p^{0.01} d^{0.64} C^{0.09}$
			$(sp)^{0.01} d^{0.18} H^{0.80}$	$(sp)^{0.01} d^{0.18} C s^{0.12} p^{0.70}$
Pt	CH ₃	CH ₃	-	$s^{0.27} p^{0.01} d^{0.82} C^{0.10}$
			-	$(sp)^{0.00} d^{0.15} C s^{0.14} p^{0.70}$

Table II. Mulliken Total Populations for $M(R_1)(R_2)$.

System			Metal Total Population		Total Population		Overlap of GVB Bond Orbitals	
M	R_1	R_2	Msp	Md	H	CH_3	M - H	M - CH_3
Pd	H	H	0.76	9.36	0.94		0.76	
Pd	H	CH_3	0.71	9.19	1.05	9.06	0.76	0.68
Pd	CH_3	CH_3	0.60	9.15		9.13		0.72
Pt	H	H	1.16	9.15	0.85		0.73	
Pt	H	CH_3	1.05	9.03	0.89	9.04	0.74	0.71
Pt	CH_3	CH_3	0.97	8.91		9.06		0.71

Table III. Summary of Energetics. Double dagger indicates transition state for the reaction.
The separate atomic state for Pt is the spin-allowed singlet (d^{10}).

Reaction	ΔE	ΔE^\ddagger	Zero Point Energy ^{a)}			ΔH_{298}° $-\Delta H_0^\circ$	ΔH_{298}^\ddagger $-\Delta H_0^\ddagger$	ΔH_{298}° ΔH_{298}^\ddagger
			MR_2	$(MR_2)^\ddagger$	$M + R_2$			
$Pd(H)_2 \rightarrow Pd + H_2$ (12)	-3.6	1.6	7.9	6.4	6.3	1.2	0.3	-4.0 0.4
$Pd(H)(CH_3) \rightarrow Pd + CH_4$ (13)	-20.1	10.4	28.4	27.2	30.1	1.2	0.3	-17.2 9.5
$Pd(CH_3)_2 \rightarrow Pd + C_2H_6$ (14)	-16.0	22.6	47.6	48.3	43.9	0.9	0.3	-18.8 23.6
$Pt(H)_2 \rightarrow Pt + H_2$ (15)	33.6	--	7.9	--	6.3	1.2	--	33.2 --
$Pt(H)(CH_3) \rightarrow Pt + CH_4$ (16)	16.1	29.0	28.4	27.2	30.1	1.2	0.3	19.0 28.1
$Pt(CH_3)_2 \rightarrow Pt + C_2H_6$ (17)	18.3	53.5	47.6	48.3	43.9	0.9	0.3	15.5 54.5
$H_2 \rightarrow \begin{array}{c} H & H \\ & \\ \text{---} & \text{---} \end{array} + \begin{array}{c} Pt \\ \\ \text{---} \end{array}$	(-20.9)		8.6	6.3	6.3	-2.1		-20.7
	(-15.4)		8.6		6.3	-2.1		-15.2
$CH_4 \rightarrow \begin{array}{c} H \\ \\ \text{---} \end{array} + \begin{array}{c} H_3 \\ C \\ \\ \text{---} \end{array} + \begin{array}{c} Pt \\ \\ \text{---} \end{array}$	(-3.4)		27.3	30.1	30.1	-2.1		-8.3
	(1.1)		27.3	30.2	30.2	-2.1		-3.9
$C_2H_6 \rightarrow \begin{array}{c} H_3 \\ C \\ \\ \text{---} \end{array} + \begin{array}{c} H_3 \\ C \\ \\ \text{---} \end{array} + \begin{array}{c} Pt \\ \\ \text{---} \end{array}$	(-5.6)		46.0	43.9	43.9	-1.8		-5.3
	(-0.7)		46.0	43.9	43.9	-1.8		-0.4

a) We have assumed that methyl groups bonded to the metal atom have free rotation about the M-C bond.

Table IV. Average M-R Bond Energies.

M	R	Adiabatic	Intrinsic
		Bond Energy	Bond Energy
		D_A	D_I
		(kcal/mol)	(kcal/mol) ^{a)}
Pd	H	50	60
Pt	H	69	62
Pd	CH ₃	36	45
Pt	CH ₃	53	47

^{a)} State splittings are those determined at the GVB-RCI level (see Section V).

Table V. Mulliken Populations and Geometries Along Reaction Path for Pd + H₂ → PdH₂. The transition state is at a H-Pd-H angle of 51°.

H-Pd-H Angle (deg.)	Mulliken Population Pt sp	Mulliken Population Pt d	Mulliken Population H	Pd-H distance (Å)	H-H distance (Å)
90	0.80	9.28	0.958	1.51	2.14
80	0.79	9.31	0.949	1.51	1.94
70	0.76	9.36	0.940	1.51	1.73
60	0.71	9.41	0.939	1.52	1.52
50	0.62	9.49	0.948	1.55	1.31
40	0.50	9.59	0.957	1.60	1.10
30	0.36	9.71	0.963	1.71	0.89
20	0.14	9.88	0.989	2.12	0.74
0	0	10.0	1.00	∞	0.73

Table VI. Atomic State Splittings (kcal/mol) for Ni Triad.

Config.	Term	Ni			Pd			Pt		
		Exp ^{a)}	GVB-RCI ^{b)}	HF ^{c)}	Exp ^{a)}	GVB-RCI ^{b)}	HF ^{c)}	Exp ^{a)}	GVB-RCI ^{b)}	HF ^{c)}
s ¹ d ⁹	³ D	0.0	0.0	0.0	0.0	0.0	0.0	0.0	0.0	0.0
d ¹⁰	¹ S	40.0	40.6	99.5	-21.9	-19.0	12.7	11.0	12.7	31.4
s ¹ d ⁹	¹ D	7.7	7.9	18.4	11.4	11.2	13.8	32.1	25.9	27.0
s ² d ⁸	³ F	0.7	21.3	-15.3	56.0	65.7	54.5	14.7	18.8	8.4

a) Reference 14.

b) GVB-RCI(5/10) total energies in hartrees for the ³D states of Ni, Pd, and Pt, are -39.238987, -29.150011, -27.551978, respectively.

c) Total energies in hartrees for the ³D states of Ni, Pd, and Pt are -39.152853, -29.111329, -27.506192, respectively, at the HF level.

Table VII. The Effect of Maximum Number of Open Shells and Level of Optimization on GVB-RCI(5/10) State Splittings in Pt Atom.

State	State Splittings (kcal/mol)		
	six open shells		ten open shells
	GVB-PP Orbitals	GVB-RCI Orbitals	GVB-RCI Orbitals
$^3D(d^9s^1)$	0 ^{a)}	0 ^{b)}	0 ^{c)}
$^1S(d^{10})$	12.3	12.7	12.5
$^1D(d^9s^1)$	26.1	25.9	25.9
$^3F(d^8s^2)$	18.5	18.8	18.9

^{a)} Total energy in hartrees for the 3D state of Pt is -27.551297 for GVB-RCI(5/10) with GVB-PP orbitals and restricted to six open shells.

^{b)} Total energy in hartrees for the 3D state of Pt is -27.551978 for GVB-RCI(5/10) with optimized orbitals and restricted to six open shells.

^{c)} Total energy in hartrees for the 3D state of Pt is -27.552461 for GVB-RCI(5/10) with optimized orbitals.

Table VIII. The Effect of Electron Correlation on R_1-M-R_2 Equilibrium Bond Angles.

System			Bond Angle (deg.)		
M	R_1	R_2	HF	GVBCI(2/6)	GVB-RCI(4/8) ×GVBCI(2/6)
Pd	H	H	68	73	73
Pt	H	H	84	81	84
Pd	H	CH ₃	83	83	80
Ni	H	H	99 ^{a)}	81 ^{a)}	76 ^{a)}

^{a)} Bond length frozen at geometry of Blomberg and Siegbahn.^{37a}

Table A-I. Results for NiH_2 .

Wavefunction ^{a)}	Total Energy at minimum (hartrees)	Optimum Angle (degrees)	Number of Confgs.	Number of SEF's	Number of Nonzero CI Matrix Elements
HF	-40.075637	99.4	1	1	1
GVB-CI(2/6)	-40.152318	81.0	48	57	1,018
CASSCF(3/5)	-40.158219	82.3	25	28	287
CASSCF(3/5) ^{b)}	-40.161980	84.5	25	28	287
RCI(4/8)×GVB-CI(2/6)	-40.317295	76.3	3,360	8,568	403,712
CISD ^{b)}	-40.333400	69.0	6,324	19,740	8,560,651
CISD+Q ^{b)}	-40.350557	69.0	--	--	--

a) All of these wavefunctions used orbitals belonging to irreducible representations of C_{2v} .

b) These wavefunctions included p's on the H atom.

Table B-I. Geometries and Energies Along Reaction Path for $\text{Pd} + \text{H}_2 \rightarrow \text{PdH}_2$.

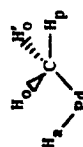
Geometric Parameters ^{a)}			Energy ^{b)}		
PdH_2 angle (deg.)	Pd-H distance Å	H-H distance Å	HF (kcal/mol)	GVBCI(2/6) (kcal/mol)	GVB-RCI(4/8) ×GVBCI(2/6) (kcal/mol)
90	1.510	2.136	21.0	2.13	6.33
80	1.508	1.939	18.4	0.0	4.04
70	1.512	1.734	17.6	-0.31	3.55
60	1.524	1.524	17.8	1.15	4.44
50	1.550	1.310	17.5	3.47	5.09
40	1.601	1.095	13.1	3.55	2.44
30	1.714	0.887	3.8	0.66	-4.61
20	2.124	0.738	0.0	-2.13	-4.42
0	∞	0.734	0.0	0.0	0.0

^{a)} Each geometry optimized at the HF level with H-Pd-H angle held fixed.

^{b)} Total energies (in hartrees) at the dissociated limit are -30.237961 at the HF level, -30.265687 at the GVB-CI(2/6) level, and -30.336364 at the GVB-RCI(4/8)×GVB-CI(2/6) level.

Table B-II. Geometries and Energies Along Reaction Path for $\text{Pd} + \text{CH}_4 \rightarrow \text{Pd}(\text{H})(\text{CH}_3)$. All angles in degrees; all distances in angstroms; all energies in kcal/mol.

Geometric Parameters ^{b)}										Energy ^{a)}	
H-Pd-CH ₃ angle	Pd-H ₂ distance	Pd-C distance	C-H ₂ distance	H ₂ -C-C-Pd angle c)	H ₂ -C-H ₂ distance	H ₂ -C-H ₂ angle	H ₂ -C-Pd angle	H ₂ -C-H ₂ angle	H ₂ -C-H ₂ angle	HF	GVBCI(2/6) x GVBCI(4/6)
86	1.51	1.95	2.39	172.2	149	1.09	1.08	101.4	112	36.63	16.41
80	1.53	1.96	2.26	176.4	142	1.09	1.08	104.2	111	36.66	16.48
70	1.52	1.96	2.04	170.2	145	1.10	1.08	100.7	113	38.67	19.30
60	1.53	2.01	1.82	161.8	151	1.09	1.08	91.9	117	41.85	24.96
50	1.55	1.99	1.55	154.2	156	1.10	1.08	84.7	118	42.89	31.18
40	1.70	2.15	1.36	142.8	165	1.09	1.08	73.5	124	29.4	24.28
30	2.03	2.44	1.22	137.6	170	1.09	1.09	61.6	126	10.20	6.52
20	2.64	3.08	1.08	123.4	180	1.08	1.08	53.5	128	0.04	-0.39
0	∞	∞	1.08	--	180	1.08	1.08	--	--	0	0



- a) Each geometry optimized at the HF level with the H-Pd-CH₃ held fixed.
b) Total energies in hartrees at the dissociated limit are -69.292703 for HF, -69.317023 for GVBCI(2/6), and -69.387700 for RCI(4/6)*GVBCI(2/6).
c) H₂Me is defined to be the center of mass of the methyl protons.

Table B-III. Geometries and Energetics Along Reaction Path for $\text{Pd} + \text{C}_3\text{H}_6 \rightarrow \text{Pd}(\text{CH}_3)_2$. All angles in degrees; all distances in angstroms; all energies in kcal/mol.

Geometric Parameters ^{a)}											Energy ^{b)}			
C-Pd -C angle	Pd-C distance	C-C distance	C-H _p distance	C-H _o distance	H ^{Me} C-Pd C-C(c) angle	H ^{Me} C-C(c) angle	H _o -C-Pd angle	H _p -C-Pd angle	H _o -C-C angle	H _p -C-C angle	H _o -C-H _p angle	H _o -C-H _o angle	HF	GVB-CI(2/6) x GVB-CI(4/6)
91.9	1.96	2.82	1.09	1.06	176	140	106	112	87	150	109	109	33.0	14.3
80	2.01	2.56	1.09	1.06	175	135	112	105	84	155	109	110	35.9	15.2
70	2.04	2.34	1.09	1.06	169	136	113	102	84	157	108	111	44.7	24.3
60	2.20	2.20	1.09	1.09	149	151	122	83	95	143	106	109	60.2	43.0
50	2.33	1.97	1.06	1.06	132	163	126	60	101	125	111	107	49.5	39.7
40	2.70	1.85	1.06	1.09	119	171	126	46	106	116	110	107	28.3	22.2
20	4.43	1.54	1.06	1.06	100	180	121	32	112	112	107	107	2.4	2.3
0	∞	1.54	1.09	1.09	90	180	--	--	111.1	111	108	108	0	0

a) Geometry optimized at the HF level with the C-Pd-C angle held fixed except for the 91.9° angle, which was fully optimized.

b) Total energies in hartrees at the dissociated limit (C-Pd-C angle = 0°) are -108.312972 for HF, -108.334426 for GVB-CI(2/6) and -108.405102 for RC(4/6)*GVB-CI(2/6).

c) H^{Me} is defined to be the center of mass of the methyl protons. Key:

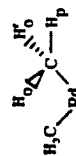


Table B-IV. Geometries and Energetics Along Reaction Path for Pt + H₂ → PtH₂.

Geometric Parameters ^{a)}			Energies ^{b)}		
PtH ₂ angle (deg.)	Pt-H distance Å	H-H distance Å	HF (kcal/mol)	GVBCI(2/6) (kcal/mol)	GVB-RCI(4/8) ×GVBCI(2/6) (kcal/mol)
90	1.47	2.07	-25.8	-30.6	-33.1
82.5	1.46	1.93	-26.2	-33.8	-33.6
70	1.47	1.68	-23.6	-31.2	-31.3
60	1.48	1.48	-18.7	-25.6	-26.5
50	1.50	1.27	-12.7	-16.9	-14.4
40	1.55	1.06	-8.1	-10.2	-7.7
20	2.12	0.74	-3.2	-3.7	-3.9
0	∞	0.734	0	0	0

^{a)} Geometry optimized at the HF level with the H-Pt-H angle held fixed except for the 82.5° H-Pt-H angle that was the result of a full geometry optimization.

^{b)} Total energies (in hartrees) at the dissociated limit are -27.584343 for HF, -27.619193 for GVB-CI(2/6), and -27.693296 for GVB-RCI(4/8)×GVBCI(2/6).

Table B-V. Geometries and Energetics Along Reaction Path for $\text{Pt} + \text{CH}_4 \rightarrow \text{Pt}(\text{H})(\text{CH}_3)$. All angles in degrees; all distances in angstroms; all energies in kcal/mol.

Geometric Parameters ^{a)}													Energy ^{b)}	
I-Pt-CH ₃ angle	Pt-C distance	Pt-H _a distance	C-H _a distance	H ^{Me} -C-Pt angle ^{c)}	H ^{Me} -C-H _a angle ^{c)}	H _p -C distance	H _o -C distance	H _p -C-Pt angle	H _o -C-Pt angle	H _p -C-H _a angle	H _o -C-H _a angle	HF	GVBCI(2/8) × GVBCI(4/8)	
89.3	1.96	1.48	2.44	180	143	1.09	1.08	109	109	146	88	110	-3.7	-31.1
80	1.97	1.47	2.24	179	141	1.09	1.08	108	109	149	87	110	-1.8	-19.5
70	1.98	1.45	2.02	178	140	1.08	1.09	107	110	150	87	111	3.4	-14.7
60	2.02	1.46	1.81	174	142	1.09	1.08	105	111	149	87	111	11.4	-7.0
50	2.04	1.48	1.57	164	150	1.09	1.08	95	115	141	91	112	20.4	5.7
40	2.15	1.59	1.39	152	160	1.09	1.08	83	120	131	98	110	21.0	15.1
30	2.40	1.91	1.21	138	170	1.09	1.08	68	124	119	104	109	8.8	3.6
20	3.08	2.64	1.09	123	180	1.09	1.08	54	125	110	109	110	-15	-6.8
0	∞	∞	1.08	--	180	1.08	1.08	--	--	109	109	109	0	0

a) Geometry optimized at the HF level with the H-Pt-C angle held fixed except for the 89.3° H-Pt-C bond angle, which was the result of a full geometry optimization.

b) Total energies in hartrees at the dissociated limit are -67.641853 for HF, -67.670529 for GVBCI(2/8), and -67.744632 for RCI(4/8)*GVBCI(2/8).

c) H_{Me} is defined to be the center of mass for the three methyl protons. Key:

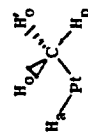


Table B-VI. Geometries and Energetics Along Reaction Path for $\text{Pt} + \text{C}_2\text{H}_6 \rightarrow \text{Pt}(\text{CH}_3)_2$. All angles in degrees; all distances in angstroms; all energies in kcal/mol.

Geometric Parameters ^{a)}														Energies ^{b)}	
CH ₃ - Pt-CH ₃ angle	Pt-C distance	C-C distance	H _{Me} ^{c)} C-Pt(c) angle	H _{Me} ^{c)} C-C(c) angle	C-H _p distance	C-H _o distance	H _p -C-Pt angle	H _o -C-Pt angle	H _p -C-C angle	H _o -C-C angle	H _o -C-H _p angle	H _o -C-H _o angle	HF	GVBC(2/6) GVBC(4/8) ×GVBC-C(2/6)	
90	1.97	3.22	178	150	1.09	1.08	109	110	150	87	109	110	-5.1	-20.3	-10.3
90	1.97	2.97	179	141	1.09	1.08	109	109	154	84	110	110	-4.0	-12.3	-12.9
80	2.00	2.78	175	138	1.09	1.08	107	112	157	85	108	110	1.9	-7.6	-7.5
70	2.03	2.57	170	135	1.10	1.08	103	114	158	84	107	111	15.6	4.6	14.7
60	2.14	2.33	160	135	1.09	1.08	93	118	153	87	108	110	39.5	19.9	19.4
50	2.35	2.14	130	140	1.09	1.08	60	125	124	101	110	110	48.1	37.7	35.2
40	2.69	1.98	118	165	1.09	1.08	49	125	119	105	109	110	28.1	21.2	20.8
30	3.00	1.84	105	173	1.09	1.08	38	123	113	111	107	108	6.1	5.1	5.1
20	4.44	1.55	100	180	1.08	1.09	32	121	112	112	107	107	2.1	1.4	1.9
0	∞	1.54	--	180	1.09	1.09	--	--	111	111	108	108	0	0	0

a) Each geometry optimized at the HF level with the C-Pt-C bond angle held fixed except for the 90° bond angle for which a full geometry optimization was done.

b) Total energies in hartrees at the dissociated limit are -106.662122 for HF, -106.687932 for GVBC(2/6), and -106.762035 for RC(4/8)*GVBC(2/6).

c) H_{Me} is defined to be the center of mass of the methyl protons.

Table B-VII. Effect of Correlation on Reaction Energetics and on Transition State Geometry. a)

All angles in degrees; all energies in kcal/mol.

Reaction	Hartree-Fock		GVB-CI(2/6)		RCI(4/8)×GVB-CI(2/6)	
	ΔE^\dagger	R-M-R [†] angle ΔE	ΔE^\dagger	R-M-R [†] angle ΔE	ΔE^\dagger	R-M-R [†] angle ΔE
$\text{Pd}(\text{H})_2 \rightarrow \text{Pd} + \text{H}_2$	0.3	55.8 -17.6	4.3	44.5 0.4	1.6	-50.6 -3.6
$\text{Pd}(\text{H})(\text{CH}_3) \rightarrow \text{Pd} + \text{CH}_4$	7.2	53.3 -36.5	14.9	49.7 -16.3	10.4	51.3 -20.1
$\text{Pd}(\text{CH}_3)_2 \rightarrow \text{Pd} + \text{C}_2\text{H}_6$	27.5	59.0 -33.0	30.9	56.5 -13.8	22.6	55.8 -16.0
$\text{Pt}(\text{H})_2 \rightarrow \text{Pt} + \text{H}_2$	--	-- 26.2	--	-- 33.8	--	-- 33.6
$\text{Pt}(\text{H})(\text{CH}_3) \rightarrow \text{Pt} + \text{CH}_4$	26.1	44.3 3.7	36.3	40.5 21.2	29.0	42.1 16.1
$\text{Pt}(\text{CH}_3)_2 \rightarrow \text{Pt} + \text{C}_2\text{H}_6$	42.8	52.0 5.1	69.3	49.8 21.7	53.1	49.8 18.3

a) R-M-R[†] denotes angle at transition state.

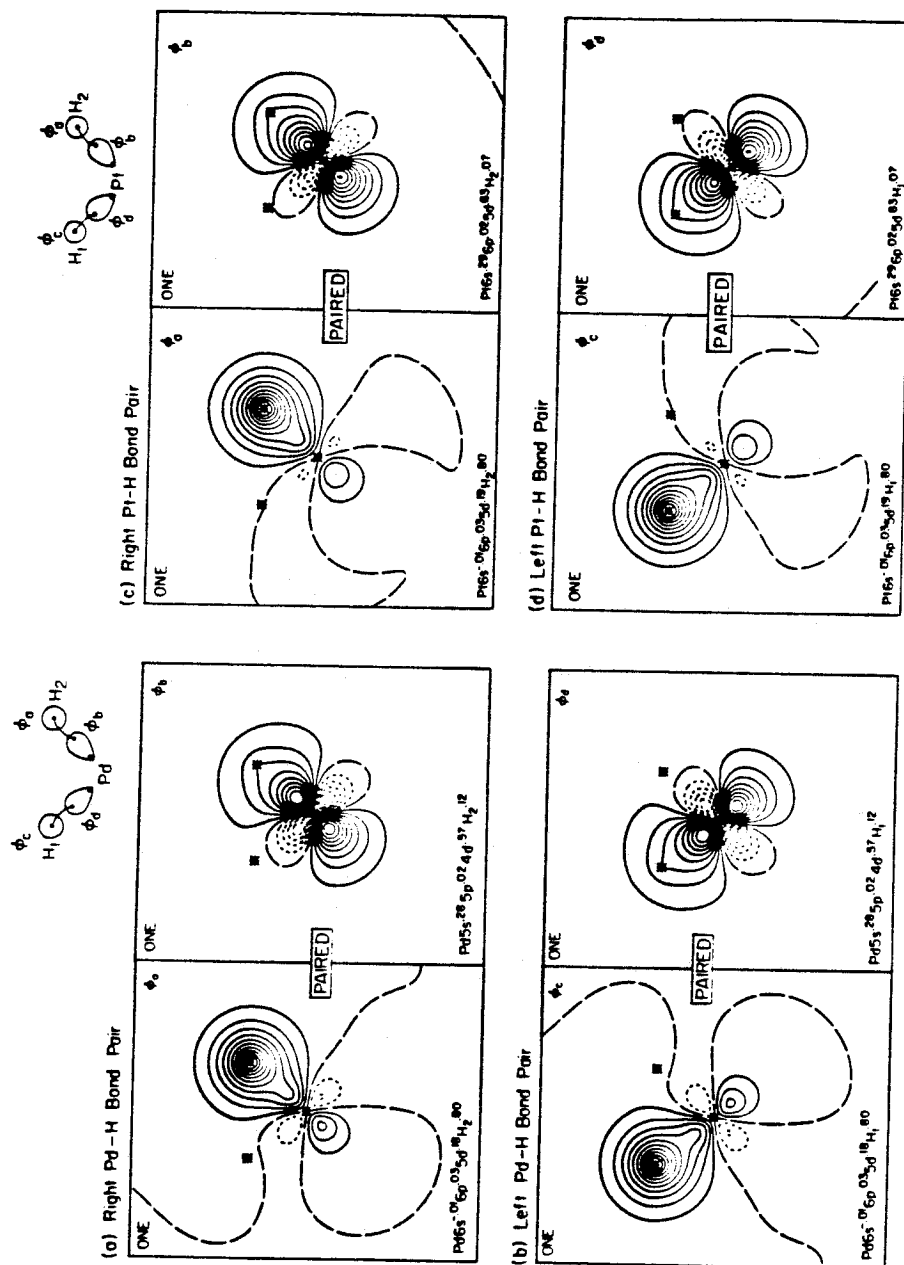


Figure 1. The GVB orbitals for PdH_2 and PtH_2 [from GVB(2/4)-PP calculations]. Nuclei in the plane are indicated by asterisks. Positive contours are solid, negative contours are dotted, and nodal lines are long dashes. The spacing between contours is 0.05. Each GVB orbital is analyzed in terms of a Mulliken population.

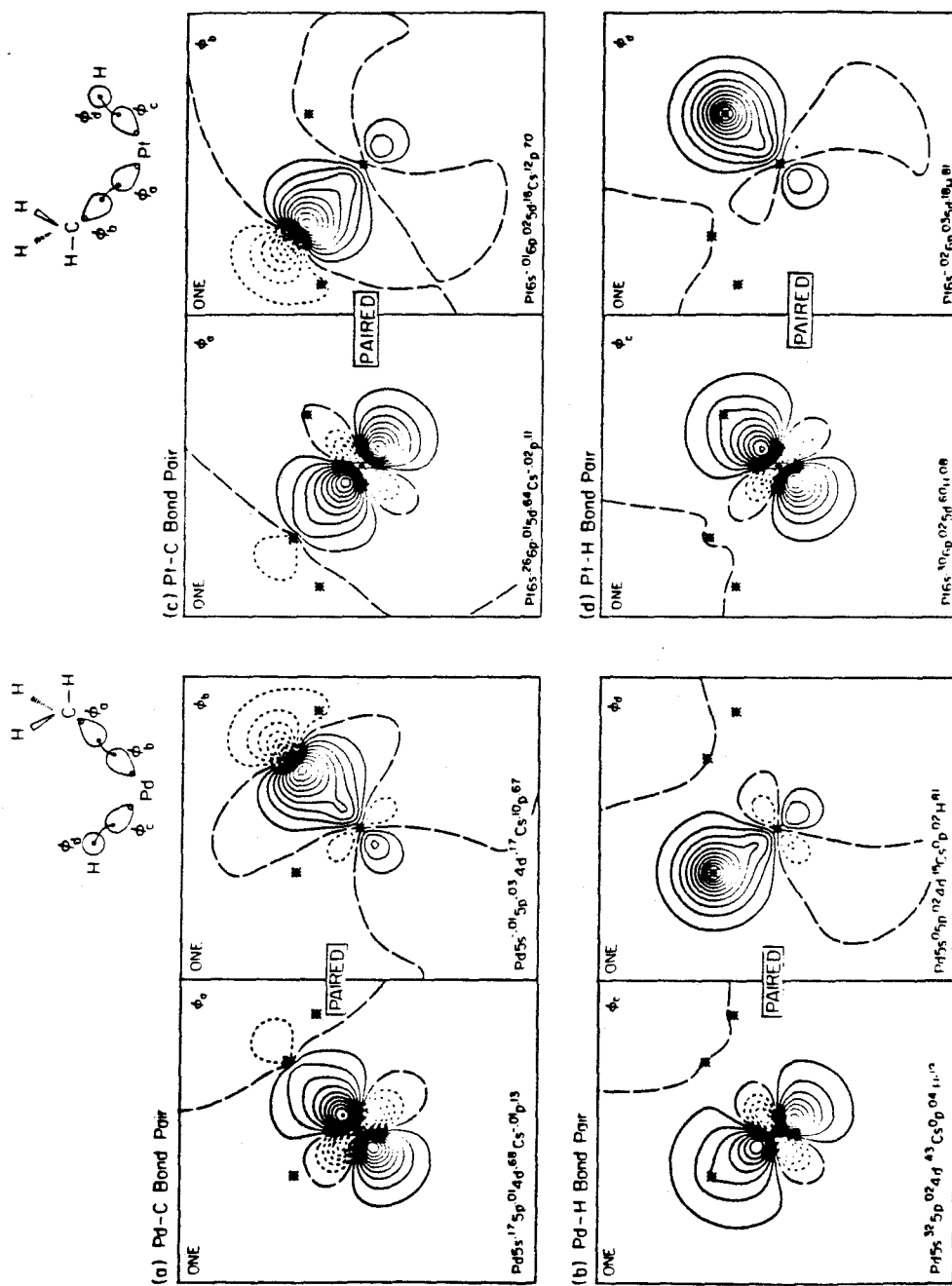


Figure 2. The GVB orbitals for $\text{PdH}(\text{CH}_3)$ and $\text{PtH}(\text{CH}_3)$ based on GVB(2/4)

calculations.

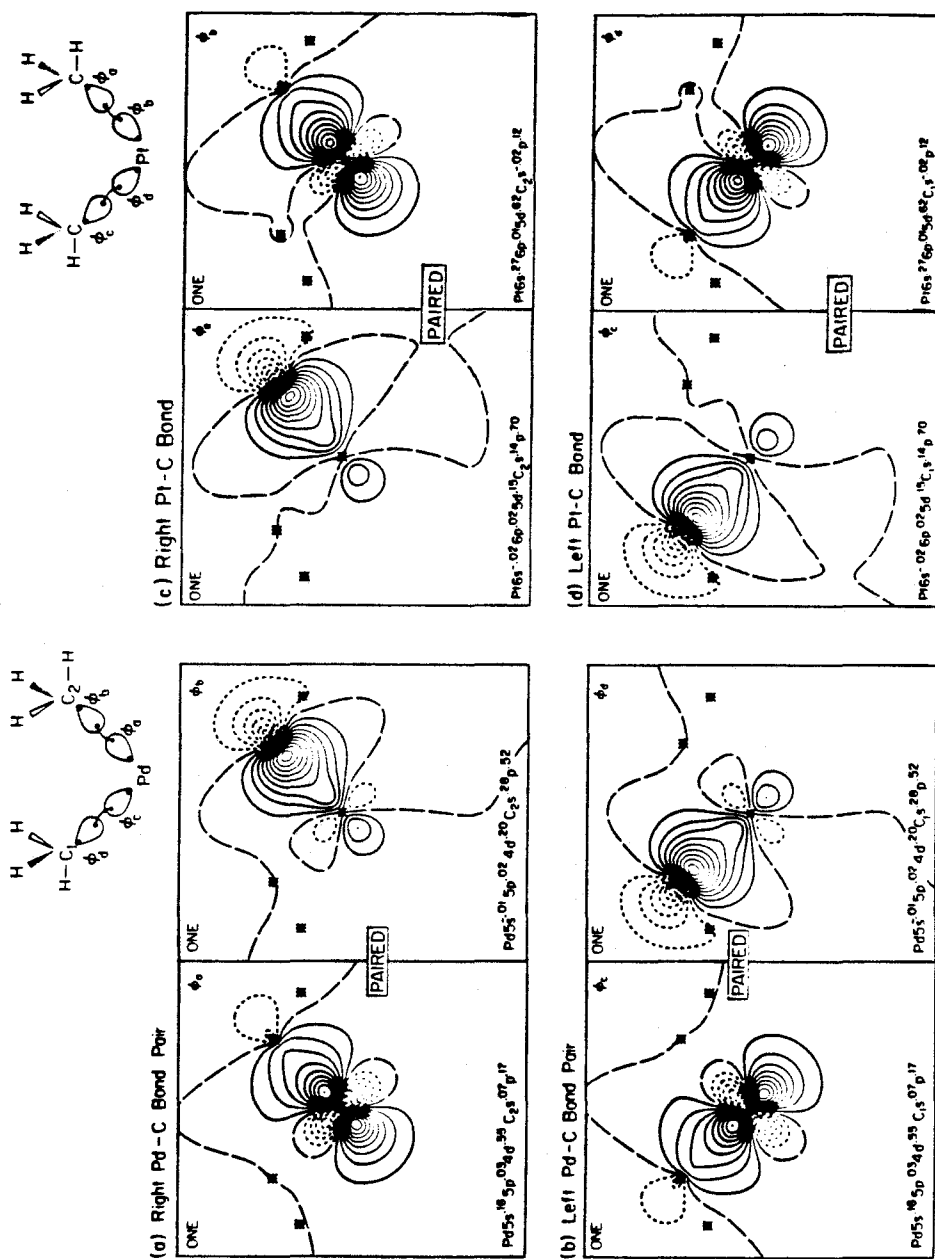


Figure 3. The GVB orbitals for $\text{Pd}(\text{CH}_3)_2$ and $\text{Pt}(\text{CH}_3)_2$ based on GVB(2/4) calculations.

Reactants	Transition State	Products
$\begin{array}{c} 1.51\text{\AA} \quad \text{H} \\ \diagdown \quad \\ \text{Pd} \quad 73^\circ \quad 1.73\text{\AA} \\ \diagup \quad \\ \text{H} \end{array}$ <p>0 kcal/mol</p>	$\begin{array}{c} 1.55\text{\AA} \quad \text{H} \\ \diagdown \quad \\ \text{Pd} \quad 51^\circ \quad 1.33\text{\AA} \\ \diagup \quad \\ \text{H} \end{array}$ <p>$\Delta E^\ddagger = 1.55 \text{ kcal/mol}$</p>	$\begin{array}{c} \text{H} \\ \\ \text{Pd} + \text{H} \end{array}$ <p>$\Delta E_r = -3.55 \text{ kcal/mol}$ 0.734 Å</p>
$\begin{array}{c} 1.52\text{\AA} \quad \text{H} \\ \diagdown \quad \\ \text{Pd} \quad 80^\circ \quad 2.39\text{\AA} \\ \diagup \quad \\ 1.95\text{\AA} \quad \text{CH}_3 \end{array}$ <p>0 kcal/mol methyl tilt = 7.8°</p>	$\begin{array}{c} 1.55\text{\AA} \quad \text{H} \\ \diagdown \quad \\ \text{Pd} \quad 51^\circ \quad 1.57\text{\AA} \\ \diagup \quad \\ 1.99\text{\AA} \quad \text{CH}_3 \end{array}$ <p>$\Delta E^\ddagger = 10.4 \text{ kcal/mol}$ methyl tilt = 25°</p>	$\begin{array}{c} \text{H} \\ \\ \text{Pd} + \text{CH}_3 \end{array}$ <p>$\Delta E_r = -20.1 \text{ kcal/mol}$ 1.08 Å</p>
$\begin{array}{c} 1.96\text{\AA} \quad \text{CH}_3 \\ \diagdown \quad \\ \text{Pd} \quad 92^\circ \quad 2.82\text{\AA} \\ \diagup \quad \\ \text{CH}_3 \end{array}$ <p>0 kcal/mol methyl tilt = 4.5°</p>	$\begin{array}{c} 2.25\text{\AA} \quad \text{CH}_3 \\ \diagdown \quad \\ \text{Pd} \quad 56^\circ \quad 2.11\text{\AA} \\ \diagup \quad \\ \text{CH}_3 \end{array}$ <p>$\Delta E^\ddagger = 22.6 \text{ kcal/mol}$ methyl tilt = 39°</p>	$\begin{array}{c} \text{CH}_3 \\ \\ \text{Pd} + \text{CH}_3 \end{array}$ <p>$\Delta E_r = -15.95 \text{ kcal/mol}$ 1.54 Å</p>

Figure 4. Summary of geometries and energetics for $\text{Pd} + \text{H}_2 \rightarrow \text{PdH}_2$,
 $\text{Pd} + \text{CH}_4 \rightarrow \text{PdH}(\text{CH}_3)$, and $\text{Pd} + \text{C}_2\text{H}_6 \rightarrow \text{Pd}(\text{CH}_3)_2$ based on GVB-
 RC(4/8)×GVBCI(2/6) calculations.

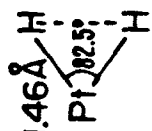
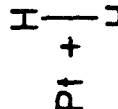
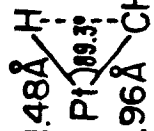
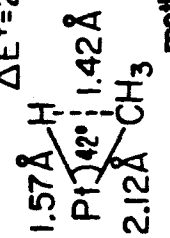
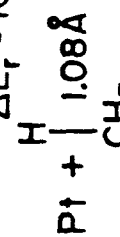
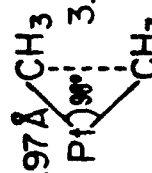
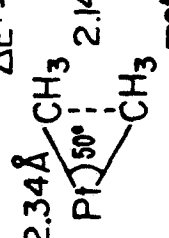
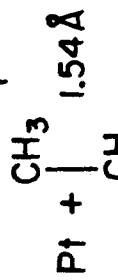
Reactants	Transition State	Products
0 kcal/mol 		$\Delta E_r = 33.6 \text{ kcal/mol}$ 
0 kcal/mol 	$\Delta E^\ddagger = 29.0 \text{ kcal/mol}$ 	$\Delta E_r = 16.1 \text{ kcal/mol}$ 
0 kcal/mol 	$\Delta E^\ddagger = 53.5 \text{ kcal/mol}$ 	$\Delta E_r = 18.3 \text{ kcal/mol}$ 

Figure 5. Summary of geometries and energetics for $\text{Pt} + \text{H}_2 \rightarrow \text{PtH}_2$, $\text{Pt} + \text{CH}_4 \rightarrow \text{PtH}(\text{CH}_3)$, and $\text{Pt} + \text{C}_2\text{H}_6 \rightarrow \text{Pt}(\text{CH}_3)_2$ based on GVB-RCI(4/8)×GVBCI(2/6) calculations.

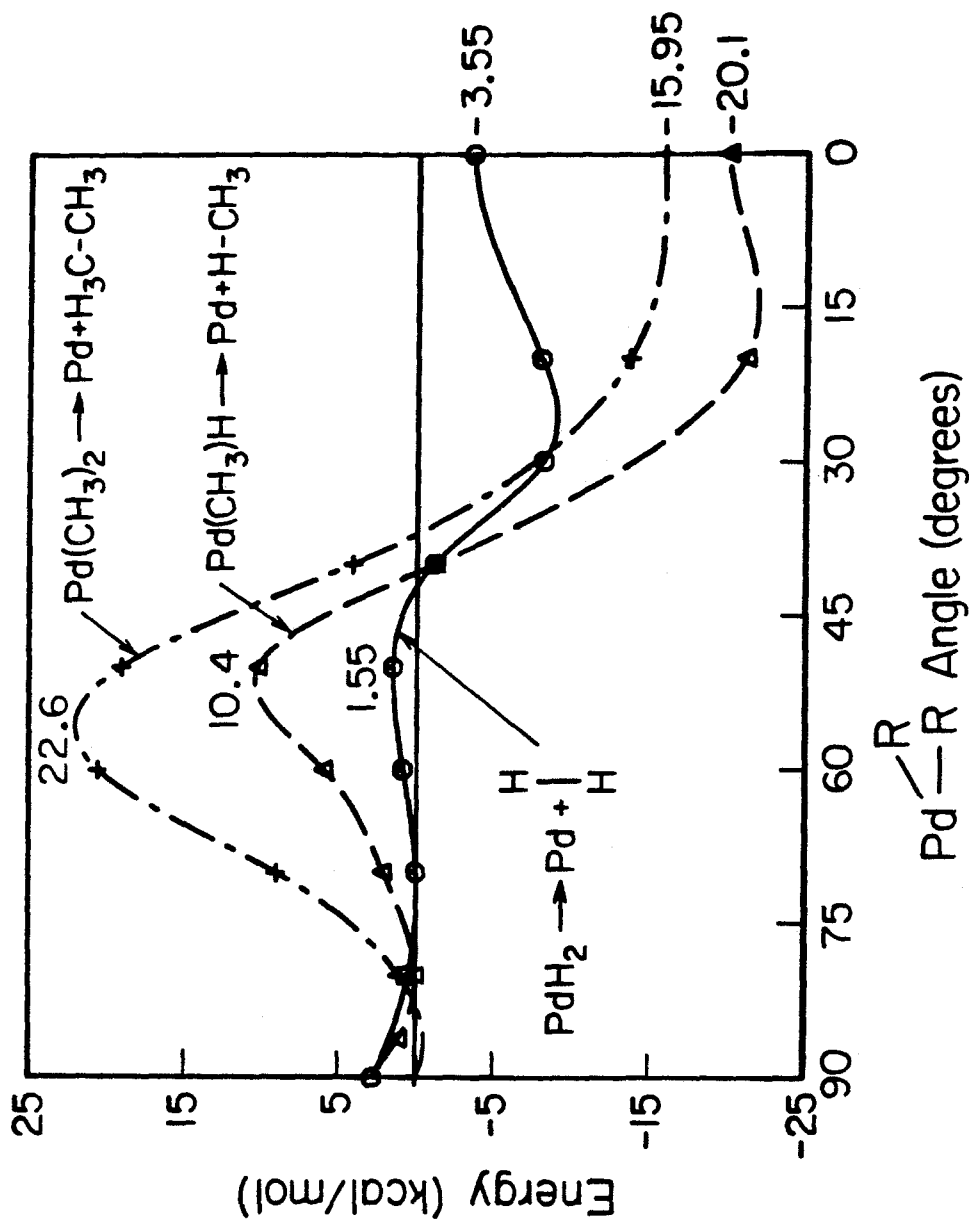


Figure 6. Potential curves for $\text{Pd} + \text{H}_2 \rightarrow \text{PdH}_2$, $\text{Pd} + \text{CH}_4 \rightarrow \text{PdH}(\text{CH}_3)$, and $\text{Pd} + \text{C}_2\text{H}_6 \rightarrow \text{Pd}(\text{CH}_3)_2$ based on GVB-RCI(4/8)×GVBCI(2/6) calculations.

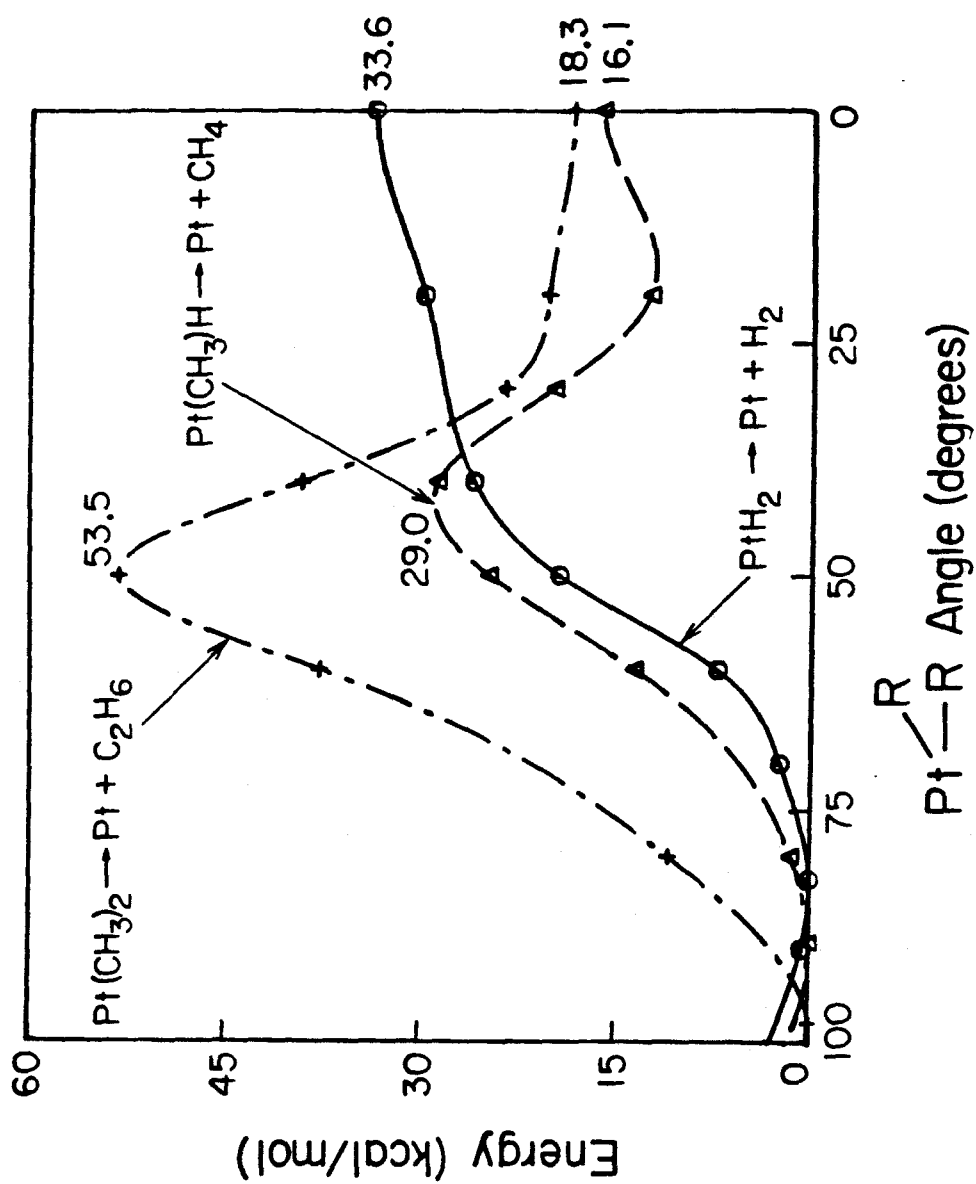


Figure 7. Potential curves for $\text{Pt} + \text{H}_2 \rightarrow \text{PtH}_2$, $\text{Pt} + \text{CH}_4 \rightarrow \text{PtH}(\text{CH}_3)$, and $\text{Pt} + \text{C}_2\text{H}_6 \rightarrow \text{Pt}(\text{CH}_3)_2$ based on GVB-RCI(4/8)×GVBCI(2/6) GVB-RCI calculations.

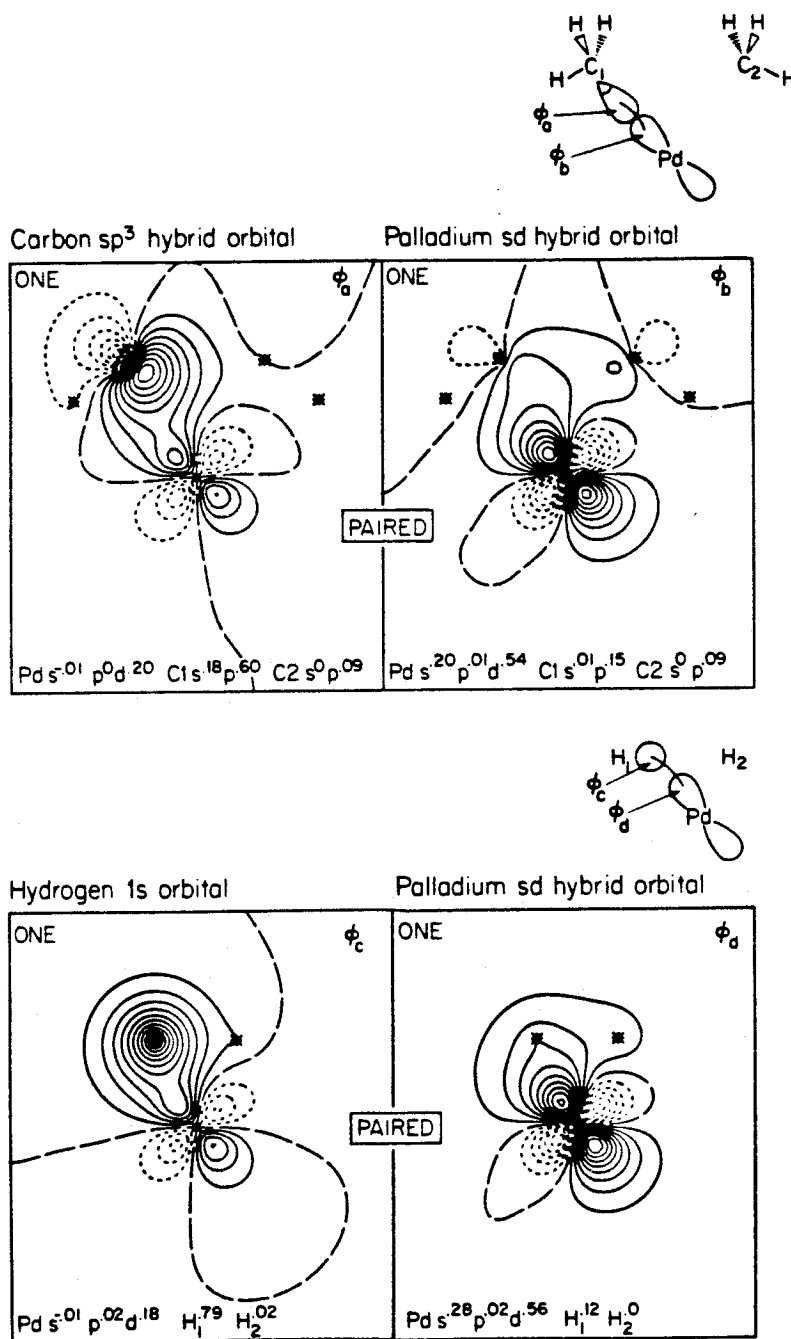


Figure 8. The GVB orbitals for PdH_2 and $Pd(CH_3)_2$ near the transition state for reductive elimination based on GVB(2/4)-PP calculations.

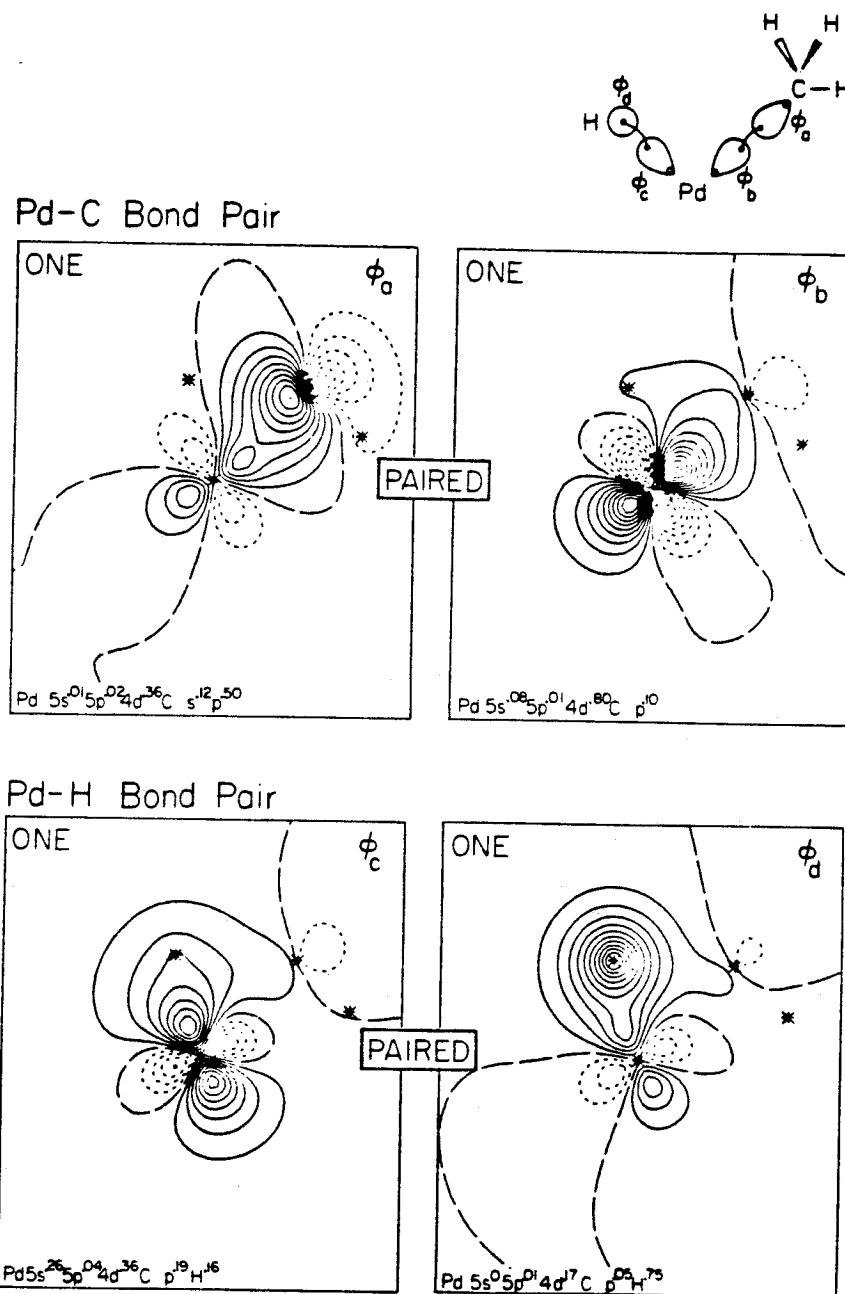


Figure 9. GVB orbitals for PdH(CH₃) near the transition state for reductive elimination based on GVB(2/4)-PP calculations.

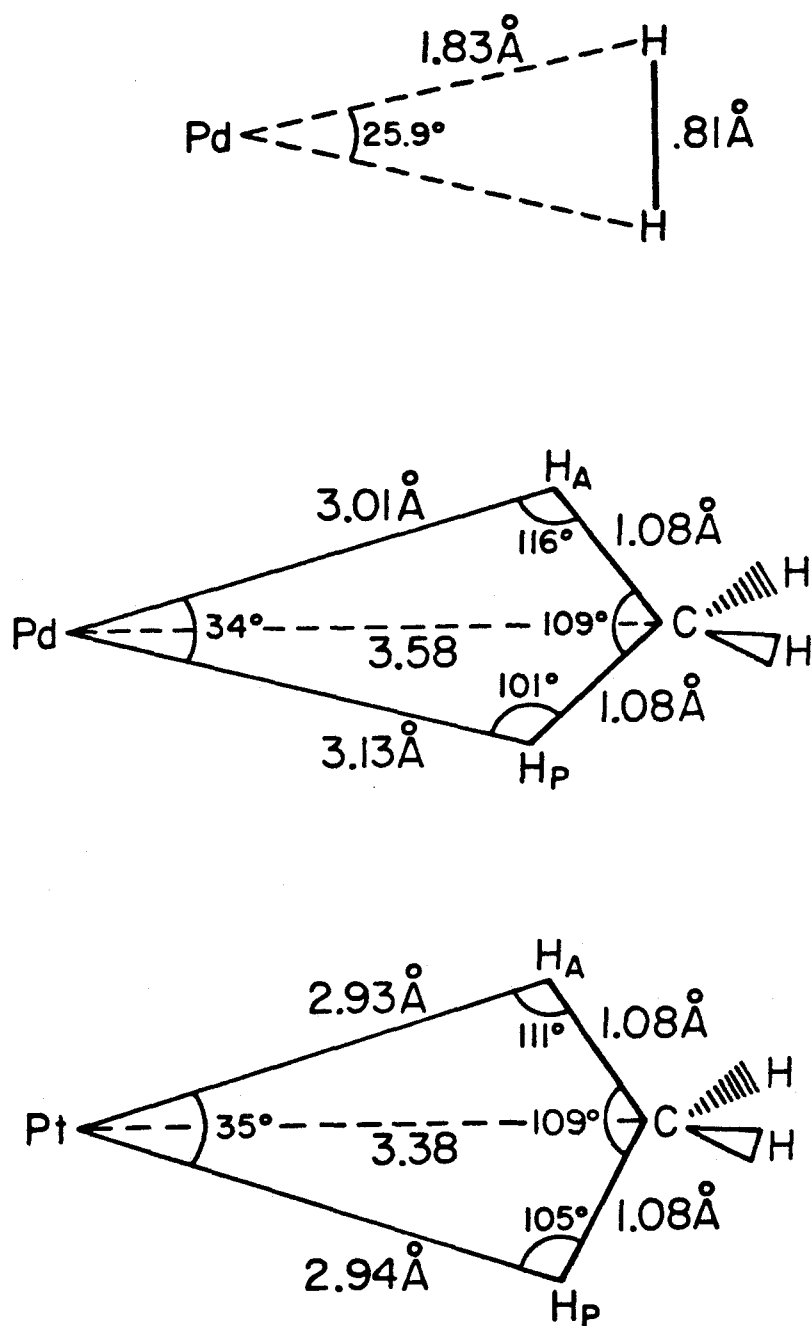


Figure 10. Geometries of Lewis acid/Lewis base complexes of Pd + H₂, Pd + CH₄, and Pt + CH₄. The bond energy with respect to dissociation is 5, 2, and 4 kcal/mol, respectively.

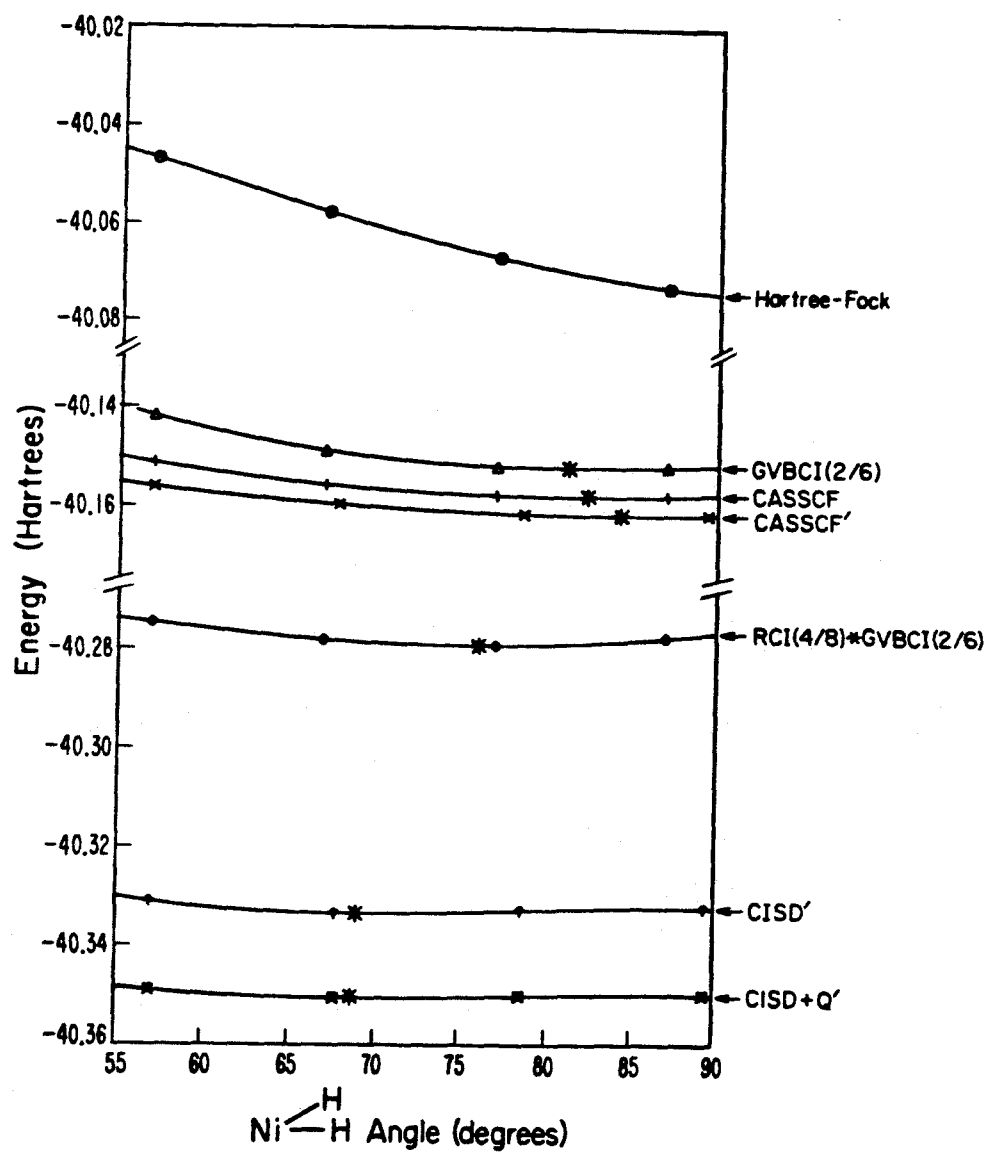


Figure 11. Total energy versus H-Ni-H angle for the lowest singlet state (1A_1) of NiH_2 . The asterisks mark the minimum of each curve. The HF minimum is at 99° (off the scale plotted here).

CHAPTER 3

Theoretical Studies of Oxidative Addition and Reductive Elimination:

III. C-H and C-C Reductive Coupling from

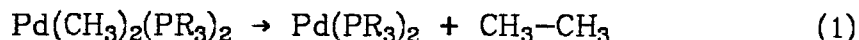
Pd and Pt Bisphosphine Complexes

The following chapter has been submitted for publication to the *Journal of the American Chemical Society*.

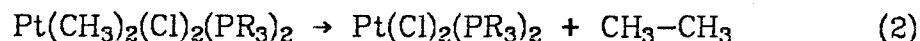
I. Introduction

In spite of the importance of oxidative addition and reductive elimination in organometallic chemistry,¹ a fundamental understanding of the electronic structure of these reactions is only just emerging.²⁻⁵ Focusing only on Pd and Pt complexes, some of the experimental observations are:

- (i) C-C coupling from Pd dialkylbisphosphines⁶

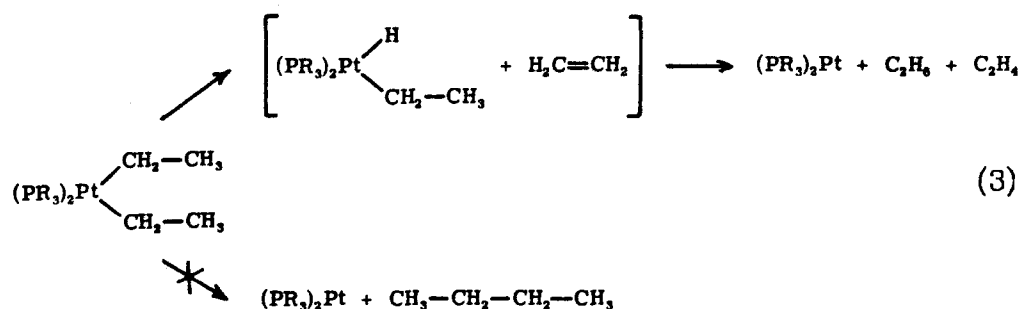


and from dimethyl, trimethyl and tetramethyl Pt(IV)⁷ complexes, e.g.,



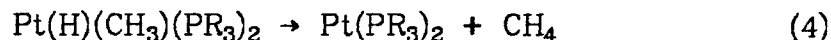
is intramolecular and consistent with a concerted process. Conversely,

- (ii) Pt dialkyls tend to decompose through β -hydride elimination⁸ if this pathway is available, even though direct C-C reductive coupling is thermodynamically favored (by 11 kcal/mol):⁹



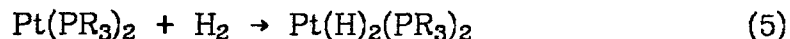
- (iii) $\text{Pt}(\text{CH}_3)_2(\text{PR}_3)_2$ complexes are thus very stable and have never been observed to undergo reductive elimination,¹⁰ while

- (iv) Pt(II) biphenyls, on the other hand, reductively couple to form C-C bonds.¹¹
- (v) In contrast, reductive H-C coupling occurs readily from Pt(II) complexes,^{12,13}



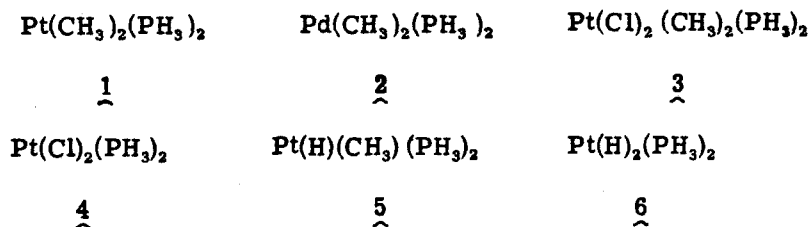
and presumably would also occur from analogous Pd(II) and Pt(IV) complexes should they be formed.

- (vi) On the other hand, the reverse (oxidative addition) reaction to (1), (2), and (4) has not been observed and oxidative addition has been observed¹⁴ only for



[and not for the analogous Pd(II) species].

In order to elucidate the general trends about reductive elimination/oxidative addition, we have carried out ab initio calculations for the species



and for the reductive coupling products



These data plus the results from previous studies² on the transition states and barriers for reductive coupling from Mt(H)_2 , $\text{Mt(H)(CH}_3\text{)}$, and $\text{Mt(CH}_3\text{)}_2$ complexes (where $\text{Mt} = \text{Pd, Pt}$) are used to estimate the energet-

ics and barriers for various reductive coupling processes in Pd and Pt bisphosphine complexes.

II. Summary of Results

A. *Nature of the Chemical Bonds*

As a basis for understanding the differences in energetics for C-C, C-H, and H-H reductive coupling from Pt(II), Pd(II), and Pt(IV) complexes, we first develop a qualitative picture for the bonding in these systems.

1. **Mt(II) Systems**

The Mt-CH₃ bond orbitals (from GVB calculations) of **1**, **2**, **3**, and **5** are shown in Figures 1-4, the Pt-Cl orbitals of **3** and **4** are shown in Figures 5 and 6, and the Pt-H orbital of **5** is shown in figure 4. The GVB orbitals are analyzed in terms of Mulliken populations in Table I and in Figures 1-6; total populations are given in Table II. The overall qualitative description is as follows:

- (1) The Mt-CH₃ bonds are covalent, with one electron in an sp³ hybrid orbital on the CH₃ and one electron in an spd hybrid orbital (60% to 75% d) mainly on the metal,
- (2) The Mt-H bonds are covalent, with one electron in an H 1s orbital and one electron in an spd hybrid orbital on the metal,
- (3) The Mt-Cl bonds are partially ionic, with one electron in a Cl p_z orbital and the other electron in an orbital that is partly on the Cl and partly on the metal (spd hybrid with 30% to 50% d character),
- (4) There are generally about ten electrons on the metal with character corresponding to either
 - (i) the atomic d¹⁰ configuration for **7** and **8** [generally denoted as Mt(0)],

- (ii) the atomic s^1d^9 configuration for **1**, **2**, **4**, **5**, and **6** [generally denoted as Mt(II)], or
- (iii) the atomic s^2d^8 configuration for **3** [generally denoted as Mt(IV)].

This focus on the ten-electron atomic configuration on the metal arises naturally from the generalized valence bond description, and we find that it provides a means for quantitative comparison of the various reaction energetics.

A more quantitative analysis of the character in the GVB orbitals is as follows (see Tables I and II). For the Pt-CH₃ bond of **1**, the metal orbital is 82% on the Pt and 17% on the C. The metal part of this orbital is 60% d, 28% s and 12% p character, very similar to other Mt-C and Mt-H bonds.¹⁵ The methyl orbital of the Pt-CH₃ bond pair is 89% on the C atom (18% s and 71% p or s^1p^4). The HCH bond angles (108°, 108° and 110°) are very close to the tetrahedral bond angles expected for sp^3 carbon. These orbitals are similar to the bond orbitals of Pt(CH₃)₂, where the metal orbital has 90% Pt character (69% d, 30% s and 1% p). The carbon in the methyl group in this complex is also sp^3 -like (18% s and 71% p or s^1p^4), with H-C-H bond angles of 109°, 109° and 110°. ^{2c} The preference for ~60% d character in covalent metal-carbon and metal-hydrogen bonds was also observed in Ti(H)₂(Cl)₂ [74%] and Zr(H)₂(Cl)₂ [58%] and has been rationalized in terms of maximal lowering of kinetic energy.¹⁵

The major effect of the phosphines here is to decrease the Pt d character (69% to 60%) and Pt s character (30% to 28%), to increase the Pt p character (1% to 12%), and to increase the charge transfer to the methyl (0.06 e⁻ to 0.13 e⁻). These changes arise because each phosphine lone pair forms a Lewis base/Lewis acid bond to the Pt by overlapping the

empty valence s and p space of the metal atom. Thus the $\text{Mt}(\text{PH}_3)_2$ complex favors the d^{10} configuration. However, with five doubly-occupied d orbitals, the d^{10} configuration cannot form covalent bonds to CH_3 or H ligands. Thus, in order to add to H-H, H-C, or C-C bonds, the metal must be promoted from d^{10} to s^1d^9 . With two singly-occupied orbitals (one s and one d that may be hybridized to form two sd hybrids pointing at 90° to each other), the s^1d^9 state can form the requisite pair of covalent bonds. The singly-occupied sd bonding orbitals must become orthogonal to phosphine lone pairs [not required for $\text{Mt}(\text{CH}_3)_2$], which they do by mixing in p character. This destabilization by the phosphines of the metal bonding orbitals makes them easier to ionize and thereby increases the ionic character of the M-C bonds.

Although Mulliken populations are always somewhat ambiguous in identifying the absolute location of charges [e.g., the dipole moment for PtH indicates that Pt is positively charged (Pt^+H^-) by an amount corresponding to a transfer of $0.26 e^-$ to H, whereas the Mulliken population indicates a positive charge on H of $0.1 e^-$],^{2a} we find these populations useful for comparisons with related systems. From Table II the total populations indicate that each phosphine in **1** is essentially neutral ($-0.06 e^-$ total charge). The total populations on the Pt for **1** lead to $(sp)^{0.73}(d)^{8.89}$, reasonably consistent with the characterization as s^1d^9 . The description of the two M-C bonds as covalent is in reasonable agreement with the Pauling electronegativities¹⁶ (2.2 for Pt and 2.5 for carbon).

Changing the metal atom from Pt in **1** to Pd in **2** leads to a small increase in charge transfer to CH_3 ($0.13 e^-$ versus $0.20 e^-$) and to PH_3 ($0.06 e^-$ versus $0.10 e^-$), to decreased sp population ($0.73 e^-$ versus 0.33

e^-), and to a slight increase in d population (8.89 e^- versus 9.09 e^-). These differences indicate that Pd has essentially the same electronegativity as Pt (the Pauling scale assigns both as 2.2) and that Pd is biased toward d^{10} relative to s^1d^9 . (This is expected since the ground state of Pd atom is d^{10} , while that of Pt is s^1d^9 .) The character of the GVB orbitals reflects these differences. Thus, comparing 1 (Pt) and 2 (Pd), the metal part of the Mt-CH₃ bond orbital has 0.17 e^- versus 0.24 e^- on the C, while the M sp character decreases by 0.09 e^- and the percentage d character on the metal part of the orbital increases from 60% to 67%.

Comparison of 1 and 4 allows us to analyse the differences between Pt-CH₃ and Pt-Cl bonds. The net effect of replacing both CH₃ by Cl is to decrease the charge on each PH₃ by 0.14 e^- and to decrease the charge on Pt by 0.07 e^- . Comparing the GVB orbitals, we see that the metal orbital is 27% on the Cl (versus 17% on the CH₃) and that the percent d character of the metal part decreases from 60% to 51%. As would be expected, the Cl-like GVB orbital is nearly pure p character (95%) with very little metal character (3%).

Summarizing, all complexes that would be described as Mt(II) in the normal oxidation state formalism are unoxidized and have s^1d^9 character on the metal. Thus *oxidative addition* of these metals to H-H, H-C, and C-C bonds is *not oxidative!* In the GVB description, we think of the two singly-occupied orbitals (s and d) as combined into sd hybrids (pointing at 90° from each other) and covalently paired with the singly-occupied ligand orbital (H, CH₃, or Cl) to form a covalent bond pair. The presence of phosphines leads to destabilization of the M s orbital, with a concomitant increase in p character and increased charge transfer to the ligand. Thus we use the notation Mt(II) to indicate the configuration (s^1d^9) capa-

ble of forming two covalent bonds.

2. **Mt(IV) Systems**

Before considering the Pt(IV) complex **3**, it is appropriate to examine the GVB description of the s^2d^8 state of Pt (and Ni and Pd). In the d^{10} state of Pt, the Hartree-Fock (HF) description has five doubly-occupied valence orbitals, while the GVB description leads to five pairs of orbitals, each of which involves two overlapping orbitals of the same character (e.g., d_{zz}) orthogonal to the other four pairs. In each pair, one of these orbitals is more compact and the other is more diffuse (reflecting the tendency of the electrons to correlate their motions so as to reduce electron-electron interaction while keeping the electrons close to the nucleus). Thus GVB describes d^{10} in terms of ten orbitals for the ten electrons, while HF uses five orbitals. However, since the GVB orbitals within each pair have a high overlap ($S = 0.91$) and similar shape, the GVB description leads to the same qualitative description as HF, and we discuss the d^{10} state as if there were five doubly-occupied orbitals.

For the s^1d^9 configuration, the ground state is 3D , which in HF is described with four doubly-occupied d orbitals, a singly-occupied d orbital, and a singly-occupied s orbital (a total of six). In the GVB description, each of the four doubly-occupied HF orbitals leads to a pair of highly overlapping GVB orbitals so that GVB again has ten orbitals for the ten electrons. Although the shapes of the singly-occupied orbitals change slightly between HF and GVB, there is again no qualitative difference in the description of the s^1d^9 state.

However, for s^2d^8 , there is a qualitative difference between HF and GVB. Here the ground state is 3F , leading in HF theory to three doubly-occupied d orbitals, a doubly-occupied s orbital, and two singly-occupied

d orbitals, for a total of six. In the GVB description there are once again ten orbitals with three pairs of highly overlapping d orbitals (corresponding to the HF pairs), two singly-occupied d orbitals, and a pair of orbitals corresponding to the HF s pair. However, this last pair of GVB orbitals differs remarkably from HF, leading to sp hybrids as shown in Figure 7. The overlap for this pair is 0.75, but most significantly these sp hybrids point to opposite sides of the atom so that they can *each participate in separate covalent bonds*. This is quite analogous to the situation in Zn, Cd, and Hg, where the valence s pair can make two covalent bonds (say to CH₃'s), leading to a 180° bond angle. Indeed, the triplet state of PtH₂, Pt(CH₃)₂, and PtCl₂ should be linear, being formed by bonding to these sp hybrids, leaving a d⁸ configuration (probably ³Δ). [For Ni there should also be similar strongly bound triplet states; however, for Pd the very high energy of the s²d⁸ state may lead to unstable triplet states.] Of course the two singly-occupied d orbitals can also be used for bonding, leading to a total of *four* possible covalent bonds for Pt s²d⁸. Electronegative ligands favor bonding to the sp hybrid orbital¹⁷ since the ionization potential of the s orbital is 2.79 eV lower (leading to Pt⁺ s¹d⁸) than the d orbital (leading to Pt⁺ s²d⁷). Thus in **3** we expect the Pt-Cl bonding to favor Pt sp, while Pt-CH₃ should favor Pt d. In addition, bonding both Cl to sp orbitals should favor trans Cl ligands.

Indeed, the geometry of **3** is essentially octahedral (vide infra). (We have assumed the Cl as trans and the CH₃ groups as cis.) Comparing the Mt-Cl bonds in **4** and **3** we see an increase in ionic character for **3** (for the metal-like orbital the number of electrons on the Cl increases from 0.27 e⁻ to 0.37 e⁻). Concomitantly, the d character on the metal part of the metal orbital decreases from 52% to 32%, while the ratio of p to s

increases from 2/3 to 4/3. Comparing the Mulliken populations in **1** and **3**, we see a slight change in polarity from Pt^+C^- to Pt^-C^+ , while remaining essentially covalent (the Pt component of the metal orbital increases from 0.82 to 0.93 e^- , while the component of C character of the methyl orbital decreases from 0.89 to 0.78 e^-). Simultaneously, the d character in the metal part of the bond pair increases dramatically (60% to 74%), as expected.

To simplify the description we will refer to the Pt-C bond in **3** as a *covalent* bond to a Pt 5d orbital and the Pt-Cl bond as a *partially ionic* bond to a Pt 6sp hybrid orbital. In this simplified picture we visually represent the Pt(IV) complexes as having the Pt atom promoted to the s^2d^8 configuration, having two sp hybrid pairs as in Mg, Al, and Si,



(6)

This state is the only one that can allow Pt atom to form four covalent bonds, two bonds to singly-occupied d orbitals and two bonds to the pair of sp lobe orbitals.¹⁸

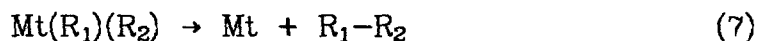
The Mulliken populations for **3** are ambiguous in assigning the electronic configuration of Pt atom. Significant amounts of charge transfer from the Pt sp orbitals to the chlorines (0.56 e^-) and from the methyl groups to the Pt d orbitals (0.28 e^-) make Pt atom appear intermediate between s^2d^8 and s^1d^9 (8.33 e^- in d orbitals and 1.12 e^- in s and p orbitals). Adjusting the Mulliken populations by assigning the excess charge on the chlorines as Pt sp and replacing the charge deficiency on the methyl groups with charge from the Pt $d\pi$ orbitals, we obtain a charge of 1.68 for sp and 8.05 for d, reasonably close to s^2d^8 .

The bonding in this Pt(IV) complex is essentially covalent, which should not be too surprising since the Pauling electronegativity¹⁶ for Pt is 2.2 versus 3.0 for Cl and 2.5 for carbon.

3. Mt(0) Systems

The ground state of Pd(0) is d^{10} , with the (triplet) s^1d^9 configuration 21.9 kcal/mol higher¹⁸ (calculated value 19.6 kcal/mol). The ground state of Pt is s^1d^9 with the d^{10} state 11.0 kcal/mol higher¹⁸ (calculated value 12.3 kcal/mol). For both Pd and Pt, reductive coupling involves s^1d^9 for the reactant and d^{10} for the product, and hence reductive coupling should be more exothermic for Pd than for Pt by $19.6 + 12.3 = 31.9$ kcal/mol (experimental value 32.9 kcal).

The lowest *singlet* state of Pt(0) is d^{10} so that the spin-allowed product of



is d^{10} in both cases. Adding two phosphines stabilizes d^{10} with respect to s^1d^9 so that the ground state of $Mt(PH_3)_2$ is the linear d^{10} singlet for both $Mt = Pd$ and Pt . This stabilization of d^{10} arises from overlap between the phosphine lone pair and the metal valence s orbital. If the Mt s orbital is empty (d^{10}), the phosphine lone pair can donate into this orbital (Lewis base-Lewis acid interaction), leading to extra bonding. If the metal s orbital is occupied, it must be orthogonalized to the phosphine lone pair, increasing the energy. The result is that reductive coupling from $Mt(PH_3)_2$ is about 20-25 kcal/mol more exothermic for both $Mt = Pd$ and Pt .

4. Summary

Our conclusion is that the oxidation state formalism for Pt and Pd

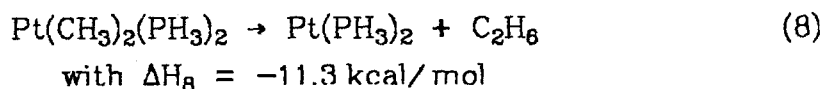
complexes should be interpreted in terms of *maximum covalency rather than degree of oxidation*. Thus, Pt(II) and Pd(II) should be considered as *neutral* atoms with a s^1d^9 configuration forming *two* covalent bonds, while Pt(IV) should be described as a neutral platinum atom in an s^2d^8 configuration forming *four* covalent bonds. We will find this view to be quite useful in rationalizing the relative reaction energetics of Pt(II) versus Pd(II) and of Pt(II) versus Pt(IV) (Section II.C), where appropriate atomic excitation energies provide excellent predictions.

B. Energetics

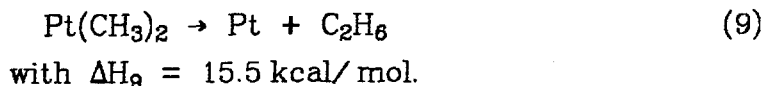
The energetics for various reactions were obtained by calculating GVB correlated wavefunctions (which give accurate s^1d^9 - d^{10} state splittings) at geometries optimized for HF wavefunctions (see Section IV for calculational details). The results are summarized in Table III.

1. Calculated Energetics for C-C Reductive Coupling

Considering C-C coupling processes, we find

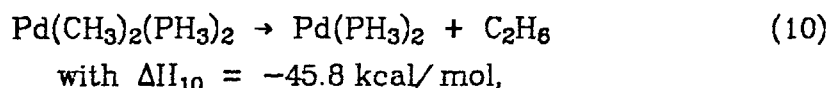


which can be compared to

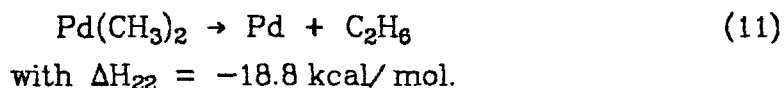


Thus, the presence of two phosphines favors reductive coupling by an extra 26.8 kcal/mol. The reason for this is that the Pt has a s^1d^9 configuration for the reactant side of (8) and (9) but a d^{10} configuration for the product side. As discussed in Section II.A.3, phosphines stabilize d^{10} relative to s^1d^9 , leading to a more exothermic reaction.

Consider next the analogous reactions with Pd,

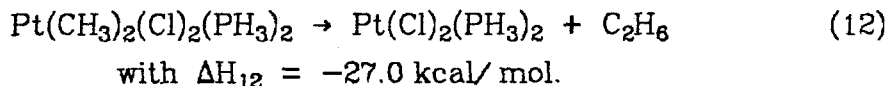


which can be compared to



The reaction enthalpies differ dramatically from those of Pt; however, these differences are easily explained. All four reactions involve converting the metal from s^1d^9 to d^{10} , but using d^{10} as the reference Pt *favors* s^1d^9 by 12.3 kcal/mol, whereas Pd *disfavors* s^1d^9 by 19.6 kcal/mol. Thus, relative to Pt, Pd has a bias against s^1d^9 of 31.9 kcal/mol. Consequently, the driving force for Pd reductive coupling should be exothermic by 31.9 kcal/mol more than for Pt. Indeed, we calculate a difference of 34.5 kcal/mol for the bisphosphine and 34.3 kcal/mol for the unsubstituted metal.

These results for Mt(II) can be compared to the Mt(IV) reaction,



Here the metal changes from s^2d^8 to s^1d^9 , which for the free atom is exothermic by 17.2 kcal/mol. Comparing to reaction (8) involving s^1d^9 to d^{10} , which is endothermic in the atom by 12.3 kcal/mol, we would expect from atomic considerations that (12) should be 29.5 kcal/mol more exothermic than (8). Of course the four-coordinate Pt(II) and six-coordinate Pt(IV) also differ in other respects; however, we find that (12) is 16 kcal/mol more exothermic than (8), so that the atomic change of configuration effects dominate.

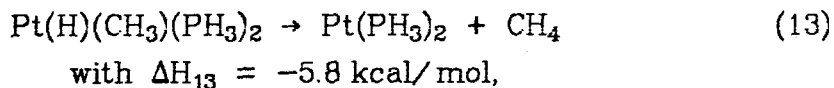
Based on differential atomic excitation energies, the Pd analog of (12) should be exothermic by an extra 45 kcal/mol, leading to a total

exothermicity (ΔE) of about 70 kcal/mol. We estimate that there is no barrier for this decomposition and hence that this species is unstable.

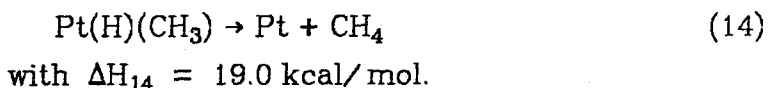
Summarizing, we find that reductive CC coupling is exothermic by 45.8 kcal/mol for Pd(II), by 27.0 kcal/mol for Pt(IV), and by 11.3 kcal/mol for Pt(II), differences that can be understood in terms of the relative atomic energies of s^1d^9 , d^{10} , and s^2d^8 configurations.

2. Calculated Energetics for C-H Reductive Coupling

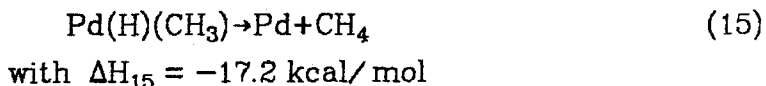
We calculate that



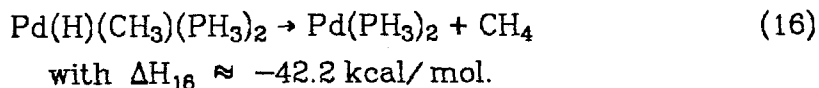
whereas



Thus two phosphines promote H-C reductive coupling by 24.8 kcal/mol, which can be compared with a promotion of 26.8 kcal/mol for C-C reductive coupling on Pt and 27.0 for C-C reductive coupling on Pd. For Pd we studied reductive coupling for the free atoms, finding

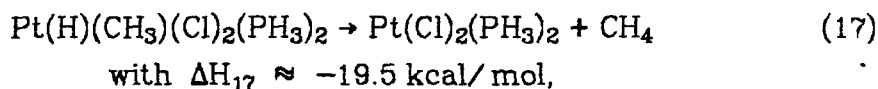


but did not calculate the H-C coupling from the bisphosphine. However, the above results suggest that for Pd the bisphosphine would promote H-C reductive coupling by ~ 25.0 kcal/mol, leading to



We did not calculate the energetics for H-C coupling from Pt(IV) or Pd(IV) complexes; however, comparisons with the C-C coupling cases sug-

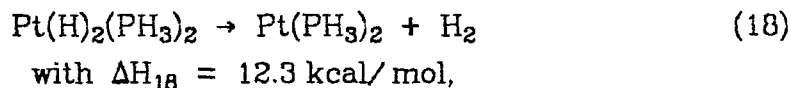
gest that



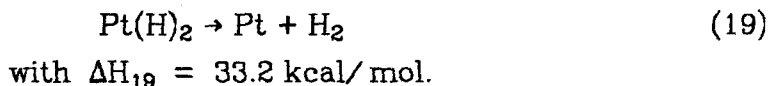
while the analogous Pd complex would not be stable.

3. Calculated Energetics for H-H Reductive Coupling

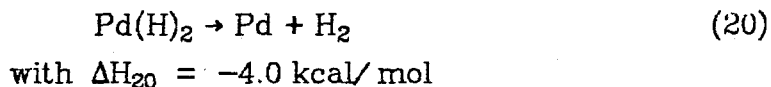
We calculate that



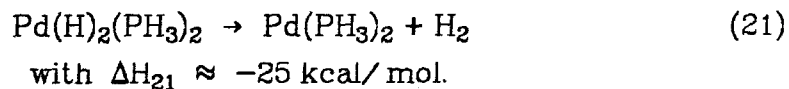
whereas



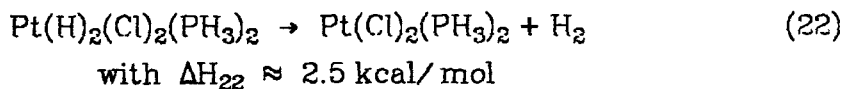
Thus the phosphines promote H-H reductive coupling by 20.9 kcal/mol, which can be compared with 24.8 kcal/mol for H-C and 26.8 kcal/mol for C-C. For Pd we studied reductive coupling from the free atom, finding



but did not calculate the reductive H-H coupling from the bisphosphine. However, the above results suggest that the phosphines would promote H-H coupling on Pd by about 21.1 kcal/mol, leading to



We did not calculate the energetics of H-H coupling from Pt(IV) or Pd(IV) complexes; however, we estimate that



and that the analogous Pd complex is unstable.

4. Adiabatic Bond Energies

Since the C-C bond energy in ethane is 90.4 kcal/mol,¹⁹ the exothermicity of 11.3 kcal/mol for (8) leads to an average Pt-C bond energy of

$$\bar{D}_{298}[(\text{PH}_3)_2\text{Pt}-\text{CH}_3] = 38.6 \text{ kcal/mol.} \quad (23)$$

Similarly, since the H-H bond energy is 104.2 kcal/mol,^{19a} the energetics in (18) correspond to an average Pt-H bond energy of

$$\bar{D}_{298}[(\text{PH}_3)_2\text{Pt}-\text{H}] = 58.3 \text{ kcal/mol.} \quad (24)$$

As a check upon the utility of such average bond energies, we can use (23) and (24) plus the C-H bond energy in CH₄ (105.1 kcal/mol)^{19b} to predict

$$\Delta H_{13} = 39.6 + 58.3 - 105.1 = -7.2 \text{ kcal/mol,}$$

in reasonable agreement with the calculated value of -5.8 kcal/mol.

The average bond energies for the bare metal are obtained from (9) and (19) as

$$\bar{D}_{298}(\text{Pt}-\text{CH}_3) = 53.0 \text{ kcal/mol} \quad (25)$$

$$\bar{D}_{298}(\text{Pt}-\text{H}) = 68.7 \text{ kcal/mol,} \quad (26)$$

which leads to a prediction of

$$\Delta H_{14} = 53.0 + 68.9 - 105.2 = +16.5 \text{ kcal/mol,}$$

in reasonable agreement with the calculated value of $\Delta H_{14} = 19.0$ kcal/mol.

The average bond energies for Pd complexes are calculated to be about 18 kcal/mol lower (see Table IV) because of the propensity for Pd to form d¹⁰ configurations.

Averaging the results for Pd and Pt, we find that M-H bonds are 18 kcal/mol stronger than M-CH₃ bonds for the bisphosphine and 15 kcal/mol stronger for the bare metal. Thus, the phosphines lead to a relative weakening of M-CH₃ versus M-H bonds. This could be simply a steric effect. If so, the bulky phosphines endemic to experiments might have even a greater bias against M-CH₃ bonds.

The Pt(IV) system leads to weaker Pt-CH₃ bonds,

$$\bar{D}_{298}[(\text{Cl})_2(\text{PH}_3)_2\text{Pt}-\text{CH}_3] = 31.7 \text{ kcal/mol.} \quad (27)$$

As discussed above, this 8 kcal/mol decrease from the value for Pt(II) is dominated by the preference of Pt to convert from s²d⁸ to d⁹s¹.

5. Intrinsic Bond Energies

It is often useful to define an *intrinsic bond strength* as the energy to break a bond A-B *without* allowing the fragments to relax. This intrinsic bond strength is then reduced by various relaxation effects that occur in the fragments A and B after the bond is broken. These relaxation effects can involve *geometric relaxation* and *electronic relaxation*. The final bond energy including all these effects is the adiabatic bond energy \bar{D}_{298} . Thus, for example, the C-H bond energy of cyclopropane is 11 kcal/mol stronger²⁰ than for H-CH(CH₃)₂ partly because geometric constraints prevent most of the geometry relaxation in cyclopropane.

A good example for the role of electronic relaxation upon bond energy is in the difference in carbon-carbon double bond strengths in C₂H₄ and C₂F₄.²¹ The double bond requires a singly-occupied σ and π orbital on each carbon corresponding to the ³B₁ state of free CH₂ or CF₂. For CH₂, the triplet state is the ground state and hence the observed (adiabatic) bond energy of 172.2 kcal/mol²² is electronically diabatic (it

involves a small amount of geometric relaxation). However, for CF_2 , the $^3\text{B}_1$ state is 56.6 kcal/mol²³ above the ground state ($^1\text{A}_1$). Thus, if the diabatic C-C double bond energy is assumed unchanged (172.2 kcal/mol), we would expect the adiabatic bond energy in C_2F_4 to be $172.2 - 2(56.6) = 59.0$ kcal/mol. This is in good agreement with the observed bond energy of 69.0 ± 2.7 kcal/mol,²² demonstrating the power in using the concept of electronic relaxation in estimating bond energies.

The adiabatic bond energies calculated in the previous section included both geometrical and electronic relaxation effects. In order to correct the average bond energies for these relaxation effects, we must add the atomic excitation energy ($d^{10} \rightarrow d^9s^1$ or $s^1d^9 \rightarrow s^2d^8$) in the complex to the driving force for reductive elimination. We calculate the energy of the triplet at the geometry of the $\text{Mt}(\text{PH}_3)_2$ [or $\text{MtCl}_2(\text{PH}_3)_2$] fragment in the $\text{MtR}_2(\text{PH}_3)_2$ [or $\text{MtR}_2\text{Cl}_2(\text{PH}_3)_2$] complex. Of course the energy of the $\text{Mt}(\text{PH}_3)_2$ [or $\text{MtCl}_2(\text{PH}_3)_2$] singlet was calculated at the equilibrium geometry. The singlet-triplet splittings calculated with these reference states include all differential relaxation effects which occur during reductive elimination from these complexes. Thus the **intrinsic bond energy** is defined as

$$D_I = \frac{1}{2}[\Delta H(\overline{\text{MR}}_2 \rightarrow \text{M} + \text{R}_2) + \delta E(\text{M} \rightarrow \overline{\text{M}}) + D_{298}(\text{R}-\text{R})], \quad (28)$$

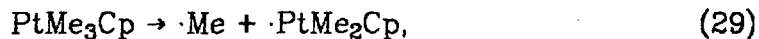
where $\delta E(\text{M} \rightarrow \overline{\text{M}})$ is the singlet-triplet excitation energy described above, M is the singlet metal complex product in its ground state geometry, and $\overline{\text{M}}$ is the triplet state of the same complex frozen at the geometry it had in the reactant complex.

Average bond energies and the relevant state splittings are presented in Table IV. The corrected bond energies show that the *intrinsic* strengths of Pt-C and Pd-C bonds are very similar and that the

relative stability toward reductive coupling is dominated by the relative energies of the s^1d^9 and d^{10} states and of bent versus linear phosphines. Comparing the intrinsic Mt-R bond strengths of bisphosphine complexes [e.g., 56 kcal/mol for $Pt(CH_3)_2(PH_3)_2$] and the corresponding MtR_2 complexes^{2c} (e.g., 47 kcal/mol for $PtMe_2$), indicates that the presence of phosphines strengthens the intrinsic Mt-R bonds by 6-12 kcal/mol. This is because the metal spd hybrid orbitals used to form the M-R bonds must be orthogonalized to the phosphines, leading to an increase in the p character of the metal hybrid. This in turn increases the overlap of the M-R bond,¹⁵ increasing the intrinsic bond strength. On the other hand, the phosphines lead to a decrease in the adiabatic bond energies [from 53 kcal/mol for $Pt(CH_3)_2$ to 40 kcal/mol for $Pt(CH_3)_2(PH_3)_2$]. This is probably because the phosphines greatly favor the d^{10} form of the product.

The intrinsic $Pt(IV)$ -C bond is 5 kcal/mol weaker than the $Pt(II)$ -C bond in bisphosphine complexes. This is probably because the Pt 6s character of the $Pt(IV)$ -C bonds is used up in the Pt-Cl bonds. Consequently, the methyl group in $Pt(IV)$ is forced to bond to metal orbitals that have mainly d character rather than the optimal hybridization¹⁵ (~60% d and 40 % sp) that is available in the $Pt(II)$ bisphosphine complex.

Few bond strengths are known experimentally for Pt-C or Pd-C. From studies of the decomposition of $PtMe_3Cp$,²⁴ an experimental Pt-CH₃ bond energy of 39 ± 5 kcal/mol has been determined. This is an adiabatic bond energy,

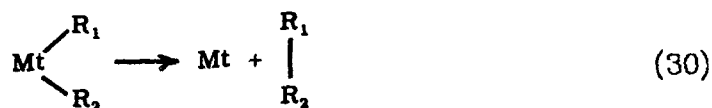


but the Pt atom no doubt retains s^2d^8 -character. Thus the exothermicity of (29) should be less than the intrinsic bond energy (51 kcal/mol) but probably larger than our estimated adiabatic bond strength of 32

kcal/mol, which involves relaxation to s^1d^9 . Thus the theory and experiment are in reasonably agreement.

C. Barriers and Rates

In previous studies of²



where Mt = Pd, Pt and $\text{R}_1, \text{R}_2 = \text{H}$ and CH_3 , we showed that the *intrinsic barrier* (i.e., the barrier exceeding the endothermicity) is

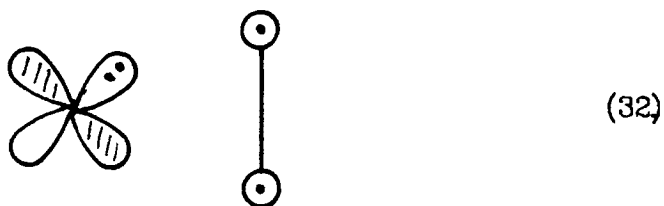
- (i) large for CC coupling (e.g., 23 kcal/mol for Pd, 54 kcal/mol for Pt),
- (ii) intermediate for CH coupling (e.g., 10 kcal/mol for Pd, 29 kcal/mol for Pt), and
- (iii) small for HH coupling (e.g., 2 kcal/mol for Pd).

The origin for such dramatic differences for H-H, H-C, and C-C coupling is found in the shapes of the H 1s and C sp^3 orbitals. At the transition state, the wavefunction involves a mixture of the s^1d^9 resonance structure (31) for the reactant



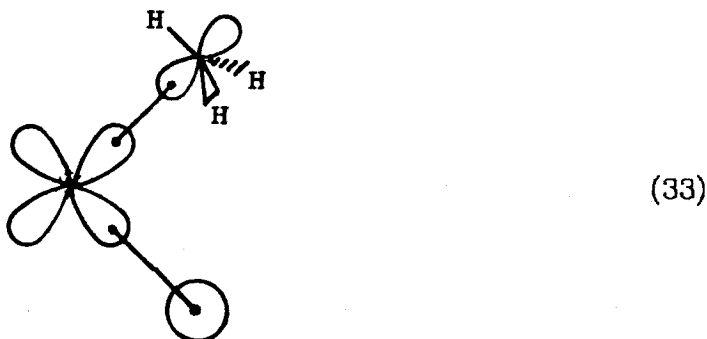
s^1d^9 Resonance Configuration

and the d^{10} resonance structure (32) of the product

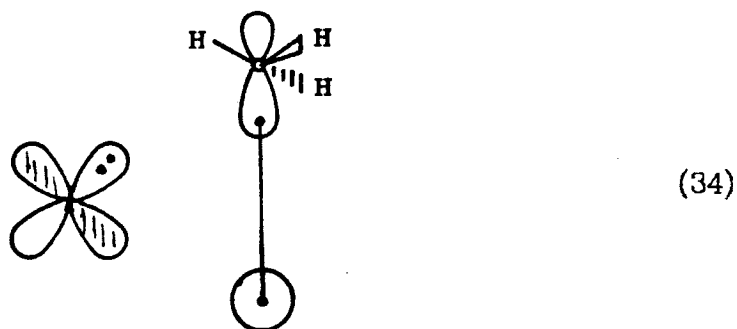


d^{10} Resonance Configuration

Since the H 1s orbital is spherical, it can simultaneously overlap either the Mt sd hybrid orbital in (31) or the valence orbital of the other R group in (32). The result is that these two resonance structures have a high overlap for $R_1 = R_2 = H$, leading to a large resonance stabilization and a low barrier. If $R_1 = H$ and $R_2 = CH_3$, then the directed form of the valence orbital for CH_3 is such that one CH_3 orientation favors (31)



while a *different* CH_3 orientation favors (32)



Consequently, at the transition state the CH_3 group has an intermediate

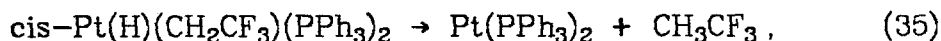
orientation which is less favorable for both (31) and (32), leading to a significant barrier. If $R_1 = R_2 = \text{CH}_3$, then there is a similar problem for *both* ligands, leading to a barrier that is roughly twice as large.

Adding two phosphines to the metal stabilizes the d^{10} state over s^1d^9 , making reductive coupling about 23 kcal/mol more exothermic (27 kcal/mol for H-H, 23 kcal/mol for H-C, and 21 kcal/mol for C-C) and should similarly decrease the activation barrier. Assuming that the transition state involves about equal parts of the d^{10} and s^1d^9 configurations, it is plausible that the barrier will be decreased by about half as much as is the reactive enthalpy. This leads to the estimated activation energies in Table III and Figure 8.

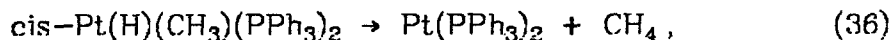
Particularly clean experiments have been carried out for H-C coupling from Pt(II),^{12,13} (13), for which we estimate

$$\Delta H^\ddagger_3 = 15.7 \text{ kcal/mol.}$$

This can be compared to



where in benzene solvents $\Delta H^\ddagger = 24.6 \pm 0.6$ and $\Delta S^\ddagger = 4.9 \pm 2.$, and to



where (in toluene at -25°C) $\Delta G^\ddagger = 18.2$.¹² Assuming $\Delta S^\ddagger \approx 5$, this latter value leads to $\Delta H^\ddagger = 17.0$ kcal/mol, in good agreement with our predictions.

Other relevant activation energies have been measured by Moravskiy and Stille^{6c} for reductive elimination of ethane from cis-Pd(CH₃)₂(PPh₂(CH₃))₂. They find activation energies (E_a) of 6-11 kcal/mol in polar-coordinating solvents (Me₂SO-d₆, Me₂CO-d₆, and CD₃CN) and 25-

28 kcal/mol in aromatic solvents ($C_6D_5CD_3$ and C_6D_6). It is uncertain how to compare these numbers with our calculations since it is likely that reductive elimination does not proceed directly from the bisphosphine complex (see Section III.A). However, we estimate

$$\Delta H_{f0}^\ddagger = 10.4 \text{ kcal/mol}$$

(at 300°K), and hence the estimated barrier (at 300°K) is $E_a = \Delta H_{f0}^\ddagger + RT = 10.7 \text{ kcal/mol}$, surprisingly close to the E_a measured in coordinating solvent.

On the other hand, our estimates lead to

$$\Delta H_8^\ddagger = 41 \text{ kcal/mol}$$

for C-C coupling on Pt(II), certainly consistent with the lack of observation of this reaction.

The calculated endothermicity ($\Delta H_{18} = 12.3 \text{ kcal/mol}$) and barrier ($\Delta H_{18}^\ddagger = 14.0 \text{ kcal/mol}$) for H-H coupling from Pt(II) are consistent with the equilibrium observed in such systems by Trogler.¹⁴ On the other hand, our calculations suggest that $\text{cis-Pd(H)}_2(\text{PH}_3)_2$ and $\text{cis-Pd(H)(CH}_3)(\text{PH}_3)_2$ would have no barrier for decomposition and hence should not be stable.

The estimated barriers for Mt(IV) complexes are much more uncertain since barriers were not calculated even for complexes without phosphines. In this case we have assumed that half of the addition exothermicity relative to Mt(II) goes into the transition state.

Brown *et al.*^{7b} have measured E_a for reductive elimination of ethane from various Pt(IV) trimethyl complexes. They find $E_a = 27.7 \pm 1.2$ for reductive elimination from $\text{PtCl(CH}_3)_3(\text{PMe}_2\text{Ph})_2$ at 353°K. Our estimate is $E_a = 34.9 \text{ kcal/mol}$ ($\Delta H_{f2}^\ddagger = 34.2 \text{ kcal/mol}$) for elimination from

$\text{PtCl}_2(\text{CH}_3)_2(\text{PH}_3)_2$. The good agreement between experiment and theory may be fortuitous since it appears experimentally that the reductive elimination takes place from a five-coordinate intermediate formed by loss of phosphine. Similar estimates for H-H and H-C coupling from Pt(IV) lead to $\Delta H^\ddagger = 9$ kcal/mol for both reactions, indicating rather unstable species. The analogous Pd(IV) complexes are predicted to be unstable.

Experimentally it is known that Pt(II) dimethyl complexes are much more stable than Pd(II) dimethyl complexes, with C-C coupling facile for Pd(II)⁶ and unobserved for Pt(II).¹⁰ In addition, it is known that Pt(IV) dimethyl, trimethyl, and tetramethyl complexes will reductively eliminate ethane,⁷ while Pt(II) dimethyl complexes do not.¹⁰ Our results are consistent with these experimental observations.

As indicated, the theoretical results are consistent with current experimental knowledge concerning reductive coupling and oxidative addition of Pt(II), Pd(II), and Pt(IV) complexes. These experiments can be understood on the basis of the changes in the electronic configuration of the metal plus simple ideas on the relative barriers for C-C versus C-H versus H-H coupling. Given results for one metal, these ideas may be used to predict the results on other metals using only atomic data.

D. Geometries

The geometries for all molecules studied in this work have been optimized for the HF wavefunctions using analytic gradient techniques. The fully optimized HF geometries of **1** $\text{Pt}(\text{Me})_2(\text{PH}_3)_2$, **2** $\text{Pd}(\text{Me})_2(\text{PH}_3)_2$, and **3** $\text{Pt}(\text{Me})_2(\text{Cl})_2(\text{PH}_3)_2$ are shown in Figures 9 and 10, and the calculational details are described in Section IV. The internal coordinates around the metal atom for the complexes studied in this work are presented in Table V. Cartesian coordinates for each molecule are given

in the Appendix. We find very good agreement between our calculated geometries and x-ray structures on related molecules, as described below.

The calculated Pt-C bond distance (2.06 Å) in **1** is very close to the sum of covalent radii¹⁶ (Pt-Csp³) 2.09 Å and is in the range observed in x-ray structures of Pt(II) dialkyl complexes:²⁵ {an average of 2.05 Å in Pt₂Me₄ (μ-dppm)₂^{25c} [dppm = Ph₂PCH₂PPh₂]; 2.18 Å and 2.15 Å in PtMe₂ (tripod) [tripod ≡ 1,1,1-tris(diphenylphosphinomethyl)ethane];^{25a} and 2.05 Å and 2.12 Å in Pt(C₄H₈(PPh₃)₂)^{25b}}.

The calculated C-Pt-C bond angle in **1** of 89° is ~10° larger than the C-Pt-C angles observed in the x-ray structure of Pt₂Me₄(μ-dppm) (81.6°) and Pt(C₄H₈)(PPh₃)₂ (80.9°).²⁵ This difference is most likely due to the PH₃ ligands having less steric bulk than substituted phosphines.

The calculated Pt-Cl bond distance in **4** of 2.35 Å and the Cl-Pt-Cl bond angle of 91° match very well with the observed Pt-Cl distances (2.368 Å and 2.377 Å) observed in the x-ray structure of *cis*-Pt(PMe₃)₂Cl₂.²⁶

The calculated Pt-P bond distances are 0.1-0.2 Å longer than experiment [Pt-P = 2.23 and 2.24 Å in PtCl₂(PMe₃)₂²⁶ versus 2.44 Å calculated for (**4**); 2.279 and 2.285 Å in Pt(C₄H₈)(PPh₃)₂^{25b} versus 2.46 Å calculated in (**1**)]. This is systematic for Pt-P bonds at this level of calculation^{2a} and may be partially due to the effect of substituted phosphines versus PH₃. The P-Pt-P bond angle is apparently less sensitive, and good matches to the experimentally observed P-Pt-P angles are found [101° in (**1**) versus 98.9° in Pt(C₄H₈)(PPh₂)₂ and 102° in (**6**) versus 96.2° in PtCl₂(PMe₃)₂].²⁶

Noell and Hay^{4b} were the first to show that HF wavefunctions yield geometries of Pt and Pd complexes which compare well with x-ray

structures, indicating that HF is a reasonable level of wavefunction with which to optimize geometries.

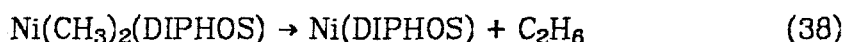
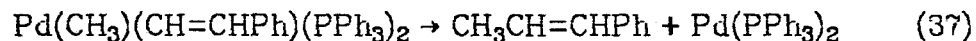
III. Discussion

A. *The Effect of Added Phosphine on the Rate of Reductive Elimination*

One of the unresolved questions in the experimental literature is the effect of added phosphines on the rate of C-C coupling. There are three classes of systems:

- (A) For PdMe_2L_2 ⁶ and AuMe_3L ^{3b,27} experiment shows that reductive elimination of ethane is *retarded* by added phosphine. This led Hoffman *et al.*^{3a,b} to propose a mechanism by which reductive elimination proceeds through a three-coordinate intermediate, an interpretation supported by Extended Hückel (EH) calculations.

- (B) Contrasted with these results are

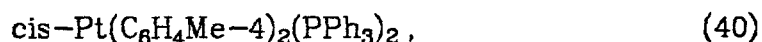


[$\text{DIPHOS} \equiv \text{Ph}_2\text{P}(\text{CH}_2)_2\text{PPh}_2$] where the addition of phosphine has no effect on the rate of C-C coupling.^{28,29} These systems apparently can reductively eliminate directly from the original four-coordinate complex.

- (C) There are also Ni(II) and Pt(II) complexes such as



and



where reductive coupling of C-C bonds is *promoted* by the addition of phosphines.^{11,28} This led Braterman and Cross³⁰ to propose a mechanism by which reductive elimination proceeds through a

five-coordinate intermediate, a mechanism that was also supported by EH calculations of Tatsumi *et al.*^{3d}

Our calculations on reductive elimination of ethane from PdR₂ and PtR₂ show that reductive elimination is favored energetically from PdR₂ because Pd prefers the d¹⁰ configuration.^{2c} It is interesting to note that the difference in ΔH^\ddagger for elimination of C₂H₆ from Pd(CH₃)₂ and Pt(CH₃)₂ (30.9 kcal/mol) is very close to the difference in the driving force for each reaction (34.3 kcal/mol). This suggests that the barrier to reductive coupling of C-C bonds is strongly coupled to the driving force. Since phosphines stabilize d¹⁰ relative to s¹d⁹, we would expect the three coordinate complexes to have a *larger* barrier for reductive elimination than the four-coordinate complex, which should in turn have a larger barrier than the five-coordinate complex.

The consideration of only the three-coordinate intermediate for systems of class A may be an oversimplification of the real system. *Intermolecular* paths clearly are important for the decomposition of AuMe₃L in some solvents [e.g., benzene, decalin, PhCl, n-Bu₂O, and Tetrahydrofuran (THF)].^{3b} More strongly coordinating solvents [Me₂SO (DMSO) and dimethylformamide (DMF)] appear to block intermolecular paths, resulting in very little crossover.^{3b} For reductive elimination of ethane from Pd(CH₃)₂L₂, crossover experiments show that reductive elimination of ethane is intramolecular *only* in DMSO or noncoordinating solvents containing dimethylmaleate (DMM).⁶ It has been assumed that DMM serves to trap the PdL₂ product before it can decompose (and thereby affect the decomposition pathway); however, Ozawa *et al.*^{6d} have shown that variation in concentration of DMM does not affect the rate of decomposition. (They did not report the rate with no added DMM.) This only proves that

DMM is not involved in the rate determining step of reductive elimination (which appears to be loss of a phosphine). The loss of phosphine could also be the rate-determining step in the formation of a four-coordinate intermediate in which one of the phosphines is replaced by DMSO, DMF, or DMM. If reductive elimination is facile from these intermediates then loss of phosphine would be the slow step which would be inhibited by added ligand.

Palladium might be expected to prefer pathways involving loss of phosphine, while other metals of the nickel triad reductively eliminate through four- and five-coordinate pathways since Pd forms weaker bonds to phosphines than Ni and Pt.³¹ Apparently reductive elimination of $\text{CH}_3\text{CH}=\text{CHPh}$ from $\text{Pd}(\text{CH}=\text{CHPh})(\text{CH}_3)(\text{PPh}_3)_2$ is *not* affected by added phosphine because the ΔG^\ddagger for elimination from the four coordinate starting complex is lower than the ΔG_f of the three coordinate intermediate.

Unfortunately it has not been possible to observe directly the three- or five-coordinate intermediates proposed for class A and C systems. Although EH calculations do support lower barriers for three and five coordinate complexes than four coordinate complexes, these predicted trends in activation energies do not correlate with our observed correlation of ΔE^\ddagger and ΔE . EH calculations are well known³² not to give accurate geometries and energetics and should not be considered as proof for the proposed mechanisms. What is needed are *ab initio* calculations of the relative barriers of reductive elimination from three, four and five coordinate intermediates.

B. *Reactivity of Metal -Carbon Bonds Involving sp^2 Hybrids Versus sp^3 Hybrids*

Another trend which has been observed but not explained is the lower stability of *cis*-methylphenyl and *cis*-biphenyl complexes relative to dimethyl complexes. Reductive elimination from *cis*-Ni(CH₃)(C₆H₅)L₂ is faster than from *cis*-Ni(CH₃)₂L₂ complexes.²⁸ The reaction of PhLi with PdCl₂(DIPHOS) yields biphenyl directly, whereas MeLi reacts with PdCl₂(DIPHOS) to give PdMe₂(DIPHOS) which eliminates ethane slowly.^{6a} Platinum diphenyl bisphosphine complexes can eliminate biphenyl¹¹ while Pt dimethyl bisphosphine complexes are very stable.¹⁰ This trend can be explained by noting that the phenyl group uses a C sp^2 hybrid orbital to form bonds while the methyl group uses a C sp^3 hybrid orbital. The increased s character of the sp^2 hybrids causes this orbital to be less directional than the sp^3 hybrids. Therefore the sp^2 hybrid can have more multicentered bonding at the transition state, leading to lower activation energies for CH₃-CH=CHPh, CH₃-Ph and Ph-Ph coupling.

It should be noted the Ph-CH₃ and Ph-Ph bond energies are 11.4 kcal/mol^{19b} and 26 kcal/mol stronger^{9c} than the H₃C-CH₃ bond energy (90.4 kcal/mol).^{19b} Thus, if the Mt-CH₃ and Mt-Ph bond energies were approximately the same, this would lead to a larger driving force for reductive elimination of sp^2 species. Evans *et al.* have made a thermochemical estimate for the Pt-Ph bond energy of 63.1³³ that is 7 kcal/mol stronger than our calculated Pt-CH₃ intrinsic bond energy. This value for the bond energy is, however, strongly dependent on their estimated Pt-Cl bond energy in PtCl₂(PPh₃)₂ [which was assumed to be the same as the Pt-Cl bond energy in PtCl₂], which could easily cause errors of ~10 kcal/mol. Therefore, there currently are insufficient data to determine

whether the diphenyl and methylphenyl Pt complexes are less stable thermodynamically than the dimethyl complex.

Thermochemical data³⁴ from $\text{ThR}_2(\text{Cp}^*)_2$ complexes demonstrate that Th-Ph bond energies are 13 kcal/mol stronger than Th-CH₃ bond energies. Therefore it does appear that diphenyl and methylphenyl complexes have approximately the same enthalpy for reductive elimination as dimethyl complexes.

Either of the above interpretations for the increased lability of sp^2 versus sp^3 carbons would suggest that alkynyl groups will reductively eliminate faster than phenyl or vinyl groups. Indeed, $\text{Ph-C}\equiv\text{C-C}\equiv\text{C-Ph}$ has been indentified in the decompostion products of $\text{cis-Pt}(\text{C}\equiv\text{C-Ph})_2\text{L}_2$.³⁵ A more careful analysis of the decompostion of dialkynyl complexes should help establish the trend of sp hybridization versus rate of reductive elimination.

C. Heat of Formation Of Pt(II) and Pd(II) salts

We have found that the difference in enthaplies $[\Delta(\Delta\text{H})]$ for reductive elimination from the corresponding Pt(II) and Pd(II) compounds is always within 5 kcal/mol of the difference in the $\text{s}^1\text{d}^9 \rightarrow \text{d}^{10}$ splittings for these metals (33 kcal/mol).¹⁸ Unfortunately, there are no reliable ΔH_f^0 's for Pt and Pd complexes available in the literature to provide a test of this theoretical trend. However ΔH_f^0 for various Pt(II) and Pd(II) salts are available.³⁶ Since Pt and Pd have the same covalent radii and electronegativities,¹⁶ we can assume that the lattice energies for the corresponding PtX_2 and PdX_2 salts are the same. Therefore the $\Delta(\Delta\text{H})$ for the reaction $\text{Mt}(\text{}^1\text{S})_{(\text{g})} + \text{X}_{2(\text{g})} \rightarrow \text{MtX}_{2(\text{s})}$ should also be approximatly equal to 33 kcal/mol. Indeed, as indicated in Table VI, the experimental $\Delta(\Delta\text{H})$ are 33 ± 3 kcal/mol, in exccllent agreement with our prediction.

The alternative interpretation based on an ionic model for Mt-C bonds would suggest that the $\Delta(\Delta H)$ is equal to the difference in the sums of the first and second ionization potentials for Pt and Pd.¹⁸ This would predict a $\Delta(\Delta H)$ of 15 kcal/mol instead of 33 kcal/mol. Therefore, our covalent bonding model is far more consistent with the experimentally observed ΔH_f^0 for these salts.

D. Comparison With Other Theoretical Studies

Hoffmann *et al.*^{3a} analyzed Extended Hückel (EH) calculations on reductive elimination from complexes of the Ni triad to obtain five conclusions concerning these reactions. The first three of which are relevant to this work since they concern reductive elimination from dimethyl bisphosphine complexes.³⁷

1. "The better the σ -donating capability of the leaving groups, the more readily the elimination reaction proceeds.
2. "Stronger donor ligands that are trans to the leaving groups give a higher barrier for the elimination reaction.
3. "Increased stability of the $MA_2 b_2$ orbital [where A indicates modified hydrogens used to model phosphines] facilitates the reductive elimination of D_2 [where D is a modified hydrogen used to model CH_3 groups]. A lower $MA_2 b_2$ energy will be given by a lower metal d orbital energy."^{3a}

Since we find essentially covalent bonding in Pt and Pd complexes, a better σ -donor leaving group is equivalent to a leaving group with lower electronegativity. Leaving groups (R) with higher electronegativities would help stabilize the s orbital of the metal atom by increasing the amount of s character in the metal sd hybrid orbital used in the M-R

bond. This will stabilize the s^1d^9 configuration of the metal atom and reduce the driving force for reductive elimination. This is in agreement with Hoffmann's first conclusion.

We have not made systematic variations in the ligands; however, the trends in going from no ligands (a very weak donor!) to two PH_3 groups are quite suggestive. We find that (due to the overlap between the phosphine lone pairs and the metal s orbital) the sd hybrid orbital used in the M-R bond has to build in p character to stay orthogonal to phosphine lone pairs. This increased p character makes the *intrinsic* M-R bond strengths slightly stronger, as expected from simple valence bond calculations.¹⁵ The σ -donating ability of substituted phosphine ligands is directly related to the overlap between the ligand lone pair and metal s orbital. The stronger the donor, the larger the overlap. The larger overlap will lead to stronger M-R bonds which may cause the barriers for reductive elimination to be higher. Therefore, our results are also consistent with the second conclusion of Hoffmann.

However, we believe that Hoffmann's third conclusion, although reasonable, does not present the complete picture. We find that the important issue here is the relative energy of the s^1d^9 and d^{10} configurations (VB language) or in MO language the relative energy of the valence s and d orbitals of the metal atom and not just the d orbital energy. The d^{10} configuration is stabilized relative to s^1d^9 by destabilizing the the s orbital relative to the d orbital. Stabilization of the d^{10} configuration leads to larger driving forces and lower barriers for reductive elimination. We have shown in an earlier paper that reductive coupling of C-C bonds from PdMe_2 is favored over PtMe_2 , both kinetically and energetically. This dramatic difference arises because relative to Pt, Pd has a 33 kcal/mol

bias for the d^{10} state. This effect is much more dramatic than the other two and should dominate the stability of these complexes.

Related trends were also observed in the CNDO calculations of Gritsenko *et al.*^{4j} where the stability of $MH_2(PH_3)_2$ complexes ($Mt = Pd, Pt$) was correlated with the Mt s character of the wavefunction.

Other ab initio theoretical calculations involving square planar complexes of the Ni triad include studies of $NiMe_2(H_2O)_2$ by Åkermark *et al.*^{4e} and $PdH_2(H_2O)_2$ by Siegbahn *et al.*^{5e} In both of these studies, H_2O was used as a model ligand. Åkermark *et al.*^{4e} found little change in the d orbital occupations upon addition of H_2O ligands, and Siegbahn actually found a small stabilization (~ 5 kcal/mol)³⁸ of the s^1d^9 singlet versus the d^{10} singlet of $Pd(H_2O)_2$ relative to the atomic state splittings of Pd . The differences between these previous studies and ours probably results from their use of H_2O ligands rather than PH_3 . The lone pairs of H_2O are much smaller than the lone pair of PH_3 . The overlap between the lone pairs of H_2O and the Pd $5s$ orbital is probably much smaller than for phosphine lone pairs. This would lead to a smaller destabilization of the s orbital, favoring the s^1d^9 configuration over d^{10} (Pd and Pt prefer "softer" ligands such as PR_3 over H_2O). The relevant experiments all involve complexes with phosphine ligands, and hence our studies using phosphines are more pertinent for understanding the observed trends in C-C coupling.

IV. Computational Details

A. Basis Sets and Effective Potentials

The basis sets and relativistic effective potentials used in this study for Pd and Pt are those of Hay *et al.*^{4b} The basis on carbon is the Dunning double zeta contraction of the Huzinaga (9s5p) basis.³⁹ The effective potential for phosphorus is the SHC potential of Rappé *et al.*⁴⁰ The SHC basis for phosphorus atom⁴⁰ was contracted to a minimum basis set using atomic calculations. Three different basis sets were used on the hydrogen atoms depending on their chemical environment. For hydrogen atoms bound to phosphorus, we used a minimum basis set contraction of the Huzinaga four-gaussian hydrogen basis (no scaling).⁴¹ Methyl protons were described using a double zeta contraction of the Huzinaga four-gaussian basis scaled by a factor of 1.2.³⁹ The active hydrogen bound to the metal atoms in the $\text{Pt}(\text{H})(\text{Me})(\text{PH}_3)_2$ and $\text{Pt}(\text{H})_2(\text{PH}_3)_2$ complexes was treated with a triple zeta contraction of the Huzinaga six-gaussian basis.⁴¹ This was necessary to allow the hydrogen to adjust for optimum bonding to the metal atom in the reactant and optimum bonding to the methyl group or H atom in the products. The chlorine potential was the SHC potential of Rappé *et al.*,⁴⁰ and the double zeta contraction of the SHC basis⁴⁰ was used.

The effective potentials for P, Cl, Pt, and Pd are expected to provide ab initio quality descriptions for these atoms. Good measures for the quality of description for Pd and Pt are the atomic state splittings as indicated in figure 11. For highly accurate calculations, polarization functions (p's on H, d's on C, P and Cl, f's on Pt or Pd) are needed. This will lead to stronger intrinsic bond energies but will probably have little effect on the ΔE for oxidative addition/reductive elimination reactions

(since bonds of reactant and product are affected similarly). The major factor in understanding these reactions is that the $s^1d^9-d^{10}$ splitting of the metal atoms be accurately described.² Although the level of basis can certainly be improved, it should be quite adequate for the purposes here, namely, the conceptual description of the differences between Pt(II), Pt(IV), and Pd(II) complexes.

B. Geometries

All geometries of the various complexes were fully optimized at the HF level using analytic energy gradients and the Newton-Raphson procedure.⁴² For the calculations on the triplet states of ML_2 and MCl_2L_2 , the geometries were frozen at the geometry of the fragment in the corresponding MR_2L_2 or $MR_2Cl_2L_2$ complex. This was done so that geometric relaxation energy would not be included in calculating intrinsic bond energies.

C. Wavefunctions

All energetics reported here involve the GVB description of electron correlation for the important valence electrons. For an electron pair that would be described as doubly-occupied in HF theory, the GVB description would allow two orbitals each optimized self-consistently with all other orbitals of the molecules,

$$\begin{aligned}\Phi^{\text{HF}}(1,2) &= \varphi(1)\varphi(2)(\alpha\beta - \beta\alpha) \rightarrow \\ \Phi^{\text{GVB}}(1,2) &= [\varphi_a(1)\varphi_b(2) + \varphi_b(1)\varphi_a(2)](\alpha\beta - \beta\alpha).\end{aligned}\tag{41}$$

When there are additional electron pairs, each may be correlated as in (41), so that the doubly-occupied orbitals $\varphi_1, \varphi_2, \dots$ of an HF wavefunction become singly-occupied orbitals [as in (41)], $\varphi_{1a}, \varphi_{1b}, \varphi_{2a}, \varphi_{2b}$ of the GVB wavefunction. Although for HF wavefunctions the doubly-occupied

orbitals can generally be taken as either delocalized (canonical) or localized, the GVB orbitals are uniquely determined and are generally localized (reminiscent of simple valence bond theory). The general form of a GVB wavefunction is

$$\mathcal{Q}[(\varphi_{1a}\varphi_{1b}\varphi_{2a}\varphi_{2b}\cdots)\chi], \quad (42)$$

where χ is an appropriate optimized spin function for N electrons. However, in calculating the GVB orbitals, it is generally convenient to choose χ as the simple valence bond function (perfect pairing)

$$\chi^{\text{VB}} = (\alpha\beta - \beta\alpha)(\alpha\beta - \beta\alpha)\cdots \quad (43)$$

In this case the orbitals for different electron pairs are taken as orthogonal, and the resulting orbitals are denoted as GVB-PP to indicate the restricted form of the wavefunction. If five pairs of electrons are so correlated (using ten orbitals), the wavefunction is denoted as GVB-PP(5/10); however, other orbitals of the wavefunction are understood to be calculated self-consistently. (This wavefunction would involve $2^5 = 32$ different orbital configurations.) Such wavefunctions quite accurately describe systems where one valence bond structure is adequate (no resonance); however, for transition metal systems, spin couplings other than (43) are often important. These spin coupling effects are usually accurately described using the GVB-PP orbitals but allowing the two electrons of each orbital pair to be either in different orbitals [as in (41)] or in the same orbital [e.g., $\varphi_a(1)\varphi_a(2)$]. Allowing a similar description for all correlated pairs leads to the GVB-RCI wavefunction. Since there are three orbital products for each pair of electrons, the GVB-RCI(5/10) wavefunction has $3^5 = 243$ orbital products. In addition to an optimized spin coupling, the RCI wavefunction includes important electron correla-

tion effects in which two electrons in one bond pair can respond instantaneously to the motions of two electrons in another bond pair (interpair correlation). The orbitals of the GVB-RCI wavefunction can be solved self-consistently; however, it is generally adequate to use the orbitals of the GVB-PP wavefunction, and we have found this to be the case for complexes of the type studied in this paper. For cases where *resonance* of simple valence bond structures would be important, it is often essential to allow readjustments in those bond pairs that would change in the resonance. Thus, for reductive C-C coupling, the two localized M-C pairs change into a C-C bond pair and a metal d pair as the bond is broken, and resonance between these configurations is important. In this case we refine the GVB-RCI(2/4) description of these two pairs by using the GVB-CI(2/4) description, where all four electrons are allowed to occupy all four orbitals in any way (leading to 19 orbital products).

We find (see Figure 11) for Ni, Pd, and Pt that the GVB description (which uses ten optimized orbital for all states) leads to a rather accurate description of the relative energies for the d^{10} , s^1d^9 , and s^2d^8 configurations and is particularly accurate for s^1d^9 versus d^{10} , the states relevant for this paper. For the s^2d^8 states the s^2 pair was polarized in the $\pm Z$ directions and d_{z^2} and the d_{xy} were singly occupied.

For the various $M(R_2)(R_2)$ complexes, it is necessary to correlate not only the ten metal valence electrons but also the additional electrons involved in the covalent $M-R_1$ and $M-R_2$ bonds. Thus, a total of 12 electrons or six electron pairs must be correlated. Consequently, we first carried out GVB-PP(6/12) calculations using 12 orbitals to correlate the motions of these six pairs (12 electrons). (All other orbitals are doubly-occupied but are solved self-consistently.) In order to include the spin-

coupling, interpair correlation, and resonance effects,^{2a,c} the energetics reported here were determined at the GVB-CI(2/4)×RCI(4/8) level.

In *previous studies* of the reaction path for reductive coupling, the necessity for simultaneous description of both the reactant (s^1d^9) and the product (d^{10}) resonance structures in the transition state region required use of three orbitals (rather than two) for each of the two bond pairs that change during the reaction². Thus, rather than GVB-PP(2/4), these two electron pairs were described with GVB-PP(2/6). In order to allow a full description of resonance effects in the transition state, all occupations of these six orbitals were allowed for all four electrons, denoted as GVB-CI(2/6). The other four pairs of electrons were correlated as usual, leading to a composite wavefunction of the form GVB-CI(2/6)×RCI(4/8). We also optimized the orbitals at this level. In the *current study*, the main interest is in overall energy differences between products and reactants, where this resonance is not so important. Consequently, we use only two orbitals for these bond pairs, and the orbitals were optimized at the GVB-PP level. However, as in the previous studies, we carry out a full CI among the (four) orbitals involving those two bond pairs [CI(2/4)]. Thus the wavefunction used in these studies is GVB-CI(2/4)×RCI(4/8).

Acknowledgments: This work was supported in part by a grant from the National Science Foundation (No. CHE83-18041). One of the authors (J.J.L.) wishes to acknowledge financial support in the form of fellowships from Exxon and ARCO.

References and Notes

- (1) Collman, J. P.; Hegedus, L. S. "Principles and Applications of Organotransition Metal Chemistry," University Science Books: Mill Valley, 1980; Chapter 4.
- (2) (a) Low, J. J.; Goddard III, W. A. *J. Am. Chem. Soc.* **1984**, *106*, 6928-6937;
(b) *ibid.* **1984**, *106*, 8321-8322;
(c) Low, J. J.; Goddard III, W. A. *Organometallics*, submitted for publication.
- (3) (a) Tatsumi, K.; Hoffmann, R.; Yamamoto, A.; Stille, J. K. *Bull. Chem. Soc. Jpn.* **1981**, *54*, 1857-1867;
(a) Komiya, S.; Albright, T. A.; Hoffmann, R.; Kochi, J. K. *J. Am. Chem. Soc.* **1976**, *98*, 7255-725;
(c) Saillard, J.; Hoffmann, R. *ibid.* **1984**, *106*, 2006-2026;
(d) Tatsumi, K.; Nakamura, A.; Komiya, S.; Yamamoto, A.; Yamamoto, T. *ibid.* **1984**, *106*, 8181-8188.
- (4) (a) Kitaura, K.; Obara, S.; Morokuma, K. *J. Am. Chem. Soc.* **1981**, *103*, 2891-2893;
(b) Noell, J. O.; Hay, P. J. *Inorg. Chem.* **1982**, *21*, 14-19;
(c) Noell, J. O.; Hay, P. J. *J. Am. Chem. Soc.* **1982**, *104*, 4578-4584;
(d) Hay, P. J. *Chem. Phys. Lett.* **1984**, *103*, 466-469;
(e) Åkermærk, B.; Johansen, H.; Roos, B.; Wahlgren, U. *J. Am. Chem. Soc.* **1979**, *101*, 5876-5883;
(f) Sevin, A. *Nouv. J. Chim.* **1981**, *5*, 233-241;
(g) Dedieu, A.; Strich, A. *Inorg. Chem.* **1979**, *18*, 2940-2943;
(h) Balazs, A. C.; Johnson, K. H.; Whitesides, G. M. *ibid.* **1982**, *21*, 2162-2174;

- (i) Gritsenko, O. V.; Bagatur'yants, A. A.; Moiseev, I. I.; Kazanskii, V. B.; Kalechits, I. V. *Kin. Kat.* **1981**, *22*, 354-358;
- (j) Gritsenko, O.V.; Bagatur'yants, A. A.; Moiseev, I. I.; Kalechits, I. V. *ibid.* **1981**, *22*, 1431-1437;
- (k) Obara, S.; Kitaura, K.; Morokuma, K. *J. Am. Chem. Soc.* **1984**, *106*, 7482-7492.
- (5) (a) Blomberg, M. R. A.; Siegbahn, P. E. M. *J. Chem. Phys.* **1983**, *78*, 986-987;
- (b) Blomberg, M. R. A.; Brandemark, U.; Pettersson, L.; Siegbahn, P. E. M. *Int. J. Quant. Chem.* **1983**, *28*, 855-863;
- (c) Blomberg, M. R. A.; Brandemark, U.; Siegbahn, P. E. M. *J. Am. Chem. Soc.* **1983**, *105*, 5557-5563;
- (d) Siegbahn, P. E. M.; Blomberg, M. R. A.; Bauschlicher, Jr., C. W. *J. Chem. Phys.* **1984**, *81*, 1373-1382;
- (e) Brandemark, U. B.; Blomberg, M. R. A.; Petersson, L. G. M.; Siegbahn, P. E. M. *J. Phys. Chem.* **1984**, *88*, 4617-4621.
- (6) (a) Gillie, A.; Stille, J. K. *J. Am. Chem. Soc.* **1980**, *102*, 4933-4941;
- (b) Loar, M. K.; Stille, J. K. *ibid.* **1981**, *103*, 4174-4181;
- (c) Moravskiy, A.; Stille, J. K. *ibid.* **1981**, *103*, 4182-4186;
- (d) Ozawa, F.; Ito, T.; Nakamura, Y.; Yamamoto, A. *Bull. Chem. Soc. Jpn.* **1981**, *54*, 1868-1880.
- (7) (a) Ruddick, J. D.; Shaw, B. L. *J. Chem. Soc. (A)* **1969**, 2969-2970;
- (b) Brown, M. P.; Puddephat, R. J.; Upton, C. E. E. *J. Chem. Soc., Dalton Trans.* **1974**, 2457-2465;
- (c) Appleton, T. G.; Clark, H. C.; Manzer, L. E. *J. Organomet. Chem.* **1974**, *65*, 275-287.

- (8) (a) Whitesides, G. M.; Gaasch, J. F.; Stedronsky, E. R. *J. Am. Chem. Soc.* **1972**, *94*, 5258-5270;
(b) McDermott, J. X.; White, J. F.; Whitesides, G. M. *ibid.* **1984**, *98*, 6521-6528;
(c) Young, G. B.; Whitesides, G. M. *ibid.* **1978**, *100*, 5808-5815;
(d) McCarthy, T. J.; Nuzzo, R. G.; Whitesides, G. M. *ibid.* **1981**, *103*, 1676-1678;
(e) *ibid.* **1981**, *103*, 3396-3403;
(f) Nuzzo, R. G.; McCarthy, T. J.; Whitesides, G. M. *ibid.* **1981**, *103*, 3404-3410;
(g) Komiya, S.; Morimoto, Y.; Yamamoto, A.; Yamamoto, T. *Organometallics* **1981**, *1*, 1528-1536.
- (9) (a) $\text{PtEt}_2(\text{PEt}_3)_2$ is known to β -hydride eliminate to give ethylene ($\Delta H_{f300}^0 = 12.5$ kcal/mol, $S_{300} = 52.4$ e.u.) and ethane ($\Delta H_{f300}^0 = -20.2$ kcal/mol, $S_{300} = 54.9$ e.u.) rather than to reductively eliminate to give n-butane ($\Delta H_{f300}^0 = -30.2$ kcal/mol, $S_{300} = 74.1$ e.u.) even though n-propane is the thermodynamically favored product ($\Delta H_{300} = -22.5$ kcal/mol, $\Delta S_{300} = -33.2$ e.u., $\Delta G_{300} = -12.5$ kcal/mol for $\text{C}_2\text{H}_4 + \text{C}_2\text{H}_6 \rightarrow \text{n-C}_4\text{H}_{10}$). The ΔH_{f300}^0 and S_{300}^0 were taken from ref 9b.
(b) Benson, S. W. "Thermochemical Kinetics," J. Wiley and Sons: New York; 1976, Second Edition, p 295.
- (10) Chatt, J.; Shaw, B. L. *J. Chem. Soc.* **1959**, 705-716.
- (11) (a) Braterman, P. S.; Cross, R. J.; Young, G. B. *J. Chem. Soc., Dalton Trans.* **1976**, 1306-1309;
(b) *ibid.* **1976**, 1310-1314;
(c) *ibid.* **1977**, 1892-1897.

- (12) (a) Abis, L.; Sen, A.; Halpern, J. *J. Am. Chem. Soc.* **1978**, *100*, 2915-2916;
(b) Halpern, J. *Acc. Chem. Res.* **1982**, *15*, 332-338.
- (13) Michelin, R.A.; Faglia, S.; Uguagliati, P. *Inorg. Chem.* **1983**, *22*, 1831-1834.
- (14) Paonessa, R. S.; Trogler, W. C. *J. Am. Chem. Soc.* **1982**, *104*, 1138-1140.
- (15) Steigerwald, M. L. Ph.D. Thesis, California Institute of Technology Pasadena, CA, 1984.
- (16) Pauling, L. "The Nature of the Chemical Bond," 3rd ed.; Cornell University Press: Ithaca, 1960.
- (17) A similar preference for p versus s character is found in carbon-halogen bonds. Goddard III, W. A.; Harding, L. B. *Ann. Rev. Phys. Chem.* **1979**, *29*, 363-396.
- (18) Moore, C. E. "Atomic Energy Levels," National Bureau of Standards: Washington, DC, 1971; Vol. III. (These state splittings were averaged over j states to cancel out spin-orbit coupling.)
- (19) The D_{298} used in these calculations are $D_{298}(\text{H-H}) = 104.2$ kcal/mol $D_{298}(\text{H-CH}_3) = 105.1$ kcal/mol and $D_{298}(\text{H}_3\text{C-CH}_3) = 90.4$ kcal/mol. These bond energies were derived from spectroscopic measurements of $\text{H}_2^{19\text{a}}$ and the reported $D_{298}^{19\text{b}}$ for $\text{H}_3\text{C-CH}_3$ and H-CH_3 .
(a) Huber, K.P.; Herzberg, G. "Constants of Diatomic Molecules," Van Nostrand: New York. 1979;
(b) McMillen, D. F.; Golden, D. M. *Ann. Rev. Phys. Chem.* **1982**, *33*, 493-552.

- (20) $D_{298} [\text{cyclopropyl-H}] = 106.3 \text{ kcal/mol}$; $^{16b} D_{298} [\text{H-CH}(\text{CH}_3)_2] = 95.1 \text{ kcal/mol}$.^{16b}
- (21) Simons, J. P. *Nature* **1965**, *205*, 1308-1309.
- (22) $D_{298} [\text{H}_2\text{C}=\text{CH}_2] = 172.2 \pm 2.07 \text{ kcal/mol}$ and $D_{298} [\text{F}_2\text{C}=\text{CF}_2] = 69.3 \pm 2.7$ were derived from the following enthalpies:
 $\Delta H_f(\text{C}_2\text{F}_4) = -157.7 \pm 0.7 \text{ kcal/mol}$ and $\Delta H_f(\text{C}_2\text{H}_4) = 12.54 \pm 0.07 \text{ kcal/mol}$ [see Stull, D. R.; Prophet, H. "JANAF Thermochemical Tables," 2nd ed.; National Bureau of Standards: Washington, DC, June 1971; NSRDS-NBS 37].
 $\Delta H_f(\text{CH}_2) = 92.35 \pm 1.0 \text{ kcal/mol}$ [Chase, M. W.; Curnett, J. L.; Prophet, H.; McDonald, R. A.; Syverd, A. N. *J. Phys. Chem. Ref. Data* **1975**, *4*, 1-175].
 $\Delta H_f(\text{CF}_2) = -44.2 \pm 1.0 \text{ kcal/mol}$ [Berman, D. W.; Bomse, D. S.; Beauchamp, J. L. *Int. J. Mass Spectrom. Ion Phys.* **1981**, *39*, 263-271].
- (23) (a) Koda, S. *Chem. Phys. Lett.* **1978**, *55*, 353-357; *Chem. Phys.* **1982**, *66*, 383-390;
(b) A theoretical calculation leads to 51.4 kcal/mol; Feller, D.; Borden, W. T.; Davidson, E. R. *Chem. Phys. Lett.* **1980**, *71*, 22-26.
- (24) Egger, K. W. *J. Organomet. Chem.* **1970**, *24*, 501-506.
- (25) (a) Kirchner, R. M.; Little, R. G.; Tau, K. D.; Meek, D. W. *J. Organomet. Chem.* **1978**, *149*, C15-C18;
(b) Biefeld, C. G.; Eick, H. A.; Grubbs, R. H. *Inorg. Chem.* **1973**, *12*, 2166-2170;
(c) Puddephatt, R. J.; Thomson, M. A.; Manojlović-Muir, L.; Muir, K. W.; Frew, A. A.; Brown, M. P. *J. Chem. Soc., Chem. Commun.* **1981**, 805-806.

- (26) Del Pra, A.; Zanotti, G. *Cryst. Struct. Comm.* **1979**, *8*, 737-742.
- (27) Tamaki, A.; Magennis, S.A.; Kochi, J.K. *J. Am. Chem. Soc.* **1974**, *96*, 6140-6148.
- (28) Komiya, S.; Abe, Y.; Yamamoto, A.; Yamamoto, T. *Organometallics* **1983**, *2*, 1466-1468.
- (29) Kohara, T.; Yamamoto, T.; Yamamoto, A. *J. Organomet. Chem.* **1980**, *192*, 265-274.
- (30) Braterman, P.S.; Cross, R.J. *Chem. Soc. Rev.* **1973**, *2*, 271-294.
- (31) Basolo, F. *Trans. N.Y. Acad. Sci.* **1969**, *3*, 676-685.
- (32) Levine, I. N. "Quantum Chemistry," 2nd ed.; Allyn and Bacon: Boston, 1974; pp 450-452.
- (33) (a) Evans, A.; Mortimer, C.T.; Puddephat, R.J. *J. Organomet. Chem.* **1975**, *96*, C58-C60;
(b) Ashcroft, S.J.; Mortimer, C.T. *J. Chem. Soc. (A)* **1967**, 930-931.
- (34) Bruno, J. W.; Marks, T. J.; Morss, L. R. *J. Am. Chem. Soc.* **1983**, *105*, 6824-6832.
- (35) Collamati, I.; Furlani, A. *J. Organomet. Chem.* **1969**, *17*, 457-461.
- (36) Hartley, F. R. "The Chemistry of Platinum and Palladium," John Wiley & Sons: New York, 1973; Chapter 2.
- (37) The last two conclusions concern the three-coordinate intermediates resulting from loss of phosphine from the square planar complexes.
- (38) This stabilization energy was derived from the results of Siegbahn *et al.*^{5e} by summing the energy needed to bend the O-Pd-O angle in Pd(OH₂)₂ from its equilibrium value of 180° to 90° (15 kcal/mol) and the diabatic d¹⁰ → s¹d⁹ singlet splitting for Pd(OH₂)₂ (20

kcal/mol), at a 90° O-Pd-O angle to give an adiabatic splitting of 35 kcal/mol. This splitting is 5 kcal/mol smaller than their calculated $d^{10} \rightarrow s^1d^9$ splitting for Pd atom of 40 kcal/mol.

- (39) Dunning, Jr., T. H.; Hay, P. J. In "Modern Theoretical Chemistry: Methods of Electronic Structure Theory," Schaefer III, H. F., Ed.; Plenum Press: New York, 1977; Vol. 3, Chapter 4, pp 79-127.
- (40) Rappé, A. K.; Smedley, T. A.; Goddard III, W. A. *J. Phys. Chem.* **1981**, *85*, 1662-1666.
- (41) Huzinaga, S. *J. Chem. Phys.* **1965**, *42*, 1293-1302.
- (42) All of the geometry optimizations were obtained by using an analytic gradient program (GVBGRAD). This program was based on subroutines from (a) the GVB2P5 program [Bobrowicz, F. W.; Goddard III, W. A. In "Modern Theoretical Chemistry: Methods of Electronic Structure Theory," Schaefer III, H. F., Ed.; Plenum Press: New York, 1977; Vol. 3, Chapter 4, pp 79-127] to evaluate density matrices for restricted HF and GVB-PP wavefunctions, (b) the HONDO program [Dupuis, M.; King, H. F. *J. Chem. Phys.* **1978**, *68*, 3998-4004] to calculate derivatives of the ab initio terms in the energy expression, and (c) routines from the GAUSS 80 program [Binkely, J. W.; Whitesides, R. A.; Krishnan, R.; Seeger, R.; DeFrees, D. J.; Schlegel, H. B.; Topiol, S.; Kahn, L. R.; Pople, J. A. "Gauss 80," Department of Chemistry, Carnegie-Mellon University: Pittsburgh, PA, 1980] to calculate the effective potential terms of the derivative. To determine the step size taken each iteration, we used a relatively simple Newton-Raphson technique in which the second derivative matrix is updated after every gradient calculation (except for the starting geometry) [Low, J. J.; Goddard III, W. A.,

manuscript in preparation].

Table I. Mulliken Populations for the GVB Bond Pairs of $M(R_1)(R_2)$. For each bond there are two listings, the top one is the metal-like GVB orbital and the bottom one is the ligand-like orbital.

		Populations in GVB Bond Orbitals	
		M-CH ₃	M-H or M-Cl
1	Pt(CH ₃) ₂ (PH ₃) ₂	s ^{0.23} p ^{0.10} d ^{0.49} C ^{0.17} (sp) ^{-0.03} d ^{0.13} C s ^{0.18} p ^{0.71}	
2	Pd(CH ₃) ₂ (PH ₃) ₂	s ^{0.17} p ^{0.07} d ^{0.49} C ^{0.24} (sp) ^{-0.02} d ^{0.15} C s ^{0.18} p ^{0.58}	
3	Pt(CH ₃) ₂ (Cl) ₂ (PH ₃) ₂	s ^{0.17} p ^{0.07} d ^{0.69} C ^{0.04} (sp) ^{0.00} d ^{0.19} C s ^{0.11} p ^{0.67}	s ^{0.19} p ^{0.25} d ^{0.21} Cl ^{0.37} (sp) ^{-0.06} d ^{0.07} Cl s ^{0.03} p ^{0.93}
4	Pt(Cl) ₂ (PH ₃) ₂		s ^{0.21} p ^{0.11} d ^{0.37} Cl ^{0.27} (sp) ^{-0.03} d ^{0.06} Cl s ^{0.01} p ^{0.95}
5	Pt(H)(CH ₃)(PH ₃) ₂	s ^{0.24} p ^{0.11} d ^{0.49} C ^{0.15} (sp) ^{-0.04} d ^{0.13} C s ^{0.18} p ^{0.72}	s ^{0.27} p ^{0.13} d ^{0.51} H ^{0.09} (sp) ^{-0.02} d ^{0.16} C ^{0.01} H ^{0.85}
	Pt(H) ₂ ^{a)}		s ^{0.29} p ^{0.02} d ^{0.63} H ^{0.07} (sp) ^{0.02} d ^{0.19} H ^{0.80}
	Pt(H)(CH ₃) ^{a)}	s ^{0.26} p ^{0.01} d ^{0.64} C ^{0.09} (sp) ^{0.01} d ^{0.16} C s ^{0.12} p ^{0.70}	s ^{0.30} p ^{0.02} d ^{0.60} H ^{0.08} (sp) ^{0.01} d ^{0.16} H ^{0.80}
	Pt(CH ₃) ₂ ^{a)}	s ^{0.27} p ^{0.01} d ^{0.62} C ^{0.10} (sp) ^{0.00} d ^{0.15} C s ^{0.14} p ^{0.70}	
	Pd(CH ₃) ₂ ^{a)}	s ^{0.16} p ^{0.03} d ^{0.55} C ^{0.24} (sp) ^{0.01} d ^{0.20} C s ^{0.28} p ^{0.52}	

^{a)} Reference 2c.

Table II. Mulliken Populations for Pt and Pd bisphosphine complexes.

Complex		Populations					Cl
		M sp	M d	CH ₃	H	PH ₃	
1	Pt(CH ₃) ₂ (PH ₃) ₂	0.73	8.89	9.13		8.06	
2	Pd(CH ₃) ₂ (PH ₃) ₂	0.33	9.09	9.20		8.10	
3	Pt(CH ₃) ₂ (Cl) ₂ (PH ₃) ₂	1.12	8.57	8.86		8.02	7.28
4	Pt(Cl) ₂ (PH ₂) ₂	0.80	8.83			7.92	7.25
5	Pt(H)(CH ₃)(PH ₃) ₂	0.85	8.99	9.12	0.93	8.05 ^{a)}	
6	Pt(H) ₂ (PH ₃) ₂	0.96	9.10		0.98		
7	Pt(PH ₃) ₂	0.38	9.51			8.07	
8	Pd(PH ₃) ₂	0.19	9.63			8.09	
	Pt(H) ₂ ^{b)}	1.16	9.15		0.85		
	Pt(H)(CH ₃) ^{b)}	1.05	9.03	9.04	0.89		
	Pt(CH ₃) ₂ ^{b)}	0.97	8.91	9.06			
	Pd(CH ₃) ₂ ^{b)}	0.60	9.15	9.13			

^{a)} This is the average occupation of the PH₃ groups in this complex. The PH₃ group trans to CH₃ has 8.04 e⁻ and the PH₃ group trans to H has 8.06 e⁻.

^{b)} Reference 2c.

TABLE III. Calculated and predicted energetics for reductive coupling processes. All energies are in kcal/mol. ΔH_{298} is the reaction enthalpy at 298°K, which is obtained from the calculated energy difference (ΔE) by adding in estimated zero point energy and temperature corrections. ΔE^\ddagger is the calculated energy barrier for reductive coupling and ΔH^\ddagger is the predicted activation barrier at 298°K. Parentheses indicate the level of approximation in obtaining an estimated value. Each level of parenthesis probably adds an additional uncertainty of ± 5 kcal/mol.

	$M(H)_2 \rightarrow M + H_2$			$M(H)(CH_3) \rightarrow M + CH_4$			$M(CH_3)_2 \rightarrow M + C_2H_6$					
	ΔE	ΔH_{298}	ΔE^\ddagger	ΔH^\ddagger	ΔE	ΔH_{298}	ΔE^\ddagger	ΔH^\ddagger	ΔE	ΔH_{298}	ΔE^\ddagger	ΔH^\ddagger
a) $M = Pt$	33.6	33.2	-- a)	-- a)	16.1	19.0	29.0	28.1	16.3	15.5	52.5	54.5
$M = Pt(PH_3)_2$	15.9	12.3	18.1	14.0	-7.2	-5.8	(17.3)	(15.7)	-6.1	-11.3	(40.3)	(41.1)
PH_3 destabilization	17.7	20.9			23.3	24.8	(11.7)	(12.4)	26.4	26.8	(13.2)	(13.4)
b) $M = Pd$	-3.6	-4.0	1.6	0.4	-20.1	-17.2	10.4	9.5	-16.0	-18.8	22.6	23.6
$M = Pd(PH_3)_2$	(-21.5)	(-25.1)	((-7.4)) ^{b)}	((-10.2)) ^{b)}	(-43.6)	(-42.2)	((-1.4)) ^{b)}	((-3.0)) ^{b)}	-42.6	-45.8	(9.3)	(10.1)
PH_3 destabilization	(17.9)	(21.1)	((9.0))	((10.6))	(23.5)	(25.0)	((11.8))	((12.8))	26.6	27.0	(13.5)	(13.5)
c) $M = Pt(Cl)(PH_3)_2$	(7.7)	(2.5)	(14.0)	((9.1))	(-22.0)	(-19.5)	((10.4))	((8.8))	-25.0	-27.0	(31.8)	(34.2)
Cl destabilization	(8.2)	(9.8)	((4.1))	((4.9))	(13.8)	(13.7)	((8.9))	((8.9))	16.9	15.7	(8.5)	(7.9)
d) $M = Pd(Cl)(PH_3)_2$	((-37.7)) ^{c)}		(((-15.5)) ^{b)}		((-67.4)) ^{c)}		(((-13.3)) ^{b)}		(-70.4) ^{c)}		(((-4.8)) ^{b)}	
Cl destabilization	((16.2))		((8.1))		((23.8))		((11.9))		(27.8)		((13.9))	

a) No barrier is found for oxidative addition.

b) No barrier is found for reductive coupling. The negative values indicate the estimated energy (relative to the product) at the geometry corresponding to the transition state for $M(H)(R_1)(R_2) \rightarrow M + R_1 + R_2$.

c) Based on correcting the $M = Pt(Cl)(PH_3)_2$ case using $\Delta E = 45.4$ kcal/mol [$Pt(d^8 s^1 - d^8 s^2) = 17.2$ kcal/mol and $Pd(d^8 s^1 - d^8 s^2) = 82.6$ kcal/mol].

Table IV. Average bond energies for $M(R)_2$ complexes (kcal/mol).

Molecule	Excitation Energy	M-H		M-CH ₃		Difference in M-H and M-CH ₃ Bond Energies \bar{D}_{298} and \bar{D}_I
		\bar{D}_{298}	\bar{D}_I	\bar{D}_{298}	\bar{D}_I	
M = Pt	-12.3	68.7	62.6	53.0	46.9	15.7
M = Pd	+19.6	50.1	59.9	35.8	45.7	14.2
M = Pt(PH ₃) ₂	+32.1 ^{a)}	58.3	(74.4)	39.6	55.7	18.7
M = Pd(PH ₃) ₂	+57.2 ^{a)}	(39.6)	(68.2)	22.3	50.9	(17.3)
M = Pt(Cl) ₂ (PH ₃) ₂	38.6 ^{a)}	(53.4)	(72.7)	31.7	51.0	(21.7)
M = Pd(Cl) ₂ (PH ₃) ₂	(84.0) ^{b)}	((33.3))	((75.3))	(10.0)	(52.0)	((23.3))

^{a)} Based on the geometry of the $M(CH_3)_2$ complex.

^{b)} Based on $\Delta E = 38.6$ kcal for Pt complex plus the differential d^9s^1 to d^8s^2 energy (45.4 kcal).

Table V. Geometric parameters around metal atom in Pt and Pd complexes (all distances are in Å and all angles are in degrees).

Molecule	M-P distance	M-C distance	misc. distance	P-M-P angle	C-M-C angle	misc. angle
1 Pt(CH ₃) ₂ (PH ₃) ₂	2.46	2.06	-	101	89	-
2 Pd(CH ₃) ₂ (PH ₃) ₂	2.50	2.02	-	98	81	-
3 PtCl ₂ (CH ₃) ₂ (PH ₃) ₂	2.44	2.03	M-Cl(2.38)	95	90	Cl-M-Cl(177)
4 PtCl ₂ (PH ₃) ₂	2.44	-	M-Cl(2.35)	102	-	Cl-M-Cl(97)
5 Pt(H)(CH ₃)(PH ₃) ₂ ^{a)}	2.46	2.06	M-H(1.50)	101	-	H-Pt-C(84)
6 PtH ₂ (PH ₃) ₂ ^{b)}	2.45	-	M-H(1.50)	100	-	H-Pt-H(79)
7 Pt(PH ₃) ₂	2.32	-	-	180	-	-
8 Pd(PH ₃) ₂	2.41	-	-	180	-	-
Pt(CH ₃) ₂ ^{c)}	-	1.97	-	-	98	-
Pt(H)(CH ₃) ^{c)}	-	1.96	M-H(1.48)	-	-	H-Pt-C(98)
Pt(H) ₂ ^{c)}	-	-	M-H(1.51)	-	83	-
Pd(CH ₃) ₂ ^{c)}	-	1.96	-	-	92	-

^{a)} This geometry was not optimized but was estimated from the geometries (1) and (6). The geometries of the Pt(CH₃)(PH₃) fragment were taken frozen at the geometry of (1), and the C-Pt-H angle was chosen to be the average of the C-Pt-C angle of (1) and the H-Pt-H angle of (6).

^{b)} Reference 2a.

^{c)} Reference 2c.

Table VI. Enthalpies (kcal/mol at 298°K) for Pt(II) and Pd(II) salts. All ΔH_f° are from ref 36, except as noted.

Compound	$\Delta H_f^\circ[\text{PtX}_2(\text{s})]$	$\Delta H_f^\circ[\text{PdX}_2(\text{s})]$	$\Delta H[\text{Pt}_{(\text{g})}({}^1\text{S}) + \text{X}_2(\text{g}) \rightarrow \text{PtX}_{2(\text{s})}]$	$\Delta H[\text{Pd}_{(\text{g})}({}^1\text{S}) + \text{X}_2(\text{g}) \rightarrow \text{PdX}_{2(\text{s})}]^{\text{c)}$	$\Delta(\Delta H)$
Mt(OH) ₂ ^{a)}	-84	-88	-184 ^{a)}	-148	36
MtCl ₂	-33	-39	-166	-132	34
MtBr ₂	-15	-25	-148	-118	30

a) $\Delta H_{f298}^\circ(\text{H}_2\text{O}_2) = -32.53$ kcal/mol, JANAF Thermochemical Tables, Second Edition, D. R. Stull and H. Prophet (National Bureau of Standards, Washington, DC; June 1971), NSRDS-NBS 37.

b) $\Delta H_{\text{sub}}^\circ(\text{Pt}) = 121.6$ kcal/mol at 25°C,³⁶ $\Delta E({}^3\text{D} \rightarrow {}^1\text{S}) = 11.0$ kcal/mol;¹⁸ consequently, $\Delta H_f^\circ[({}^1\text{S})\text{Pt}] = 121.6 + 11.0 = 132.6$ kcal/mol.

c) $\Delta H_{\text{sub}}^\circ(\text{Pd}) = 92.96$ kcal/mol.³⁶ The ground state of Pd is ${}^1\text{S}$; therefore, $\Delta H_{\text{sub}}^\circ(\text{Pd}) = \Delta H_f^\circ[\text{Pd}_g({}^1\text{S})]$.

Supplementary Material. -140-

The following seven tables contain the cartesian coordinates of the optimized geometries for the molecules studied in this paper. The eighth table contains the internal coordinates of the phosphine and methyl groups for the geometries tabulated in tables SI-SVII.

Table S.I. Cartesian Coordinates for $\text{Pt}(\text{CH}_3)_2(\text{PH}_3)_2$ (Å)

Atom	X	Y	Z
Pt	0.000000	0.000000	0.030594
C(1)	0.000000	-1.378597	1.528559
HC(1)	0.000000	-2.406768	1.173832
HC(2)	-0.883506	-1.241806	2.145267
HC(3)	0.883506	-1.241806	2.145267
C(2)	0.000000	1.378597	1.528559
HC(4)	0.000000	2.406768	1.173832
HC(5)	0.883506	1.241806	2.145267
HC(6)	-0.883506	1.241806	2.145267
P(1)	0.000000	-1.896819	-1.490378
HP(1)	0.000000	-3.237424	-0.779494
HP(2)	-1.147403	-2.175522	-2.452186
HP(3)	1.147403	-2.175522	-2.452186
P(2)	0.000000	1.896819	-1.490378
HP(4)	0.000000	3.237424	-0.779494
HP(5)	1.147403	2.175522	-2.452186
HP(6)	-1.147403	2.175522	-2.452186

Level of Wavefunction	Total Energies at This Geometry (hartrees)	Total Energies at Dissociated Limit (hartrees)	ΔE (kcal/mol)
Hartree-Fock	-791.3802	-791.4082	-19.0
GVB-CI(2/4)	-791.4183	-791.4290	-6.7
GVB-RCI(4/8) \times GVB-CI(2/4)	-791.4851	-791.4980	-8.1

Table S.II. Cartesian Coordinates for $\text{Pd}(\text{CH}_3)_2(\text{PH}_3)_2$ (Å)

Atom	X	Y	Z
Pd	0.000000	0.000000	0.055150
C(1)	0.000000	-1.305608	1.592483
HC(1)	0.000000	-2.343222	1.269129
HC(2)	-0.880756	-1.121416	2.196919
HC(3)	0.880756	-1.121416	2.196919
C(2)	0.000000	1.305608	1.592483
HC(4)	0.000000	2.343222	1.269129
HC(5)	0.880756	1.121416	2.196919
HC(6)	-0.880756	1.121416	2.196919
P(1)	0.000000	-1.885864	-1.581444
HP(1)	0.000000	-3.171799	-0.786064
HP(2)	-1.138148	-2.226994	-2.540769
HP(3)	1.138148	-2.226994	-2.540769
P(2)	0.000000	1.885864	-1.581444
HP(4)	0.000000	3.171799	-0.786064
HP(5)	1.138148	2.226994	-2.540769
HP(6)	-1.138148	2.226994	-2.540769

Level of Wavefunction	Total Energies at This Geometry (hartrees)	Total Energies at Dissociated Limit (hartrees)	ΔE (kcal/mol)
Hartree-Fock	-792.9620	-793.0295	-42.4
GVB-CI(2/4)	-793.0066	-793.0498	-27.1
GVB-RCI(4/8)×GVB-CI(2/4)	-793.0639	-793.1318	-42.6

Table S.III. Cartesian Coordinates for $\text{PtCl}_2(\text{CH}_3)_2(\text{PH}_3)_2$ (Å)

Atom	X	Y	Z
Pt	0.000000	0.000000	0.136317
C(1)	0.000000	-1.438951	1.574711
HC(1)	0.000000	-2.448813	1.169736
HC(2)	-0.902419	-1.302946	2.157062
HC(3)	0.902419	-1.302946	2.157062
C(2)	0.000000	1.438951	1.574711
HC(4)	0.000000	2.448813	1.169736
HC(5)	0.902419	1.302946	2.157062
HC(6)	-0.902419	1.302946	2.157062
Cl(1)	-2.382457	0.000000	0.066219
Cl(2)	2.382457	0.000000	0.066219
P(1)	0.000000	1.797415	-1.509749
HP(1)	0.000000	3.055002	-0.692679
HP(2)	1.187320	2.017055	-2.424796
HP(3)	-1.187320	2.017055	-2.424796
P(2)	0.000000	-1.797415	-1.509749
HP(4)	0.000000	-3.055002	-0.692679
HP(5)	-1.187320	-2.017055	-2.424796
HP(6)	1.187320	-2.017055	-2.424796

Level of Wavefunction	Total Energies at This Geometry (hartrees)	Total Energies at Dissociated Limit (hartrees)	ΔE (kcal/mol)
Hartree-Fock	-1710.3463	-1710.4079	-38.7
GVB-RCI(2/4)×GVB-CI(2/4)	-1710.4272	-1710.4554	-17.7
GVB-RCI(5/10)×GVB-CI(2/4)	-1710.4718	-1710.5116	-25.0

Table S.IV. Cartesian Coordinates for $\text{PtCl}_2(\text{PH}_3)_2$ (Å)

Atom	X	Y	Z
Pt	0.000000	0.000000	0.066550
Cl(1)	0.000000	1.683502	1.712871
Cl(2)	0.000000	-1.683502	1.712871
P(1)	0.000000	-1.905718	-1.463152
HP(1)	0.000000	-3.257738	-0.758184
HP(2)	-1.153527	-2.147114	-2.437360
HP(3)	1.153527	-2.147114	-2.437360
P(2)	0.000000	1.905718	-1.463152
HP(4)	0.000000	3.257738	-0.758184
HP(5)	1.153527	2.147114	-2.437360
HP(6)	-1.153527	2.147114	-2.437360

Level of Wavefunction	Total Energies at This Geometry (hartrees)
Hartree-Fock	-1631.2019
RCI(2/4)	-1631.2343
GVB-RCI(6/12)	-1631.2906

Table S.V. Cartesian Coordinates for Pt(H)(CH₃)(PH₃)₂ (Å)

Atom	X	Y	Z
PT	0.000000	0.000000	0.030594
C(1)	0.000000	-1.378597	1.528559
CH(1)	0.000000	-2.406768	1.173832
CH(2)	-0.883506	-1.241806	2.145267
CH(3)	0.883506	-1.241806	2.145267
H(1)	0.000000	0.960402	1.187922
P(1)	0.000000	-1.896819	-1.490378
HP(1)	0.000000	-3.237424	-0.779494
HP(2)	-1.147403	-2.175522	-2.452186
HP(3)	1.147403	-2.175522	-2.452186
P(2)	0.000000	1.896819	-1.490378
HP(4)	0.000000	3.237424	-0.779494
HP(5)	1.147403	2.175522	-2.452186
HP(6)	-1.147403	2.175522	-2.452186

Level of Wavefunction	Total Energies at This Geometry (hartrees)	Total Energies at Dissociated Limit (hartrees)	ΔE (kcal/mol)
Hartree-Fock	-791.3671	-791.3880	-13.2
GVB-CI(2/4)	-791.4085	-791.4095	-0.6
GVB-RCI(4/8)×GVB-CI(2/4)	-791.4670	-791.4785	-7.2

Table S.VI. Cartesian Coordinates for Pt(PH₃)₂ (Å)

Atom	X	Y	Z
Pt	0.000000	0.000000	0.000000
P(1)	0.000000	-2.318176	0.000000
HP(1)	0.000000	-3.097940	1.312807
HP(2)	-1.136924	-3.097940	-0.656404
HP(3)	1.136924	-3.097940	-0.656404
P(2)	0.000000	2.318176	0.000000
HP(4)	0.000000	3.097940	1.312807
HP(5)	1.136924	3.097940	-0.656404
HP(6)	-1.136924	3.097940	-0.656404

Level of Wavefunction	Total Energies at This Geometry (hartrees)
Hartree-Fock	-712.2023
GVB-CI(1/2)	-712.2080
GVB-RCI(5/10)	-712.2770

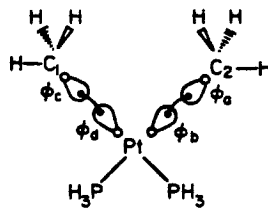
Table S.VII. Cartesian Coordinates for Pd(PH₃)₂ (Å)

Atom	X	Y	Z
Pd	0.000000	0.000000	0.000000
P(1)	0.000000	-2.405422	0.000000
HP(1)	0.000000	-3.210795	1.301985
HP(2)	-1.127552	-3.210795	-0.650993
HP(3)	1.127552	-3.210795	-0.650993
P(2)	0.000000	2.405422	0.000000
HP(4)	0.000000	3.210795	1.301985
HP(5)	1.127552	3.210795	-0.650993
HP(6)	-1.127552	3.210795	-0.650993

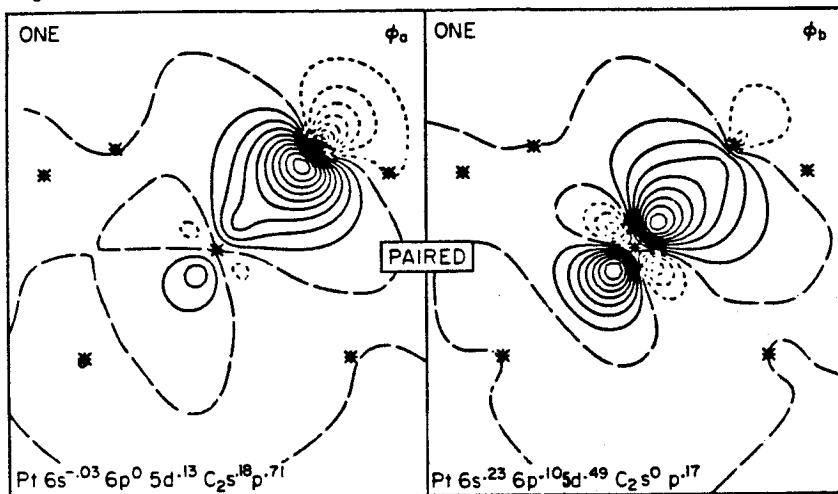
Level of Wavefunction	Total Energies at This Geometry (hartrees)
Hartree-Fock	-713.8235
GVB-CI(1/2)	-713.8288
GVB-RCI(5/10)	-713.9107

Table S. VIII. Internal Coordinates of Methyls and Phosphines.

	Pt(CH ₃) ₂ (PH ₃) ₂	Pd(CH ₃) ₂ (PH ₃) ₂	PtCl ₂ (CH ₃) ₂ (PH ₃) ₂	PtCl ₂ (PH ₃) ₂	Pt(PH ₃) ₂	Pd(PH ₃) ₂
r [C(1)-HC(1)] Å	1.09	1.08	1.09	--	--	--
r [C(1)-HC(2)] Å	1.09	1.08	1.08	--	--	--
θ [HC(1)-C(1)-HC(2)]°	108	109	108	--	--	--
θ [HC(2)-C(1)-HC(3)]°	109	109	113	--	--	--
r [P(1)-HP(1)] Å	1.52	1.53	1.50	1.52	1.53	1.53
r [P(1)-HP(2)] Å	1.52	1.53	1.52	1.53	1.53	1.53
θ [HP(1)-P(1)-HP(2)]°	98	98	98	99	96	95
θ [HP(2)-P(1)-HP(3)]°	98	96	103	98	96	95



Right Pt-C Bond Pair



Left Pt-C Bond Pair

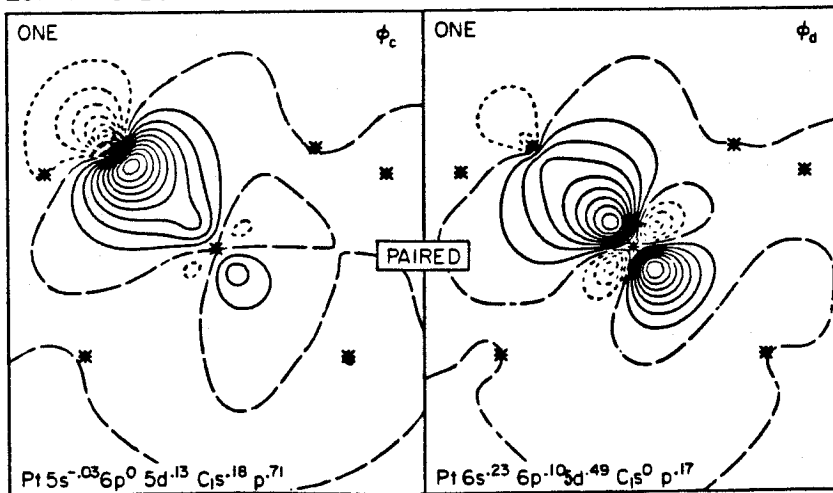
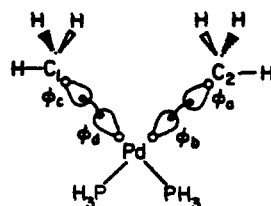
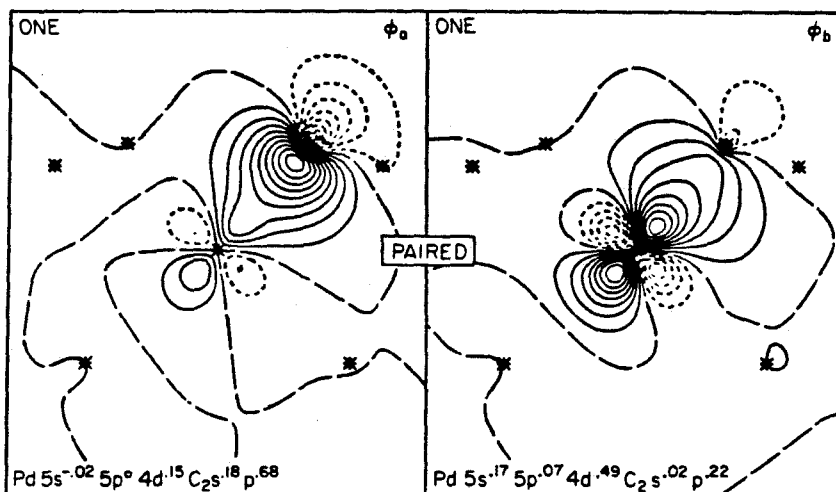


Figure 1. The GVB orbitals for 1 [from the CVB(5/10)-PP wavefunction]. Nuclei in the plane are indicated by asterisks. Positive contours are solid, negative contours are dotted, and nodal lines are long dashes. The spacing between contours is 0.05 a.u. Analysis of each GVB orbital in terms of a Mulliken population is shown.



Right Pd-C Bond



Left Pd-C Bond

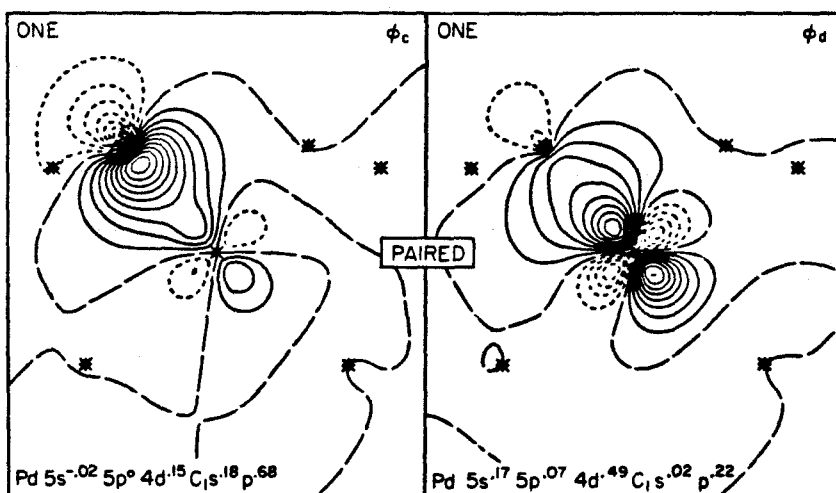
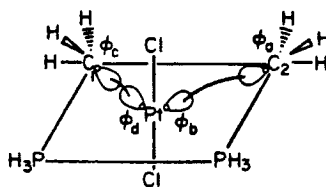
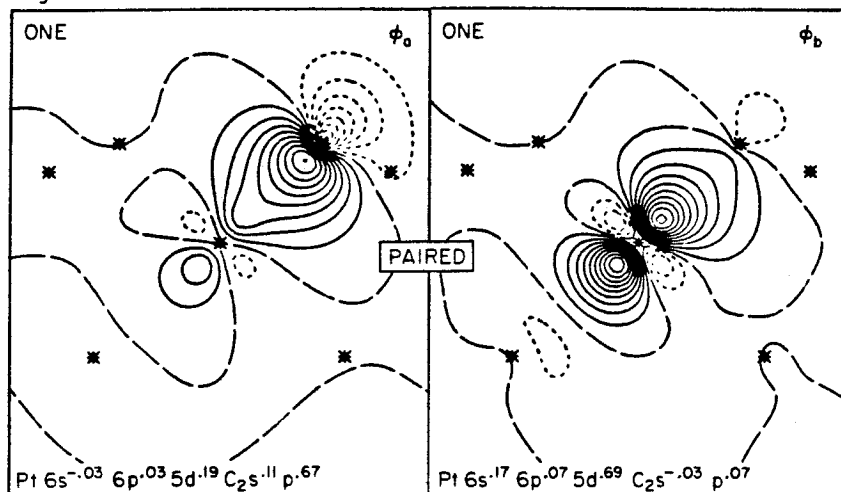


Figure 2. The GVB orbitals for the Pt-C bonds of 2.



Right Pt-C Bond



Left Pt-C Bond

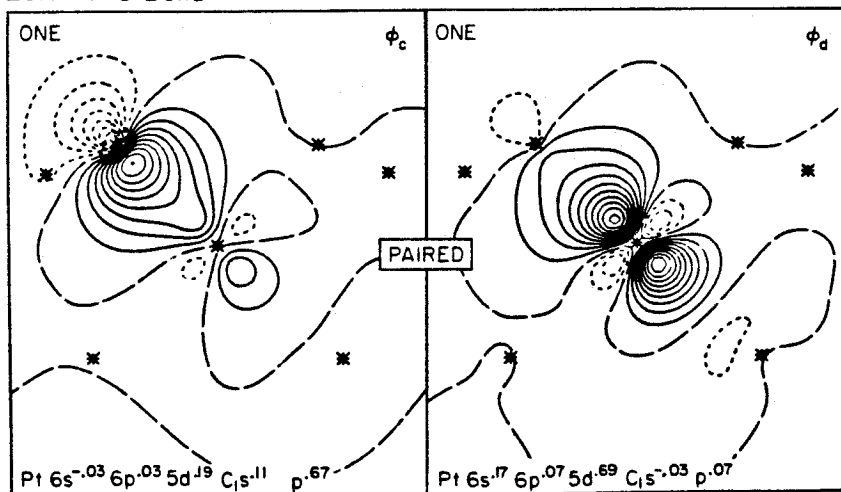
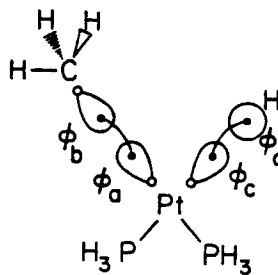
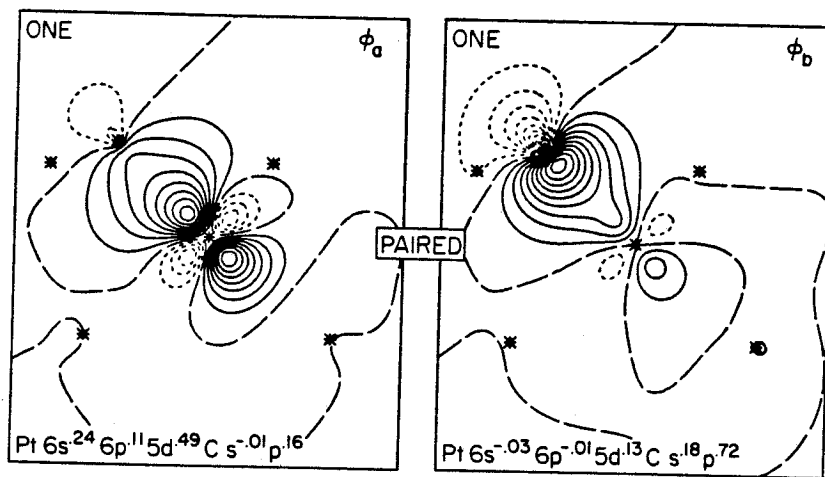


Figure 3. The GVB orbitals for the Pt-C bonds of 3.



Pt-C Bond Pair



Pt-H Bond Pair

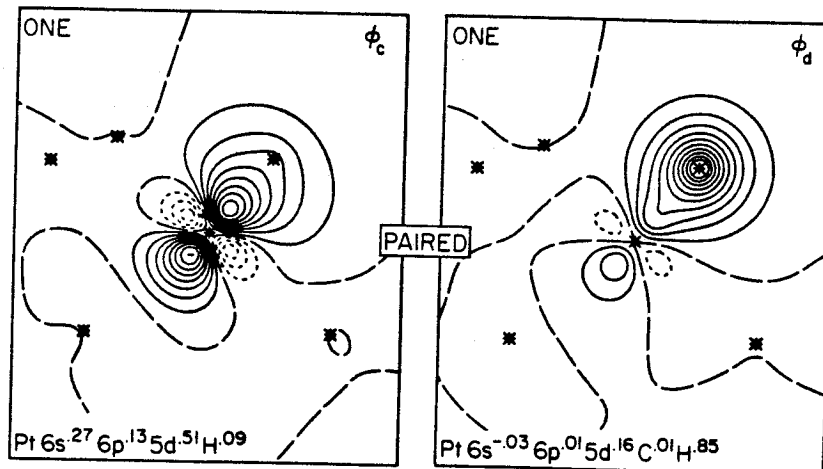


Figure 4. The GVB orbitals for the Pt-H and Pt-C bonds of **5**.

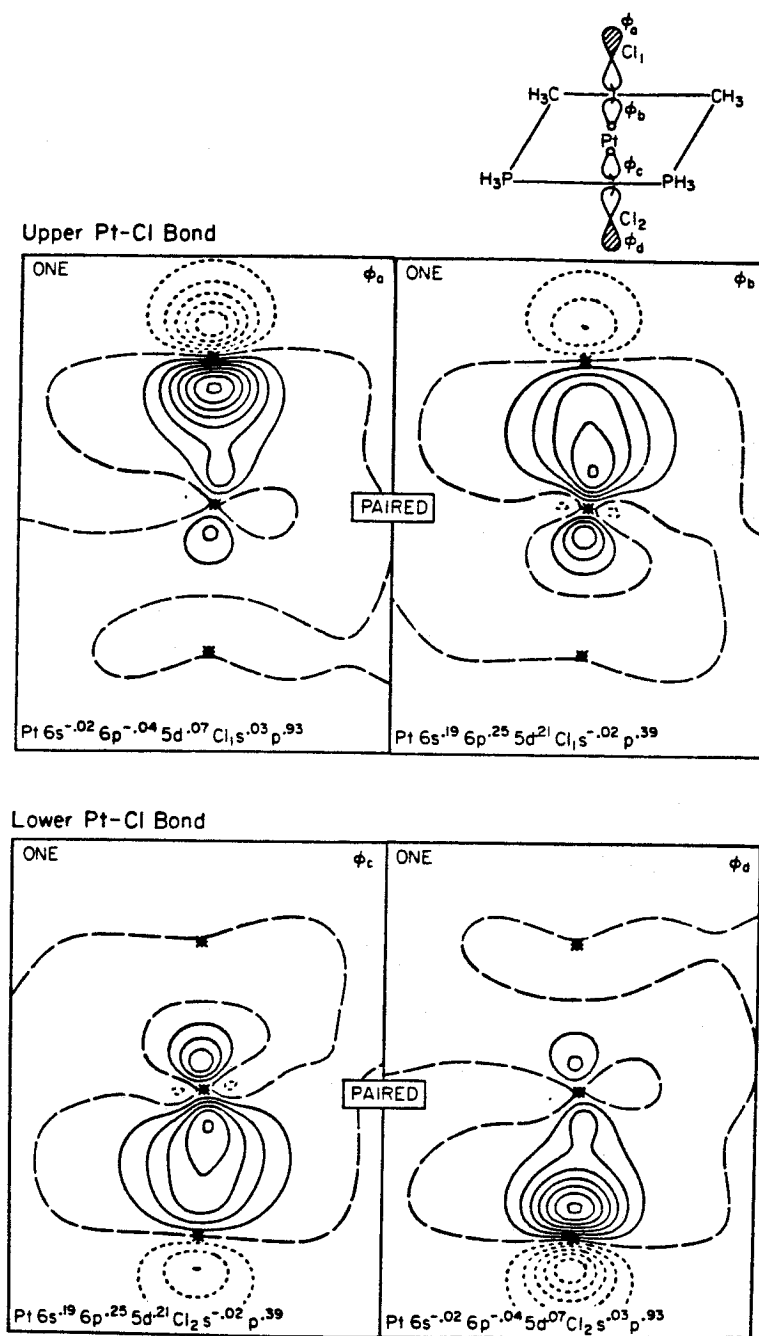
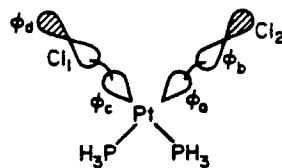
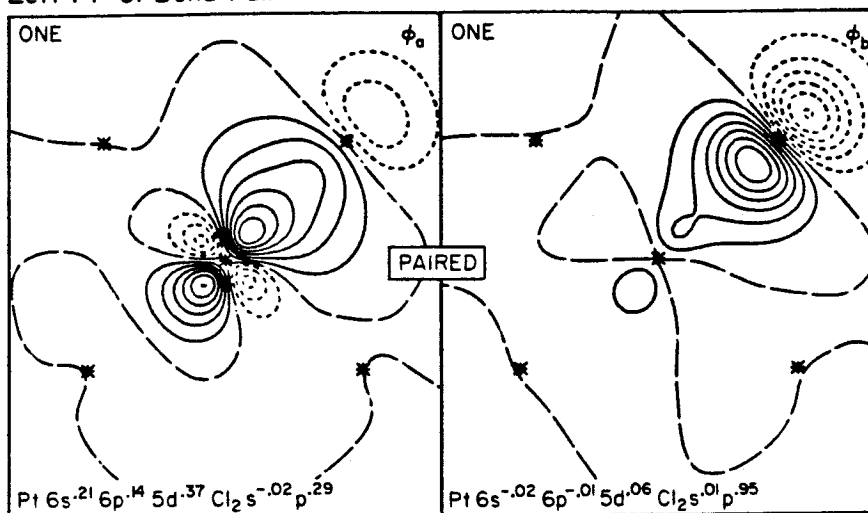


Figure 5. The GVB orbitals for the Pt-Cl bond of 3.



Left Pt-Cl Bond Pair



Right Pt-Cl Bond Pair

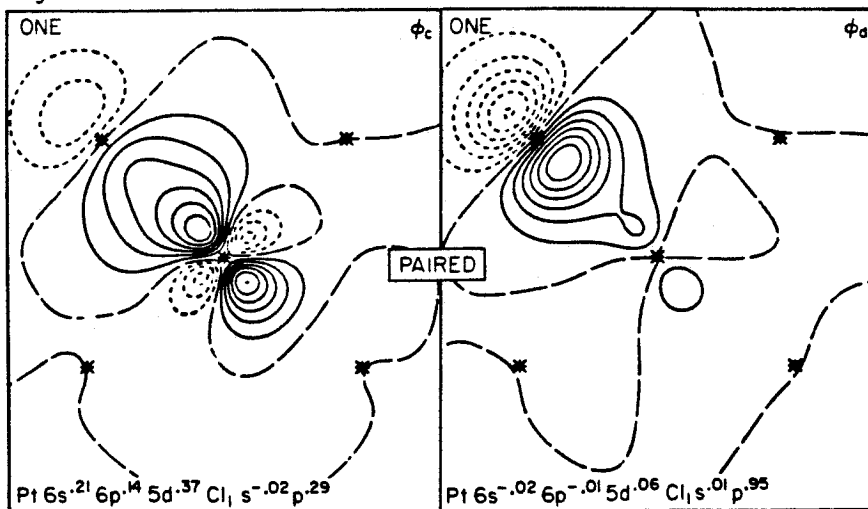


Figure 6. The GVB orbitals for the Pt-Cl bond of 4.

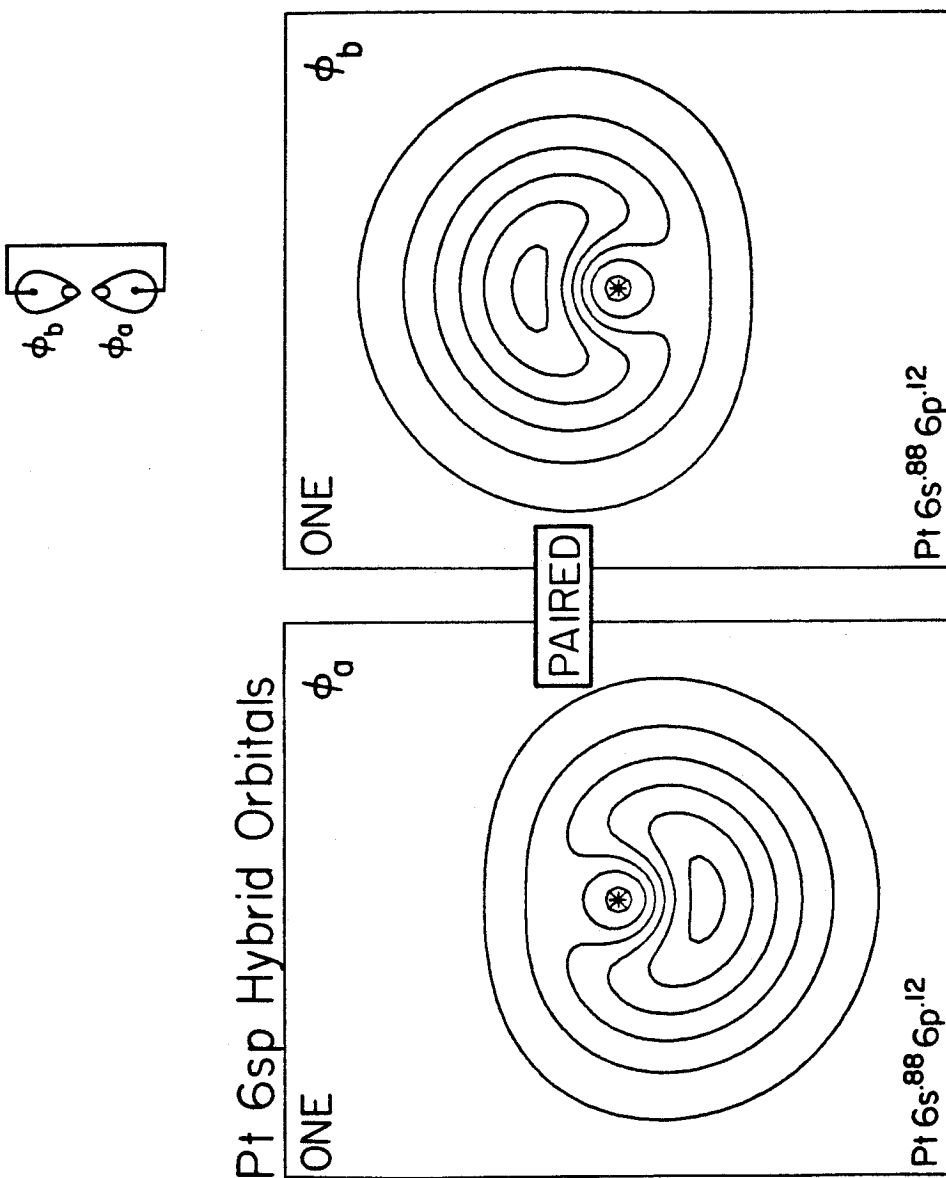


Figure 7. The GVB orbitals for the s^2 pair of the d^8s^2 state of Pt.

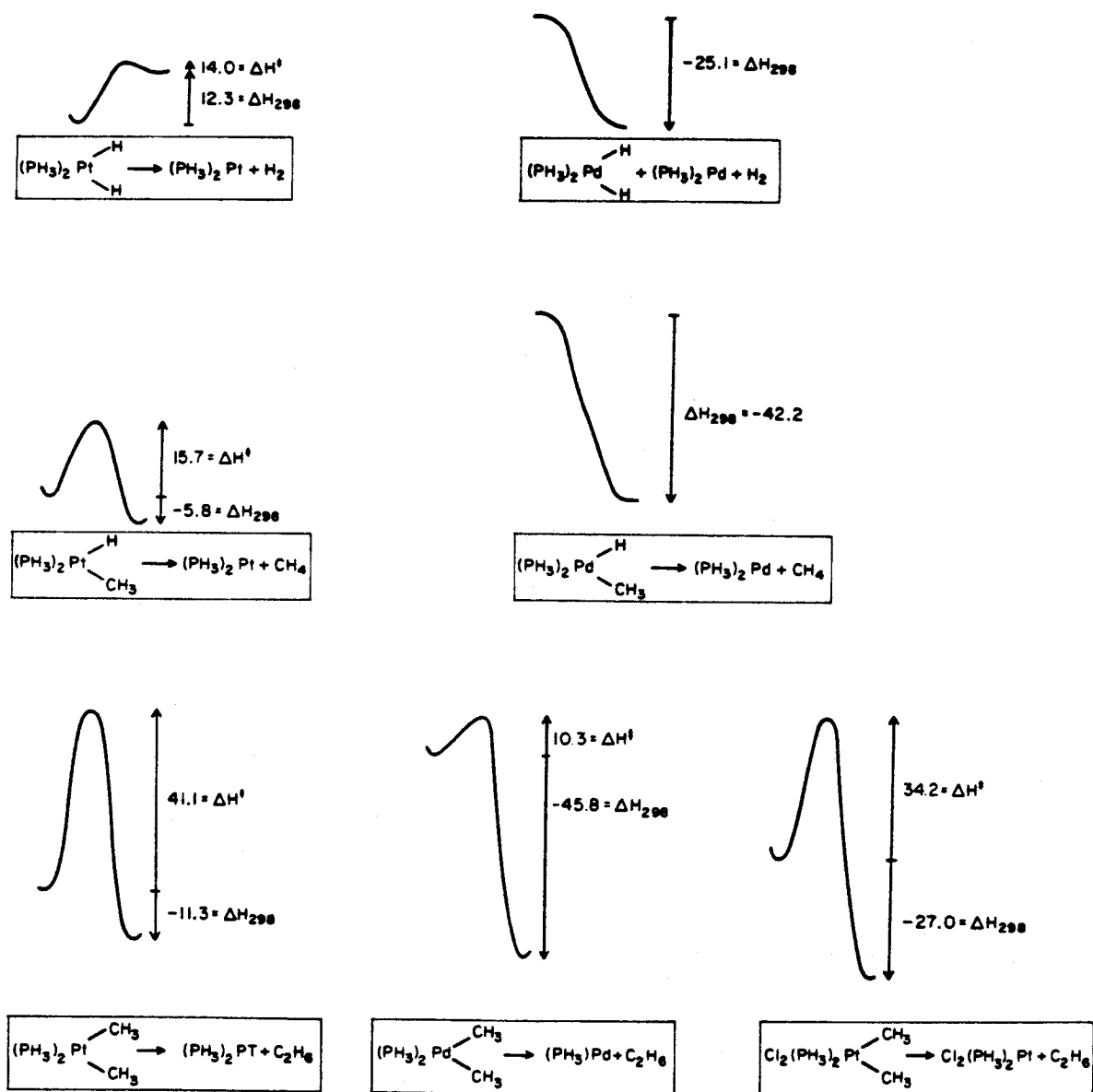


Figure 8. Estimated energetics for $\text{R}_1\text{-R}_2$ reductive coupling of $(\text{PH}_3)_2\text{Mt}(\text{R}_1)(\text{R}_2)$ complexes. All quantities are enthalpies at 298°K.

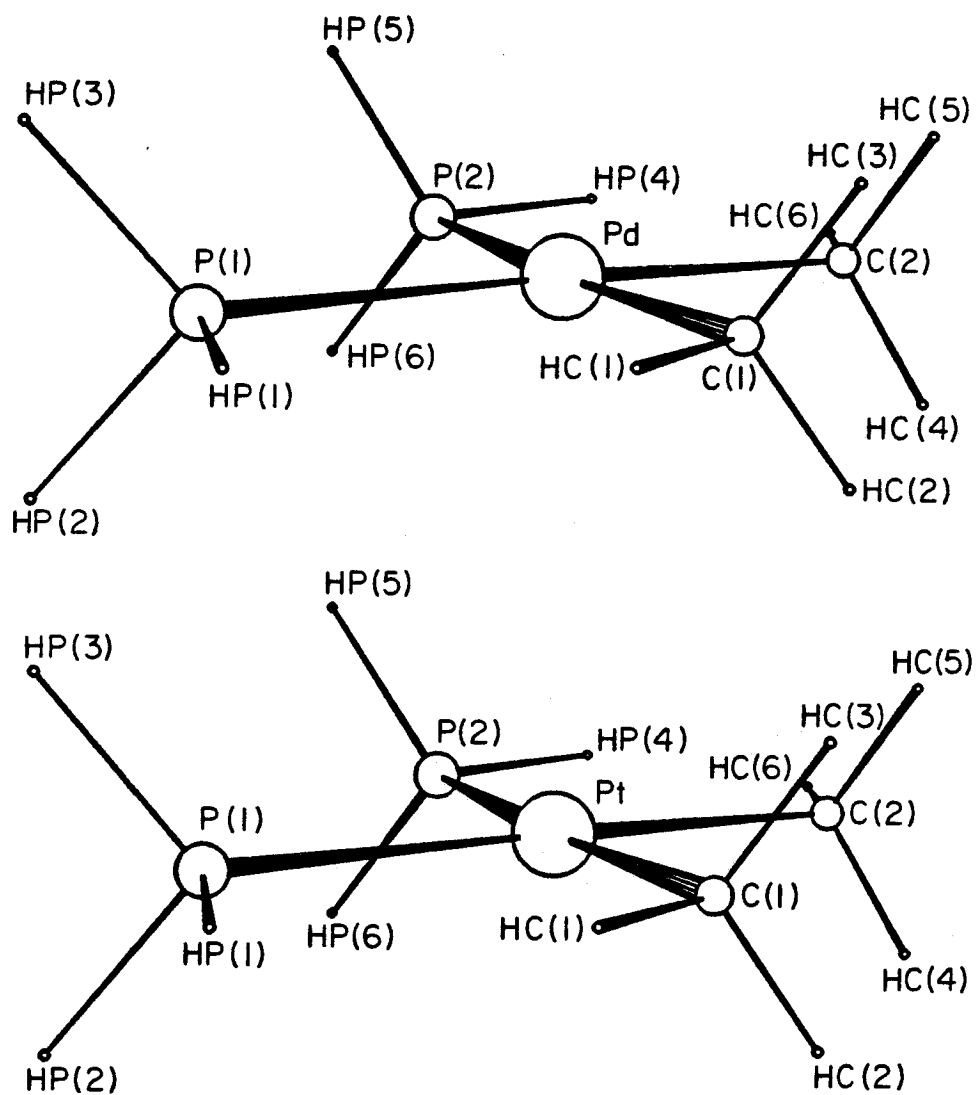


Figure 9. ORTEP plot of 1 and 2.

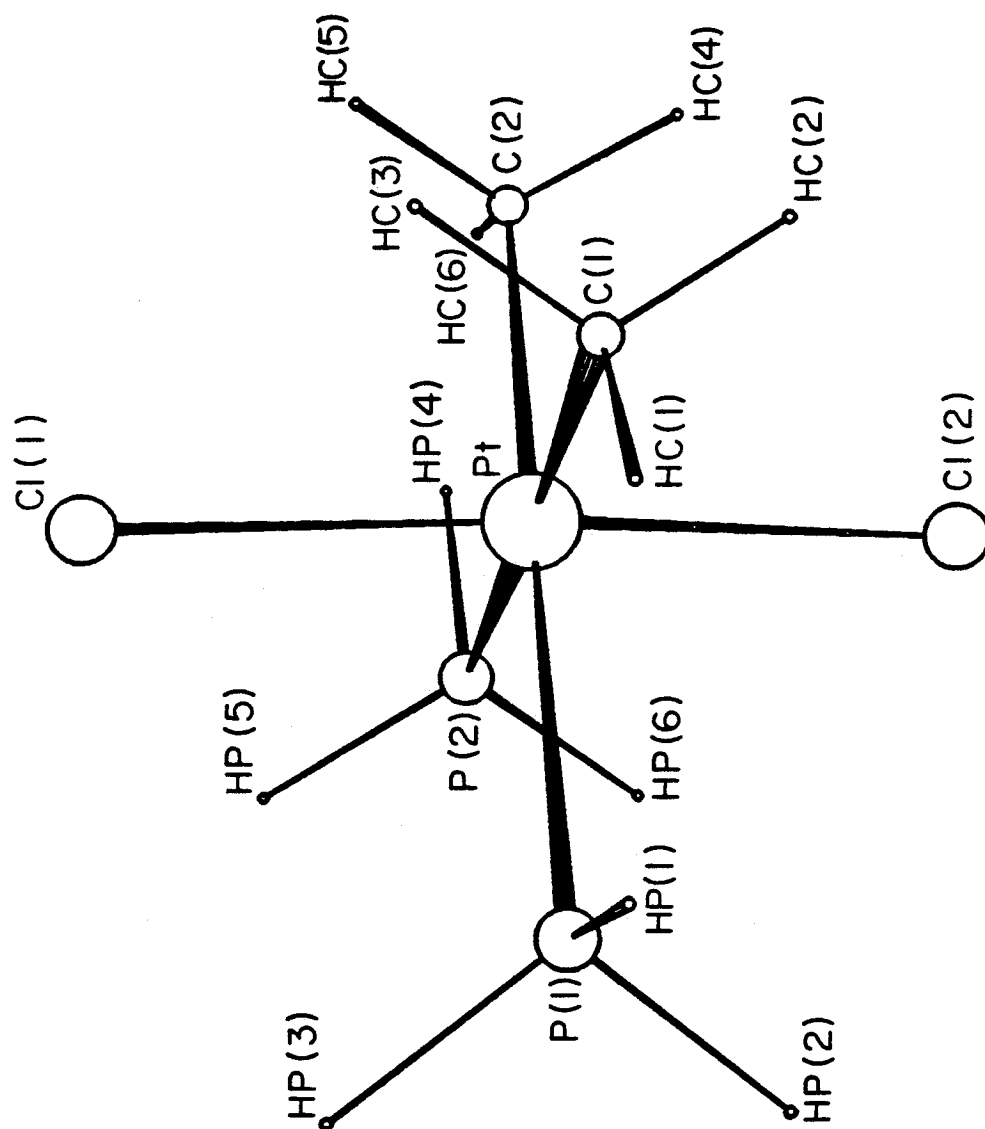


Figure 10. ORTEP plot of 3.

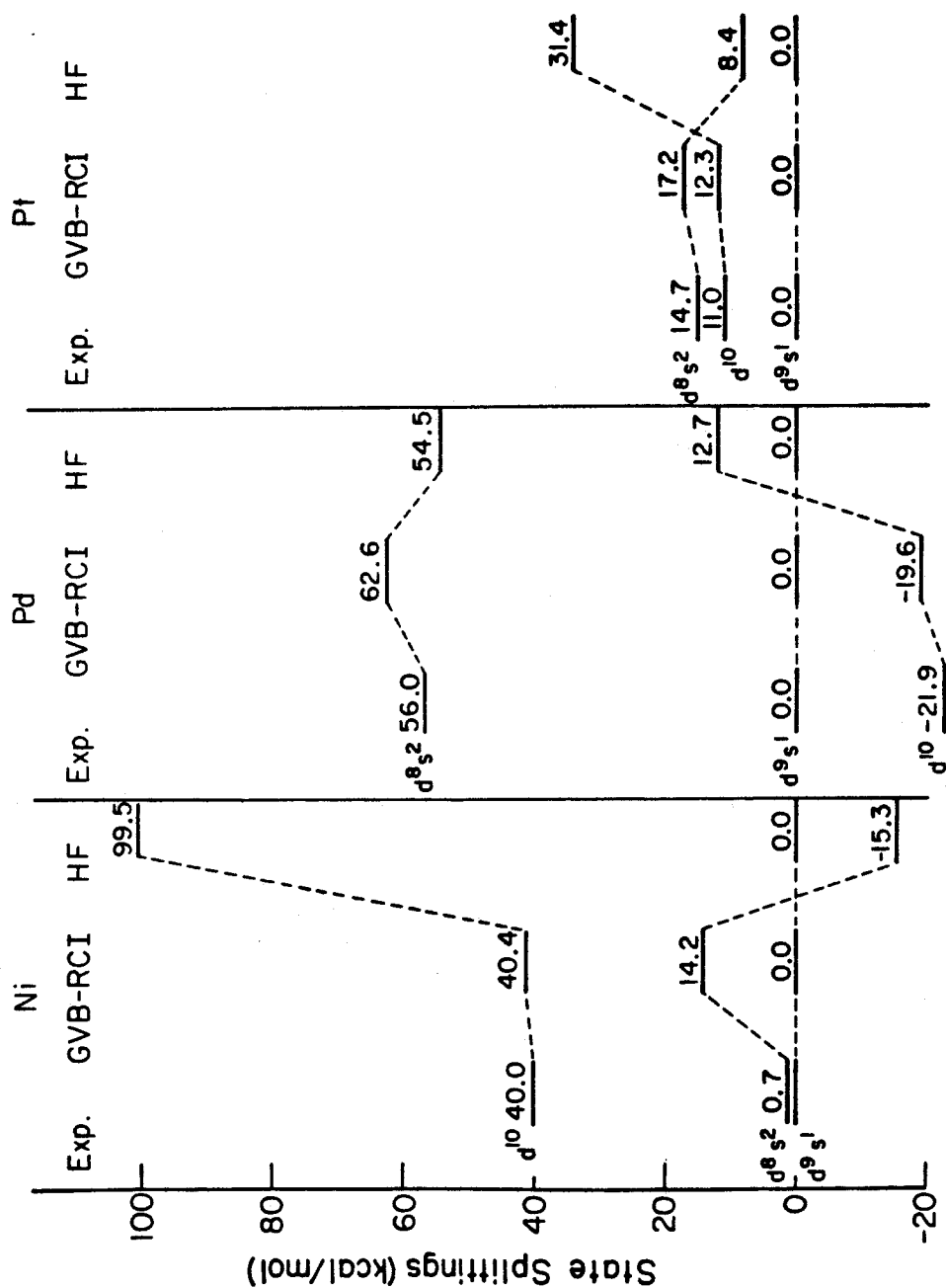


Figure 11. Atomic excitation energies for Ni, Pd, and Pt. All quantities in kcal/mol.

CHAPTER 4

Theoretical Studies of CH_x and NH_x

Species Chemisorbed on Ni Clusters

I. Introduction

The chemisorption of small molecules on metal surfaces has been the subject of many experimental¹ and theoretical² studies. The low index surfaces of metals have been used to model many catalytic reactions including methanation³ and ammonia decomposition on metal surfaces.⁴ The problem with experimental studies is that critical intermediates are often very unstable and cannot be observed under typical experimental conditions. The advantage theory has is that a theorist can perform calculations on the various proposed intermediates and compare their relative energetics to see whether the proposed mechanism is reasonable or not.⁵ The problem that a theorist has is that the system to be modelled is very large, which forces him to make various approximations in his calculations. These approximations affect the results in various ways that should be accounted for when attempting to relate theory to experiment.

In this paper we examine theoretically cluster models for the various intermediates important for methanation and ammonia decomposition on Ni surfaces. We have used the one-electron modified effective potential (MEP) of Upton and Goddard (UG)⁶ to simulate the Ni atoms of the cluster. This approximation involves replacing the Ar core and 3d⁹ shell of Ni by the MEP. Only the Ni 4s electrons are treated explicitly. This method allows the use of large clusters (13-20 atoms) to model the metal surface for chemisorption. The method has been used with considerable success in modelling chemisorption of H, O, S, Cl,⁶ and CO⁷ on Ni surfaces.

We have used the four-coordinate site of the Ni₁₃ cluster (see Figure 1) to model chemisorption of small molecules on the Ni(100) surface. This site allows the singly-occupied orbitals of the radical to have the largest overlap with the conduction band orbitals. This should lead to radical

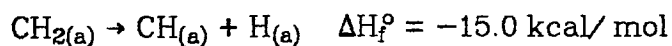
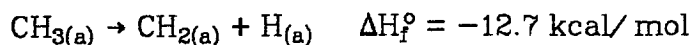
species forming the strongest bonds on high coordination sites. Carbon has been observed to bond to a similiar site in various carbidocarbonyl clusters⁸ (i.e., $\text{Fe}_5\text{C}(\text{CO})_{15}$). Akylidynes have been observed to be coordinated to three metal atoms in various metal cluster compounds.⁹ Since such a site is not available on the $\text{Ni}(100)$ cluster, methylidyne and carbon should both prefer the four-coordinate site. Methylene, on the other hand, has only been observed to bind to metal clusters at two-coordinate bridge sites.¹⁰ In this work we intend a first pass at the relative energetics for these chemisorbed intermediates. For these purposes the four-coordinate site of Ni_{13} is quite adequate. We have used the Ni_{14} (see figure 2) cluster to model chemisorption of closed shell molecules (i.e., NH_3 and CO) where the bonding is dominated by lewis acid/base interactions. More quantitative results would require larger clusters and perhaps higher levels of theory. This work is intended to provide a qualitative understanding of the nature of the surface chemical bond and to help organize further theoretical study in this area.

II. Results

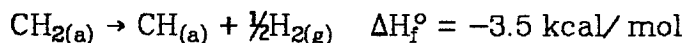
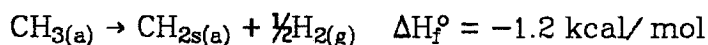
A. Qualitative Description of Bonding

The ${}^4T_{1g}$ ($1a_{1g}^2 t_{1u}^6 t_{2g}^4 e_g^1$) excited state of the Ni_{13} cluster was chosen to model the bulk for the four-coordinate site of Ni(100). This state is 5.6 kcal/mol above the ${}^2T_{1g}$ ($1a_g^2 t_{1u}^6 t_{2g}^5$) ground state. This state was chosen because it had orbitals available for forming σ and π bonds to the various intermediates studied here. The ${}^2T_{1g}$ ground state only had a singly-occupied orbital of π symmetry available for forming bonds. In the ground state of all the CH_x and NH_x complexes studied here, the Ni_{13} cluster was in its ${}^4T_{1g}$ electronic state. (For more details about the low lying states of the Ni_{13} cluster see Appendix A.) The ${}^1A_{1g}$ ground state of Ni_{14} cluster⁷ was chosen to model the bulk for the one-coordinate site of Ni(100). The calculated geometries, vibrational frequencies and energetics are shown in Table I.

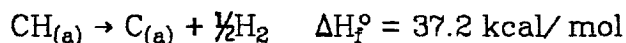
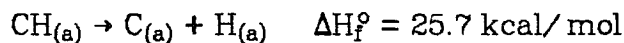
The GVB orbitals for methyldiyne (CH), methylene (CH_2), and methyl (CH_3) are shown in Figures 3-5. In general, the bonding of these species can be characterized as forming a high-overlap ionic σ -bond and low-overlap covalent π bonds. The surface bonds for methyldiyne, methylene, and methyl are best described as triple (1σ and 2π), double (1σ and 1π), and single (1σ) bonds, respectively. The carbon-surface π bonds in these systems are quite strong. This causes the decomposition of chemisorbed CH_x to chemisorbed CH_{x-1} and chemisorbed H to be about 14 kcal/mol downhill for $x=(2 \text{ and } 3)$.



By assuming a C-H bond strength of 98 kcal/mol¹¹ and a surface-H bond strength of 63 kcal/mol,¹² we estimate a surface-carbon π bond strength of 49 kcal/mol. This is only 5 kcal/mol stronger than our calculated surface-carbon σ bond strength of 43.6 kcal/mol for chemisorbed methyl. The surface-carbon π bond strength is close to the difference in the C-H bond strength (98 kcal/mol) and half of the H-H bond strength (52.1 kcal/mol)¹³ which causes the dehydrogenation of chemisorbed methyl or methylene to give dihydrogen and chemisorbed methylene or methyldiyne to be essentially isoenergetic processes.

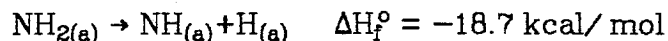
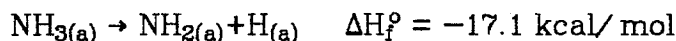


Carbon atom bonds to the surface in a very different manner (see the GVB orbitals in Figure 6). The chemisorbed carbon atom is best described as a C^- , which has formed two covalent π bonds to the surface. An electron from the cluster has moved to the C $2p_z$ orbital. This implies that the maximum number of bonds that a CH_x species can form to the surface is three. When the last C-H bond is broken in chemisorbed methyldiyne to yield chemisorbed carbon, the carbon electron involved in the C-H bond is not able to form another bond to the surface. Thus the chemisorbed carbon ends up having significant radical character. Therefore it is uphill energetically to dissociate methyldiyne to carbon and hydrogen atoms on our clusters. This will have a significant impact on the surface chemistry of carbon, which will be discussed in the next section.



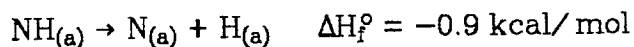
The GVB orbitals for imidogen (NH), amidogen (NH₂), and ammonia (NH₃) are shown in Figures 7-9. In general, these species make σ bonds that can be characterized as donor-acceptor bonds and covalent π bonds. The bonds that imidogen, amidogen, and ammonia make to the surface are triple, double, and single bonds, respectively. Nitrogen atom (see GVB orbitals in Figure 10) forms a triple bond to the surface. The three bonds consist of an ionic σ bond and two covalent π bonds to the surface that are similar to the methylidyne surface bonds.

Just like the CH_x species, the NH_x species also makes fairly strong π bonds to the surface. This causes the decomposition of NH_{x(a)} to NH_{x-1(a)} and H_(a) to be downhill by about 18 kcal/mol for x=(2 and 3). Assuming a N-H bond strength of 106 kcal/mol,¹⁴ we can estimate a surface-N π bond energy of 61 kcal/mol.



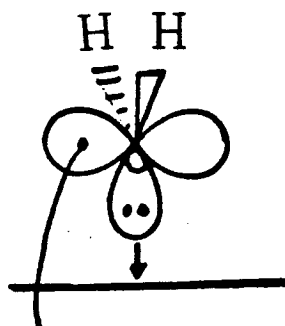
When chemisorbed imidogen decomposes to chemisorbed nitrogen and hydrogen, the lewis acid/base surface-N bond and N-H bond are replaced by a surface-N ionic bond and surface-H bond. The difference between these two bond energies is apparently very close to difference in energy between a N-H (106 kcal/mol) and a surface-hydrogen bond (63

kcal/mol) which causes the decomposition of chemisorbed imidogen to chemisorbed nitrogen and hydrogen to be essentially isoenergetic.

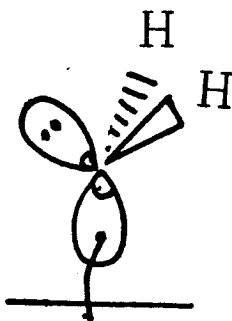


The bond that ammonia makes to the four-coordinate site of Ni_{13} is very weak (2.04 kcal/mol). In fact, when the zero point energy is added, it is unbound by 1.6 kcal/mol. Ammonia is bound by 10 kcal/mol to the one-coordinate site of the Ni_{14} cluster. This shows that the donor/acceptor bond of ammonia is stronger when bound to the one-coordinate site than to higher coordination sites. The lone pair of ammonia favors the on-top site because it can form a lewis acid/base bond to the metal center, without disrupting metal-metal bonding in the cluster. Even though the lone pair of ammonia would be stabilized by more metal centers at a higher coordination site through lewis acid/base interactions, it would also have higher overlap with the occupied orbitals of the conduction band (4s) electrons. We therefore believe that ammonia prefers sites where it is coordinated to only a single metal center.

We find that the surface-carbon and surface-nitrogen π bonds are very important in the nature of the surface chemical bond. In general, we find that these π bonds are slightly stronger than the corresponding σ bonds for CH_x species. This is also true for NH_x species, because we have found that these species prefer to bind oriented perpendicular to the surface where it can make a π bond and a lewis acid/base σ bond



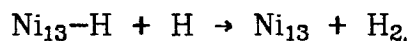
rather than to bend over where it can only make a σ bond.



We find that oxygen atom binds to the surface by making an ionic σ bond and a covalent π bond (see figures 11 and 12). This state is very similar to the oxide state found on Ni_{20} by UG.⁶

B. Quantitative Discussion

The parameters calculated for chemisorbed species discussed above are shown in Table I. In general, in going from single to double to triple bonds, the bond energy increases. The calculated bond energies for the multiple surface bonds appear to be systematically high. The worst case is for the surface oxygen bond of 157 kcal/mol, which is much higher than the experimental estimates of 94-135 kcal/mol.¹⁵ The calculated bond energy for H on Ni_{13} (66 kcal/mol) is fortuitously close to the experimental value for hydrogen bound to Ni surfaces (63 kcal/mol).¹² If we examine the process



we calculate a ΔH_f° for this reaction of -23.3 kcal/mol compared to experimental ΔH_f° of -40.1 kcal/mol. This means that the calculated D_0 for the chemisorbed hydrogen is 16.8 kcal/mol too strong, assuming that the correlation error is the same for the surface H bond as it is for the H-H bond. This error can arise from either the small cluster size or the tendency of the MEP to have systematically large bond energies.¹⁶

In order to account for this bias toward stronger bond strengths, we have used the error in the Ni-H bond to account for the errors made in carbon-surface and nitrogen-surface bonds. The procedure we have used is essentially an equibondedness approach,¹⁷ in which the total number of bonds and the number of bonds to the surface were held fixed (see Computational Details). All of the bonds made through donor-acceptor bonds to the surface have been assumed to have no correlation error. This appears to be reasonable in light of the bond strength (10.9 kcal/mol) of NH_3 to Ni_{14} , which compares well to the experimental chemisorption energy of NH_3 to nickel surfaces (~ 12 kcal/mol)⁴. The reactions used to calculate enthalpies of formation at 0°K are shown in Table II. The enthalpies for any particular intermediate are predicted from the change in the calculated energies and from enthalpies known either from experiment (see Table III) or previous equibondedness reactions. We have used the experimental enthalpies of methane, ammonia, chemisorbed H and chemisorbed CO^{18} as references. The ΔH_f° calculated in this manner along with experimental ΔH_f° (see table III and IV) can then be used to calculate the corrected D_0 shown in Table I and to compare the relative enthalpies of various intermediates.

A good test of these energetics is to compare them to two simple reactions which are known to proceed on Ni surfaces.¹⁹ Our calculated enthalpy for the disproportionation reaction of CO (the Boudouard Reaction)^{19a}



indicates that our carbon-surface bond strength is reasonable, but we calculate the reduction of chemisorbed oxygen^{19b}



to be uphill energetically, indicating that our corrected oxygen-surface bond strength is still too high.

The enthalpies of formation at 0° K for NH_x intermediates are shown in Figure 13. The enthalpy changes for the steps shown in figure 13 are tabulated in table V. Chemisorbed imidogen is calculated to be the most stable NH_x intermediate. Decomposition of ammonia has been observed to occur at low temperature (200° K) in an electron beam on Ni(111) surfaces²⁰ and the decomposition product was tentatively assigned to chemisorbed imidogen by ultraviolet photoelectron spectroscopy. Ammonia also decomposes on Ni(110) at temperatures above 150° K to some unidentified NH_x intermediate.^{21,22} Hüttlinger and Küppers²³ have performed thermal desorption spectroscopy (TDS) experiments suggesting that chemisorbed amidogen is formed by exposing ammonia to Ni(110) at temperatures below 350° K. This species decomposes at 410° K to give H_2 and chemisorbed nitrogen atom. Exposure of ammonia to Ni(110) at 400° K yields chemisorbed imidogen which decomposes at ~800° K to give N_2 and H_2 . Ammonia gas also been observed to decompose when exposed to Ni(100) at room temperature.²⁴ The intermediates were assigned to a

imidogen and amidogen intermediates by X-ray Photoelectron Spectroscopy. Unfortunately, all of the experimental work for ammonia decomposition only really shows that chemisorbed amidogen and imidogen are kinetically stable and not necessarily energetically stable. The experimental work does indicate that it is energetically favorable to dissociate ammonia on Ni surfaces, which is in agreement with our results, but the activation energy for dissociative chemisorption is higher than that for desorption of NH_3 molecules.

The relative enthalpies at 0°K for the various intermediates relevant for methanation are shown in Figure 14. The enthalpy changes for the steps shown in figure 14 are tabulated in table VI. These enthalpies imply that methylidyne is the most stable CH_x intermediate on Ni. Experimentally it is known that both acetylene and ethylene will decompose to chemisorbed methylidyne on $\text{Ni}(100)^{25}$ and $\text{Ni}(111)$,²⁷ suggesting that methylidyne is the most stable CH_x intermediate on Ni. Kinetic experiments²⁸ suggest that the most abundant species on supported Ni catalysts during methanation is chemisorbed carbon and chemisorbed methylidyne. Both of these experiments are consistent with our calculated energetics and proposal that methylidyne is the most stable CH_x intermediate on Ni surfaces.

The first step in dissociation of CO to chemisorbed carbon and oxygen is calculated to be downhill by 10.3 kcal/mol. Experimentally it is known that the dissociative chemisorption of CO does not occur for the low index faces of $\text{Ni}[(111) \text{ and } (100)]^{29,30}$ for temperatures below 450°K , at this temperature CO will have desorbed under ultra high vacuum conditions. This implies that the activation barrier for CO decomposition is larger than for molecular desorption. Dissociative chemisorption of CO takes

place at low temperatures (180° K) on Ni(110) surfaces³¹ and on stepped surfaces of Ni.³⁰ This is most probably caused by a lower activation energy at steps on these surfaces. This experimental evidence supports favorable energetics for CO dissociation.

Unfortunately the removal of chemisorbed oxygen by hydrogen molecule or chemisorbed hydrogen (reactions 3 and 9 in figure 14) is calculated to be extremely endothermic (35.1 kcal/mol and 58.1 kcal/mol). These enthalpies do not appear to be reasonable in light of kinetic experiments which give an activation barrier of 24.7 kcal/mol for the methanation reaction.³ Water was a principle product under the conditions under which these experiments were carried out. Although the observations of the chemistry of chemisorbed oxygen do not agree with our estimates, the relative energetics of the various chemisorbed CH_x and NH_x intermediates appear to be reasonable and consistent with experimental results.

There has been considerable controversy regarding the geometry of O on Ni(100). UG have carried out calculations on Ni_{20} to model this system and found two low lying electronic states:⁶ an "oxide" state with a surface-oxygen distance of 0.55 Å and vibrational frequency of 218 cm^{-1} and a "radical" state with a surface-oxygen distance of 0.88 Å and vibrational frequency of 371 cm^{-1} . In order to model higher coverages UG⁶ carried out calculations on Ni_{20}O^+ and obtained a $R_1=0.26$ Å and a vibrational frequency of 266 cm^{-1} . These results provided an explanation for why the metal-oxygen stretching frequency (310 cm^{-1}) in the c(2x2) O overlayer was lower than in the p(2x2) O overlayer (430 cm^{-1})³² on Ni(100). Parameters derived from these calculations were used in detailed calculations of the low frequency phonon spectrum which agreed

well with experiment.³³ This led to the conclusion that the c(2x2) O overlayer had chemisorbed oxygen atoms in the "oxide" state with an $R_1=0.26$ Å and the p(2x2) O overlayer contained chemisorbed oxygen atoms in the "radical" with an $R_1 = 0.88$ Å state. However, many experiments have been performed since then which find a longer surface-oxygen distance of 0.8 to 0.9 Å for the c(2x2) overlayer,³⁴ although some experiments do support the shorter Ni-O bond distance.^{34c,d,35} Bauschlicher *et al.*³⁶ have performed calculations on the Ni₅O cluster in which they found that the inclusion of Ni 4p functions to the double- ζ basis of UG⁶ increased the surface-oxygen distance from 0.57 Å to 0.68 Å for the oxide state at the HF level. Their final surface-oxygen distance of 0.74 Å and vibrational frequency of 320 cm⁻¹ was calculated at the singles and doubles CI level. In our GVB-CI calculations we have used a basis of the same quality as Bauschlicher *et al.* (see appendix) and find a surface-oxygen distance of 0.712 Å and vibrational frequency of 380 cm⁻¹ for Ni₁₃O. We have also carried out calculations on Ni₂₀O with the same cluster basis and found an R_1 of 0.647 Å and a vibrational frequency of 358 cm⁻¹ at the GVB-CI level. The results are in good agreement with the Ni₅O calculations and fair agreement with the experimental geometries of 0.8-0.9 Å.

Our calculated geometry for H chemisorbed at the four fold site of Ni₁₃ ($R_1=0.74$ Å) is also substantially longer than that calculated by UG⁶ at the same site ($R_1=0.30$ Å). A recent experimental determination of geometry for deuterium on Ni(100) by transmission tunneling gives a value of $R_1 = 0.5 \pm 0.1$ Å³⁷. Helium diffraction experiments³⁸ gave a geometry for chemisorbed hydrogen on Ni(100) with an R_1 of 0.9-1.0 Å. Our calculated value of 0.74 Å lies in between the two experimental results, which does support the longer R_1 we are finding with a more com-

plete cluster basis. However, our calculated vibrational frequency of 845 cm^{-1} for the surface-hydrogen stretch does not agree as well with the experimental³⁹ frequency of 596 cm^{-1} as that calculated by UG⁶ (589 cm^{-1}).

The experimental determination of the geometry of carbon on Ni(100) has been hampered by significant reconstruction of the substrate.⁴⁰ The LEED data has been shown to be consistent with two structures. In one structure the carbon atoms are 0.9 Å from the surface and in the other structure the carbon atoms are 0.1 Å from the surface. The best fit was found for the second structure and helium diffraction experiments³⁸ also support the shorter R_1 . However, we calculate a surface-carbon distance of 0.858 Å which is in better agreement with the $R_1=0.9$ Å structure. Since we have held the Ni atoms in our cluster fixed we cannot rule out the shorter surface-C distance, which could be favored if the Ni atoms were allowed to relax.

III. Computational details

In all of the calculations presented here the Ni atoms were described by the MEP of UG.⁶ The double- ζ basis of UG⁶ plus bond functions (DZB) at octahedral and tetrahedral interstitials with exponents of 0.208 and 0.310 respectively was used to describe the Ni cluster. In the appendix we compare the DZB basis with a cluster basis in which the double- ζ basis is augmented by a single- ζ Ni 4p function with an exponent of 0.14. The exponents for the bond functions and single- ζ Ni 4p function were optimized for an averaged field wavefunction of Ni₁₃, in which one-third of an electron was placed in the $2a_{1g}$ and $1e_g$ orbitals, four-thirds of an electron was placed in the $1t_{2g}$ orbitals, and the $1a_{1g}$ and $1t_{1u}$ orbitals were doubly occupied. This wavefunction corresponds to an average of all electronic states in which one electron occupies a $1e_g$ or $1a_{1g}$ orbital and four electrons with triplet spin occupy the t_{2g} set of orbitals. This average field wavefunction includes many of the low lying states of the Ni₁₃ cluster and should give a basis which is unbiased toward any particular state of the cluster. Dunning's valence double- ζ contraction (9S5P|3S2P) augmented by polarization functions (D exponents 0.75, 0.80, 0.85) was used for carbon, nitrogen, and oxygen.⁴¹ Hunzinger's four gaussian⁴² basis contracted double zeta and scaled by a factor of 1.2⁴¹ was used for hydrogens bound to nitrogen, carbon and oxygen. Hydrogen bound directly to the cluster was described by a double zeta contraction of Hunzinger's four gaussian basis⁴² unscaled.

The internal coordinates and orientation relative to the surface of each chemisorbed species were optimized with the Ni₁₃ cluster described by the double zeta basis (DZ) without bond functions at the Hartree-Fock level. Every CH_x and NH_x intermediate was found to have its axis of sym-

metry oriented perpendicular to the surface. The calculated internal coordinates of each chemisorbed molecule is listed in table VII. The distance of each molecule from the surface (R_1) was reoptimized with the double zeta plus bond functions basis at the GVB-CI level, while holding the internal coordinates fixed. The nearest neighbor distance between Ni atoms in the clusters was fixed at 2.487 Å.⁶

The GVB-CI wavefunction is a full configuration interaction (CI) calculation in which the orbitals were optimized at the GVB perfect-pairing (GVBPP) level.⁴³ For every complex studied here, except Ni_{13}C , we have used a GVBPP wavefunction where only the electrons in adsorbate valence orbitals and metal-surface bonds were correlated. This generally corresponded to wavefunctions which contained four GVB pairs described by two orbitals each [GVB(4/8)]. The GVB-CI wavefunction for nitrogen on Ni_{13} , which has zero spin, contains 331 configurations and 492 spin eigenfunctions. The chemisorbed carbon atom is an exception in that only seven electrons were localized on the carbon and in surface-carbon bonds. The wavefunction used to describe this complex was a full CI in the orbitals described by three GVB pairs and the singly occupied C_{2p_z} orbital.

In appendix A we show results from RCI wavefunctions. This CI wavefunction involves single and double excitations within each pair times single and double excitations in all other pairs. Excitations between pairs are not allowed. This calculation was felt to be a good test of basis set effects. The RCI wavefunction for nitrogen on Ni_{13} contains 81 configurations and 150 spin eigenfunctions.

The equibondedness reactions used to cancel correlation errors are shown in Table II. The total energies, zero point energies and enthalpies

used to calculate the enthalpies of Table I are tabulated in Table I, II and III. The ΔH_f° for these reactions represent the difference in total energies from our calculations and estimated zero point energies. In each of these reactions the number of bonds to the surface and the total number of H-H, C-H and N-H bonds were held constant. Chemisorbed carbon did not fit well into this scheme because it appears to make between two and three bonds to the surface (two metal-carbon π bonds and a one-electron ionic σ bond). Two reactions are shown to predict the ΔH_f° of chemisorbed carbon. The second reaction ($\text{Ni}_{13}\text{CH} + \text{Ni}_{13}\text{H} \rightarrow \text{Ni}_{13}\text{C} + \text{H}_2 + \text{Ni}_{13}$) was not considered a fair cancellation of errors because in order for this reaction to be considered an equibondedness reaction chemisorbed carbon would have to make four bonds to the surface, which it is not able to do. We felt that using singlet methylene in the first reaction ($2\text{Ni}_{13}\text{H} + ({}^1\text{A}_1)\text{CH}_2 \rightarrow \text{Ni}_{13}\text{C} + 2\text{H}_2 + \text{Ni}_{13}$) to cancel correlation errors was better because methylene is divalent and has a doubly occupied 2s orbital, like chemisorbed carbon atom which has two surface π bonds and a doubly occupied 2s orbital. Unfortunately carbon has also picked up an extra electron from the cluster, which we have not accounted for in our equibondedness scheme. This will cause larger errors in our corrected surface-carbon enthalpy estimate.

As a test of the accuracy of the equibondedness schemes we have calculated the enthalpy change for hydrogen abstraction from various gas phase CH_x and NH_x species. The results of these calculations are tabulated in Table VIII and give C-H and N-H bond energies which agree with the experimental enthalpies to within ± 6 kcal/mol, which justifies its use in these cluster calculations.

Our calculated surface-O bond energy (157.2 kcal/mol) in Ni_{13}O is

disturbingly large. This is much larger than the experimental values (94-134 kcal/mol)¹⁵ but the experimental estimates are very uncertain since chemisorbed oxygen will tend to form oxides at higher temperatures. The fact that we calculate the reduction of oxygen to be uphill is disturbing and means that we must be overestimating the surface-oxygen bond strength by as much as 30 kcal/mol. This is most likely due to the small size of the cluster. We have calculated a surface-oxygen bond energy of 142.6 kcal/mol in Ni₂₀O at the same level of electronic correlation and basis set.⁴⁴ We can use this difference in bond energies to estimate a "cluster effect" of 15 kcal/mol. This correction applied to the Ni₁₃O results derived from the equibondedness analysis gives a bond energy of 136 kcal/mol for oxygen chemisorption on Ni. This is in the range of bond energies found for oxygen on Ni polycrystalline films which range from 94 to 134 kcal/mol.¹⁴

IV. Conclusions

These results are at best qualitative estimates of the heat of formation for various chemisorbed intermediates on Ni(100). Each step of the equibondedness procedure gives errors of approximately ± 7 kcal/mol. The Ni_{13} cluster appears to give bond strengths which are too large; an attempt to correct this bias yields reasonable energetics for NH_x ($x = 0-3$) and CH_x ($x = 1-3$). The energetics for carbon and oxygen chemisorption appear to have larger errors which are most likely due to cluster effects. Our results do indicate that it is energetically favorable to decompose NH_3 on Ni, that imidogen is the most stable NH_x intermediate, and that methylidyne is the most stable CH_x intermediate on Ni, all of which are consistent with experiment.

We find that nitrogen-surface and carbon-surface π bonds are slightly stronger than the corresponding σ bonds. This causes both CH_x and NH_x species to be oriented perpendicular to the surface and favors species which are multiply bonded to the surface. We feel that this is a general trend and can be extrapolated to the surface of bulk metals.

Appendix A.

A. Introduction

Upton and Goddard (UG)⁶ have developed the basic approximations used in this work and applied them to large clusters of Ni atoms (up to 87 atoms).⁴⁵ The heart of this method involves simulating the Ni atoms by a modified effective potential⁶ (MEP) in which the Ar core and d⁹ shell of electrons are included in the MEP. Only the 4s electrons of the Ni atoms are treated explicitly.

UG made several tests of the frozen d⁹ shell approximation, both for the electronic structure of the Ni₁₃ cluster⁴⁶ and for chemisorption of hydrogen on Ni₂₀.^{6,46} These tests showed that the frozen d⁹ shell was a good approximation for large clusters of Ni atoms and for chemisorption on them.

UG⁴⁶ felt that large clusters of atoms (20-87 atoms) were needed to simulate the bulk for chemisorption. This was only made feasible by using an unpolarized basis that contained a double zeta (DZ) 4s function for each Ni atom. In spite of the relatively large differences in the ionization potential (IP) (1.42, 2.46, and 1.63 eV for 13-, 19-, and 20-atom clusters), electron affinity (EA) (1.34, 1.89, and 1.47 eV), and cohesive energy (0.62 and 0.48 eV/atom) for the 13- and 19-atom clusters between the polarized and unpolarized basis sets,⁴⁵⁻⁴⁷ UG felt that in order to mimic the bulk for chemisorption, it was more important to use large clusters approximately than to do highly accurate calculations on small clusters. This approximation appeared to be justified in that the IP and EA of large clusters approached those of the bulk metal as the clusters grew larger.⁴⁵ This result implied that the effect of polarization functions was less important for large clusters than small ones.

Siegbahn *et al.*⁴⁸ have also done tests on the effects of including Ni 3d electrons explicitly in cluster models of hydrogen chemisorption. These results basically confirm the conclusions of UG in that the replacement of d electrons by the MEP did not significantly affect the equilibrium properties of chemisorbed hydrogen atom. However, Siegbahn *et al.*⁴⁸ did find that the addition of polarization functions significantly altered the energetics (~ 10 kcal/mol per H atom) calculated for hydrogen chemisorption.

Siegbahn *et al.*⁴⁸ found that freezing the Ni d orbitals significantly affected their calculated barriers for the dissociative chemisorption of H_2 . They found a barrier of 4.4 kcal/mol in calculations which include d orbitals, while they find a barrier of 48 kcal/mol for calculations in which the d orbitals were included in the MEP. These results indicate that the d orbitals played an important role in the barrier for activation of dihydrogen but not for the equilibrium structure of hydrogen chemisorption. Upton⁴⁹ has presented arguments based on the orbital phase continuity principle⁵⁰ that suggest that low barriers for H_2 dissociation on Ni can be obtained by just considering the s and p bands of the bulk. Although he did not completely optimize the transition state H_2 dissociation, the lowest barrier he finds is 10 kcal/mol. This result directly contradicts the results of Siegbahn *et al.* We believe that Upton's barrier is more reliable since the wavefunction he used allowed the electrons in the conduction band of the cluster to have the optimum spin coupling at the transition state. Since dissociative chemisorption of H_2 on Ni surface is known to be an unactivated process, the barrier height calculated by various methods should be a good test of their validity. Upton's results show that the frozen d^9 shell approximation is valid for this process as well.

Bauschlicher *et al.*³⁶ have carried out calculations on chemisorption of oxygen atoms on a small Ni cluster (five atoms) to test the effect of Ni polarization functions on the calculated parameters for oxygen chemisorption. They found that polarization functions caused an increase in the distance of the oxygen atom from the surface (0.11 Å) and a small increase in the vibrational frequencies (39 cm⁻¹ out of 290 cm⁻¹). Bauschlicher and co-workers have also tested the importance of d electrons for oxygen chemisorption on Ni(100)⁵¹ and for CO chemisorption on Ni(100).⁵² In both cases MEP Ni atoms were replaced by all-electron Ni atoms at the Hartree-Fock level (AEHF). The differences in these calculations are not surprising in light of the fact that AEHF Ni atoms have a 28.7 kcal/mol bias⁵³ favoring the ³F (s²d⁸) versus ³D (s¹d⁹) state of Ni atom, while the 10 e⁻ MEP⁵⁴ was constructed to match the experimental state splitting (0.07 kcal/mol).⁵⁵ It is very likely that the Ni atoms in these studies have a significant amount of d⁹ character that would have increased the 4s population of their wavefunction. This could very likely explain the long oxygen-surface distance (1.05 Å AE versus 0.68 Å MEP) for Ni₅O. It is well known that errors in the state splittings for Ni atom at the AEHF level can cause significant errors in description of the electronic structure of molecules containing Ni. For example, AEHF predicts the ground state for NiCO to be ³Δ while good quality CI calculations predict the ground state to be ¹Σ.⁵⁶ Thus all tests of the d⁹ frozen shell approximation carried out with the 10 e⁻ MEP have shown that this approximation is valid. The AEHF tests conducted so far have given different results because of their bias towards the s²d⁸ configuration and are therefore not fair tests. Until it becomes possible to do all electron CI calculations for Ni clusters in which the ³F-³D state splitting is well

described, the MEP is a necessary and reasonable approximation for describing Ni clusters.

In this appendix we demonstrate that for a large number of cases, the double- ζ cluster basis is not an adequate basis set for modelling chemisorption. Clusters described at the double- ζ level have basis set deficiencies which cause errors in geometries, vibration frequencies and bond energies. It is shown that augmenting the double- ζ cluster basis with s gaussians placed at the tetrahedral and octahedral interstitials of the cluster (bond functions) give results as good as those in the basis set included p polarization functions.

B. Results and Discussion

The results of Siegbahn *et al.*,⁴⁸ Bauschlicher *et al.*,^{36,51} and the results presented in this appendix show that polarization functions are necessary for accurate cluster chemisorption studies. Test calculations for hydrogen (see Table AI) and nitrogen (see Table AII) chemisorption on Ni_{13} show that clusters described by the DZ basis of UG are basis set deficient. In chemisorption studies, this basis set deficiency causes the cluster to compensate by using the basis set of the adsorbate, leading to bond energies that are too large and bond distances that are too short.

Polarization functions also affect the ordering of electronic states in the cluster (see Table AIII). Basically, the lack of polarization functions favors high spin states because of weaker bonds between Ni atoms in the cluster. The major disadvantage of using p functions to polarize the basis set is that the size of the polarized basis is factor 3.5 times that of the DZ basis. For Ni_{13} , the DZ basis contains 26 basis functions, while the DZ plus single- ζ p functions basis (DZP) contains 65 basis functions. The larger basis set will increase the computational effort by a factor of approximately 39 ($= 2.5^4$). The high computational cost of the DZP basis will make the study of the chemisorption of polyatomic molecules (i.e., CH_4 or NH_3) unpractical with the technology currently available to quantum chemists. An intermediate basis that corrects the basis set deficiency of clusters described with the DZ basis is one that uses bond functions at the octahedral and tetrahedral interstitials of the metal cluster. This basis set was found to mimic quite well the DZP results for hydrogen and nitrogen chemisorption (see Tables AI and AII) and the ordering of electronic states for the Ni_{13} cluster (see Table AIII). The advantage of bond functions is that the improvement in the basis set is concentrated where

it is most needed, inside the cluster. This improvement is accomplished with smaller basis sets and considerable savings in cost. For Ni_{13} , the DZ plus bond functions (DZB) basis, which contains 40 functions (26 Ni 4s functions plus one bond function each at six octahedral and eight tetrahedral interstitial sites), yielded a savings of 25 functions and 85% [$1 - (40/65)^4$] of the computation effort over the DZP basis. The DZB basis should not be as flexible as the DZP basis in calculating geometries or cohesive energies of the clusters themselves. However, since we are holding the geometry of the cluster fixed in these studies, the use of bond functions is an appropriate way to correct the artifacts due to the basis set deficiencies of clusters described by the DZ basis. A comparison of the results for various CH_x and NH_x species is shown in Table AIV for clusters described by the DZ and DZB basis sets.

In general, the DZ basis results have shorter surface adsorbate distances (R_{\perp}) and larger dissociation energies than the DZB results. For larger R_{\perp} , this basis set error gets smaller. This is consistent with the cluster using adsorbate basis functions at the DZ level, in that the effect appears to get smaller as the adsorbate moves farther away from the cluster.

It is strongly recommended that all future calculations are performed either with the DZB or DZP basis sets. Although the other approximations made in this work may affect the accuracy of these calculations, correcting the basis set deficiency makes the method self-consistent in that larger basis sets should not affect the results to a significant extent. Because of the large number of atoms and the complicated nature of transition metals, a highly accurate method that would include all of the valence electrons and the differential electronic correlation effects of

large clusters is not yet feasible.

References

- (1) For a recent review, see "The Chemical Physics of Solid Surfaces and Heterogeneous Catalysis," King, D. A.; Woodruff, D. P., Eds., Elsevier: New York, 1982; Vol. 4.
- (2) For a recent review, see Grimley, T. B. In "The Chemical Physics of Solid Surfaces and Heterogeneous Catalysis," King, D. A.; Woodruff, D. P., Eds., Elsevier: New York, 1983; Vol. 2, Chapter 5.
- (3) Kelly, R. D.; Goodman, D. W. In "The Chemical Physics of Solid Surfaces and Heterogeneous Catalysis," King, D. A.; Woodruff, D. P., Eds., Elsevier: New York, 1982; Vol. 4, Chapter 10.
- (4) Grunze, M. In "The Chemical Physics of Solid Surfaces and Heterogeneous Catalysis," King, D. A.; Woodruff, D. P., eds., Elsevier: New York, 1982; Vol. 4, Chapter 5.
- (5) (a) Rappé, A. K.; Goddard III, W. A. *J. Am. Chem. Soc.* **1982**, *104*, 3287-3294;
(b) Allison, J. N.; Goddard III, W. A. *J. Catal.* **1985**, *92*, 127-135.
- (6) Upton, T. H.; Goddard III, W. A. In "Chemistry and Physics of Solid Surfaces," Vanselow, R.; England, W., Eds., CRC Press: Boca Raton, 1982; Vol. 3, pp. 127-162.
- (7) Allison, J. N.; Goddard III, W. A. *Surf. Sci.* **1982**, *115*, 553-568.
- (8) Bradley, J. S. *Adv. Organomet. Chem.* **1983**, *22*, 1-58.
- (9) Seyferth, D. *Adv. Organomet. Chem.* **1976**, *14*, 97-144.
- (10) Herrman, W. A. *Adv. Organomet. Chem.* **1982**, *20*, 159-263.
- (11) $E(\text{C-H})_p = 98.19 \text{ kcal/mol}$ is the C-H bond strength for primary carbons in hydrocarbons. Cox, J.D.; Pilcher, G. "Thermochemistry of Organic and Organometallic Compounds," Academic Press: New

York, 1970.

- (12) Weinberg, W. H. *Survey of Progress in Chemistry* **1983**, *10*, 1-59.
- (13) Herzberg, G. "Electronic Spectra of Polyatomic Molecules," Van Nostrand-Reinhold: New York, 1966; Huber, K. D.; Herzberg, G., "Constants of Diatomic Molecules," Van Nostrand-Reinhold: New York, 1979.
- (14) The N-H bond strength was assumed to be the same as that in NH_3 , which was derived from the experimental enthalpies in Tables V and VII.
- (15) Toyoshima, I.; Somorjai, G. A. *Catal. Rev. - Sci. Eng.* **1979**, *19*, 105.
- (16) Bauschlicher, Jr., C. W.; Cox, B. N. *Surf. Sci.* **1981**, *108*, 483-502.
- (17) Rappé, A. K., Goddard III, W. A. In "Potential Energy Surfaces and Dynamics Calculations," Truhlar, D.G., Ed., Plenum Press: New York, 1981; pp. 661-684.
- (18) Bertolini, J. C.; Tardy, B. *Surf. Sci.* **1981**, *102*, 131-150.
- (19) (a) Goodman, D.W.; Kelly, R.D.; Madey, T.E.; White, J.M. *J. Catal.* **1980**, *64*, 479-481;
(b) Dadayan, K.A.; Boreskov, G.K.; Savchenko, V.I.; Bulgakov, N.N. *Kinet. Catal. (Engl. Trans.)* **1977**, *18*, 480-481; *Kinet. Katal.* **1977**, 574-575; Dadayan, K.A.; Boreskov, G.K.; Savchenko, V.I.; Bulgakov, N.N.; Smolikov, M.D. *Dokl. Acad. Nauk. SSR (Engl. Trans.)* **1978**, *239*, 234-237; *Dokl. Acad. Nauk. SSR* **1978**, *239*, 356-359.
- (20) Seabury, C. W.; Rhodin, T. N.; Purtell, R. J.; Merrill, R. P. *Surf. Sci.* **1980**, *93*, 117-126.
- (21) Grunze, M.; Golze, M.; Driscoll, R. K.; Dowben, P. A. *J. Vac. Sci. Technol.* **1981**, *18*, 611-615.

- (22) Jacobi, K.; Hensen, E. S.; Rhodin, T. N.; Merrill, R. P. *Surf. Sci.* **1981**, *108*, 387-410.
- (23) Hüttinger, M.; Küppers, J. *Surf. Sci.* **1983**, *130*, L277-L282.
- (24) Grunze, M.; Dowben, P. A.; Brundle, C. R. *Surf. Sci.* **1983**, *128*, 311-324.
- (25) Demuth, J. E. *Surf. Sci.* **1980**, *93*, 127-144.
- (26) Demuth, J. E. *Surf. Sci.* **1977**, *69*, 365-384.
- (27) Lehwald, S.; Ibach, H. *Surf. Sci.* **1979**, *89*, 425-445.
- (28) Otarod, M.; Ozawa, S.; Yin, F.; Chew, M.; Cheh, H. Y.; Happel, J. J. *Catal.* **1983**, *84*, 156-169.
- (29) Bradshaw, A. M. *Surf. Sci.* **1979**, *80*, 215-225.
- (30) Erley, W.; Wagner, H. *Surf. Sci.* **1978**, *74*, 333-341.
- (31) Rosal, R.; Ciccaci, F.; Memeo, R.; Caputi, L. S.; Pagano, L. J. *Catal.* **1983**, *83*, 19-24.
- (32) Lehwald, S.; Ibach, H. In "Vibrations at Surfaces," Caudano, R.; Guilles, J.-M.; Lucas, A.A., Eds., Plenum Press: New York, 1982.
- (33) Rahman, T.; Black, J.E.; Mills, D.L. *Phys. Rev. Lett.* **1981**, *46*, 1469-1472.
- (34) (a) Norman, D; Stöhr, J.; Jaeger, R.; Durham, P.J.; Pendry, J.B. *Phys. Rev. Lett.* **1983**, *51*, 2052-2055;
(b) Stöhr, J.; Jaeger, R.; Kendelewicz, T. *Phys. Rev. Lett.* **1982**, *49*, 142-146;
(c) Demuth, J.E.; Dinardo, N.J.; Cargill III, G.S. *Phys. Rev. Lett.* **1983**, *50*, 1373-1376. In this paper the authors propose a structure for the c(2x2) O overlayer in which the oxygen atom has moved 0.3 Å along the <110> direction. This results in two shorter Ni-O

distances of 1.74 Å and two longer distances of 2.14 Å. The shorter distance is in agreement with the Ni-O distance calculated by UG⁶ of 1.78 Å.

(d) Tong, S.Y.; Lau, K.H. *Phys. Rev. B* **1982**, *25*, 7382-7387. The analysis of the LEED data in this paper was shown to be consistent with a surface-oxygen distance of either less than 0.1 Å or 0.9 Å.

- (35) Petersson, L.G.; Kono, S.; Hall, N.F.T; Goldberg, S.; Lloyd, J.T.; Fadley, C.S.; Pendry, J.B. *Mater. Sci. Eng.* **1980**, *42*, 111-119.
- (36) Bauschlicher, Jr., C. W.; Walch, S. P.; Bagus, P. S.; Brundle, C. R. *Phys. Rev. Lett.* **1983**, *50*, 864.
- (37) Stensgaard, I.; Jakobsen, F. *Phys. Rev. Lett.* **1985**, *54*, 711-713.
- (38) Reider, K.H.; Wilsch, H. *Surf. Sci.* **1983**, *131*, 245-257.
- (39) Andersson, S. *Chem. Phys. Lett.* **1978**, *55*, 185-188.
- (40) Onuferko, J.H.; Woodruff, D.P.; Holland, B.W. *Surf. Sci.* **1979**, *87*, 357-374.
- (41) Dunning, T. H.; Hay, D. J. In "Modern Theoretical Chemistry," Schaefer III, H. F., Ed.; Plenum Press: New York, 1977; Vol. 3, Chapter 1, pp 1 - 27.
- (42) Huzinaga, S. *J. Chem. Phys.* **1965**, *42*, 1293-1302.
- (43) Bobrowicz, F. W.; Goddard III, W. A. In "Modern Theoretical Chemistry: Methods of Electronic Structure Theory," Schaefer III, H. F., Ed.; Plenum Press: New York, 1977; Vol. 3, Chapter 4, pp 79-127.
- (44) The same Ni₂₀ cluster was used by UG⁶ to model the bulk for chemisorption.

- (45) Melius, C. F.; Upton, T. H.; Goddard III, W. A. *Solid State Commun.* **1978**, *28*, 501-504.
- (46) Upton, T. H., Ph.D. Thesis, California Institute of Technology, Pasadena, CA, 1980.
- (47) Upton, T. H.; Goddard III, W. A. *J. Vac. Sci. Technol.* **1979**, *16*, 531-535.
- (48) Siegbahn, P. E. M.; Blomberg, M. R. A.; Bauschlicher, Jr., C. W. *J. Chem. Phys.* **1984**, *81*, 2103-2111.
- (49) Upton, T.H. *J. Am. Chem. Soc.* **1984**, *106*, 1561-1571.
- (50) Goddard III, W.A. *J. Am. Chem. Soc.* **1972**, *94*, 793-807.
- (51) Bauschlicher, Jr., C. W.; Bagus, P. S. *Phys. Rev. Lett.* **1984**, *52*, 200-203.
- (52) Bagus, P. S.; Bauschlicher, Jr., C. W.; Nelin, N. J.; Laskowski, B. C.; Seel, B. C. *J. Chem. Phys.* **1984**, *81*, 3594-3602.
- (53) Martin, R. L.; Hay, P. J. *J. Chem. Phys.* **1981**, *75*, 4539-4545.
- (54) Sollenberger M., M.S. Thesis, California Institute of Technology, Pasadena, CA, 1977.
- (55) Moore, C. E. "Atomic Energy Levels," National Bureau of Standards: Washington, DC, 1971; Vol. II. (These state splittings were averaged over j states to cancel out spin-orbit coupling.)
- (56) (a) Rives, A. B.; Fenske, R. F. *J. Chem. Phys.* **1981**, *75*, 1293-1302;
(b) Ha, T.; Nguyen, M. T. *J. Mol. Struct. (Theochem)* **1984**, *109*, 331-338.

Table I.
GVB-CI Parameters for Chemisorption on Four-Coordinate (100) Site of Ni₁₃.

Chemisorbed Species	R(Ni-X) (Å)	R ₁ (Å)	$\omega_1^a)$ (cm ⁻¹)	D _e (kcal/mol)	Total Energy (a.u.)	Corrected D ₀ (kcal/mol)	Corrected ΔH_f^p (kcal/mol)	Ground State	Zero Point Energy ^{b)} (kcal/mol)
C	1.957	0.858	390	142.1	-42.1654	144.8	24.8	² A ₁	1.7
CH	1.991	0.934	457	175.5 ^{c)}	-42.8130	153.6	-12.4	¹ A ₁	8.5
CH ₂	2.051	1.056	430	111.8	-43.3735	101.1	-8.9	² B ₂	15.6
CH ₃ ^{d)}	2.223	1.360	341	53.4	-43.8383	43.6	-7.7	³ A''	22.9
N	1.848	0.569	347	141.3	-58.8581	134.6	-22.1	¹ A ₁	1.5
NH	1.980	0.910	482	129.4	-59.4426	117.0	-32.7	¹ A ₁	9.2
NH ₂	2.102	1.152	424	81.3	-59.9987	70.6	-25.5	³ B ₂	17.2
NH ₃ ^{d)}	2.702	2.052	129	2.04	-60.5369	-1.6	-7.7	⁴ A''	24.6
NH ₃ ^{d,e)}	2.092	2.092	354	15.0	-61.0079	10.0	-19.3	¹ A'	26.0
CO ^{e)}	2.017	2.017	330	17.5	-117.6332	30.0 ^{f)}	-57.2 ^{f)}	¹ A ₁	5 ^{g)}
O	1.897	0.712	380	157.2	-79.3137	151.3	-92.3	² E	1.6
H	1.908	0.740	845	65.6	-4.8394	63.1 ^{h)}	-11.5 ^{h)}	³ A ₂	3.6

a) The reduced mass used to calculate vibrational frequencies was the same as a diatomic in which one atom had a mass equal to the mass of four Ni atoms and the other atom had the mass of the chemisorbed species.

b) The zero point energies were based on ω_1 , frequencies from calculations with the DZ cluster basis and estimated frequencies.

c) Relative to ⁴Σ⁻ methylidyne dissociated limit (Total energy of ⁴Σ⁻ methylidyne is -38.2976 hartrees.)

d) Geometry optimized at the GVB-perfect pairing level.

e) Chemisorption on one-coordinate site of Ni₁₄.

f) Experimental value for D₀ (M-CO). (see ref. 18)

g) Not evaluated since not used in equibondedness reactions (see table II).

h) Experimental value for D₀ (M-H) (see ref. 11)

Table II.

Equibondedness Reactions Used to Calculate ΔH_f°
for Chemisorbed Species Shown in Table I.
(All energies are kcal/mol.)

Reaction	ΔH_f°	Calculated Quantity
$\text{CH}_4 + \text{Ni}_{13}\text{H} \rightarrow \text{Ni}_{13}\text{CH}_3 + \text{H}_2$	19.6	$\Delta H_f^\circ(\text{Ni}_{13}\text{CH}_3) = -7.7$
$\text{Ni}_{13}\text{CH}_3 + \text{Ni}_{13}\text{H} \rightarrow \text{Ni}_{13}\text{CH}_2 + \text{H}_2 + \text{Ni}_{13}$	10.5	$\Delta H_f^\circ(\text{Ni}_{13}\text{CH}_2) = -8.9$
$\text{Ni}_{13}\text{CH}_2 + \text{Ni}_{13}\text{H} \rightarrow \text{Ni}_{13}\text{CH} + \text{H}_2 + \text{Ni}_{13}$	8.0	$\Delta H_f^\circ(\text{Ni}_{13}\text{CH}) = -12.4$
$2[\text{Ni}_{13}\text{H}] + ({}^1\text{A}_1)\text{CH}_2 \rightarrow \text{Ni}_{13}\text{C} + 2\text{H}_2 + \text{Ni}_{13}$	-53.5	$\Delta H_f^\circ(\text{Ni}_{13}\text{C}) = 24.8$
$\text{Ni}_{13}\text{C}-\text{H} + \text{Ni}_{13}-\text{H} \rightarrow \text{Ni}_{13}\text{C} + \text{H}_2 + \text{Ni}_{13}$	62.9	$\Delta H_f^\circ(\text{Ni}_{13}\text{C}) = 39.0$
$\text{Ni}_{13}\text{NH}_3 + \text{Ni}_{13}\text{H} \rightarrow \text{Ni}_{13}\text{NH}_2 + \text{H}_2$	-6.3	$\Delta H_f^\circ(\text{Ni}_{13}\text{NH}_2) = -25.5$
$\text{Ni}_{13}\text{NH}_2 + \text{Ni}_{13}\text{H} \rightarrow \text{Ni}_{13}\text{NH} + \text{H}_2$	4.3	$\Delta H_f^\circ(\text{Ni}_{13}\text{NH}) = -32.7$
$\text{Ni}_{13}\text{NH} + \text{Ni}_{13}\text{H} \rightarrow \text{Ni}_{13}\text{N} + \text{H}_2$	22.1	$\Delta H_f^\circ(\text{Ni}_{13}\text{N}) = -22.1$
$2[\text{Ni}_{13}\text{H}] + \text{H}_2\text{O} \rightarrow \text{Ni}_{13}\text{O} + 2\text{H}_2 + \text{Ni}_{13}$	-12.2	$\Delta H_f^\circ(\text{Ni}_{13}\text{O}) = -92.3$

-193-
Table III.

**Total Energies, Zero Point Energies, and ΔH_f°
for Molecules Used in Table II.**

Molecule	Total Energy ^{a)}	Zero Point ^{b)}	$\Delta H_f^{\circ c)$
	GVB-CI (hartrees)	Energy (kcal/mol)	(kcal/mol)
H ₂	-1.1445	6.3	0.0
CH ₄	-40.2771	27.1	-16.0
NH ₃	-56.2979	21.0	-9.3
H ₂ O	-76.1495	12.9	-57.1
CO	-112.9192	3.1	-27.2
(¹ A ₁) CH ₂	-38.9396	15.6	101.3 ^{d)}
(⁴ T _{1g}) Ni ₁₃ ^{e)}	-4.2357	-	0.0
(¹ A _{1g}) Ni ₁₄ ^{e)}	-4.6861	-	0.0

a) Calculated at experimental geometry; (ref. 13)

b) Calculated with experimental vibrational frequencies (ref. 13).

c) D. R. Stull and H. Prophet, *JANAF Thermochemical Tables*, National Standard Reference Data Series (National Bureau of Standards, Washington, DC, 1971), NSRDS-NBS 37.

d) $\Delta H_f^\circ[(^3B_1)(CH_2)] + \Delta E(^3B_1 \rightarrow ^1A_1)$, state splitting (9.1 kcal/mol), from L. B. Harding and W. A. Goddard III, *Chem. Phys. Lett.*, **55**, 217-220 (1978).

e) We have assumed that the heat of formation of the Ni cluster is the same as the bulk and that the zero point energy of the cluster is essentially constant during the reactions studied here. The geometries of the Ni₁₃ and Ni₁₄ clusters are described in the text.

-194-
Table IV.

**Calculated Total Energies, Zero Point Energies and
Experimental Enthalpies at 0°K for Various Radicals
Used in This Paper.^{a)}**

Molecule	Total Energy	Zero Point	ΔH_f°
	GVB-CI(hartrees)	energy (kcal/mol)	(kcal/mol)
H	-0.4993	0.0	51.6
C	-37.7033	0.0	169.6
CH	-38.3100	4.1	141.2
CH ₂	-38.9597	10.4	92.2 ^{b)}
CH ₃	-39.6176	18.2	35.9 ^{c)}
N	-54.3972	0.0	112.5
NH	-55.0008	4.7	84.3 ^{d)}
NH ₂	-55.6335	11.2	45.1 ^{e)}
O	-74.8274	0.0	59.0

^{a)} Values are from JANAF [footnote (c), Table V] unless otherwise specified. Geometries and vibrational frequencies are those of reference 13.

^{b)} McMillen, D. F.; Golden, D. M., *Ann. Rev. Phys. Chem.*, **33**, 493-532 (1982). This value was extrapolated to 0° K from $\Delta H_{f298}^\circ = 35.1$ kcal/mol.

^{c)} Chase, M.W.; Curnutt, J.L.; Prophey, H.; McDonald, R.A.; Syverud, A.N., *J. Phys. Chem. Ref. Data*, **1975**, *4*, 1-175.

^{d)} Foner, S.N.; Hudson, R.L., *J. Chem. Phys.*, **1981**, *74*, 5017-5021.

^{e)} Bohme, D.K.; Hemsworth, R.S.; Rundle, H.W., *J. Chem. Phys.*, **1973**, *59*, 77-81.

**-195-
Table V.**

**Reactions for Ammonia Decompositon.
(see figure 13)**

			ΔH_f°
			(kcal/mol)
1	$\text{NH}_{3(g)} \rightarrow \text{NH}_{3(a)}$		-10.0
2	$\text{NH}_{3(a)} \rightarrow \text{NH}_{2(a)} + \frac{1}{2} \text{H}_{2(g)}$		-6.2
3	$\text{NH}_{2(a)} \rightarrow \text{NH}_{(a)} + \frac{1}{2} \text{H}_{2(g)}$		-7.2
4	$\text{NH}_{(a)} \rightarrow \text{N}_{(a)} + \frac{1}{2} \text{H}_{2(g)}$		10.6
5	$\text{N}_{(a)} \rightarrow \frac{1}{2} \text{N}_{2(g)}$		22.1
6	$\text{NH}_{3(a)} \rightarrow \text{NH}_{2(a)} + \text{H}_{(a)}$		-17.7
7	$\text{NH}_{2(a)} \rightarrow \text{NH}_{(a)} + \text{H}_{(a)}$		-18.7
8	$\text{NH}_{(a)} \rightarrow \text{N}_{(a)} + \text{H}_{(a)}$		-0.9

Table VI.

Reactions for Methanation.
(see figure 14)

		ΔH_f° (kcal/mol)
1	$\text{CO}_{(g)} \rightarrow \text{CO}_{(a)}$	-30.0
2	$\text{CO}_{(a)} \rightarrow \text{C}_{(a)} + \text{O}_{(a)}$	-10.3
3	$\text{O}_{(a)} + \text{H}_{2(g)} \rightarrow \text{H}_2\text{O}_{(g)}$	35.2
4	$\text{C}_{(a)} + \frac{1}{2} \text{H}_{2(g)} \rightarrow \text{CH}_{(a)}$	-37.2
5	$\text{CH}_{(a)} + \frac{1}{2} \text{H}_{2(g)} \rightarrow \text{CH}_{2(a)}$	3.5
6	$\text{CH}_{2(a)} + \frac{1}{2} \text{H}_{2(g)} \rightarrow \text{CH}_{3(a)}$	1.2
7	$\text{CH}_{3(a)} + \frac{1}{2} \text{H}_{2(g)} \rightarrow \text{CH}_{4(g)}$	-8.3
8	same as 1	
9	$\text{O}_{(a)} + 2\text{H}_{(a)} \rightarrow \text{H}_2\text{O}_{(g)}$	58.2
10	$\text{C}_{(a)} + \text{H}_{(a)} \rightarrow \text{CH}_{(a)}$	-25.7
11	$\text{CH}_{(a)} + \text{H}_{(a)} \rightarrow \text{CH}_{2(a)}$	15.0
12	$\text{CH}_{2(a)} + \text{H}_{(a)} \rightarrow \text{CH}_{3(a)}$	12.7
13	$\text{CH}_{3(a)} + \text{H}_{(a)} \rightarrow \text{CH}_{4(g)}$	3.2

Table VII. Internal coordinates of AH_x (where A = N or C) used in this study.

Chemisorbed Species	Internal Coordinate of Fragment	
	A-H distance (Å)	H-A-H angle (degrees)
NH	1.013	
NH ₂	1.017	97.7
NH ₃	1.003	105.1
CH	1.095	
CH ₂	1.107	100.4
CH ₃	1.094	104.1

Table VIII. Test of Equibondedness Reactions (in kcal/mol).

Reaction	ΔH_f° (exp)	ΔH_f° (GVB-CI)	Error
$C + H_2 \rightarrow CH + H$	23.2	21.9	-1.3
$CH + H_2 \rightarrow CH_2 + H$	2.6	-2.8	-5.4
$CH_2 + H_2 \rightarrow CH_3 + H$	-5.0	-6.5	1.5
$CH_3 + H_2 \rightarrow CH_4 + H$	-0.3	-6.4	-6.1
$N + H_2 \rightarrow NH + H$	23.4	24.5	1.2
$NH + H_2 \rightarrow NH_2 + H$	12.4	7.6	-4.8
$NH_2 + H_2 \rightarrow NH_3 + H$	-2.8	-8.5	-5.7

Table AI.
Basis Set Effects on
Hydrogen Chemisorption on Ni₁₃.^{a)}

Level of Calculation	Basis Set	R_1 (Å)	ω_1^b (cm ⁻¹)	Bond Energy (kcal/mol)	Total Energy (hartrees)
HF	DZ	0.355	637	60.0	-4.6190
GVB(1/2)	DZ	0.385	659	67.1	-4.6301
RCI(1/2)	DZ	0.388	661	67.3	-4.6304
HF	DZP	0.690	828	58.6	-4.9125
GVB(1/2)	DZP	0.726	814	66.7	-4.9254
RCI(1/2)	DZP	0.724	804	66.9	-4.9256
HF	DZB	0.730	891	57.2	-4.8266
GVB(1/2)	DZB	0.764	871	65.4	-4.8393
RCI(1/2)	DZB	0.740	845	65.6	-4.8394

^{a)} The bond lengths (R_1), vibrational (ω_1), bond energies, and total energies are extrapolated from spline fits to calculated values.

^{b)} The vibrational frequencies were calculated using the reduced mass for a hydrogen atom and a particle four times the mass of a nickel atom; $\mu = 1.0035$ atomic mass units.

-200-
Table AII.
Basis Set Effects on
Nitrogen Chemisorption on Ni₁₃.^{a)}

Level of Calculation	Basis Set	R ₁ (Å)	ω ₁ ^{b)} (cm ⁻¹)	Bond Energy (kcal/mol)	Total Energy (hartrees)
HF	DZ	0.157	410	71.5	-58.4584
GVB(4/8)	DZ	0.205	387	106.6	-58.5173
RCI(4/8)	DZ	0.232	352	146.2	-58.5804
HF	DZP	0.442	325	52.7	-58.7239
GVB(4/8)	DZP	0.550	308	93.4	-58.7917
RCI(4/8)	DZP	0.511	332	133.5	-58.8556
HF	DZB	0.487	325	50.7	-58.6370
GVB(4/8)	DZB	0.612	320	91.8	-58.7055
RCI(4/8)	DZB	0.550	320	130.7	-58.7675

^{a)} The bond lengths (R₁), vibrational (ω₁), bond energies, and total energies are extrapolated from spline fits to calculated values. The Nitrogen basis used for these calculations was a double-ζ contraction of Rappé's "fours" basis (see table AV).

^{b)} The vibrational frequencies were calculated using the reduced mass for a nitrogen atom four times the mass of a nickel atom; μ = 13.2084.

Table AIII.
Basis Set Effects on State Splittings of Ni₁₃.

State	Configuration ^{a)}						State Splittings (kcal/mol)		
	t_{2g} (xy)	t_{2g} (xz)	t_{2g} (yz)	e_g (x^2-y^2)	e_g ($3z^2-r^2$)	$2a_{1g}$	DZ	DZP	DZB
$2T_{2g}$	2	2	1				0 ^{b)}	0 ^{c)}	0 ^{d)}
$4T_{2g}$	2	1	1	1			17.5	13.8	10.2
$4T_{1g}$	2	1	1		1		18.4	8.2	5.6
$4T_{1g}$ ^{e)}	2	1	1			1	-2.1		
$6A_{1g}$	1	1	1	1	1			10.7	8.1
$6E_g$	1	1	1	1		1	2.2	19.8	11.9

a) The $1a_{1g}$ and $1t_{1u}$ orbitals which are doubly occupied for all of these states are not shown.

b) The total energy for Ni₁₃ in the DZ basis is -4.0206 h.

c) The total energy for Ni₁₃ in the DZP basis is -4.3324 h.

d) The total energy for Ni₁₃ in the DZB basis is -4.244628 h.

e) Only the lowest energy $4T_{1g}$ state was solved for in the DZP and DZB basis sets.

Table AIV. Effects of Bond Functions on AH_x (where $A = N$ or C) on the Four-Coordinate Site of Ni_{13} .^{a)}

Ground State	Chemisorbed Species	R_1 (Å)		ω_1 (cm ⁻¹)		D_e (kcal/mol)		Total Energy (hartrees)	
		DZ	DZB	DZ	DZB	DZ	DZB	DZ ^{b)}	DZB
¹ A ₁	N	0.232	0.551	352	337	146.2	134.1	-58.5804	-58.8467
² A ₁	NH	0.807	0.908	476	484	129.5	127.7	-59.1793	-59.4364
³ B ₂	NH ₂	1.068	1.15	462	426	93.6	80.9	-59.7242	-59.9932
⁴ A"	NH ₃	1.57	2.05	292	129	20.8	2.3	-60.2589	-60.5319
² A ₁	C	0.355	0.833	333	413	148.3	138.9	-41.9636	-42.1803
¹ A ₁	CH	0.742	0.934	464	457	190.6	173.9	-42.6220	-42.8071
² B ₂	CH ₂	0.895	1.057	401	430	121.1	111.8	-43.1725	-43.3692
³ A"	CH ₃	1.282	1.36	375	341	88.7	53.4	-43.7288	-43.9350

^{a)} These calculations were all performed at the RCI(4/8) level.

^{b)} The nitrogen basis for DZ calculations was a double- ζ contraction of Rappé's "Fours" basis (set table AV).

Table AV.

The (7s4p|3s2p) Contraction of Rappé's "Fours" Nitrogen basis set^{a)}

Component	Type	Exponent	Coefficient
1	S	588.790042	0.0207721952
2	S	88.7013675	0.142129065
3	S	19.8226575	0.479025723
4	S	5.26862757	0.500943653
1	S	7.003173828	-0.195396724
2	S	0.767161436	1.07488965
1	S	0.231739294	1.00000000
1	P	13.5561742	0.0589506223
2	P	2.92431073	0.320281888
3	P	0.799357604	0.753138039
1	P	0.219198754	1.00000000

^{a)} Rappé, A.K.; Goddard, W.A., III, unpublished results

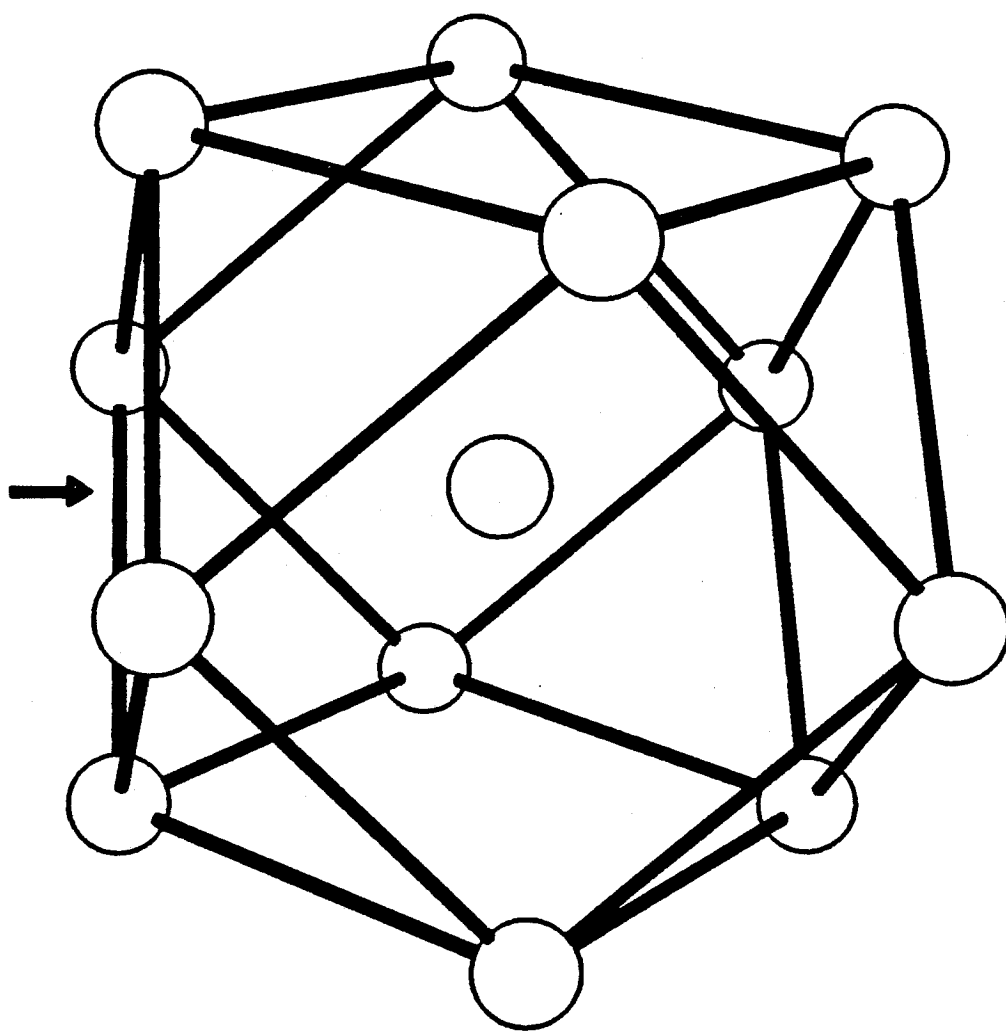


Figure 1. The Ni_{13} cluster. The arrow marks the four-coordinate site.

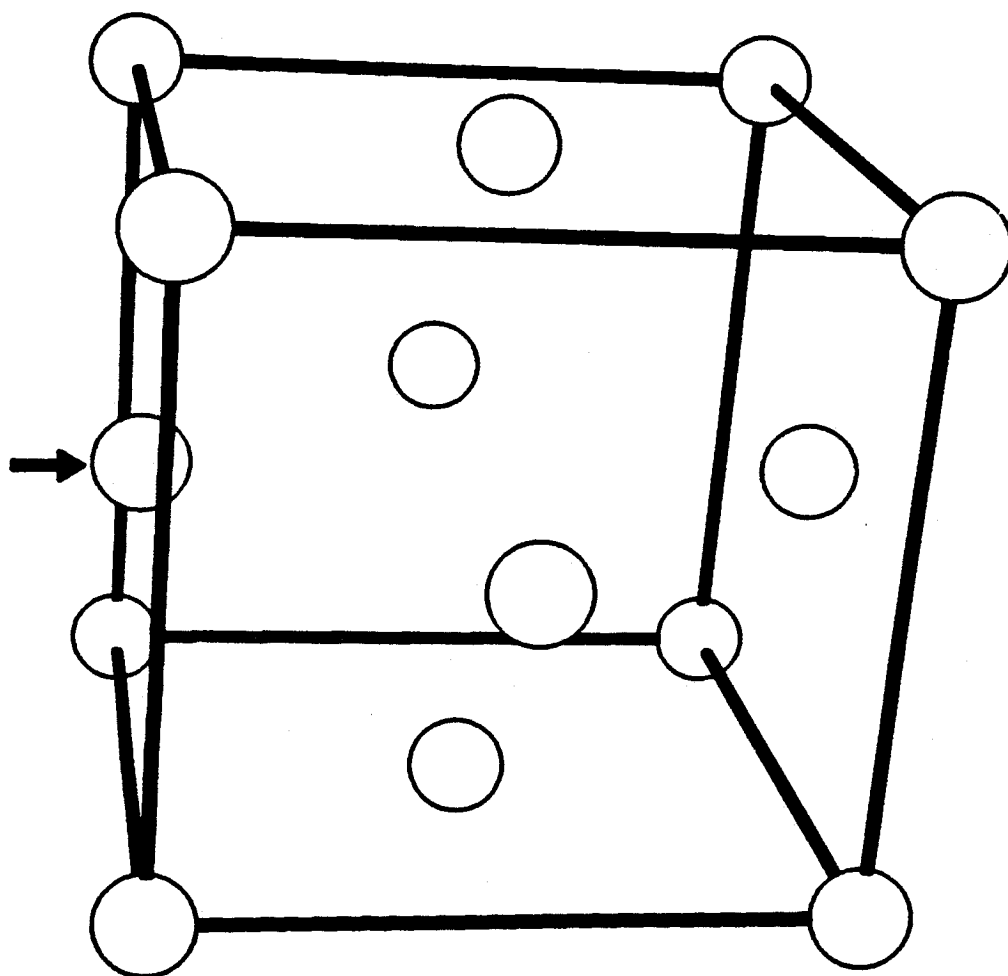


Figure 2. The Ni₁₄ cluster. The arrow marks the one-coordinate site.

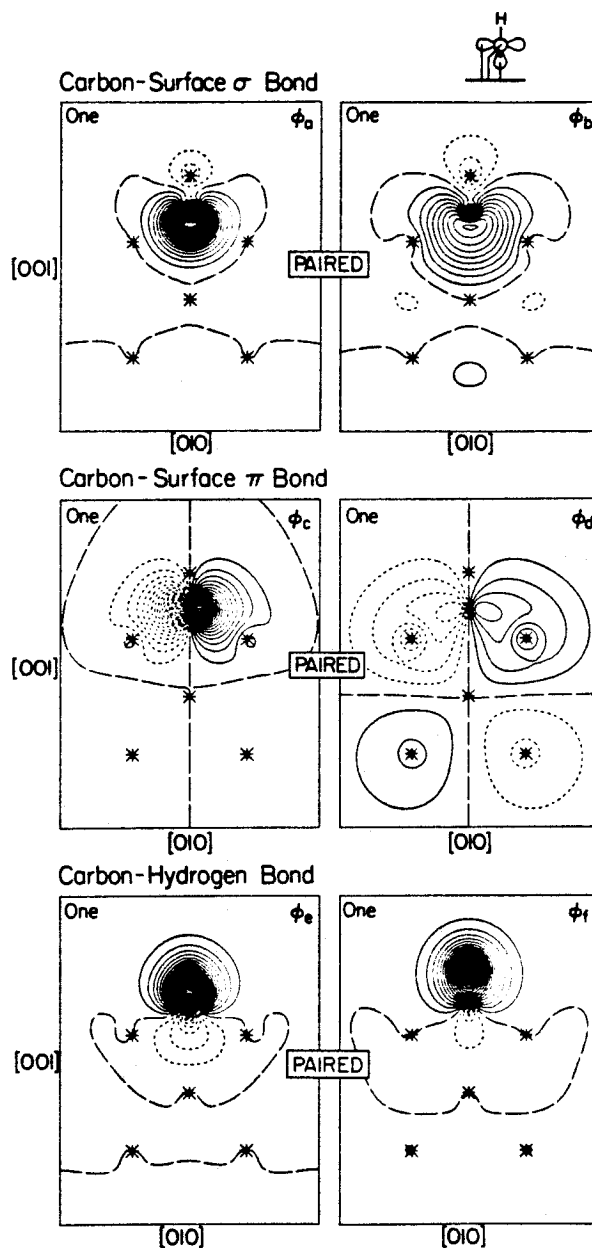


Figure 3. The GVB orbitals for Ni_{13}CH [from the GVB(4/8)-PP wavefunction]. Nuclei in the plane are indicated by asterisks. Positive contours are solid, negative contours are dotted, and nodal lines are long dashes. The spacing between contours is 0.02 a.u.

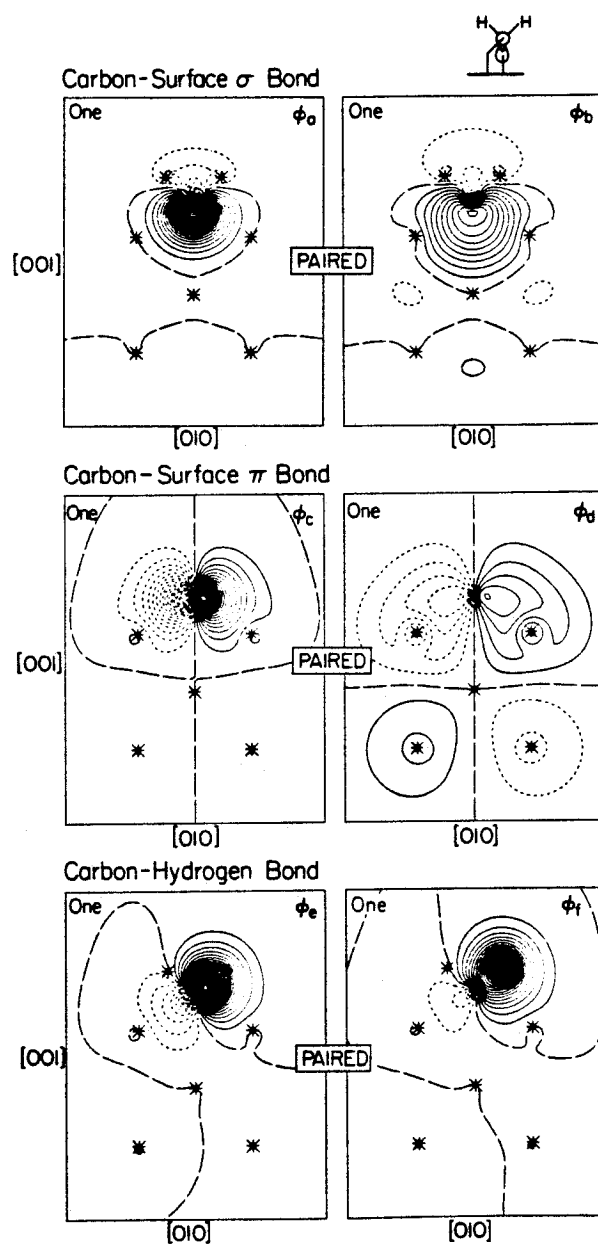


Figure 4. The GVB orbitals for the $\text{Ni}_{13}\text{CH}_2$ cluster.

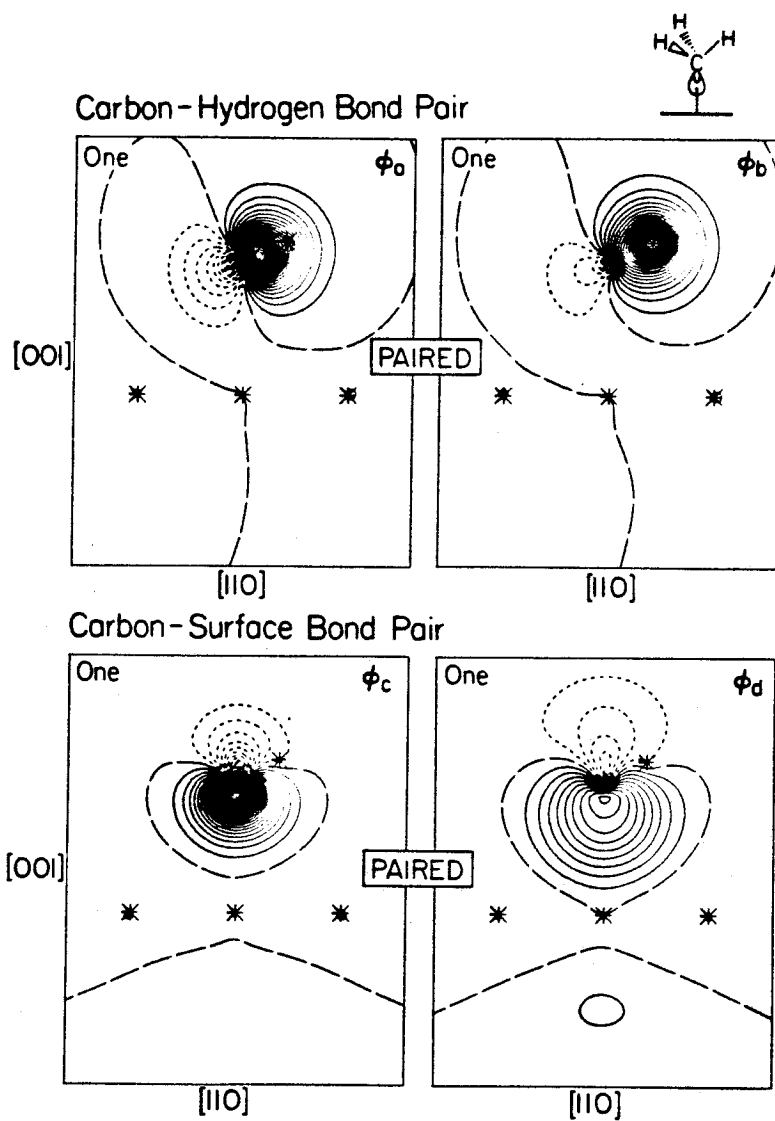


Figure 5. The GVB orbitals for the $\text{Ni}_{13}\text{CH}_3$ cluster.

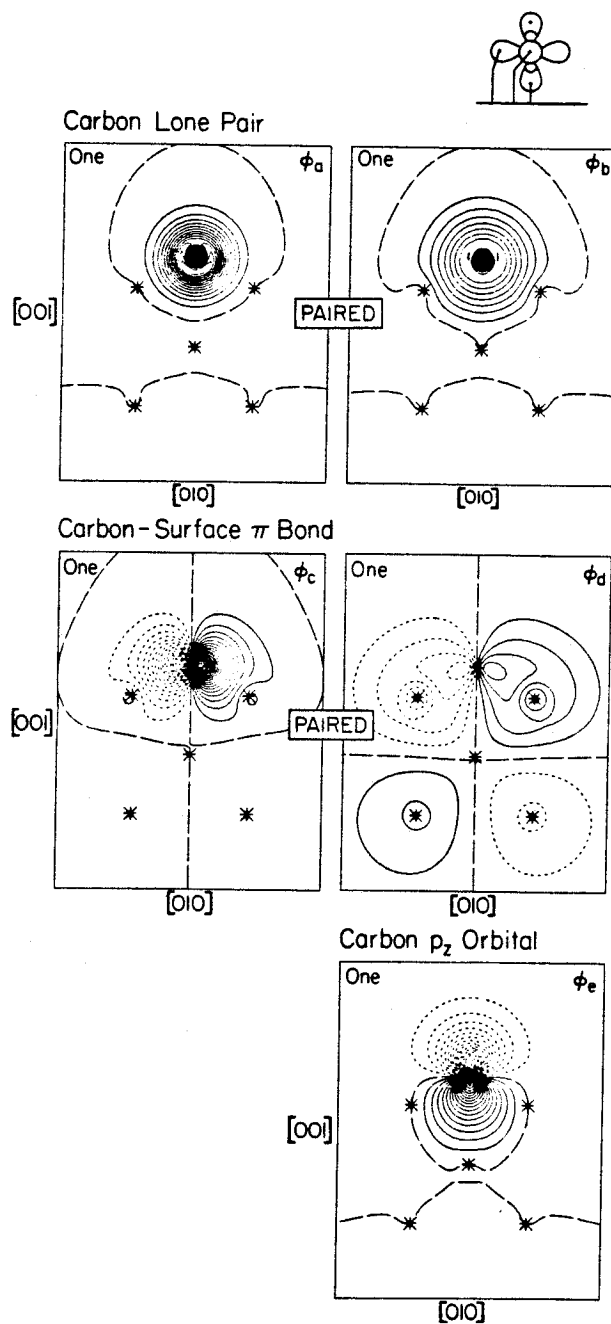


Figure 6. The GVB orbitals for the Ni_{13}C cluster.

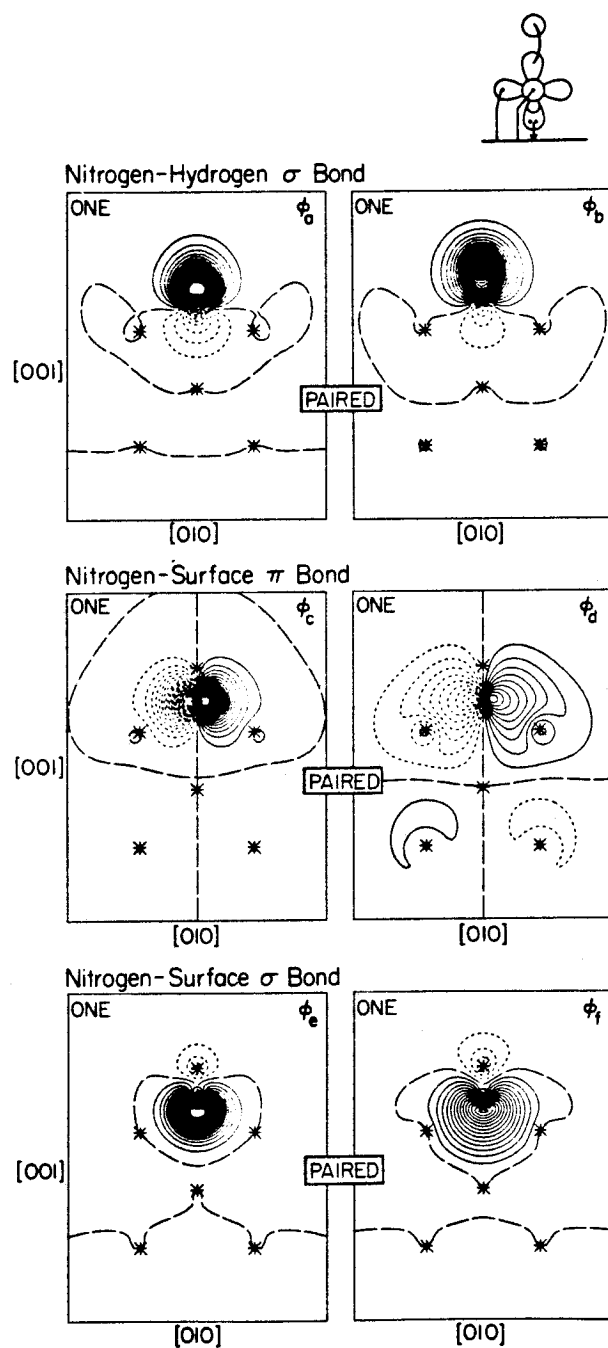


Figure 7. The GVB orbitals for the Ni_{13}NH cluster.

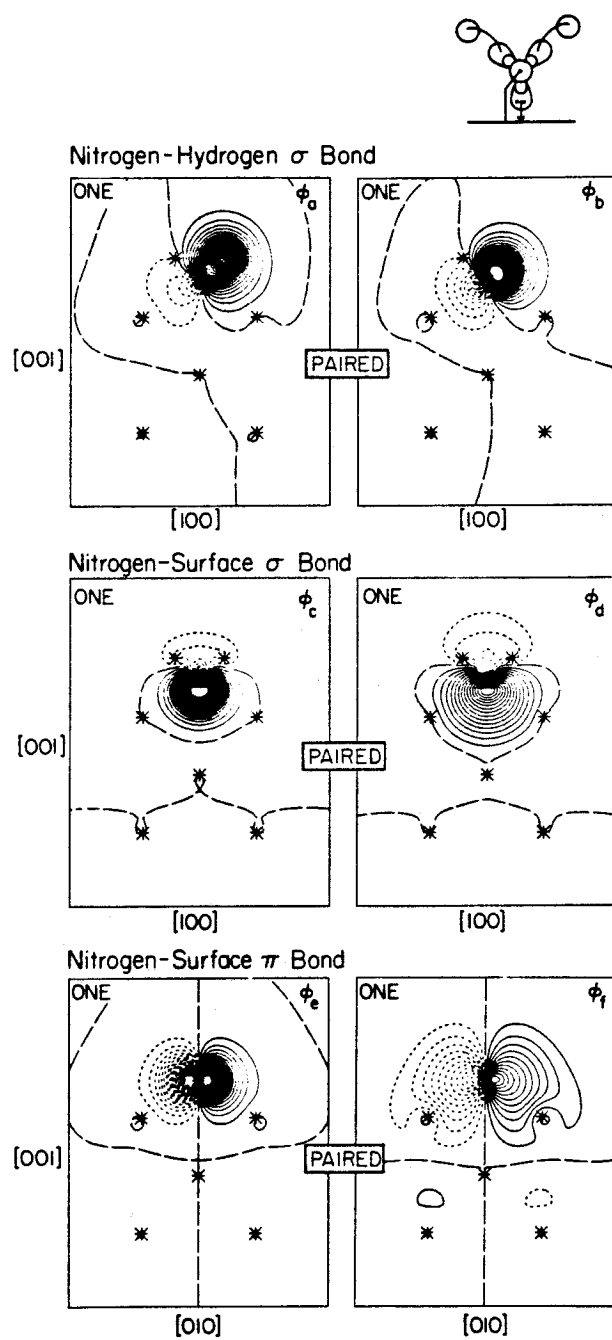


Figure 8. The GVB orbitals for the $\text{Ni}_{13}\text{NH}_2$ cluster.

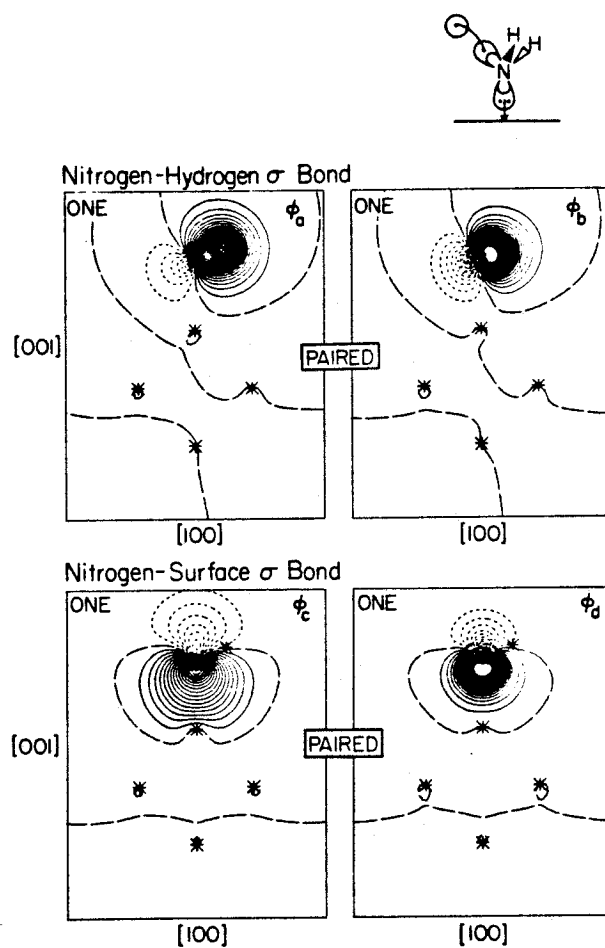


Figure 9. The GVB orbitals for the $\text{Ni}_{13}\text{NH}_3$ cluster.

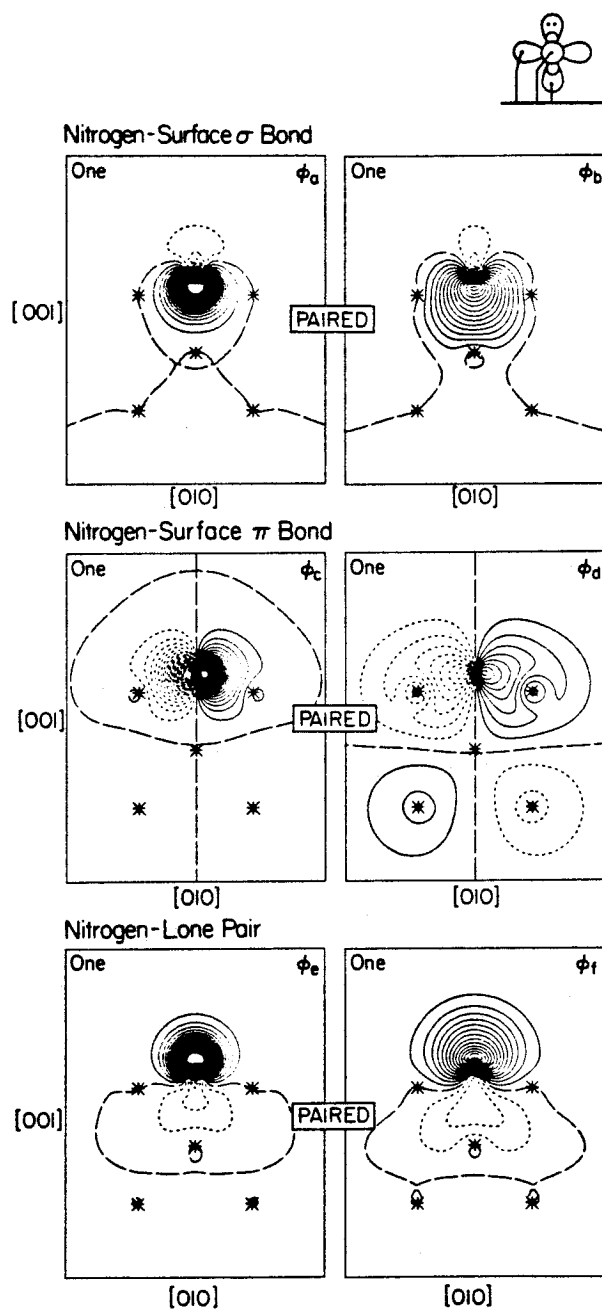


Figure 10. The GVB orbitals for the Ni_{13}N cluster.

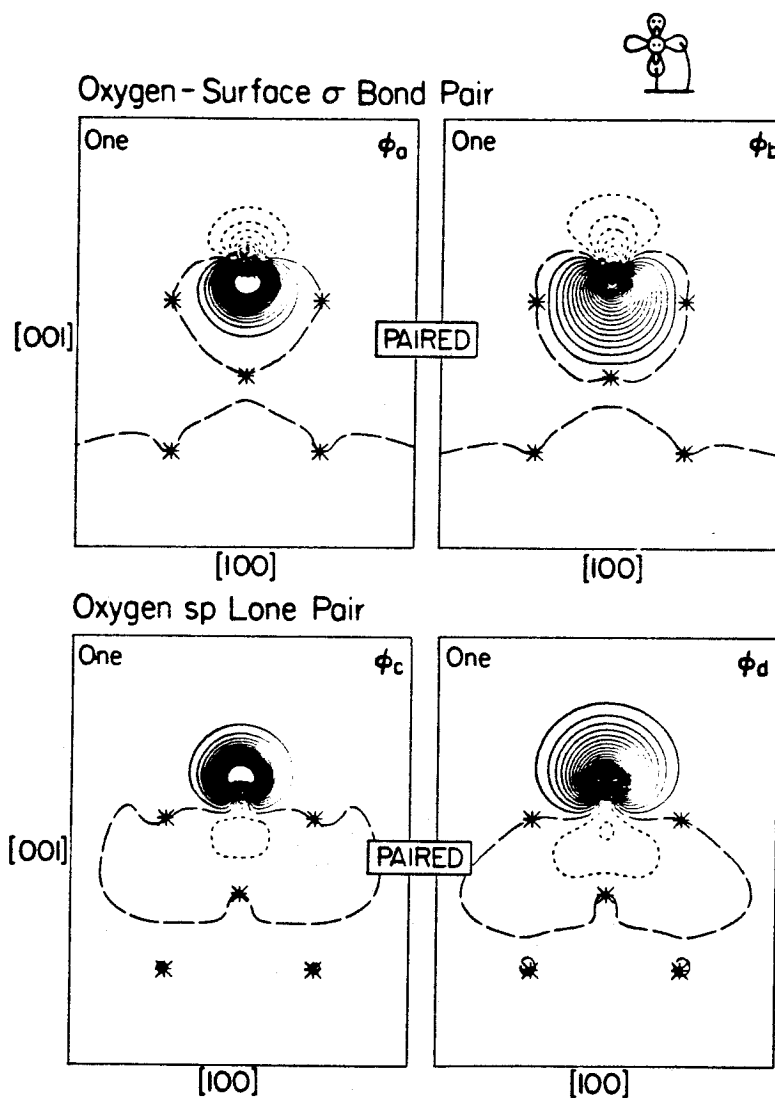


Figure 11. The GVB orbitals for the σ orbitals of the Ni_{13}O cluster.

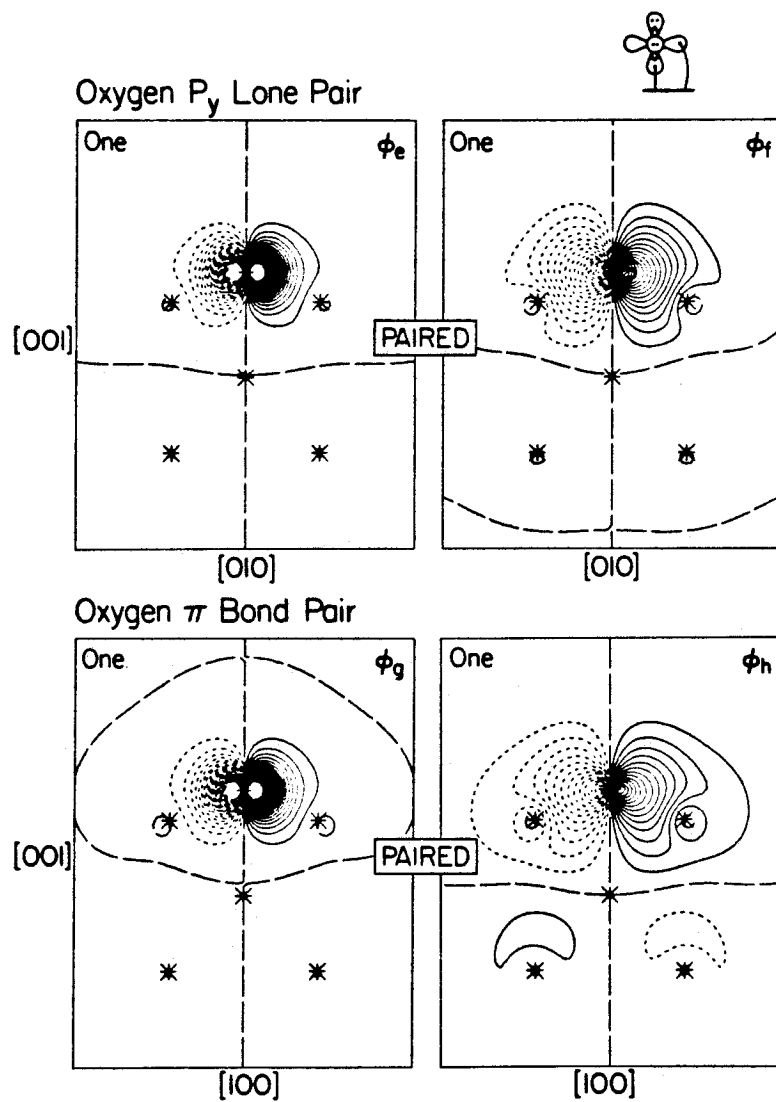


Figure 12. The GVB orbitals for the π orbitals of the Ni_{13}O cluster.

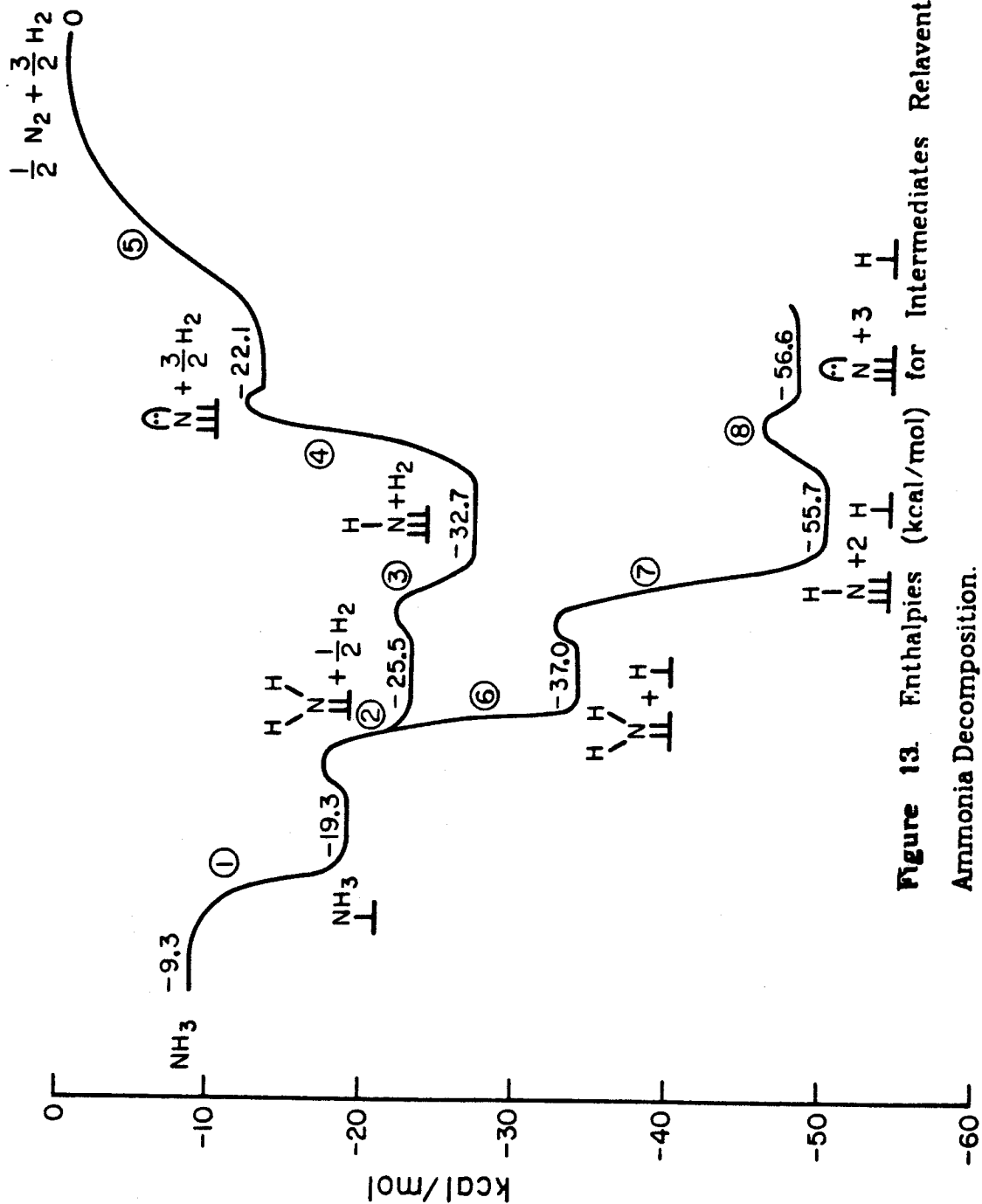


Figure 13. Enthalpies (kcal/mol) for Intermediates Relevant for Ammonia Decomposition.

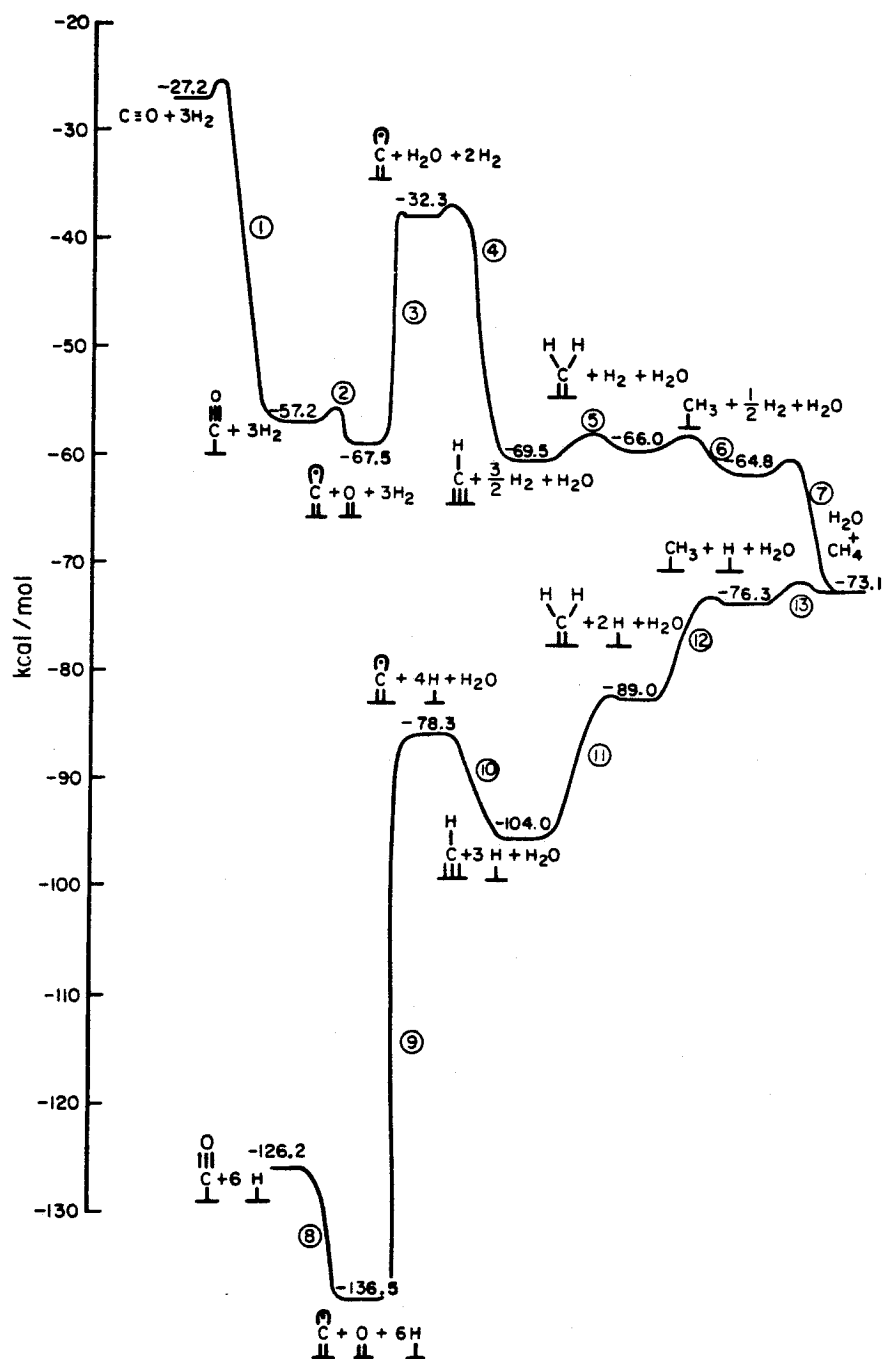


Figure 14. Enthalpies (kcal/mol) for Intermediates Relevant for Methanation.